



**SAPIENZA**  
UNIVERSITÀ DI ROMA

SAPIENZA UNIVERSITY OF ROME



DOCTORATE OF PHILOSOPHY IN INFORMATION AND COMMUNICATION  
TECHNOLOGY – CURRICULUM ELECTRONICS ENGINEERING  
XXXV CYCLE

**Occupational exposure to electromagnetic fields: risk  
assessment of operators performing Transcranial  
Magnetic Stimulation (TMS) treatments**

**Candidate**

Simona D'Agostino

*ID Number 1249619*

**Thesis Advisor**

Prof. Francesca Apollonio  
Dr. Rosaria Falsaperla

**Thesis Co-Advisor**

Prof. Rita Asquini  
Prof. Marta Cavagnaro  
Prof. Micaela Liberti

A.Y. 2021/2022





**SAPIENZA**  
UNIVERSITÀ DI ROMA

SAPIENZA UNIVERSITY OF ROME



DOCTORATE OF PHILOSOPHY IN INFORMATION AND COMMUNICATION  
TECHNOLOGY – CURRICULUM ELECTRONICS ENGINEERING  
XXXV CYCLE

**Occupational exposure to electromagnetic fields: risk  
assessment of operators performing Transcranial  
Magnetic Stimulation (TMS) treatments**

**Candidate**

Simona D'Agostino

*ID Number 1249619*

**Thesis Committee**

Prof. Francesca Apollonio (Thesis Advisor)

Dr. Rosaria Falsaperla

Prof. Rita Asquini

Prof. Marta Cavagnaro

Prof. Micaela Liberti

**Reviewers**

Prof. Rita Massa

Prof. Marta Parazzini

A.Y. 2021/2022

**Occupational exposure to electromagnetic fields: risk assessment of operators performing Transcranial Magnetic Stimulation (TMS) treatments**

Ph.D. Thesis - Sapienza University of Rome

© 2021 Simona D'Agostino. All rights reserved.

Thesis submitted in partial fulfillment of the requirements for the degree of Doctor of Philosophy Information and Communication Technology – Curriculum Electronics Engineering.

Author's address:

Simona D'Agostino

Sapienza - University of Rome

Via Eudossiana 25, 00184 Rome, Italy

e-mail: [simona.dagostino@uniroma1.it](mailto:simona.dagostino@uniroma1.it)

# CONTENTS

---

<b>Abstract .....</b>	<b>17</b>
<b>Introduction and Purpose of the research .....</b>	<b>20</b>
<b>Section I. EMF applications: occupational exposure and legislative .....</b>	<b>27</b>
<b>I..... Chapter</b>	<b>29</b>
1.1. State of art: an overview of occupational exposure in the work environment .....	29
1.2. The EM source of interest: Transcranial Magnetic Stimulation (TMS).....	35
1.3. TMS device: physical principle, device models, and applications.....	39
<b>II..... Chapter</b>	<b>44</b>
2.1. Reference legislation: Directive and technical standards .....	44
2.2. Risk assessment: compliance with LG ICNIRP 2010.....	51
<b>Section II. Numerical modeling and computational dosimetry in the risk assessment ..</b>	<b>55</b>
<b>III..... Chapter</b>	<b>57</b>
3.1 Numerical analysis: an overview of the computational methods.....	57
3.2 EM characterization of TMS device: validation & verification of the coil models .	63
3.3 Standardization of worker position in TMS treatments .....	75
<b>IV..... Chapter</b>	<b>79</b>
4.1 Occupational exposure conditions during TMS treatment: methods and modeling	79
4.2 Results of the analysis of risk for male clinician performing the TMS treatments .	83

4.3	Discussion of the results .....	97
4.4	Conclusions .....	102
<b>V. Chapter</b>	.....	<b>104</b>
5.1	Exposure gender-dependent: possible differences in risk assessment between male and female operator .....	104
5.2	Assessment of gender exposure to TMS: comparison of the results .....	105
5.3	Conclusions and suggestions for a better analysis of the risk .....	116
<b>Section III. AN Innovative approach to the analysis of the risk in the occupational exposure .....</b>		<b>119</b>
<b>VI. Chapter</b>	.....	<b>121</b>
6.1	Drawback of the female models and enhancement of Ella model.....	121
6.2	Numerical dosimetry with Enhanced Ella: exposure dependent on anatomical structure.....	122
6.3	Conclusions and suggestions.....	131
<b>VII. Chapter</b>	.....	<b>134</b>
7.1	Human exposure variability and the importance of the anatomical characteristics in the risk assessment .....	134
7.2	Methods of analysis: four different human subjects to provide an intersubject variability.....	136
7.3	Comparison of the results among the human models.....	140
7.4	Discussions .....	149
7.5	Conclusions .....	154
<b>VIII. Chapter</b>	.....	<b>155</b>
8.1	Possible health effects during TMS treatments: possible neuronal stimulation response .....	155

8.2	Neuronal analysis: Jeduk and Yoon-Sun neurofunctional models.....	157
8.3	Results .....	162
8.4	Discussions and conclusions.....	169
<b>Section IV. Technical support in INAIL mission .....</b>		<b>172</b>
<b>IX. Chapter.....</b>		<b>174</b>
9.1	Aims of the Institute and measurement campaigns.....	174
9.2	An overview of the contributions to the research activity in INAIL .....	187
9.3	Working Group of physical agents portal- PAF: presentation of the database for the prevention and protection from the physical agents.....	193
<b>Conclusions .....</b>		<b>197</b>
<b>Bibliography .....</b>		<b>206</b>

# LIST OF FIGURES

---

Figure I. 1 (a) Welding Machine <sup>24</sup> ; (b) Industrial induction oven, 30 kHz - 24kW, .....	30
Figure I. 2.(a) Electrosurgical unit <sup>24</sup> ;(b) MRI, figure adapted from Siemens Corporation website.....	31
Figure I. 3. TMS device, figure adapted from PAF website <sup>24</sup> .....	33
Figure I. 4. Operating principle of the TMS device during the treatment .....	35
Figure I. 5 Models of coil: (a) circular and (b) figure of eight. Images adapted from the Magstim website .....	41
Figure I. 6 Double-cone coil, from Magstim website .....	42
Figure I. 7 Commercial coils for clinical treatments: (a) Circular coil, (b) Hased coil, (c) Crown coil, (d) Figure-of-eight coil, (e) Double cone coil, and (f) C-core coil. Image adapted from Zhi-De Deng et al. 2013 <sup>90</sup> . .....	43
Figure III. 1. (a) Evaluation of B-field at 80 mm from the center of the coil; (b) Evaluation of B-field at 65 mm from the center of the coil; (c) on the top coil placed in the plane xy, on the bottom B-field around the coil in the free space.....	64
Figure III. 2: Measurement setup .....	66
Figure III. 3 Modeled coil in simulation environment: (A) coil in the grid (mesh) set in the simulation environment, (B) circular coil numerical model, (C) distribution of the magnetic flux density B(T) on the surface of the coil in corresponding of the windings, (D) distribution of B(T) in corresponding on the surface in the position of the coating .....	67
Figure III. 4 B-field (T) <i>along the line through the center of the coil in the outer surface</i> .....	67
Figure III. 5: Coil position with respect to the operator model: h = 29.2 cm (case #A), h = 49.2 cm (case #B), and h = 9.2 cm (Case #C). Figure adapted from Bottauscio et al.2016.....	69
Figure III. 6: Distribution of B-field produced by the modeled MC125 circular coil, (A) distribution of the magnetic flux density B(T) on the surface of the coil in	



corresponding of the windings, (B) distribution of B(T) on the surface at the position of the coating, i.e.4mm away from the windings. ....	70
Figure III. 7. Figure-of-eight coil .....	71
Figure III. 8 Mapping of B on surface of the Std. Double coil 9925-00. The maximum B-field 1.2 T is achieved at the center of the coil.....	72
Figure III. 9  B  along radial direction, through the center and the two lobes, on the surface of the coil .....	73
Figure III. 10:  B  along radial direction, through the center and the two lobes, on the plane 4 mm away from the surface of the coil.....	73
Figure III. 11: Circular coil .....	74
Figure III. 12: a) Mapping of B-field on the plane at 4 mm from surface of the coil. b) B-field along radial axis, that is highlighted by the green line in a).....	75
Figure III. 13. TMS treatment with use of plastic tool. Figure adapted from <a href="https://www.smarttms.co.uk">https://www.smarttms.co.uk</a> .....	76
Figure III. 14. Exposure of lower abdomen with use of bed support for patient. Figure adapted from GEA solution website.....	77
Figure III. 15. Exposure of chin/neck of the operator. Figure adapted from website <a href="https://www.cincinnatichildrens.org/research/divisions/n/neurology/labs/gilbert-wu">https://www.cincinnatichildrens.org/research/divisions/n/neurology/labs/gilbert-wu</a> .....	77
Figure III. 16: Typical relative vertical positions between the TMS coil and the clinician: examples of real scenarios and identification of the exposed anatomical areas: (A) exposure of the chin/neck, (B) exposure of the chest, (C) exposure of the abdomen, and (D) exposure of the lower abdomen.....	78
Figure IV. 1 The dosimetric model. Two coil orientations (I and II) and four vertical positions: case A-exposure of the chin/neck ( $h_1 = 153.5$ cm), case B-exposure of the chest ( $h_2 = 136$ cm), case C-exposure of the abdomen ( $h_3 = 112$ cm), case D-exposure of the lower abdomen ( $h_4 = 95.3$ cm). For orientation I, the distance between the center of the coil and the surface of the clinician's body model ( $d_1$ ) is	

21 cm, whereas for orientation II, the distance between the edge of the coil and the surface of the clinician's body $d_{II}$ is 12 cm. ....	80
Figure IV. 2. Explanatory image of the exposure conditions of the hand. (a) distance considered, (b) closed hand, (c) open hand. ....	82
Figure IV. 3. Streamline distribution map at a simulation output of 100%. Worst case exposure of: (a) Std. Double coil 9925-00, Magstim, (b) circular coil 9784-00, Magstim.....	84
Figure IV. 4. E-field map at 50% of the maximum output for orientation I: (1) Exposure to the Double coil 9925-00 in the four cases, A-B-C-D; (2) Exposure to the Circular coil 9784-00 in the four cases, A-B-C-D.....	85
Figure IV. 5. E-field map at 50% of the maximum output for orientation II: (1) Exposure to the Double coil 9925-00 in the four cases, A-B-C-D; (2) Exposure to the Circular coil 9784-00 in the four cases, A-B-C-D.....	86
Figure IV. 6. 99 <sup>th</sup> percentile of induced E-field for case D - lower abdomen (worst case scenario in orientation I owing to exposure to circular coil Magstim 9784-00) as a function of the distance from the center of the coil.....	88
Figure IV. 7. 99 <sup>th</sup> percentile of induced E-field for case C - abdomen (worst case scenario in orientation II owing to exposure to circular coil Magstim 9784-00) as a function of the distance from the coil windings edge.....	89
Figure IV. 8. Safe distances as a function of the MSO%. Red line the lower abdomen exposure in the I orientation; blue line the abdomen exposure in II orientation. ...	90
Figure IV. 9. Induced E-field map at 50% of the maximum output for orientation II. Coil placed in correspondence to: (a) chin/neck- case A, (b) chest- case B, (c) abdomen- case C, (d) lower abdomen -case D. ....	91
Figure IV. 10. Exposure condition: (a) On the top the human model of the Dukeposable model, on the bottom the illustration of hand's distance $d$ ; (b) $E_{F_{induced}}$ on the surface of the closed hand 5 cm from coil edge; (c) $E_{F_{induced}}$ on the surface of the open hand 2.5 cm from coil edge.....	93
Figure IV. 11 Dose metric of the exposure in hand district. ....	95

Figure IV. 12. Bar graph representing the 99th percentile of the current density induced in the whole body (blue) and in the Central Nervous System CNS only (red) by the circular coil (A) and the figure-of-eight coil (B) for two cases of exposure: neck/chin (case-A orientation I) and the abdomen (case-C orientation II).....96

Figure V. 1. The exposure conditions. Two coil orientations (I and II) and four vertical positions: case A-exposure of the chin/neck ( $h_1 = 141.3$  cm), case B-exposure of the chest ( $h_2 = 125$  cm), case C-exposure of the abdomen ( $h_3 = 103$  cm), case D-exposure of the lower abdomen ( $h_4 = 87.7$  cm). For orientation I, the distance between the center of the coil and the surface of the clinician's body model is 21 cm, whereas, for orientation II, the distance between the edge of the coil and the surface of the clinician's body is 12 cm (as previously defined). ..... 106

Figure V. 2. Streamline distribution with 100% MSO. Exposure case B (chest) produced by circular coil 9784-00, Magstim. (a) Duke male model, (b) Ella female model..... 107

Figure V. 3. E-field map at 50% MSO for orientation II: (a) Exposure of Ella to circular coil 9784-00 in the four cases, A-B-C-D; (2) Exposure of Duke to the Circular coil 9784-00 in the four cases, A-B-C-D. The maximum color bar is set to the limit suggested by ICNIRP guidelines..... 110

Figure V. 4. Exposure to the circular coil, orientation II, in the A (chin/neck). Electric field distribution in body tissues at 100%MSO (a) Duke, (b) Ella. .... 112

Figure V. 5. Exposure to circular coil in orientation II, case B. Panel 1 refers to Duke, panel 2 refers to Ella. Distribution of the induced E-field (a)-(b) on a transversal plane at the height of the coil of Duke and Ella respectively; (c)-(d) on a transversal plane in correspondence of the chest on the plane below 4.5 cm from the surface of the coil, in Duke and Ella respectively. (e)(f) slices of tissues in the correspondence of the Duke and Ella chest respectively. .... 114

Figure V. 6. Exposure to circular coil in orientation II, case C. Panel 1 refers to Duke, panel 2 refers to Ella. Distribution of the induced E-field (a)-(b) on the transversal plane at the height of the coil of Duke and Ella respectively; (c)-(d) in a slice of the hip, below the coil; (e)(f) slices of the tissues corresponding to the hip slice. .... 115

Figure VI. 1. Blender manipulation. (a) Basic tissues- the first step, (b) reconstruction of the real shape – second step, (c) improvement region of the thoracic area obtained- improved model. ....	123
Figure VI. 2. Comparison between the anatomical female human models. (a) a panel of Ella original, with a section of tissues in 3D, sagittal and axial views, followed by the profile of the model; (b) panel of Enhanced Ella, with a section of tissues in 3D, sagittal and axial views, followed by the profile of the model respectively. ....	124
Figure VI. 3. Exposure to circular coil, orientation II: (a) exposure of the abdomen ( $h_2 = 112$ cm), the distance ( $d_0=12$ cm) was taken for both models, (b) exposure of the chest ( $h_1 = 136$ cm) with Original Ella ( $d_0 = 12$ cm), (c) exposure of chest of Enhanced Ella (in green $d_1 = 12$ cm, in purple $d_2 = 10.3$ cm, and in orange $d_3 = 8.6$ cm); (c.1) explanation of the distances in Ella Enhanced .....	126
Figure VI. 4. Induced E-field distribution at 70% MSO on sagittal planes. Exposure of abdomen, orientation II: (a) Ella slices with steps of 5 cm, (b) Enhanced Ella slices. ....	127
Figure VI. 5. Induced E-field distribution at 70% MSO on sagittal planes. Exposure of chest, orientation II: (a) Ella slices with steps of 5 cm, (b) Enhanced Ella slices at three different distances.....	129
Figure VI. 6. Comparison between Ella and Enhanced Ella , of the normalized probability of the distribution of E-field intensity ( $ E $ ) induced by TMS inside the tissues, in the case of exposure of the chest. ....	131
Figure VII. 1. The dosimetric exposure scenarios, representative of the intersubject analysis. The two coil positions are described: (a) at the height $h$ of the abdomen; (b) at the height $h$ of the chest. Both in the defined Orientation II.....	136
Figure VII. 2. Position of the coil as a function of the human height. The coil, marked with a cross, in (a) exposure of abdomen and (b) exposure of chest, in the four human models: Duke (light blue), Ella (pink), Jeduk (orange), Fats (green).....	139

Figure VII. 3. Exposure of Abdomen at 70% MSO. Induced E-Field behavior along the body of human models. Marked with cross the position of the coil.....	141
Figure VII. 4. Exposure of Chest at 70% MSO. Induced E-Field behavior along the body of human models. Marked with cross the position of the coil.....	142
Figure VII. 5. Metric dose of the percentiles of the induced E-field in the exposure of the abdomen. Comparison among the four human models. ....	144
Figure VII. 6. Metric dose of the percentiles of the induced E-field in the exposure of the chest. Comparison among the four human models.....	144
Figure VII. 7. Transverse slice, coil at height of the Abdomen at 70% MSO. Induced E-field (1), the conductivity of tissues (2), and real body tissues. ....	145
Figure VII. 8. Transverse slice, coil at height of the Chest at 70% MSO: Induced E-Field (1), the conductivity of tissues (2), and real body tissues. ....	147
Figure VII. 9. Exposure of the Chest at 70% MSO. Box-plot of the E-field in SAT, fat, skin, and breast tissues, referred to a local area of the body in front of the coil.....	148
Figure VIII.1. Exposure operator-dependent. Distribution of the induced E-field with the figure-of-eight inclined of about $55^\circ$ on the head of the patient. (a)whole body exposure on the surface, (b) focus on the limb, (c) focus on the central slice of the body. ....	160
Figure VIII. 2 Choice of the trajectories to involve in the neuron study. (a) All the trajectories present in the upper part of the body, (b) selected trajectories forming part of the body region in which we have a relevant E-field. ....	161
Figure VIII. 3 Exposure conditions. (a) Position $\alpha$ , ear of the patient facing the chest of the operator, that keeps the coil in positions with both hands, (b) Position $\beta$ , nape of the neck of the patient facing the chest of the operator, that keeps the coil in positions with both hands. Coil inclined of about $55^\circ$ . ....	162
Figure VIII. 4. Distribution of the induced E-field in the surface of the body of the Jeduc model, in the two configurations: $\alpha$ on the left and $\beta$ on the right. Maximum color bar set to the limit. ....	163

Figure VIII. 5. Distribution of the induced E-field in the surface of the body of the Yoon-Sun female model, in the two configurations: $\alpha$ on the left and $\beta$ on the right. Maximum color bar set to the limit. ....	165
Figure VIII. 6. Trajectories under test for the Titration analysis. Sensory MRG neuron of 20 $\mu\text{m}$ diameter. ....	167
Figure VIII. 7. Trajectories under test for the Titration analysis. Sensory MRG neuron of 20 $\mu\text{m}$ diameter. ....	168
Figure IX. 1 Applicator of the aesthetic device. (a) dimension of the coat of the coil, (b) an image of the interior with the scheme of the windings of the coil, (c) an example of the exposure. Image adapted by the user manual. ....	176
Figure IX. 2 Measurement chain of instrument NARDA ELT 400 .....	177
Figure IX. 3 Measurement set-up. Points of measure are chosen along the radial direction. The applicator is positioned with the active surface facing the ground on support at 80 cm from the ground. ....	180
Figure IX. 4, Measurement set-up. Points of measure are chosen along the axial direction. The applicator is positioned with the axis of the active surface perpendicular to the ground. It is also on support at 80 cm from the ground. ....	182
Figure IX. 5 Measurement setup: (a) GTEM cell; (b) Generator, amplifiers, and measurement instrument; (c) PVC cylindrical phantom with PM. ....	185

# LIST OF TABLES

---

<b>Table II- 1</b> Health effects ELVs for internal electric field strength from 1 Hz to 10 MHz Table A2 from the Directive 2013/35/EU.....	49
<b>Table II- 2</b> ICNIRP-2010 BRs for occupational exposure to time-varying electric and magnetic fields.....	49
<b>Table III - 1.</b> Features of the devices.....	65
<b>Table III - 2</b> Measured B-Field.....	66
<b>Table III - 3.</b> Measurements of B (mT) along the radial direction.....	68
<b>Table III - 4.</b> Measurements of B (mT) along the axial direction.....	68
<b>Table III - 5.</b> Features of MC125 circular coil .....	69
<b>Table III - 6.</b> Comparison of results .....	70
<b>Table III - 7.</b> Features of the coils .....	75
<b>Table IV - 1.</b> Exposure conditions.....	81
<b>Table IV - 2.</b> Orientation I - percentiles of detected induced E-field (V/m) as a function of %MSO .....	87
<b>Table IV - 3.</b> Orientation II - percentiles of detected induced E-field (V/m) as a function of %MSO .....	87
<b>Table IV - 4.</b> 99 <sup>th</sup> percentile of induced E-field (V/m) .....	91
<b>Table IV - 5.</b> Percentiles of the Induced E-field (V/m) in the operator’s hand as a function of the percentage of stimulator output .....	94
<b>Table V - 1.</b> Orientation I - percentiles of detected induced E-field (V/m) in Ella as a function of %MSO.....	108
<b>Table V - 2.</b> Orientation II - percentiles of detected induced E-field (V/m) in Ella as a function of %MSO.....	108

<b>Table V - 3.</b> Orientation II – percentiles Induced E-Field (V/m) -exposure to a circular coil .....	111
<b>Table V - 4.</b> Percentiles of the Induced E-field (V/m) in the tissues.....	113
<b>Table VI - 1.</b> Induced E-field (V/m) in the human female models.....	128
<b>Table VI - 2.</b> Induced E-field (V/m) in the human female models.....	130
<b>Table VII - 1.</b> Characteristics of the human anatomical models .....	137
<b>Table VII - 2.</b> Percentiles of the induced E-field (V/m) in the human models .....	140
<b>Table VII - 3.</b> The 99 <sup>th</sup> percentile of Induced Electric Field (V/m) for tissues of interest ...	149
<b>Table VIII - 1.</b> The 99 <sup>th</sup> percentiles of the induced E-field (V/m) in the district of the hand .....	164
<b>Table VIII - 2.</b> The 99 <sup>th</sup> percentiles of the induced E-field (V/m) in the district of the hand .....	165
<b>Table VIII - 3.</b> Results of the Titration analysis .....	169
<b>Table IX - 1.</b> AL for environmental magnetic fields at frequencies between 1Hz – 10 MHz .....	178
<b>Table IX - 2.</b> Limits for the electric, magnetic and electromagnetic fields (0 Hz – 300 GHz). From Recommendation 1999/519/EC.....	179
<b>Table IX - 3.</b> Measurements along radial direction for the I <sub>WP</sub> index.....	181
<b>Table IX - 4.</b> Measurements along axial direction for the IWP index .....	182
<b>Table IX - 5.</b> Measured values of the unperturbed E-field and produced Power.....	186



# ABSTRACT

---

The assessment of the risk from occupational exposure to electromagnetic fields (EMF) has attracted the attention of those involved in safety in the workplace, in particular after the updating of European legislation, with the publication for EMFs, of Directive 2013/35/EU<sup>1</sup> of the European Parliament and of the Council, which made the risk assessment mandatory for this type of physical agents. The issue is made even more relevant by the proliferation of industrial and health applications using EMF even of considerable intensity. However, the rapid technological development has not always been accompanied by adequate growth in the culture of prevention and safety. Many devices expose both operators and persons of the general public to significant risks, but often, these risks are not adequately reported by the manufacturer, nor mentioned in the instruction manual, as would be expressly required by the harmonized standards.

In this general framework is placed this Ph.D. research project, whose aim is to analyze possible conditions of risk in the workplace, considering only the environment where the EMF sources potentially expose the operator to risk. The research project involves a joint collaboration between two Institutions: the National Institute for Insurance against Accidents at Work - INAIL and of course Sapienza University of Rome.

The project is developed in a multidisciplinary manner, providing experimental and numerical investigations to achieve the required goals, also considering the literature review and comparison for a more realistic analysis of the risk, in terms of human exposure to EMF. The work is based on a multiphysics approach to obtain a complete evaluation of the risk in the workplace, with the prospective to improve the current approach in the assessment of the risk and eventually suggest some indications to the operator for better use of the device under test.

Therefore, the starting point has been a review of the workplaces to identify any gaps and critical issues in relation to the risk assessment and therefore for which it is considered

necessary to deepen the protectionist issues. A literature analysis of the state of the art on the risk in the workplace is first carried out.

This has been followed by numerical and accurate modeling of the device under test as well as the workers in a real reproduced work condition of exposure. Of paramount importance is the understanding of all the parameters that can affect the distribution of the induced EM quantities, which are essential for the risk assessment and the verification of compliance with the regulations system. To do this, it was necessary to study human exposure in-depth, also using different human body models available for dosimetric analysis on dedicated software.

All the research has traveled on two parallel tracks, on the one hand, the need to fill the scientific gaps in the research area of exposure assessment of workers and on the other one to take into account the regulatory aspects, essential for a correct evaluation of professional exposure. Therefore, as a last step of the overall work, a possible new protocol of risk assessment analysis is proposed to move forward on the improvement of safety and security in the workplace.



# INTRODUCTION AND PURPOSE OF THE RESEARCH

---

The rapid development of technology has not always been accompanied by the growth of a culture of prevention and safety: many equipment based on the use of EMF expose to important risks, especially for employees directly involved in the use of those devices, which require the presence of the operator near the source, as in the case of the use of welding machines, electrosurgery, transcranial magnetic stimulators, magnetic resonance imaging, etc. As a result, it follows that the number of workers exposed to EMF is really huge and thus it's likely that a possible relevant occupational health risk exists for the vast majority of occupationally exposed operators<sup>2</sup>. On a general scale, we can consider that, whenever electric and/or magnetic fields or currents are used, EMF are generated, thus all workers could be potentially exposed, albeit differently depending on the class of the equipment. For most workers, the field strength is of a level that does not cause harmful effects, but in some work environments, the field strength may nevertheless present a risk. According to this premise, the importance of an assessment of the risk from exposure in the workplace is clear and becomes even more important depending on the type of source that is used. Although the focus on health and safety in the workplace is currently a highly important issue, accompanied by legislation to reduce risks and improve health in the workplace, there are circumstances in which not all safety aspects have been investigated or investigated appropriately.

It should be noted, in fact, that while in the industrial field, the technical regulations have already addressed some aspects related to operator exposure with reference to the most widespread equipment such as for example the various families of welding machines, in the electromedical sector, if we exclude the case of Magnetic Resonance Imaging (MRI), the international technical regulations have not yet addressed this aspect, limiting themselves to setting only the requirements related to electrical safety and electromagnetic (EM)

compatibility. Considering welding machines for example, a fairly complete regulatory framework exists, consisting of a product standard (EN 62822-1<sup>3</sup>) and for the case of arc welding machines a second standard (EN 62822-2<sup>4</sup>) both published in 2008<sup>5,6</sup> and updated in 2016 and 2018 respectively. EN 62822-1 and even more so EN 62822-2 set out the procedures that individually address the various aspects of exposure assessment and thus provide all the indications regarding the standardization of the exposure scenario and the measurement procedure. On the other hand, regarding MRI, for example, countless documents relating to risk assessment are made available, also in the Italian national framework. This is because the exposure of workers to MRI presents several critical issues, both related to occupational exposures to static magnetic fields, (the movement of the operator inside the magnet room) and related to variable fields (gradient and radiofrequency fields), without neglecting the complexity of the systems and technology used, particularly in superconducting magnets. Therefore, the approach to risk assessment in MRI is one of the most operationally relevant from a safety point of view and most explored. The Section for Technical Support to the National Health System on Radiation of the Department of Medicine, Epidemiology, Occupational and Environmental Hygiene of INAIL is the national supervisory authority on installations that use magnetic resonance tomography for clinical purposes, and it is because of this role, with a total of more than 2000 inspections carried out, that it has contributed decisively to the standardization of risk assessment approaches for this specific field. In addition, there are several international publications on the exposure of workers in MRI<sup>7,8</sup>. Both of the previously described apparatuses are extensively dealt with in the Non-Binding Guide to Good Practice<sup>9</sup>, where it is also possible to find other assessment methods for certain apparatuses more generally used in both medical and industrial practice.

For the Transcranial Magnetic Stimulator (TMS), conversely, it is known that to date, there aren't International Electrotechnical Commission (IEC) particular standards<sup>10</sup>, and in fact observing the user manuals of the instrument, in the section concerning the *construction in conformity*, the only reference is made to the general standard on electrical safety and to the collateral one concerning electromagnetic compatibility<sup>11,12</sup>, while there is nothing on how

to carry out a risk assessment or how to use the instrument safely. This means a gap in the standardization of the products, thus resulting in great variability in the design and realization requirements of the instrumentation adopted by different countries. Further, during the TMS treatments, the clinician is typically very close to the EM source, since he/she keeps in position the device over the head of the patient. It is also important to observe, that during the work shift, the operator could be exposed to the source for several hours, and this can happen for several days during the week and for some months, since this is usually the protocol for treatment.

Based on these assumptions, among all the equipment that causes potential risk for the workers, in this work we have chosen to analyze the exposure of the working operator to the variable magnetic field produced by various kinds of TMS, since for this specific source we have found a lack both in the scientific literature and in the regulatory system. What has been done in this study is, first, to reconstruct the real working conditions of the operator, during clinical treatments with TMS, to provide a classification of all the possible conditions of exposure based on realistic scenarios. Successively, since at frequencies lower than 10 MHz, international guidelines and standards adopt the electric field induced in the body as the measure for limiting human exposure to EM fields, and in the case of realistic exposure scenarios, such induced field can only be estimated using computational methods combined with anatomically realistic body models, numerical dosimetry techniques typical of low frequency (LF) applications have been applied to the evaluation of exposure to the TMS.

LF numerical dosimetry needs to be adopted taking care of different issues as: i) possible numerical errors; ii) electric properties of tissues; iii) differences in human body models; iv) estimation of neuronal stimulation threshold.

Regarding estimated electric fields, they can be affected by various sources of error and uncertainty. To account for numerical errors, ICNIRP<sup>13,14</sup> recommends calculating the 99<sup>th</sup> percentile of the induced electric field, which discards the highest 1% of induced electric field values. Nevertheless, it is demonstrated that the 99<sup>th</sup> percentile can produce a large

underestimation of the highest electric field, for localized exposure<sup>15,16</sup>. Therefore, in these cases, it is suggested to also use percentiles higher than the 99<sup>th</sup>, like the 99.9<sup>th</sup> and 99.99<sup>th</sup>.

Considering electrical properties of tissues, in particular conductivity values, in Laksoo et al. 2020<sup>17</sup>, two comparative simulations were performed using the human NORMAN model<sup>18</sup> exposed to uniform magnetic fields to illustrate the effect of tissue conductivity on the induced electric field. Two different sets of tissue conductivity values were used. Set 1 was obtained from Dimbylow's study<sup>18</sup> and set 2 was obtained from a widely used tissue property database from the IT'IS Foundation (Zurich, Switzerland)<sup>19</sup>. The results, related to the brain, show that Set 2 (higher brain conductivity) produced a significantly weaker electric field strength than Set 1 (lower brain conductivity). Therefore, we can understand from these results that uncertainty in tissue properties can have a strong impact on the induced electric fields.

Regarding the anatomical differences between subjects, a study by Aga et al. 2018<sup>20</sup> considered the variability of the induced electric field between anatomical models. The comparison between five adult models and one child model showed relatively significant differences between them. For example, there was a 40% difference in the lowest and highest electric field values induced in the brains of the adult models<sup>20</sup>. Similarly, earlier work on two adults and six children (5-14 years) suggested similar or larger differences<sup>21</sup>. But, in both studies, the number of subjects was inadequate to draw definitive conclusions. Nonetheless, it seems clear that larger body size tends to produce higher induced electric field strengths due to Faraday's law of induction, but too few data currently exist to assess variability due to other anatomical factors, precisely because human variability from an induced electric field analysis perspective is not a sufficiently thorough issue to date.

Finally, another important aspect related to the induced electric field are the stimulation thresholds. To this regard, the study of Soldati et al. 2018<sup>22</sup>, indicated that the order of magnitude of the stimulation thresholds obtained using empirical models of nerve fibers was consistent with the value of the calculated electric field. Therefore, we can consider using the computational method to study the correlation between stimulation thresholds and the induced electric field in human models.

The main purpose of the present research study is focused within this scientific context. Thus, in Section I of the work, we want to give a general overview of the occupational exposure, placing it in the current regulatory framework, considering the International Commission on Non-Ionizing Radiation Protection guidelines, the European Directive, and technical reference documents. Successively, a focus is given to the EM source under test, the TMS coil, which based on our studies, needs further information about the risk associated with its use. Thus, it has been necessary to characterize the model of the source using a numerical approach and also considering experimental data and literature comparison.

In Section II, by means of a review of all the possible scenarios that may occur during a TMS treatment, a thorough numerical dosimetry analysis is carried out, with the aim to reproduce the real work conditions of the exposure for clinicians using this device and to provide a classification of all the possible exposure conditions. It has been particularly important to study all the variables that can play a decisive role in the risk assessment of TMS treatment, trying to bring new knowledge in the field of safety, and also providing new indications and/or suggestions that can make the worker more aware of the risk. Therefore, the numerical assessment of risk has been based on the human male model Duke<sup>23</sup> (Virtual population of Sim4Life software), which represents in this context the model of a generic medical operator performing the treatments. Then a successive step was to reproduce the same exposure conditions with a model of a female operator, with the idea of evaluating possible differences in exposure and thus a specificity of the behavior to be assumed during the treatment in order to reduce the risk (gender-dependent risk assessment).

Based on the results obtained in Section II, the importance of the anatomical characteristics of the operator (physical conformation, height, robustness, etc.) emerged, and therefore in Section III an improvement of the female model is performed as well as a complete and exhaustive analysis based on an inter-subject variability: an innovative approach in the field of risk assessment for workers. Several human anatomical models have been considered in different exposure conditions. This analysis includes a study of the dielectric properties of



tissues, as well as the tissues distribution in the human apparatus, and their role in the exposure. All the analyses provided have led to results that could be useful on one hand for greater awareness of the risk in exposure for the TMS operators, on the other hand for an improvement in safety in the workplace where this kind of medical treatment is used, and for a possible protocol of future risk assessment, since to date, no one is currently available.

Moreover, to link the numerical dosimetric assessment with physiological induced effects due to the EM exposure, in Section III we also evaluated the aspect of the sensory effects and therefore the possible stimuli (sensory or muscular) that an operator can experience during the use of TMS, if even locally (for example in the hand), the exposure limits identified by the guidelines are exceeded (overexposure condition).

Finally, Section IV provides an overview of the mission of the National Institute for Insurance against Accidents at Work (INAIL) Research Center. This is because, the Ph.D. research project is a study mutually conducted by the Department of Information Engineering, Electronics and Telecommunications – DIET of the Sapienza University of Rome, and the Department of Medicine, Epidemiology, Occupational and Environmental Hygiene DiMEILA of INAIL.



**SECTION I. EMF APPLICATIONS:  
OCCUPATIONAL EXPOSURE AND  
LEGISLATIVE**

---



# I. CHAPTER

---

## 1.1. State of art: an overview of occupational exposure in the work environment

EMFs are produced by a wide variety of sources to which workers can be exposed in the workplace. The EMFs are generated and used in many work activities, for example for manufacturing processes, research, communications, medical applications, power generation, transmission and distribution, broadcasting, sea and air navigation, safety area, and so on. EM fields can also be incidental, such as fields generated near electrical energy distribution cables inside buildings, or due to the use of electrical equipment and devices. However, it may happen that, since most fields are electrically generated, they disappear when the power supply is turned off<sup>2</sup>.

As before mentioned, important exposure scenarios can occur both in the industrial application area as well as in the medical field and in these workplaces, there are several tools that currently attract attention due to their risk of exposing workers to excessive levels of radiation (i.e., overexposure condition). For example, in industrial applications, we can consider the exposure caused by the welding machines (Figure I.1 (a)), for which the potential for exposures above the limits for health effects and the intrinsic difficulty of bringing these exposures below the regulatory limits relating to the induced quantities without having to incur in excessive costs is well known.

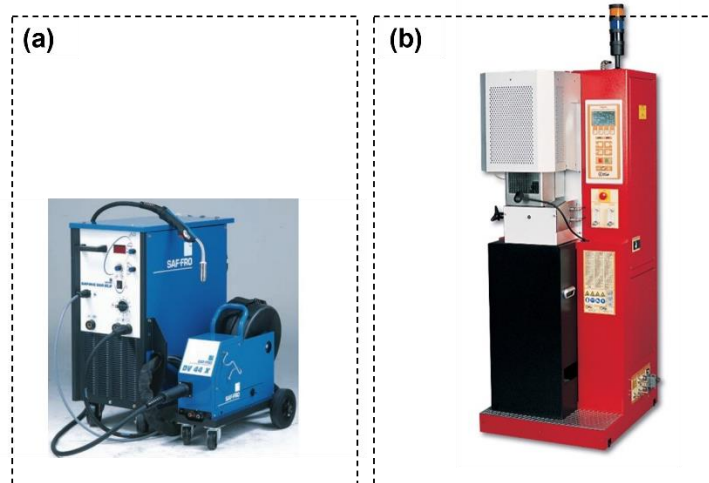


Figure I. 1 (a) Welding Machine<sup>24</sup>; (b) Industrial induction oven, 30 kHz - 24kW,

The signal emitted by the welding machines is impulsive with spectral components up to frequencies of the order of a few hundred kHz, but it is not the only signal that can cause a significant exposure of the operator since in correspondence to the electric arc (in the case of arc welding machines) there are field peaks due to the transients of the quantities (current and voltage); this field corresponding to the trigger of the arc could cause the greatest peaks of exposure. Typically the rated operating current ranges from hundreds of Amperes up to kA<sup>9</sup>. Welding machine operators usually stand or sit near the machines during welding, and their hands are as close as possible to the machines. When using a spot bench welding machine and a continuous welding machine, the operator holds the material to be welded, and therefore the hands may be near the welding electrodes. It follows that in the vicinity of the torch the operator is subjected to fields that exceed the relevant regulatory limits<sup>25</sup>, as it happens when the subject stops near the cable, or worse, for reasons of convenience, wraps the cable of the welding machine on the shoulder. Another apparatus of particular importance in terms of human safety could be the industrial induction oven (Figure I.1 (b))<sup>26</sup>. In this case, the power is of the order of tens of kW and the working frequency is of the order of a few dozen kHz. For these types of equipment, a further detailed risk assessment is required, allowing operators to work safely. It is found that within 25 cm from the source the regulatory levels are exceeded, therefore the apparatus requires usage indications, for the safety of the operators<sup>24</sup>.

Conversely, considering the medical area, different working conditions could lead to an overexposure of the operator, among these we could mention as an example the electrosurgery (Figure I.2 (a)), and the magnetic resonance imaging technology (Figure I.2(b)).

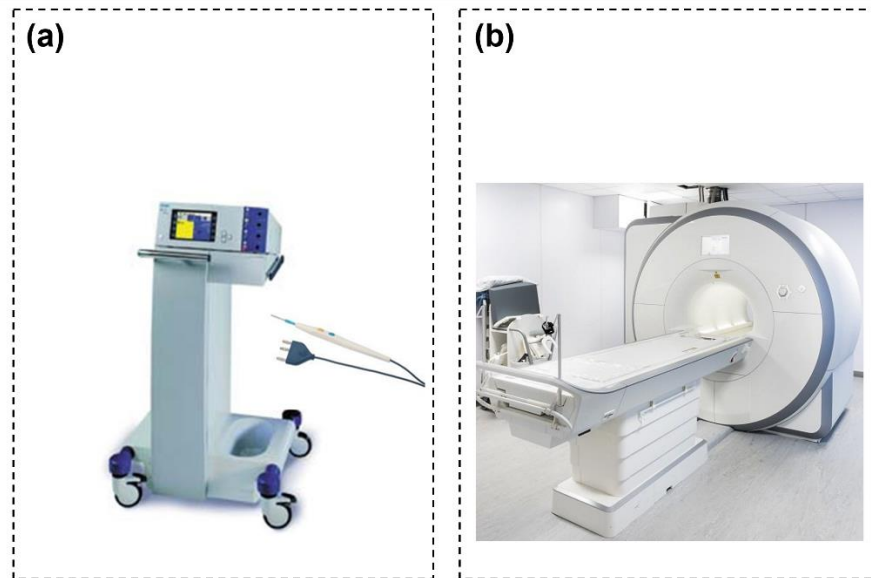


Figure I. 2.(a) Electrosurgical unit <sup>24</sup>;(b) MRI, figure adapted from Siemens Corporation website

The first is an instrument typically used in surgery and which obviously requires the operator to hold it during its operation. Electrosurgical units are widely used in health practices. Applying a sinusoidal or pulsed voltage in the frequency range of 0.3 - 5 MHz at the tip of the electrode, the desired mixture of coagulation and cutting is obtained. Due to the high voltage and current in the cable, strong electromagnetic fields appear near the electrosurgical units. The surgeon and others within the operating room such as nurses, anesthesiologists, etc., will be highly exposed to these fields. Therefore, healthcare workers could be exposed to the field so high that they exceed the limits<sup>27,28</sup>. All electrosurgery provides the surgeon with two basic operating modes: cutting and coagulation. In the cutting mode, the waveform of the working current is approximately sinusoidal (with a frequency of the order of hundreds kHz), the voltage applied to the handpiece is usually between 0.5 and 2 kV peak, and in some models even 3 kV peak and finally the current up to one or a few amperes. In the coagulation mode, the waveform is more complex and

consists of pulses or trains of damped sinusoids, this mode corresponds to the situation in which the voltage applied to the blade is maximum (up to values even above 5 kV peak in some models). The handpiece with its blade and the conductors that connect it to the generator are the main elements that disperse EMF in the surrounding environment. In this case, the exposure reduction measures that are suggested for example are the shielding of the supply cable, keeping it as short as possible, and suspending it instead of letting it rest on the body. Further, keeping distance and reducing exposure time are general organizational measurements to reduce the level of exposure.

The second equipment is the RMI. As beforementioned, it exposes the workers to different sources of risk, which are: the static magnetic field (and in particular the movement in the static magnetic field), the variable EMF due to the radiofrequency- RF gradient field, the superconducting magnets, and also all transverse risks related to the use of the machine (e.g., the presence of cryogenic fluids in superconducting magnet resonances and so on). For these reasons, as explained above, MRI in healthcare is one of the most operationally relevant aspects from a safety point of view. It is no coincidence, in fact, that the risk assessment of MRI equipment is extensively investigated in order to provide all the information necessary for risk reduction.

However, many other working conditions could expose workers to intense sources of EMF, causing the overcoming regulatory limits. Along with those just described, the diathermy device, certainly deserve to be mentioned in the healthcare field, while in the industrial one, we can think of demagnetizers (mechanical workshops), cells for electrolysis, and also both electrical substations and telecommunications sites, which are identified as critical environments for occupational exposure to EMFs. In fact, the limits established for 50 Hz electric fields (E-fields) can be exceeded in the 400 kV electrical substations where workers are usually present<sup>29</sup>, while limits for radiofrequency fields can be exceeded, at telecommunications sites, in areas accessible to workers near the antennas<sup>30</sup>. In this regard, it is also important to point out that to date, for the prevention and early diagnosis of the effects related to electromagnetic fields in exposed workers, no guidelines are available and only a few indications can be found mainly related to overexposure situations<sup>31,32,33</sup>.



However, at the same time, general technical and organizational preventive measures are widely recognized, including the individual protections to be adopted in the workplace and the risk assessment practices to be followed<sup>2</sup>. Providing adequate information to workers about the risk, the exposure levels, and the EMF-related effects, including the conditions possibly inducing a particular susceptibility, is also a fundamental part of appropriate prevention for EMF-exposed workers.

In these cases, just exposed, the physical quantities to which referring when considering the possibility that there may be an overcoming of the regulatory limits, are clearly both the environmental ones, that is, obtainable by radiometric measurements, but also the induced quantities. This latter occurs, in all those cases in which the operator is extremely close to the source, such as the clinician holding the source in his hand (as in the cases of electrosurgery or TMS), the exposure itself cannot be evaluated with radiometric methods (i.e. with measurements of the electric and magnetic field in the environment), but it is necessary instead to resort to dosimetric methods (i.e. the numerical calculation of the E-field induced inside the human tissues) based on specific modeling of the exposure environment. This concept is expressed in the ICNIRP-2010 guidelines<sup>13</sup>, where it is stated: “for a very localized source with a distance of a few centimeters from the body, the only realistic option for the exposure assessment is to determine dosimetrically the induced E-field, case by case”, and is also reiterated in the European Directive<sup>1</sup>.

Actually, this exposure condition exactly occurs with the TMS (Figure I.3), that is another important equipment that needs to be taken into account in the medical area, since it could cause a possible overexposure of the worker.



Figure I. 3. TMS device, figure adapted from PAF website<sup>24</sup>

This device is widely used in the clinical practice, both for the diagnosis and for the treatment of several diseases. This instrument operates at frequencies between 1-3 kHz, generating variable magnetic induction fields that can reach up to 3 T. The criticalities of this instrument are actually due to the need of the operator to hold the device with his hands, which for its functionality, must be held in place on the patient's head. This configuration of operation implies exposure of both the limbs and the whole body of the clinician, that during the treatment typically remains close to the patient. Although the use of this device is well-established in medical practice, unlike, for example, MRI, it is by no means accompanied by adequate literature dealing with the critical issues, nor are there any product standards in the (national and international) regulatory framework (as there are for the welding machines) that deal with the issue of risk assessment. For these reasons, this tool is among those that need more in-depth study, precisely in order to increase safety for the clinician. Obviously, the first measure to reduce exposure is certainly to increase the distance from the device, but in most cases, the working conditions do not always allow it, therefore a specific analysis should be carried out.

Finally, we can conclude that there are also many other equipments in workplaces that produce such low EMFs that they are identified as conforming "a priori". They do not even exceed the limits set for the general public (well below those set for workers)<sup>34</sup>. These include, for example, computers and computer equipment, such as electric fans, fixed telephones, photocopiers, and so on. For all this equipment, it is not necessary to carry out a risk assessment for exposure to EMFs.

## 1.2. The EM source of interest: Transcranial Magnetic Stimulation (TMS)

TMS device consists of a signal generation system and a maniple that must be positioned appropriately on the patient's head.

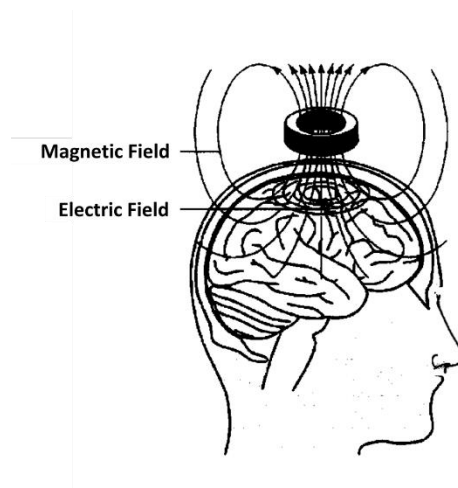


Figure I. 4. Operating principle of the TMS device during the treatment.

This maniple consists of a coil crossed by current, which generates a variable magnetic induction field in the surrounding space, as can be seen in Figure I.4. The mode of use of TMS requires that the operator to remain close to the patient, in order to keep the coil in place on the patient's head during treatment. Therefore, because the TMS magnetic field spreads in the space around the stimulating coil<sup>35</sup>, the clinician also undergoes an undesired exposure several times a day during treatments. In clinical practice, different relative positions between the patient and the clinician can be assumed, causing the local exposure of different body parts of the operator, depending on the specific therapy. Furthermore, since the operator handles the device, he/she may hold a part of the coil with the hand or both hands, while the device is active, for example, to increase the coil's stability, and so this could produce an induced E-field in a part of the body rich in peripheral nerve innervation (the median, ulnar and radial nerves). From these assumptions and considering the exposure not to be underestimated, it is clear the need to carry out further analyses regarding the safety of the operator. The risk assessment for occupational exposure to TMS

has not been adequately addressed in the scientific literature, where safe distances between the coil and the operator are suggested, derived from considerations that lack of in-depth analysis on this topic<sup>36,37</sup>. For example, a study focused on the exposure of TMS workers was conducted in 2006 by Karlström et al., and they experimentally estimated a distance of 70 cm to avoid overexposure to magnetic pulses, as recommended by the ICNIRP Guidelines in 2003<sup>38</sup>. For several years, this work remained the only one addressing the problem of occupational exposure during TMS treatments; therefore, it was considered a reference in the Safety Guidelines for the use of TMS proposed in 2009<sup>39</sup> by a group of TMS experts. Since the publication of these results, the ICNIRP 2003 guidelines and Directive 2004/40/EC have been update<sup>1,40,41</sup>; however, to date, there are no standardized requirements for the conformity assessment of TMS<sup>10</sup>, consequently, there is great variability in the adopted methodologies. Moreover, since to date, there is neither a specific product compliant to the standard nor a procedure for assessing conformity to the limits, the state of art leaves space for a wide variety of analysis methods, which could obviously lead to different results. Thus, the need for a particular international standard concerning TMS devices that could improve safety in work environments has increased in recent years.

The present work, therefore, aims to be a possible starting point for the creation of ad hoc protocols for risk assessment, and on the other hand, it wants to be able to deepen the theme of workers' exposure by filling those shortcomings that have been found in the literature.

Few studies have been performed over the last decade to address this topic. Particularly, two studies conducted in 2010<sup>42</sup> and 2016<sup>43</sup> numerically investigated the exposure of workers to TMS systems, finding safety distances of 110 cm and 40 cm, respectively. Despite having the same objective, these two studies considered different human body models (Brooks Air Force Laboratory (BAFL)<sup>42,44</sup> and Virtual Population<sup>23,45</sup>) and different exposure conditions (TMS feeding equal to 7.7 kA at 3.6 kHz in Lu et al., 2010<sup>42</sup> and 5.6 kA at 3.45 kHz in Bottauscio et al., 2016<sup>43</sup>). Furthermore, Lu et al., 2010<sup>42</sup> investigated two coil geometries (i.e. circular and figure-of-eight) for different orientations, but the clinician body was limited to one vertical position, whereas Bottauscio et al., 2016<sup>43</sup> studied only the circular coil for

different orientations and vertical positions. However, an in-depth investigation of the exposure should account for the specificity of TMS devices, in terms of coil geometry and feeding system, and examine the exposure as a function of the device's stimulator output, since each output depends on the treatment, which needs of a different setup because of the specificity of the disease that must be treated. This is an important aspect because the stimulation intensity in clinical practice is always related to the resting motor threshold of the patient, and it is usually below the maximum output available from the machine<sup>46,47</sup>. Furthermore, many different coil positions and orientations should be considered because clinicians may hold the coil at different heights concerning their trunk, depending on the patient-holder support (bed, chair, or recliner), the sort of patient (tall, in pediatric age, uncooperative), based on the bodily characteristics of the operators themselves, and finally they may rotate the coil to optimize the treatment. Such analysis would allow the investigation of the exposure of specific body parts and resulting in detection of the worst-case scenario. Previous studies have only partially considered these aspects by analyzing one or the other<sup>42,43</sup> or even nothing (as the variability of the maximum stimulator output-MSO). Another important aspect is the position of the operator's arm and hand while holding the coil, as this area is inevitably exposed to higher intensities<sup>48,49</sup>. Determining the entity of the exposure in this district is of primary importance since this is the first part of the body directly exposed to the source and based on the type of treatment never can be moved off. In this direction can be considered the study of A. De Leo et al. 2014<sup>50</sup>, which addressed the possibility of reduction of the exposure of the operator using the presence of a tile of ferrite on the surface of the coil. The presence of this layer on the device effectively reduces the exposure in the operator side, but at the same time, causes a reduction in the pulse that is less enhanced in the patient region. Further, these results are strongly dependent on the model of the coil under test. Therefore, the possibility to cover the coil with a tile is probably not the right way to solve the problem. This is because it would mean making a specific change directly in the manufacture of the TMS coil by the manufacturer since the same tile cannot be used on all types of coils and for all available treatments. Therefore, an aspect that needs to be addressed is the possibility of the biological effect in

the hands of the clinician. This could mean the perception of skin disorders or tingling sensations, therefore transient sensory effects. Even worse it could be muscle stimulation effects if the fields reach high values. In the literature, no study has been found that analyzed these aspects, neither locally (hand or otherwise) nor whole-body, therefore this aspect of nerve stimulation is also evaluated in this work.

Finally, another important consideration is related to the way that exposure is dependent on the human body conformation of the operator who is performing the treatment. In this sense, the aim is to carry out an assessment analysis of the induced electric field that is dependent on the body characteristics of the operator. This means carrying out an exposure assessment, taking into account that the induced quantities may operator - dependent (tall, short, slim, overweight, and so on). The impact of human variability on risk assessment is largely unexplored to date; typically when the variability was addressed in the occupational field, it regarded not the influence that the properties of the tissues could have in the distribution of the electric field inside the human body, but only the differences in sensitivity of the subjects and the inter-individual variations in populations' response to the EMF<sup>51</sup>. Typically scientific research deepens the study of how the sensitivity<sup>52</sup> and human variability influence the estimated thresholds<sup>53</sup> for effects and dose-response relationships, thus for the quantitative risk assessment. In the frame of the risk assessment, a recent study by Hirata and co-workers<sup>54</sup> addressed the topic of the importance to use accurate human body models jointly to the right dielectric properties, highlighting the necessity to carry out an accurate measurement of dielectric human tissue properties for evaluating the induced field strength. However, the paper aimed to make review of the most up to date dosimetric studies (considering human body modeling and tissue dielectric properties) and to analyze the standardization process for compliance of certain products based on exposure standards such as human safety in wireless energy transfer (WPT). It does not conduct a comparative study on how the body anatomy could influence the induced E-field. Conversely, a study conducted by S. Gallucci et al. 2022<sup>55</sup> shows that a difference in terms of exposure-response exists due to gender. In this study, a numerical assessment of the risk of human exposure to RF-EMFs emitted by a wearable antenna is

performed. Results showed how the value of SAR depends on gender, which means that the anatomy models could impact the exposure level.

To conclude, the present study aims to perform a comprehensive analysis that investigates TMS operator exposure in the low frequency range, considering all the variables that could influence the entity of the exposure, as above mentioned, in order to suggest safer general working instructions for clinicians and eventually suggest a protocol for the risk assessment for this device.

### 1.3. TMS device: physical principle, device models, and applications.

TMS is a neurostimulation and neuromodulation technique developed in the early 80's<sup>56</sup> and it is used as a neuro-investigation and diagnostic tool<sup>57</sup>, as well as in clinical practice for therapeutic purposes<sup>58</sup>. When applied over the cerebral cortex, TMS can interfere with neuronal connections, providing important insights in the field of brain connectivity, particularly relevant for brain mapping applications<sup>59,60</sup> or for diagnosing neurodegenerative diseases<sup>61</sup>. Furthermore, because it is non-invasive and minimally painful, it is currently being investigated as a potential treatment for several psychological disorders, including major depression<sup>62</sup> and obsessive-compulsive disorders<sup>63</sup>, for both of which it received FDA approval; neurological impairments due to stroke<sup>64</sup>, Parkinson's<sup>65</sup>, tinnitus<sup>66</sup>, epilepsy<sup>67</sup>, chronic pain<sup>68</sup>, and Spinal Injury<sup>69</sup>. The main advantage, that makes this instrument particularly appreciated, is the reduced scalp pain sensation for the patients, compared to the electrical stimulation<sup>69</sup>. This device was created for use in diagnostic and experimental applications for humans, therefore many studies have been conducted on healthy volunteers to allow doctors to interact directly with the neuronal activity in progress and understand its importance for a given task at particular times, as well as to understand that TMS stimulation may be able to improve the brain's natural ability to adapt to damage and recover lost performance<sup>70</sup>. TMS is based on the principle of electromagnetic (EM) induction, where a time-varying current flowing inside a conductive wire produces a time-

varying magnetic field that is responsible for secondary currents induced inside the cerebral tissue<sup>57</sup> of the patient under treatment. Additionally, owing to the conductive properties of the patient's head tissue, it induces an intense E-field (i.e., of the order of 100 V/m) that alters the brain neuronal activity<sup>57,71</sup>, achieving the desired clinical or experimental response. Depending on the intensity of the stimulation and on the position and type of stimulating coil, such induced E-field can depolarize superficial axons and activate neural networks in the cortex<sup>72</sup>. Thus, during TMS applications, the stimulating coil placed over the patient's head generates a high-intensity pulsed magnetic field, up to 3 T, that crosses the scalp. The path and strength of an electrical field generated in the brain by TMS depend on many physical and biological parameters such as magnetic pulse waveform; shape and orientation of the coil, intensity, frequency, and pattern of stimulation, the orientation of the current lines induced in the brain and excitable neural elements. TMS can deliver two different waveforms of the magnetic pulse, that are monophasic pulses and biphasic pulses<sup>73</sup>. Monophasic magnetic pulses are commonly used for single-pulse experiments, whereas biphasic stimulus waveforms are usually required in rTMS (repetitive TMS) experiments because of the lower energy requirements<sup>74,75</sup>. Studies regarding the single-pulse treatment demonstrated that they are different in the effectiveness of these sorts of waveforms, from a clinical point of view. It is known that, for a given initial amplitude of the stimulation pulse, biphasic stimulation is more powerful than monophasic stimulation<sup>73,76</sup>. Less is known about the differences between monophasic and biphasic repetitive TMS (rTMS), being a more complex mechanism often linked to moderate interindividual variability<sup>77</sup>. Although it is necessary to understand the mechanism behind this device, to have a whole overview of clinical applications and its functionality and to consider what happens in the patient's brain tissues and study the mechanism of nerve stimulation caused by the TMS pulse, it is beyond the scope of this study. Conversely, is paramount to consider that there are different shapes of the coil used for clinical practice. The model of the coils is relevant since the geometry has an impact on the produced variable magnetic field. Many types of coils have been developed with different geometries and sizes, including the circular coil



(Figure I.5 (a)), figure-of-eight (Figure I.5 (b)), double-cone, air-cooled coil, and more recently Hesed coil, the C-Core, and circular crown<sup>78,79</sup>.

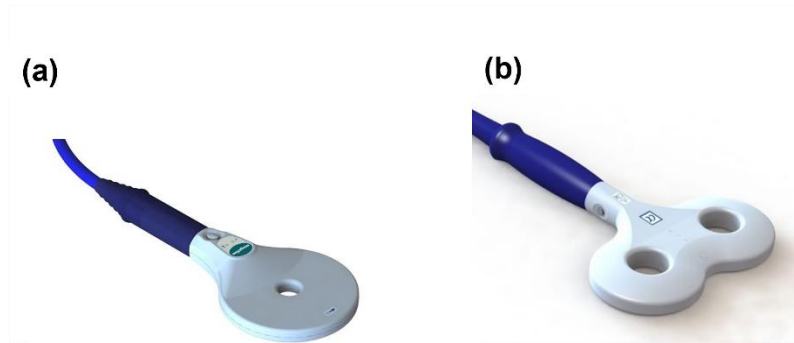


Figure I. 5 Models of coil: (a) circular and (b) figure of eight. Images adapted from the Magstim website.

Going by order, the circular coils typically have a diameter that ranges from 80 mm to 150 mm<sup>80</sup> and can generate a spherical magnetic field perpendicular to the coil itself, such to induce an E-field that would have its minimum below the center of the coil and maximum below its perimeter, potentially stimulating a ring-shaped area of the brain, therefore, lacking in spatial selectivity<sup>81,82</sup>. Thus the currents induced by circular coils widely spread under the windings and activate superficial cortical layers and, for this reason, circular coils are rarely used to investigate TMS clinical effects, while they are still considered for investigational purposes<sup>83,84</sup>. The figure-of-eight coil, first proposed in 1988<sup>85</sup>, provides to enhance the focality of the circular coil. It consists of copper wires continuously wound to create two connected circular coils, with currents owing in opposite directions, so the E-field is at its maximum under its center (hot spot), where the two rings meet. Such geometrical composition allows for to maximization of the E-field at the center of the coil, increasing the focality for a more accurately defined area<sup>86,87</sup>. For both these types of coils, the induced E-field remains confined in the superficial cortical area, therefore for deep stimulation, a solution could be the E-field of double-cone coils (Figure I.6), which can reach deep cortical layers. It consists of a figure-of-eight with the two wings bent closer together, typically forming an angle of 120°.



*Figure I. 6. Double-cone coil, from Magstim website*

Nevertheless, the disadvantage of the double cone coil is the loss of focality<sup>88</sup>. Following, we find the air-cooled coil, which can be a figure-of-eight as well as a circular coil, equipped with a cooler system, which is a fan. This latter transports the heat away from the coil and thus allows a much longer stimulation time than, for example, a non-cooled stimulation coil. Then, a better compromise between depth and focus may be obtained with new types of coils that allow a lesser rate of decrease of field magnitude as a function of distance, such as the Hersed-coil (H-coil), C-core coil, and circular crown-coil. The Hersed coil<sup>79</sup> with a complex three-dimensional windings pattern enables effective stimulation of deep brain regions without inducing an unbearable field in cortical regions<sup>89</sup>. The C-Core is a coil with a ferromagnetic core with a wide opening angle that generates a figure-of-eight shaped E-field and has a depth–focality ratio commensurate with figure-of-eight coils, whereas the crown coil is a large circular coil wound around the perimeter of the head like a crown. All the coils exposed are reported in Figure I. 7.

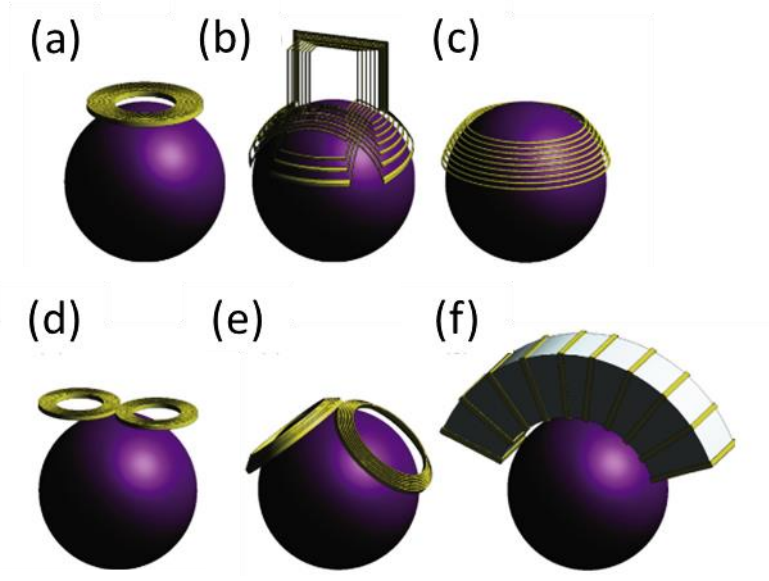


Figure I. 7 Commercial coils for clinical treatments: (a) Circular coil, (b) Heschl coil, (c) Crown coil, (d) Figure-of-eight coil, (e) Double cone coil, and (f) C-core coil. Image adapted from Zhi-De Deng et al. 2013<sup>90</sup>.

Among these coils, the two most usually used in TMS treatment are the circular and the figure-of-eight coils, both constructed from wound copper wire, properly insulated, and placed in a plastic case. Today, the figure-of-eight coil is one of the most extensively used in TMS studies for both investigational and therapeutic purposes. Therefore, this study will be analyzed these two shapes of coils (circular and figure-of-eight), since the aim is to reproduce the real exposure conditions, using the most usual devices that we can find in clinical practice.

## II. CHAPTER

---

### 2.1 Reference legislation: Directive and technical standards

In a working environment where there are EM sources, in the context of risk assessment two important steps must be considered. The first is to identify which workers are professionally exposed to EMF. They are considered as such, those who for their specific work activity, are exposed to electric, magnetic, and electromagnetic fields, and therefore, for them occupational limits, established by the legislation, will apply. The second step is to identify those who carry out an activity for which exposure to electromagnetic fields is not foreseen, they must be considered a "general population", and for them, the levels reported in the guidelines of the International Commission on Non-Ionizing Radiation Protection (ICNIRP) 1998<sup>91</sup>, relating to the population exposure, will have to be respected. At this point, having identified the type of subjects exposed, it is necessary to identify the sources present in the workplace. In this phase, the EN 50499<sup>34</sup> standard "Procedure for the assessment of workers exposed to electromagnetic fields" is of fundamental importance, it provides for the first phase of the intervention, called initial assessment, which basically consists of a census of places and work equipment. These must be classified according to criteria concerning the possibility that the reference levels for the population may be exceeded. In particular, the following shall be considered "a priori compliant":

- all equipment that is not capable of emitting fields of intensity higher than the reference levels for the population<sup>92</sup> is considered to comply a priori with the standard (and are sometimes referred to as justifiable sources);
- all workplaces where the reference levels for the population are respected are also considered to comply a priori.

According to the standard, in workplaces where only "a priori-compliant" equipment is present, the risk assessment essentially ends with the initial census. In workplaces where there are devices capable of emitting fields of intensity higher than the reference levels

for the population, the standard indicates instead as necessary a further evaluation procedure. To facilitate the task of the assessor, the EN 50499 contains two tables, the first of which includes all places and work equipment that comply a priori, while the second is a non-exhaustive list of equipment for which further assessment is required. This method has been further detailed in the Non-Binding Guide to Good Practice<sup>93</sup> for the implementation of Directive 2013/35/EU<sup>1</sup> of the European Commission. In particular, Table 1 contained in EN 50499 concerning "a priori compliant" equipment, i.e., those inherently safe, has been expanded and detailed in the first volume of the Non-Binding Guide to Good Practice, in Table 3.2. In this latter are reported the devices for which are not necessarily specific assessment and also the devices for which it is required (such as for the TMS device). In general, once the sources and areas have been identified, it is essential to provide for a procedure called "zoning" by defining the following Zones:

- Zone 0: is the area where the levels of electric, magnetic, and electromagnetic fields respect the limits for the general population, or in which all the sources present are "a priori compliant". This area can be accessed by anyone, including those with contraindications to exposure, such as wearers of metal prostheses or implanted electronic devices, pregnant women, and minors.
- Zone 1: it is the area where the reference levels for the population may be exceeded, but in which the employment limits are certainly respected. Access to this area must be allowed only to those involved in the specific processing carried out in it, these must be properly trained and informed. Access must instead be precluded to all other workers, to individuals of the population, and to subjects with contraindications.
- Zone 2: is the area where exposure levels may exceed occupational limit values. Access to this area must as a rule be forbidden to anyone.

At this point, having identified the potential exposure scenarios and the type of subjects exposed, it is necessary to choose which limits to refer to for the verification of conformity of the equipment. In Europe, a specific directive, that is the 2013/35/EU of the

European Parliament and of the Council of 26 June 2013 “on the minimum health and safety requirements regarding the exposure of workers to the risks arising from physical agents (electromagnetic fields) and repealing Directive 2004/40/EC<sup>94</sup>”, is currently adopted in a large number of the European member states, and requires an EMF-related risk assessment in workplaces. However, for a better understanding of the limits reported in the Directive, firstly it is important to define some aspects related to the exposure mechanisms. The ascertained mechanisms of interaction of electromagnetic fields with biological matter are substantially divided into two fundamental effects: induction of currents in electrically stimulable tissues and transfer of energy with thermal rise. Such effects are called direct effects because of a direct interaction of the fields with the human body. At lower frequencies and up to about 1 MHz, non-thermal effects such as stimulation of nerves, muscles, and sensory organs prevail. As the frequency increases, the transfer of energy into the tissues through the rapid oscillatory movement of ions and water molecules, with the development of heat and heating, becomes increasingly significant. At frequencies above about 10 MHz, this last effect is the only one to remain, and above 10 GHz, the absorption is exclusively present in the skin. The direct effects manifest themselves above specific induction thresholds: the current framework of knowledge allows us to have a "rationale" (i.e., a logical-scientific basis) for the definition of exposure limit values that prevent their occurrence in the exposed subjects. In addition to direct effects, there are indirect effects that can have serious repercussions on health and safety and therefore must be prevented, among them we find: interference with equipment and other electronic medical devices, involuntary triggering of detonators, electric shock or burns due to contact currents, risk of projectiles due to non-fixed ferromagnetic objects in a static magnetic field, etc. The aforementioned Directive aims to prevent both direct and indirect biophysical effects, while the scope does not concern protection from possible long-term effects for which, as indicated by the Directive itself, there is currently no conclusive scientific evidence capable of establishing a causal relationship. At this point, to delve into the issue of compliance with regulatory limits, the following definitions should be made:

- Exposure limit values (ELVs), pursuant to Directive 2013/35/EU<sup>1</sup>, are those values established based on biophysical and biological considerations, in particular, the acute and short-term direct effects scientifically ascertained, i.e. thermal effects and electrostimulation of tissues. The ELVs below 1 Hz are limits for the static magnetic field, for frequencies from 1 Hz to 10 MHz are limits for electric fields induced in the body from exposure to time-varying electric and magnetic fields, and for external magnetic flux density from 0 to 1 Hz. Therefore ELVs refer to quantities that are not directly measurable and are conceptually equal to the Basic Restrictions (BRs) suggested by the ICNIRP guidelines<sup>13,14</sup>;
- Action Levels (ALs), within the meaning of Directive 2013/35/EU, means those operational levels established to simplify the process of demonstrating compliance with the relevant ELVs or, where appropriate, to take appropriate protection or prevention measures. ALs correspond to calculated or measured electric and magnetic field values at the workplace, the overcoming of which determines the obligation to adopt certain appropriate prevention and protection measures. They are conceptually coincident with the reference levels (RLs) suggested by the ICNIRP guidelines<sup>14</sup>;

Further, the Directive stated, “The physical quantities, ELVs and ALs, laid down in this Directive are based on the recommendations of the International Commission on Non-Ionizing Radiation Protection (ICNIRP) and should be considered in accordance with ICNIRP concepts, save where this Directive specifies otherwise”. And in fact, in line with the logic of the ICNIRP, with regard to low frequency, Directive 2013/35/ EU introduces a double system of exposure limits (ELVs), distinguishing the stimulation effects on the central nervous system of the head ("minor" sensory effects, i.e. transient disturbing effects such as phosphenes or minor cognitive disorders, for frequencies below 400 Hz) from those affecting the peripheral nerves throughout the rest of the body (health effects, such as painful stimulation or involuntary muscle contraction up to arrhythmias.). The directive specifies that "minor" sensory effects can be risky for safety depending on the activity carried out by the worker, since the symptoms, even if temporary, can affect cognitive

abilities or other brain or muscle functions and therefore can adversely affect a worker's ability to work safely (safety risks).

Finally, it should be noted that the Directive, as well as the ICNIRP guidelines, also for low frequency (1 Hz- 100 kHz), take a flexible approach. That is, it is expected that a worker can experience minor sensory effects, and therefore the limits on the central nervous system of the head can be exceeded, provided that any negative consequences are kept under control through the adoption of specific protection measures. The motivation is well expressed in the text of the ICNIRP 2010 Guidelines where it says: "Following the recommendations made concerning guidelines on limits of exposure to static magnetic fields (ICNIRP 2009<sup>95</sup>), ICNIRP considers that there are occupational circumstances where, with appropriate advice and training, it is reasonable for workers voluntarily and knowingly to experience transient effects such as retinal phosphenes and possibly minor changes in some brain functions, since they are not believed to result in long-term or pathological health effects. Exposure of all parts of the body in these circumstances should be limited in order to avoid peripheral and central myelinated nerve stimulation".

Since the rationale of the Directive and the ICNIRP guidelines is matching, it is possible to refer to the latter, to establish a concept, that is the following. "The reference levels for electric and magnetic field exposure may be exceeded if it can be demonstrated that the basic restrictions are not exceeded". Thus, it is a practical or "surrogate" parameter that may be used for determining compliance with the Basic Restrictions.

If the measured or calculated value exceeds the reference level, it does not necessarily follow that the basic restriction will be exceeded. However, whenever a reference level is exceeded, it is necessary to test compliance with the relevant basic restriction and to determine whether additional protective measures are necessary. What is just reported, as a general rule, is not valid for a localized exposure. In this case, the ICNIRP guidelines stated that "for a very localized source with a distance of a few centimeters from the body, the only realistic option for the exposure assessment is to determine dosimetrically the induced electric field, case by case". Therefore, since the operator during the TMS treatment is close to the source,



in this study we considered carrying out a dosimetric analysis, to verify the compliance to the BRs expressed as induced E-Field.

In the following are reported the exposure limits of the Directive (ELVs) and the ICNIRP guidelines (BRs):

**Table II- 1 Health effects ELVs for internal electric field strength from 1 Hz to 10 MHz**

*Table A2 from the Directive 2013/35/EU*

<i>Frequency range</i>	<i>Health effect ELVs</i>
1 Hz ≤ f < 3 kHz	1.1 Vm <sup>-1</sup> (peak)
3 kHz ≤ f ≤ 10 MHz	3.8 × 10 <sup>-4</sup> f Vm <sup>-1</sup> (peak)

In Table II-1, f- frequency is in Hz. The health effects ELVs for the internal electric field are spatial peak values in the entire body of the exposed.

**Table II- 2 ICNIRP-2010 BRs for occupational exposure to time-varying electric and magnetic fields**

<i>Exposure characteristic</i>	<i>Frequency range (Hz)</i>	<i>Internal E-field (Vm<sup>-1</sup>)</i>
Occupational Exposure CNS tissue of the head	1–10 Hz	0.5/f
	10 Hz–25 Hz	0.05
	25 Hz–400 Hz	2 × 10 <sup>-3</sup> f
	400 Hz–3 kHz	0.8
All tissues of the head and body	3 kHz–10 MHz	2.7 × 10 <sup>-4</sup> f
	1 Hz–3 kHz	0.8
	3 kHz–10 MHz	2.7 × 10 <sup>-4</sup> f

In Table II-2, f- frequency is in Hz. The internal E-field is expressed in rms.

To conclude is important to mention the legislation directly related to the device in terms of electric and electronic equipment. IEC is the International Electrotechnical Commission, which provides a wide range of requirements also for medical devices, which are used by regulatory authorities for conformity assessment. As previously stated, for the TMS, up to this point, there is no IEC particular standard. Nevertheless, for TMS devices, it is necessary to take into account the EN-60601 series, promulgated by the IEC, which deals with various aspects of basic safety and essential performance for electrical medical devices. However,

being a general standard, it provides precisely general requirements and serves as a basis for standards. For example, collateral standards are defined as those specifying general requirements for basic safety and essential performance applicable to a subgroup of equipment or a specific characteristic of all equipment not covered in the more general document (60601-1). These standards are identified by type codes 60601-1-X, for example, we find among them the 60601-1-2<sup>12</sup> standard for Electromagnetic compatibility and also the 60601-1-3<sup>6</sup> concerning X-ray - radiation protection. There are also specific standards (with the format 60601-2-X) that can modify, replace, or eliminate the requirements contained in the general standard, as appropriate for a specific type of electrical equipment. These include, for example, 60601-2-1<sup>97</sup> for the Medical accelerator, 60601-2-33<sup>98</sup> for Magnetic Resonance Imaging and 60601-2-2<sup>99</sup> for the HF surgical equipment, and so on. What we found in reference to the requirements for the TMS, in the user manual of the manufacturer, regards the compliance only to the 60601-1<sup>11</sup> (general) and the 60601-1-2<sup>12</sup> (compatibility). In fact in the section of the product manual, typically under the voice "Performance Standard", we found that the TMS is designed to comply with the requirements of the Safety Standard EN60601-1 (Medical Electrical Equipment - Part 1: General requirements for basic safety and essential performance - Ed 3.1, 2005 + CORR.1:2006 + CORR.2:2007 + A1:2012 AND 2006 + AC:2010 + A1:2013), including amendment 1 and amendment 2, and EMC Standard EN 60601-1-2 (Medical Electrical Equipment - Part 1-2: General requirements for basic safety and essential performance - Collateral standard: Electromagnetic compatibility - Requirements and test, Ed 4 2014). Thus, no specific standards are stated, neither related to the explain how to carry out a risk assessment for this specific device nor is it evidently required of the manufacturer to comply with rules relating to medical devices, such as Regulation 745/2017 of the European Union<sup>100</sup>. This lack, for example, impact also in the possibility to apply the derogations allowed by the Directive, in reference to the ELVs health effects (a concept not included in the ICNIRP guidelines), that could be exceeded in specific cases. This is because derogations from the compliance to health effects ELVs could apply if there is a particular standard, as for example occurs in the case of MRI equipment, where the derogation could be applied following the instructions for safe use provided by the

manufacturer in accordance with European standard EN 60601-2-33<sup>98</sup> (specific for the MRI device). Following this European standard, severe effects like cardiac stimulation are prevented, the possibility of intolerable stimulations is confidently ruled out, and the only foreseen effects are of minor importance consisting just of non-painful perceptions. As regards other sectors or specific activities different from MRI, the above considerations should be addressed in specific technical standards, taking into account that the balance of health risks for workers with benefits to the patient should be considered in the medical applications<sup>101</sup>. To date, no technical standard exists for a TMS device that could be used for this permitted derogation. Therefore, this confirms the need for the harmonization in conformity assessment and thus the international particular standard with appropriate requirements for the TMS devices. What has just been said, confirms again the choice to deepen the issue related to the risk assessment for the TMS device.

## 2.2 Risk assessment: compliance with LG ICNIRP 2010

As mentioned earlier, the ICNIRP guidelines are taken as a technical-scientific reference by Directive 2013/35/EC laying down minimum requirements for the protection of workers from exposure to electromagnetic fields in the frequency range between 0 Hz and 300 GHz. In this study, since we considered a source positioned close to the operator, we refer to BRs suggested by ICNIRP 2010 guidelines<sup>13</sup>, and thus to the last update 2020<sup>14</sup>, to verify the exposure compliance to the regulatory system. The physical quantity used to specify the BRs during exposure to EM fields is the strength of the induced electric field, as it affects the nerves and other electrically sensitive cells. The limits, reported in Table II-2, are frequency-dependent, thus we have to compare the calculated induced quantity to a correspondent value of the working frequency of the device. At ~3 kHz (typical TMS frequency), the BRs assume the value of 0.8 V/m (rms), corresponding to 1.13 V/m (peak). The guidelines also suggest considering the local induced electric field as a value averaged in a tissue volume of  $2 \times 2 \times 2 \text{ mm}^3$ , and for a specific tissue, the 99<sup>th</sup> percentile of the induced E-field distribution is the relevant value to be compared with the BR. Therefore, in this study, we compared the ICNIRP limits by computing the 99<sup>th</sup> percentile of the induced E-field inside

the human body of an operator performing TMS treatment, which was discretized in  $2 \times 2 \times 2 \text{ mm}^3$  voxels in the numerical evaluation. Using this analysis, it is also possible to estimate the safety distance, that is the distance in which the induced E-field gets below the limits, and so it is possible to obtain the position in which is reached the compliance with the limits. It is clear that this analysis strongly depends on the device under test, thus should be carried out for each coil model and each possible exposure scenario. So, the results strongly depend on the exposure conditions examined.

Nevertheless, some studies consider that the evaluation of the 99<sup>th</sup> percentile in a local exposure condition isn't the best way for the risk assessment, since where the majority of significant induced electric field values may be concentrated in a small volume<sup>15</sup>. The maximum electric field (100<sup>th</sup> percentile) value depends on the resolution of the numerical grid and is susceptible to staircase error<sup>102</sup>, so the influence of human model resolution on computed quantity induced by the external fields<sup>102,103</sup>, led the research studies and also the ICNIRP guidelines to use the 99<sup>th</sup> in order to reduce this error. However, Laakso et al. 2012<sup>15</sup>, assume that, in a local exposure, taking into account only the 99<sup>th</sup> percentile, leads to an underestimation of the risk, since excluding the 1%, means ignoring the real values that should be considered. Therefore, Laakso et al. 2013<sup>104</sup> propose using 99.9<sup>th</sup> as a dose metric. In this study, were considered three human models (male Taro, female Norman, and child Thelonious) and the aim is to investigate the magnitude of the numerical errors that affected the induced E-field, thus the authors examine the correlation between the 99.9<sup>th</sup> percentile and the 100<sup>th</sup> percentile and the 99<sup>th</sup> percentile of the electric field. What they found is that there was a strong correlation between the 99.9<sup>th</sup> percentile and 99<sup>th</sup> percentile of the electric fields, whereas a slightly weaker correlation between the 100<sup>th</sup> percentile electric field and the 99.9<sup>th</sup> percentile. Therefore, to reduce numerical errors affecting the 100<sup>th</sup> percentile and on the other hand, to improve the underestimation relative to the 99<sup>th</sup> percentile, the authors obtain as result, and so suggest, that the 99.9<sup>th</sup> percentile is reasonable the value that should be used for the assessment of exposure. In agreement with each other, are Ahn et al. 2021<sup>105</sup>, that propose yet the use of the 99.9<sup>th</sup> percentile for the exposure analysis. In this study, five anatomical human models and a simplified model are considered, and the paper aims to

carry out an improvement of the method for the safety assessment introduced by IEC about the exposure to a Low-Frequency wireless power transfer system. This assessment is based on the concept of the calculation of coupling factor (as suggested by IEC 62233<sup>106</sup> and 62311<sup>107</sup>), which in turn implies the calculation of induced quantities. The author in order to reduce the computation artifacts due to abnormal peak (100<sup>th</sup> percentile) proposes an improved method by applying the 99.9<sup>th</sup> percentile in calculating the coupling factor without underestimation (present in the case of the use of the 99<sup>th</sup> percentile). The results of this study show that the use of the 99.9<sup>th</sup> percentile for the evaluation of the induced quantities reduces the computational errors by up to 65.3% compared to a conventional method, that uses the 99<sup>th</sup> percentile. Thus, they suggested that the 99.9<sup>th</sup> is the value that could be used to obtain an assessment of exposure without an underestimation. For what has just been dealt with, in this study, it was considered important to report both the 99<sup>th</sup> percentile, to take into account the ICNIRP guidelines (and thus the Directive), but also the 99.9<sup>th</sup> percentile to take into account the knowledge gained from the scientific literature.



## **SECTION II. NUMERICAL MODELING AND COMPUTATIONAL DOSIMETRY IN THE RISK ASSESSMENT**

---





# III. CHAPTER

---

## 3.1 Numerical analysis: an overview of the computational methods

As aforementioned, the main scope of the work is to evaluate an exposure assessment for working operators during the TMS treatments, carefully reproducing a real work exposure scenario. In particular, through the classification of all possible orientations adopted by the clinician with respect to the patient and thus to the TMS coil, a computational numerical dosimetry analysis is carried out. EM dosimetry is a scientific discipline aimed at studying the coupling mechanisms between an EM field and a biological object exposed to it. Coupling is the first step in an interaction process, which can manifest itself with biological or health effects<sup>108</sup>. The whole process of interaction is inherently multidisciplinary, as it involves engineering, physics, biology, and physiology. However, coupling itself is simply a physical process involving the laws of interaction between EM fields and objects of complex shapes, such as human models. At the basis of this mechanism of interaction, there are indeed the so-called dosimetric quantities. These quantities can properly correlate the intensities of the external fields and the effects observed inside the exposed subjects (the operator in this case). As just mentioned, the dosimetric quantity that needs to be assessed for our scope is the induced E-field within human tissue (understood as the 99<sup>th</sup> percentile), which then needs to be compared with the BRs limits, as suggested by the ICNIRP guidelines, to verify exposure compliance. Therefore, first of all, an understanding of the methods used to obtain this dosimetric quantity is needed.

The TMS coil device works in a range of frequencies of about 1 kHz – 3 kHz, with a circulating current of dozens of kA (typically from 4 kA up to 10 kA). Therefore, the operational field of the TMS is in the low-frequency range, since this latter includes the frequencies ranging from 300 Hz up to 100 kHz. To study the distribution of the EM field in the environment due to the TMS source, Maxwell's equations must be solved. These equations describe exactly how the EM field, generated by a source, is distributed in the surrounding space:

$$\nabla \times \mathbf{H} = \mathbf{J} + \frac{\partial \mathbf{D}}{\partial t} \quad (3.1)$$

$$\nabla \times \mathbf{E} = -\frac{\partial \mathbf{B}}{\partial t} \quad (3.2)$$

$$\nabla \cdot \mathbf{D} = \rho \quad (3.3)$$

$$\nabla \cdot \mathbf{B} = 0 \quad (3.4)$$

where  $\mathbf{H}$  is the magnetic (H-)field,  $\mathbf{E}$  is the electric (E-)field,  $\mathbf{D} = \epsilon\mathbf{E}$  is the electric displacement, accounting for the polarization of the material in an electric field,  $\mathbf{B} = \mu\mathbf{H}$  is the magnetic flux density, accounting for the magnetization of a material and  $\mathbf{J}$  is the current density. It is possible to express the equation in the frequency domain:

$$\nabla \times \mathbf{E} = -j\omega\mathbf{B} \quad (3.5)$$

$$\nabla \times \mathbf{H} = j\omega\mathbf{D} + \mathbf{J} \quad (3.6)$$

$$\nabla \cdot \mathbf{D} = \rho \quad (3.7)$$

$$\nabla \cdot \mathbf{B} = 0 \quad (3.8)$$

Where  $\omega$  is the angular frequency and  $j = \sqrt{-1}$ . Further, equations that consider the material behavior in the presence of EMF must also be considered, that are the constitutive relations of the material:

$$\mathbf{D} = \epsilon_0\epsilon_r\mathbf{E} \quad (3.9)$$

$$\mathbf{B} = \mu_0\mu_r\mathbf{H} \quad (3.10)$$

$$\mathbf{J} = \sigma \mathbf{E} + \mathbf{J}_0 \quad (3.11)$$

Where  $\epsilon_0$  and  $\mu_0$  are respectively the permittivity and the permeability in the free space, while  $\epsilon_r$  and  $\mu_r$  are the permittivity and the permeability in the material. The last equation is the EM representation of the law of Ohm, where  $\sigma$  is the conductivity of the material and  $\mathbf{J}_0$  represents an external current source. Maxwell's equations can be solved both in the time domain and in the frequency domain. Typically, the numerical methods used are based on differential or integral equation solvers, which precisely discretize the differential or integral form of Maxwell's equations. What is essentially done is a spatial discretization of the equations in the region of space to be analyzed (or possibly a temporal discretization). In this way, the geometry involved in the problem is divided into elements, called cells, in which the differential equations can be calculated. The entire environment thus discretized is called *Grid* or *mesh*. Once the mesh has been defined, the relationships of the physical system within each element of the numerical space must be found. Once the spatial discretization has been done, what must be defined is the algorithm capable of solving the physical problem in the discretized space for the specific characteristics chosen. Depending on the characteristics of the problem, one numerical algorithm may be more suitable than the other, thus providing more accurate results. In the case of this study, which is a low-frequency application of numerical dosimetry, it is possible to take advantage of the quasi-static approximation (QSA), which has been extensively applied up to a few tens of MHz. However, the QSA, for the analysis of the mechanism of the interaction between human models and low-frequency EMF can be used if three conditions are satisfied<sup>109</sup>:

1. The dimensions of the involved objects and their mutual distances should be small when compared to the free-space wavelength (i.e., up to 40 MHz for the human body);
2. The size of the exposed subject should be comparable to, or smaller than, the skin depth in the biological materials (for the frequencies considered in this work, we found that the skin depth<sup>109</sup> of the human tissues are included between 19 m, for

blood, and up to 1314 m, for skin dry)<sup>109</sup>, therefore this requirement is certainly fulfilled in our case;

3. The electric displacement current is neglected with respect to ohmic currents and the induced currents in the human body are assumed not to perturb the external magnetic field.

In the case of this study, all the conditions are satisfied, thus the QSA can be used. Based on this approximation a simplified version of the Maxwell's equations, which finds the EM solution by decoupling the B-field and E-field calculations, is applied. The solution to the B-field was obtained according to Biot–Savart law (equation 3.12) and equation 3.13.

$$A(\mathbf{r}) = \frac{\mu_0}{4\pi} \int_{\Omega} \frac{J_0(\mathbf{r}')}{|\mathbf{r} - \mathbf{r}'|} d^3r' \quad (3.12)$$

where  $\mathbf{A}$  is the magnetic vector potential;  $J_0$  is the current source;  $\mu_0$  is the magnetic permeability (constant over the entire domain  $\Omega$ );  $\mathbf{r}$  and  $\mathbf{r}'$  are the position vector inside the domain and the position vector of the source, respectively.

$$\mathbf{B} = \nabla \times \mathbf{A} \quad (3.13)$$

Where  $\mathbf{B}$  is the magnetic flux density and  $\mathbf{A}$  is the magnetic vector potential.

Subsequently, the finite element method (FEM) was applied to solve the Laplace equation and compute the E-field distribution, in the hypothesis of ohmic current domination:

$$\nabla \cdot \sigma \nabla \phi = -j\omega \nabla \cdot (\sigma \mathbf{A}) \quad (3.14)$$

where  $\sigma$  is the conductivity of each tissue,  $\omega$  is the angular frequency, and  $\phi$  is the electric scalar potential.

In order to carry out the computational dosimetry of this study, it is decided to use the commercial electromagnetic simulation software Sim4Life (Zurich MedTech, AG)<sup>110</sup>. It is

important to highlight that this software is widely used in the research literature for dosimetric purpose<sup>111,112,113</sup>.

Additionally, since as anticipated, a neuronal analysis is performed in this work, it is important to underline that the commercial software Sim4Life is capable to simulate the effect of EM fields on neuronal dynamics. This sort of solver library is developed at Yale University<sup>114</sup>. The tool allows us to directly couple the results obtained by the EM simulations with the neuronal dynamics. When exposed to an EM field, a nerve fiber reacts by changing the electrical activity of its membrane<sup>115,116,117</sup>. This latter results in temporally and spatially limited changes in the transmembrane potential<sup>118</sup>, which, if above a certain threshold, may cause the activation of spikes or action potentials that propagate along the fiber. Inhomogeneity and rapid changes in the EM field may impose localized potential gradients along the neuron, which could then depolarize the membrane inducing transmembrane flow of ionic currents. As stated, if the depolarization is of sufficient strength, an action potential or spike could be initiated, and typically, it is precisely these nerve stimulation thresholds that play a very important role in defining safety limits and standards. It is obvious that various factors influence the reaction and so the possible stimulation of the neurons to EM exposure, among them are certainly the geometric characteristics<sup>119</sup> of the fiber (such as the diameter) and the orientation of the fiber with respect to the field. Thus, from a physical point of view of the solver, the neuron exposed to an EM field detects an electric potential ( $\phi$ ) distribution that can be extracted directly as the quantity of QS LF solvers or derived from the E-field for EM solvers that do not produce the electric potential. The E-field is defined as the negative of the gradient of the potential (equation 3.15):

$$\mathbf{E} = -\nabla\phi \quad (3.15)$$

Where:

$$\phi = V_{ext} = - \int_C \mathbf{E} dl \quad (3.16)$$

where  $C$  is a linear path that connects each data point to an arbitrary zero-voltage reference, and  $dl$  is the integral of the path length. In the context of the Neuron solver,  $\phi$  and  $V_{ext}$  are the data that are passed to the *Neuron Solver* to obtain the solution. Another important function, for the scope of this work, and available in this solver, is the Titration. By means of the Titration analysis, it is possible to determine the threshold above which a peak is generated along the fibers. The titration factor obtained is used to further scale the electrical potential ( $\phi = V_{ext}$ ) detected by the neuron. Thus, the final threshold field is the product of the static potential from the initial EM field  $\phi$ , the modulating pulse  $a(t)$ , and the titration factor  $T$ .

$$\phi_T(t) = \phi \cdot T \cdot a(t) = - \int_C \mathbf{E} dl \quad (3.17)$$

Therefore,  $T$  is a scale factor indicating the proportion or multiple of the actual modulated electric potential needed to generate an action potential. There are also different neuronal models that can be set in the simulation, each of them has specific characteristics that determine the stimulation response. These models consider the ionic currents that cross the membrane and the excitability thresholds. The software integrates, among others, the following neuronal models, more aligned with the purposes of the present work:

- Sensory modify MRG model<sup>120</sup>: describe the membrane dynamics of myelinated sensory axon fibers;
- Motor modify MRG model<sup>120</sup>: describe the membrane dynamics of myelinated motor axon fibers;

These two models are named “modify”, since they are obtained thanks to a change in the basic model, implemented by McIntyre, Richardson, and Grill (MRG)<sup>121</sup>. These new modified models, compared to the initial model, take into account the electrophysiological

differences between sensory and motor fibers. The two models benefit from accepting continuous values of fiber diameters, instead of discrete values as for the original MRG model. The main characteristics of the MRG model are that they incorporate a double cable structure, with explicit representation of the nodes of Ranvier, paranodal, and internodal sections of the axon as well as a finite impedance myelin sheath. Thus, these models were able to reproduce a wide range of experimental data on the excitation properties of mammalian myelinated nerve fibers. By means of these explained tools, it was possible to carry out the assessment risk and the scientific analysis of the topic covered in this study.

### 3.2 EM characterization of TMS device: validation & verification of the coil models

During the research project, different TMS coils have been characterized through a Verification and Validation process (V&V)<sup>122</sup>. The Verification is a static process that consists of analyzing documents, data, and literature, to correctly implement a source. The question to ask yourself at this stage is "Am I building the source correctly?". The Validation is a dynamic process, which involves mathematical solvers, software, etc., during which a comparison of the results is made. At this stage, the question to ask yourself is: Is the source working as it should?

For instance, in the Validation process, a comparative evaluation was also carried out using different analysis methods. In particular, for one of the coils, the characterization of which will be dealt in detail below, a comparison between numerical and analytical models was performed. Using the latter, we have found a solution for the Biot-Savart law by considering the coil fed with a stationary electric current, by means of two different analytical methods. The evaluation referring to the circular coil Magstim, consisting of 14 windings, with an outer radius of 120 mm and an inner radius of 70 mm, supplied with a maximum current of

5.6 kA (3 kHz). The data obtained using the two methods (i.e., analytical and numerical), are shown in the multi graph reported below.

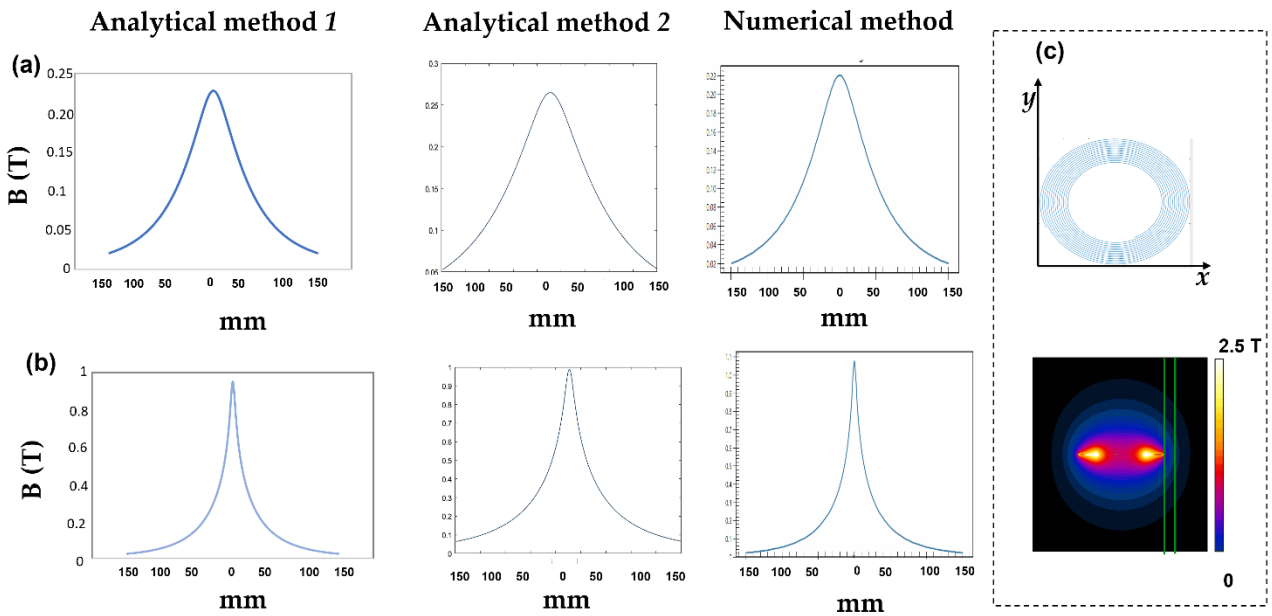


Figure III. 1. (a) Evaluation of B-field at 80 mm from the center of the coil; (b) Evaluation of B-field at 65 mm from the center of the coil; (c) on the top coil placed in the plane  $xy$ , on the bottom B-field around the coil in the free space.

In the graph, the first two columns refer to the data obtained from two different analytical method, while the third column reports those obtained from the numerical method. In addition, in the in the right-hand box are also reported the map of the distribution of B-field (with the two distances highlighted) in the free space around the coil, that on the top is geometrically reported in the plane  $yz$ , that is the plane perpendicular to the surface of the coil.. By analyzing the graph, the panel in the row (a) shows the data obtained at distance equal to 80 mm from the center of the coil, along the line highlighted in green in the box (c) on the maps of the B-field. While panel (b) reported the values of B-field, along the line highlighted in green, that distance from the center is 65 mm. As we can see, the results showed good agreement. Therefore, we can conclude that B-field produced by the coil is sufficiently reliable.

At this point, we can start with the characterization of the sources.



The first device chosen for dosimetric analysis has been derived from experimental data acquired during a measurement campaign<sup>123</sup> conducted by the group of INAIL Research Center in November 2009. During this campaign, the commercial Magstim MAG-9784-00 circular coil fed by the BiStim appliance<sup>124,125,126</sup> has been used. In Table III-1, the features of the entire system are analyzed:

*Table III - 1. Features of the devices*

<b>Circular coil Magstim MAG-9784-00</b>	
<b>Power system</b>	BiStim
<b>Frequency</b>	1 kHz
<b>Current (MSO*)</b>	9.7 kA
<b>Inner diameter</b>	7 cm
<b>Outer diameter</b>	12.2 cm

\*MSO: maximum stimulator output

The current signal that flows inside the TMS is assimilated to a pure sinusoid at equivalent frequencies obtained from the pulse period, as literature studies have shown that this assumption leads to a negligible error<sup>127,128</sup> when compared with the time-dependent signals. The experimental acquisitions have been conducted in a medical center and the measurement conditions have been provided considering the machine working in real operating conditions (70% MSO), obviously avoiding the exposure of the patient. To this end, a plastic container with a capacity of 3 L, filled with a 0.01 molar solution of NaCl in water was placed in the position normally occupied by the patient's head (Figure III.2). The circular coil was placed in contact with the container and oriented with the axis parallel to the walking plane. The measuring points were chosen both at the position normally occupied by the operator and along the radial and axial direction of the actuator to reconstruct the spatial distribution of the field. It is declared that the estimated uncertainty about the measures is 5%. In Figure III.2, is reported the measurement setup.

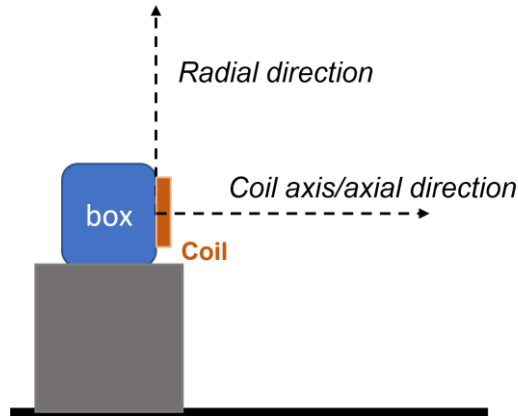


Figure III. 2: Measurement setup

We define D1, as the axial direction, whereas D2 is the radial direction. The measurements of the magnetic flux density (B-field) recorded during the campaign are reported in Table III-2:

**Table III - 2. Measured B-Field**

POINTS OF MEASURE			
	D1 [cm]	D2 [cm]	$B(\mu\text{T})_{peak}$
1	4	0	667000
2	64	0	494
3	96	0	153
4	0	32	1827
5	0	64	251

The second step is to reproduce and numerically model the source validating its performances through a comparison with the values obtained during the experimental campaign. Therefore, following the features reported in Table III-1, the coil model was reproduced using the numerical software Sim4Life (v.7, ZMT, Zurich MedTech AG). In the environment of simulation, it consisted only of the windings, without the outer coating, as done by current literature on TMS modeling<sup>129</sup>. Therefore the coil was reproduced in the simulation environment as dimensionless wires placed at the center of the real wires<sup>129,130</sup>. This implied a 2D coil approximation that may slightly underestimate the induced E-field, but the overall error was typically below 2%<sup>129,131</sup> in the range of work frequency here

considered. In Figure III.3, it is reported the modeled coil in numerical software and the distribution of the magnetic field produced.

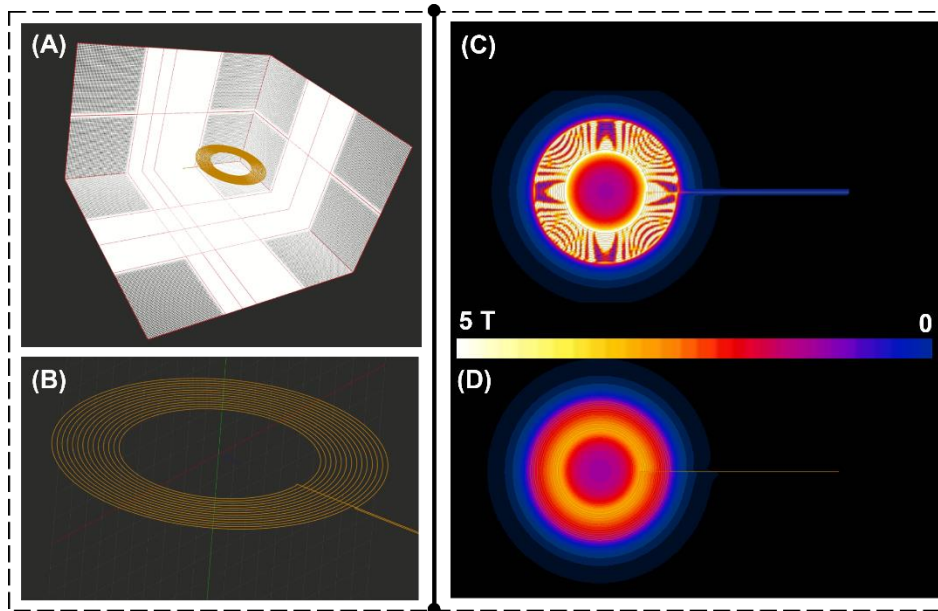


Figure III. 3 Modeled coil in simulation environment: (A) coil in the grid (mesh) set in the simulation environment, (B) circular coil numerical model, (C) distribution of the magnetic flux density  $B(T)$  on the surface of the coil in corresponding of the windings, (D) distribution of  $B(T)$  in corresponding on the surface in the position of the coating.

At this point, the analysis of the B-field around the coil is detected. Since we have the exact position in which the B-field is recorded, we move in the same direction in the simulation environment to compare the B-field. Figure III.4 shows the behavior of the B-field, with the maximum peak achieved in the corresponding of the inner turn of the coil (as the geometry of the coil suggests).

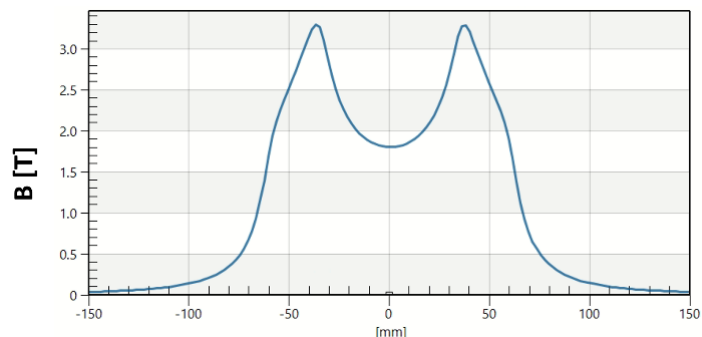


Figure III. 4 B-field (T) along the line through the center of the coil in the outer surface.

The comparison with experimental measurements, along the two directions, is summarized in Table III-3 and Table III-4:

**Table III - 3. Measurements of B (mT) along the radial direction**

<i>Distance</i>	<b>Measured values</b> 70% MSO	<b>Simulated values</b> 70% MSO
32 cm	1.827	2.2
64 cm	0.251	0.268

**Table III - 4. Measurements of B (mT) along the axial direction**

<i>Distance</i>	<b>Measured values</b> 70% MSO	<b>Simulated values</b> 70% MSO
4 cm	667	669.9
64 cm	0.494	0.52
96 cm	0.153	0.158

The source modeled in the numerical environment returns roughly the same values of the measurement campaign. With a maximum percentage variation, between the measured and simulated value, of 5.26%.

As a whole, we can conclude that the V&V process is successfully completed.

The characterization of the second coil, modeled in Sim4Life, is carried out from a comparison of the results obtained by Bottauscio et al. 2016<sup>43</sup>, where an assessment of risk for occupational exposure to a circular commercial coil MC125 is conducted. Bottauscio et

al. obtained from the experimental analysis, the feature of the coil under test. They measured a peak current equal to 5.6 kA, for which is achieved the  $B_{\max}$  measured in the inner turn of the coil. The waveform of the current, and thus the B-field in the free space, is assimilable to a dampened sinusoid with a period  $T= 290 \mu\text{s}$ . Since the current signal is assimilated to a pure sinusoid with an equivalent frequency obtained from the inverse of the period, the authors set the operative frequency at 3.45 kHz. The features of the circular coil MC125 used in the study of Bottauscio et al., are following reported:

**Table III - 5. Features of MC125 circular coil**

<b>TMS SUPPLY</b>	<b>MAGPRO R30</b>
Max initial dB/dt	<b>41 kT/s</b>
Inner diameter	<b>28 mm</b>
Outer diameter	<b>114 mm</b>
Turns	<b>13</b>
Current <sub>peak</sub>	<b>5.6 kA</b>
Frequency	<b>3.45 kHz</b>

Moreover, since a risk assessment study is considered, the 99<sup>th</sup> percentile of the induced E-field in the human male model Duke (member of the ViP of Sim4Life<sup>132</sup> software) is evaluated, also considering the induced quantity in a specific tissue, i.e. the central nervous system (CNS). Three vertical positions (heights  $h$ ) of the coil with respect to the operator body, and also different distances ( $d$ ) of the coil from the operator body axis are considered, as reported in Figure III.5.

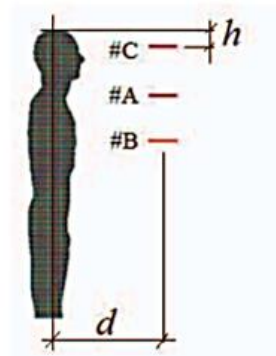


Figure III. 5: Coil position with respect to the operator model:  $h = 29.2 \text{ cm}$  (case #A),  $h = 49.2 \text{ cm}$  (case #B), and  $h = 9.2 \text{ cm}$  (Case #C). Figure adapted from Bottauscio et al.2016.

The authors considered as worst case the #B position, thus in the present study, we chose to reproduce this exposure condition. As previously done, also in this case the coil is first geometrically modeled and then the magnetic field in the free space analyzed. The coil is fed by 5.6 kA (100% MSO) at 3.45 kHz. Following the distribution of the B-field obtained:

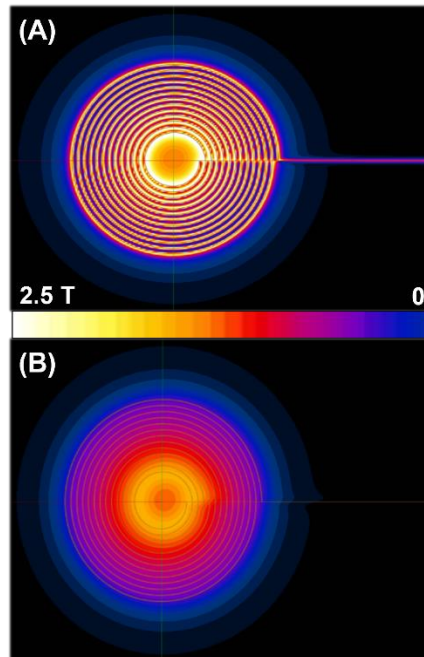


Figure III. 6: Distribution of B-field produced by the modeled MC125 circular coil, (A) distribution of the magnetic flux density  $B(T)$  on the surface of the coil in corresponding of the windings, (B) distribution of  $B(T)$  on the surface at the position of the coating, i.e., 4mm away from the windings.

The human body model Duke is considered and positioned in the simulation as done by Bottauscio et al. (2016). This exposure condition results in  $h= 49.2$  cm from the top of the model and in two distances  $d$  from the axis of the operator (40 cm and 60 cm). Reproducing these cases in our computational environment, we evaluated the 99<sup>th</sup> percentile of the induced E-field, in the total body and in a localized tissue (i.e., CNS). Further, we have considered two voxel dimensions, that are 4 mm and 2 mm, as done also by Bottauscio et al., since they stated that the use of 4 mm voxels leads to a slight conservative overestimation in the CNS ( $\sim 5\div 7\%$ ) in comparison with the results given by the 2 mm voxels. Data are reported in Table III-6:

*Table III - 6. Comparison of results*

	<b>Voxel</b>	<b>Distance</b> from body axis	<b>Results</b> of this work	<b>Results</b> of Bottauscio et al.
<i>Total body</i>	<i>4 mm</i>	<i>40 cm</i>	<b>1.80 V/m</b>	<b>1.91 V/m</b>
<i>Total body</i>	<i>4 mm</i>	<i>60 cm</i>	<b>0.57 V/m</b>	<b>0.69 V/m</b>
<i>CNS</i>	<i>4 mm</i>	<i>40 cm</i>	<b>0.59 V/m</b>	<b>0.57 V/m</b>
<i>CNS</i>	<i>2 mm</i>	<i>40 cm</i>	<b>0.57 V/m</b>	<b>0.55 V/m</b>

As can be observed from the Table, the E field calculation in the CNS tissue for the case of 2 mm voxel resolution is perfectly reproduced; in the case of lower resolution discretization of 4 mm, the difference between the two models (Bottauscio and ours) goes from 5% to 20% as a function of the distance between the coil and the human body model. Thus, we can conclude that we have obtained the characterization of the MC125 device powered by the MagPro R30.

Finally, the other two coil models coming from the company Magstim Co.Ltd.<sup>133</sup> are characterized through the information found in the user manuals<sup>134–136</sup>. In fact, in the user manual or in the guide of the products typically it is possible to find the information regarding the geometry of the coil and the B-field maximum (100% MSO) produced by the system. From this information, we conducted a backward analysis from the known data. Thus, knowing the  $B\text{-field}_{\max}$  produced by the power system at 100% MSO, we were able to derive the current needed to obtain that field value at the working frequency of the coil.

We start with the Std. Double coil 9925-00, Magstim. This coil will be referred as figure-of-eight. Typically the commercial figure-of-eight coil is powered by the two-phase generator Magstim Rapid2<sup>135</sup>.



Figure III. 7. Figure-of-eight coil.

From the user manual, it is known that the maximum magnetic field produced by the coil is 1.2 T at the external surface. Starting from this indication and knowing the geometrical characteristics provided by the manufacturer, the coil model has been implemented on the EM simulation software Sim4Life v.4.4 (ZMT, Zurich MedTech AG). The coil model reproduces the real geometry with a  $\sim 90$  mm diameter per lobe, and a long feeding handle of about 205 mm. The simulation environment was discretized by a maximum size of the grid cells equal to 2 mm, considering extremely fine refinement. The feeding signal, corresponding to a cycle of the damped sinusoid, was herein approximated as a pure sine with the equivalent frequency of 3 kHz, equal to the inverse of the damped sine period ( $340 \mu\text{s}$ )<sup>137</sup>. In our model, we used a coil consisting of only windings, without the surrounding coating. To consider the presence of the external plastic shell, we fed the coil so as to have the maximum B-field 4 mm away from the windings, considering that this thickness represents the coating, inhere not modeled. In Figure III-8 the B-field map is reported, obtained when the coil is supplied by  $\sim 1.6$  kA. This shows the case in which the maximum B-field output (1.2 T) is achieved in the corresponding of the windings of the coil, approximately in the center of the coil (that is in the plane xy, with x-axis along the handle of the coil and y-axis crossing the two lobes and the center of the coil, i.e., radial direction).

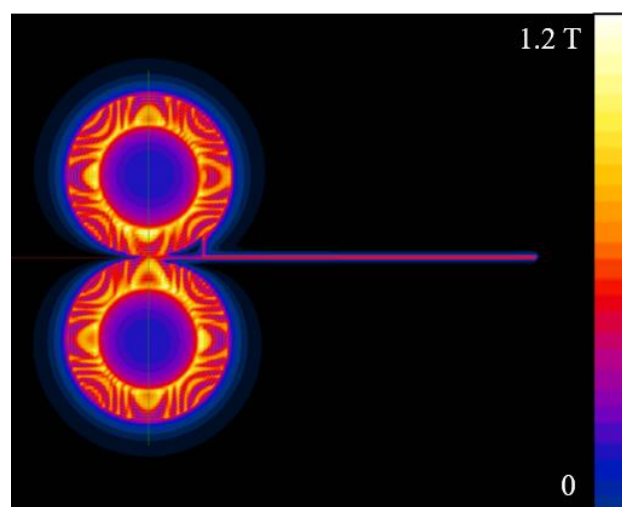


Figure III. 8 Mapping of B on the surface of the Std. Double coil 9925-00. The maximum B-field 1.2 T is achieved at the center of the coil.



The data of the B-field along the y-axis on the plane that contains the coil windings is shown in Figure III.9, whereas the same data in the plane away 4 mm from the windings is shown in Figure III.10:

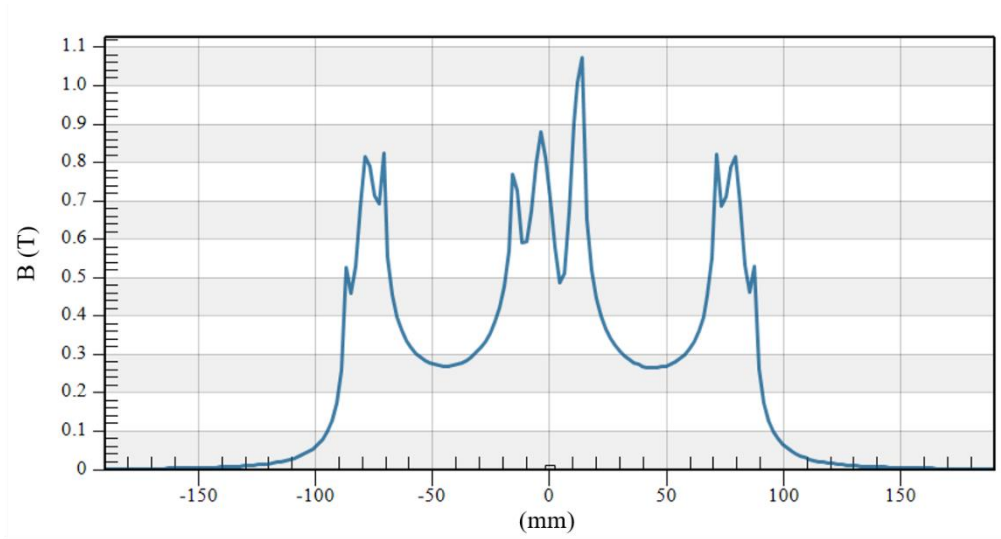


Figure III. 9 |B| along radial direction, through the center and the two lobes, on the surface of the coil

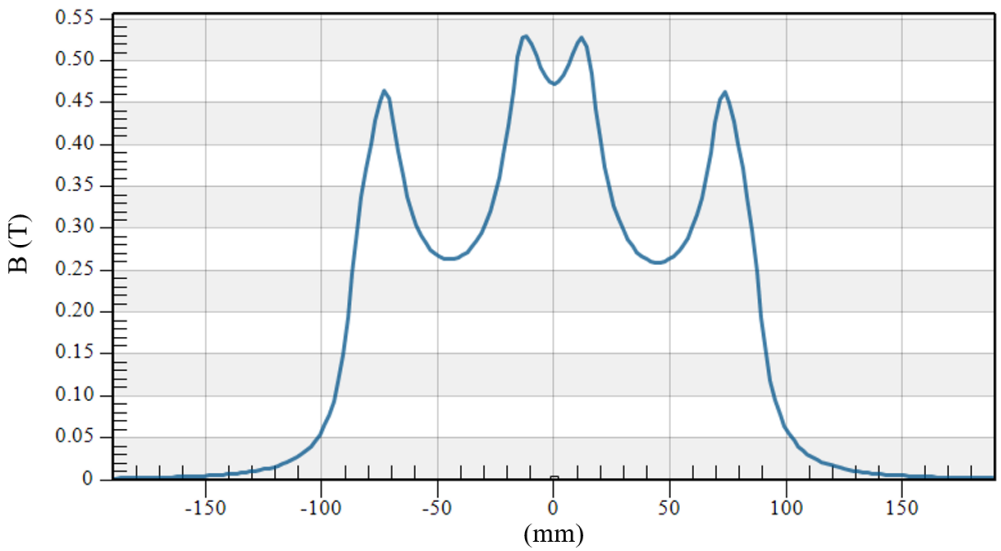


Figure III. 10: |B| along radial direction, through the center and the two lobes, on the plane 4 mm away from the surface of the coil.

Following these results, to have a  $B_{\max} = 1.2$  T (maximum output of Magstim Rapid<sup>2</sup>) on the plane at 4 mm from the windings, the current to be used should be equal to 4085 A.

The second Magstim coil considered is the circular coil 9784-00. The circular coil is powered by the mono-phasic generator Magstim200. With this type of coil, the maximum B-field occurs near the inner turns and is equal to 2 T peak field.



*Figure III. 11: Circular coil*

Using the same method followed for the figure-of-eight, the model of the circular coil was created in Sim4Life v4.4 and the EM problem was solved considering the Magnetic Quasi-Static module. The coil is characterized by an internal radius of 70 mm, an external radius of 120 mm, and 14 windings<sup>138</sup>. The simulation environment was discretized with the same step as before and also considering the extremely fine refinement of the grid surrounding the coil. The simulation takes place at the fixed equivalent frequency of work of the coil, equal to 3 kHz. To obtain a  $B_{\max}$  equal to 2 T, the required current supply is 5.6 kA. Below in Figure III.12 (a) is the mapping of B-field in the plane xy, 4 mm away from the surface of the coil, which as mentioned, represents the thickness of the coil case and, therefore, where the maximum B output should be achieved. On this plane, the plot of B-field along the axis highlighted green that through the center of the coil was extracted (Figure III.12 (b)).

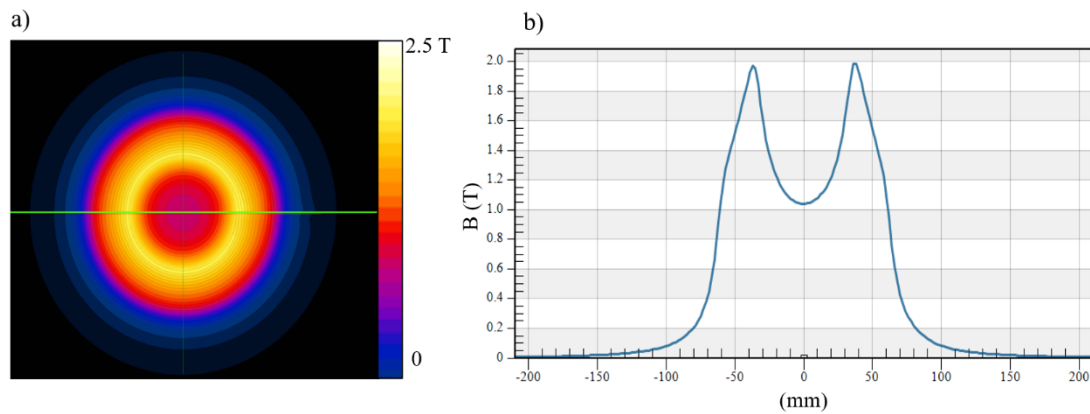


Figure III. 12. a) Mapping of B-field on the plane at 4 mm from the surface of the coil; b) B-field along the radial axis, that is highlighted by the green line in a).

The figure shows that the desired B-field max is guaranteed with a supply of 5.6 kA, at the frequency of 3 kHz. The features of the four coils characterized are summarized in the following:

*Table III - 7. Features of the coils*

	Figure-of-eight Coil	Circular Coil	Circular coil	Circular Coil
<i>Supply:</i>	Magstim Rapid2	Magstim 200	Magstim BiStim	MagPro R30
<i>Max B Output:</i>	1.2 T	2 T	3.2 T	1.8 T (= 41 kT/s)
<i>Inner Diameter</i>	52 mm	70 mm	70 mm	28 mm
<i>Outer Diameter</i>	88 mm	122 mm	122 mm	114 mm
<i>Turns</i>	Double turn	14	14	13
<i>Current</i>	4 kA	5.6 kA	9.7 kA	5.6 kA
<i>Frequency</i>	3 kHz	3 kHz	1 kHz	3.45 kHz

### 3.3 Standardization of worker position in TMS treatments

We collected information on typical positions assumed by clinicians during TMS treatments by searching different documental sources, such as company user manuals, websites<sup>139</sup>,

papers<sup>140</sup>, and pictures obtained during the measurement campaigns made by the National Institute for Insurance against Accidents at Work (INAIL)<sup>141</sup>. Thus, we stored approximately 65 pictures representing clinical scenarios, through which the positions taken by the worker during TMS treatment were identified. It is observed that the position of the stimulating coil with respect to the clinician depends on several factors, such as the available equipment, e.g., type of coil, presence of a supporting system, and geometry of the supporting system. We need to consider that the geometry of the coil could influence the position of the operator, since, as mentioned above, typically he/she holds the coil with the hands. Further, some coils are equipped with a supporting tool (a sort of plastic stick) that helps the clinician to keep in position the coil, remaining a greater distance from the source; although this solution is rarely used in clinical practice, it does not exclude completely the occupational exposure (Figure III. 13):



*Figure III. 13. TMS treatment with use of plastic tool. Figure adapted from <https://www.smarttms.co.uk>*

Another factor is the patient's holder, i.e., bed or chair because both determine the position of the patient's head with respect to the frontal axis of the clinician. For example, the presence of a bed and thus the patient lying down, implies the exposure of the lower abdomen of the clinician, since the position taken by the operators appears to be that of Figure III.14:



Figure III. 14. Exposure of lower abdomen with use of bed support for patient. Figure adapted from GEA solution website.

Also, the height of the clinician and that of the patient may influence the exposure conditions: for instance, pediatric patients would likely force the clinician to bend over, bringing the stimulator closer to the chin/neck area (Figure III.15):

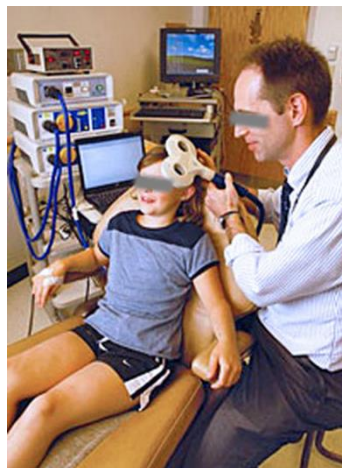


Figure III. 15. Exposure of chin/neck of the operator. Figure adapted from website <https://www.cincinnatichildrens.org/research/divisions/n/neurology/labs/gilbert-wu>.

Based on the results of these reviews, it was possible to classify the exposure in four anatomical positions of the coil with respect to the body of the operator. These conditions are summarized in the following Figure III.16:

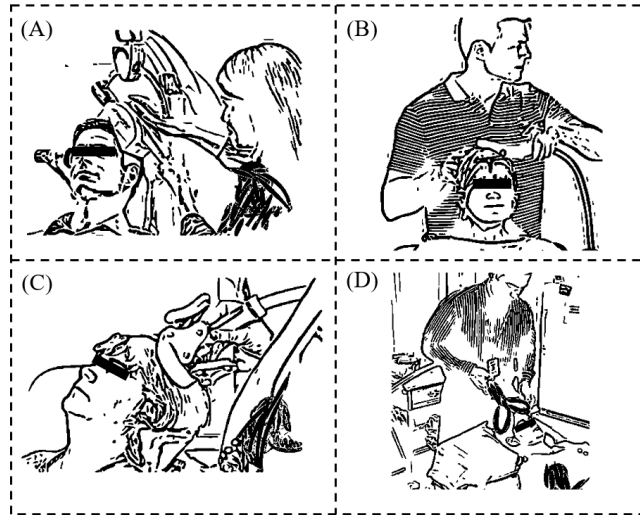


Figure III. 16: Typical relative vertical positions between the TMS coil and the clinician: examples of real scenarios and identification of the exposed anatomical areas: (A) exposure of the chin/neck, (B) exposure of the chest, (C) exposure of the abdomen, and (D) exposure of the lower abdomen

Therefore, this exposure mainly involves four anatomical areas of the clinician, which we have classified below with capital letters:

- A. Chin/neck, Figure III.16 (A);
- B. Chest, Figure III.16 (B);
- C. Abdomen, Figure III.16 (C);
- D. Lower abdomen, Figure III.16 (D);

The computation analysis carried out in this work start from these assumptions, since they represent the real exposure condition actually detected in typical workplaces.

# IV. CHAPTER

---

## 4.1 Occupational exposure conditions during TMS treatment: methods and modeling

In this chapter<sup>142</sup>, it is considered the exposure of a TMS operator to two kinds of commercial coils: the Magstim MAG-9925-00 standard double (simply called the figure-of-eight) and the Magstim MAG-9784-00 circular coil. TMS pulses were assimilated to pure sinusoids at equivalent frequencies, as aforementioned. The features of the TMS devices here considered are listed in Table III-7. As before mentioned, the coils were reproduced in the simulation environment as dimensionless wires placed at the center of the real wires<sup>35,143</sup>. This implied a 2D coil approximation that may slightly underestimate the induced E-field, but as reported, the overall error was detected as below to 2%<sup>35,144</sup>

To model the presence of the operator, we considered an anatomical human body model, Duke, a standard young adult male (34-year-old, 1.77 m, 70.2 kg), member of the Virtual Population (ViP., v.3.0)<sup>145</sup>. Duke is a surface-based model obtained from the MRI scans of a healthy volunteer and it has 319 different body structures. Additionally, we considered aposable Duke (ViP., v.3.1<sup>145</sup>), which allows for changes in body posture, in order to reproduce also the real position of the worker that grips the handle of the coil. The dielectric properties of the tissues were assigned from LF IT'IS database v.4<sup>146</sup> embedded in Sim4Life (software chosen for the simulations, see above paragraph 3.1).

Furthermore, the dosimetric analysis included the patient's head, modeled by the simplified two-tissue head phantom Sam (IEEE Standards Coordinating Committee 34, Sub Committee 2, Working Group 1 - SCC34/SC2/WG1), available in Sim4life. This phantom consisted of two compartments, shell, and liquid, with conductivities of 0.01 S/m and 0.33 S/m<sup>147</sup> respectively. The phantom was placed approximately 1 cm below the surface of the coil and positioned at the center of the simulation domain. By considering the patient's head, we ensured the representation of a realistic scenario, with the TMS coil properly coupled.

However, it is beyond the aim of this study to analyze the EM quantities induced inside the patient's head.

To consider the exposure of the operator's anatomical districts previously identified (Figure III.16), four vertical positions of the TMS coils were chosen, with different distances  $h$  from the ground and they are denoted, as before stated, as cases A, B, C, and D (Figure IV.1).

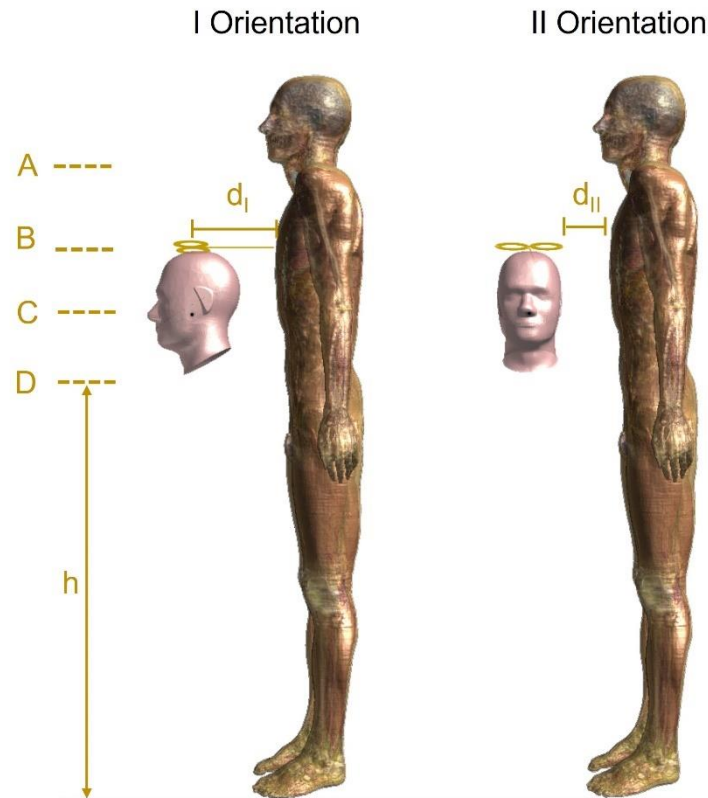


Figure IV. 1 The dosimetric model. Two coil orientations (I and II) and four vertical positions: case A-exposure of the chin/neck ( $h_1 = 153.5$  cm), case B-exposure of the chest ( $h_2 = 136$  cm), case C-exposure of the abdomen ( $h_3 = 112$  cm), case D- exposure of the lower abdomen ( $h_4 = 95.3$  cm). For orientation I, the distance between the center of the coil and the surface of the clinician's body model ( $d_I$ ) is 21 cm, whereas for orientation II, the distance between the edge of the coil and the surface of the clinician's body  $d_{II}$  is 12 cm.

Additionally, two different orientations of the ensemble coil/Sam were considered for each vertical position, as shown in Figure IV.1. For orientation I, the model of the clinician is placed behind the coil handle (coil angular positions  $0^\circ$ ) and a distance of 21 cm is kept constant between the center of the coil and the surface of the clinician's body model. This distance considers the 20.5 cm length of the coil's handle, plus 0.5 cm as the closest possible distance between the handle edge and the surface of the human model. For orientation II, the clinician's body model is placed on the side of the coil (coil angular position  $90^\circ$ ) at a



distance of 12 cm from the extremity of the outermost coil winding to consider the length of the forearm. Both distances are considered with respect to the surface of the Duke's body. In addition, is important to highlight that these two distances take into account different considerations. In particular:

- The classification of the work environments made from company user manuals, websites, and papers allowed us to consider such distances  $d_{II}$  as reasonable;
- The conclusions of the study by Rutherford et al.<sup>147</sup>, which finds a distance of 12.3 cm from the torso in which the limits are exceeded;
- The length of the forearm when the arm is kept bent at 90 ° attached to the torso, where this value is considered equal to about 12 cm.
- Conversely, the choice of 21 cm from the coil center ( $d_I$ ), considered in orientation I, corresponds to a minimum possible distance (i.e., 0.5 cm) from the coil handle, which is 20.5 cm long, as reported in <sup>87</sup>; this value is as well found from company user manuals, websites, papers and also in the real work environment during measurements campaigns.

Moreover, as suggested by the 2010 ICNIRP guidelines, at low frequencies, 20 cm is the maximum distance from a source, to keep the exposure localized. The ICNIRP 2010 guidelines states in fact: *“For a very localized source with a distance of a few centimeters from the body, the only realistic option for the exposure assessment is to determine dosimetrically the induced electric field, case by case. When the distance exceeds 20 cm, the distribution of the field becomes less localized but is still non-uniform, in which case it is possible to determine the spatial average along the body or part of it <sup>148, 149</sup>.”*

A summary of the analyzed conditions is presented in Table IV-1.

**Table IV - 1. Exposure conditions**

	<b>I Orientation</b>	<b>II Orientation</b>
<i>Coil angular positions</i>	0°	90°
<i>Distance of surface of Duke (d)</i>	21 cm <i>From the center of coil</i>	12 cm <i>From coil windings edge</i>
<i>Vertical position (h)</i>	A, B, C, D	A, B, C, D

All the exposure conditions were numerically simulated for the two coil models of Magstim for a total of 16 positions. Additionally, we reproduced the clinician while holding the figure-of-eight TMS coil, which was implemented by arranging the arm and hand of the Duke model using the Poser tool embedded in Sim4life. In this latter case, the dosimetric analysis mainly focused on the hand of the human model, as it is the anatomical district closer than the others to the source. We evaluated both closed (Figure IV.2 (b)) and open hand (Figure IV.2 (c)) conditions, considering distance  $d$  between the outermost coil winding and the thumb (Figure IV.2 (a)) as follows:

1. Closed hand, with distance from coil  $d = 5$  cm;
2. Open hand, with distance from coil  $d = 5$  cm;
3. Open hand, with distance from coil  $d = 2.5$  cm;

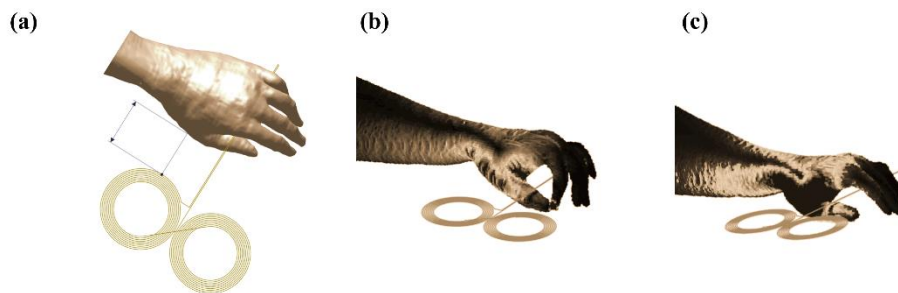


Figure IV. 2. Explanatory image of the exposure conditions of the hand. (a) distance considered, (b) closed hand, (c) open hand.

The Duke model was discretized with a uniform step of 2 mm along the three Cartesian directions, which corresponded to approximately 73 MCells. To estimate the induced E-field, produced by the TMS, inside the operator, we could not automatically exclude the use at 100% of MSO, because the stimulator output of the coils can be different between treatments. Therefore, it was necessary to consider other values for the identification of the motor stimulation threshold<sup>150</sup> for single patients, which requires different output power from the generator. As aforementioned, the coils are typically used with a percentage of MSO<sup>151</sup> in a range of 30% to 80%, values with which it was considered to conduct the

dosimetric analysis, jointly with the 100% (maximum output), starting from the features of the Magstim coils listed in Table III-7. To assess compliance with the ICNIRP 2010 guidelines, for each coil configuration, we compared the 99<sup>th</sup> percentile of the E-field induced inside the Duke model with the limits reported in Table II-2. Since these limits are frequency dependent, for the occupational exposure at the frequency of work of the coils, is fixed at  $\sim 1.13$  V/m (peak value). Furthermore, for both orientations, after finding the worst-case exposure condition, it is evaluated the distance at which the induced E-field decreased below these limits. To obtain these data, we performed further simulations, in which the human model was slowly moved away from the source, gradually increasing the distance. Herein, we refer to the ICNIRP 2010 Guidelines and not to the 2020 update, as the changes referred to the EMF frequency range between 100 kHz and 10 MHz are not considered.

## 4.2 Results of the analysis of risk for male clinician performing the TMS treatments

First, we evaluated the streamline of the B-field produced by the two TMS coils. The flux expanded in the free space and through the clinician's body, as shown in Figure IV.3 for the two coils placed at the level of the abdomen (case C) and oriented according to orientation II. Notably, both simulation domains had the same dimensions and the same spatial resolution for a better comparison of the extent of the exposure.

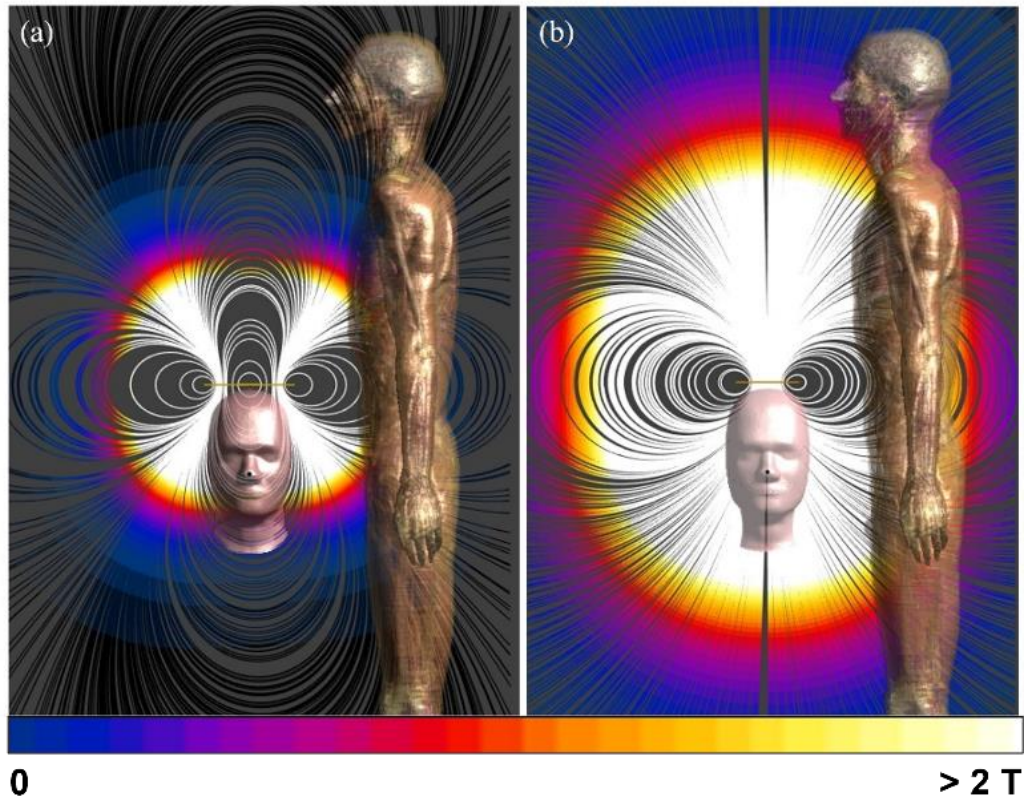


Figure IV. 3. Streamline distribution map at a simulation output of 100%. Worst case exposure of: (a) Std. Double coil 9925-00, Magstim, (b) circular coil 9784-00, Magstim.

As expected, the B-field distribution generated by the circular coils (Figure IV.3 (b)) differs from that generated by the figure-of-eight because the latter remains confined in a smaller region (Figure IV.3 (a)). This is because the figure-of-eight coil has a better focality inside the patient's head, compared to the circular one, whose generated B-field is characterized by a greater dispersion. At this point, the focus shifts to what occurs within the human model exposed to this B-field that spreads in the environment occupied by the operator. Therefore, in Figures IV.4 and IV.5, the induced E-field distributions inside the operator's body are reported for the two Magstim coils placed at each exposure scenario described in Figure IV.1. In particular, the results from orientation I are presented in Figure IV.4, and those from orientation II are presented in Figure IV.5. In both cases, the feeding condition at MSO of 50% was considered. The two figures show the induced E-field on the Duke's sagittal plane, passing through the center of the coil, and the maximum full-scale value was set as the limit suggested by the ICNIRP 2010 guidelines, that is 1.3 V/m at 3 kHz.

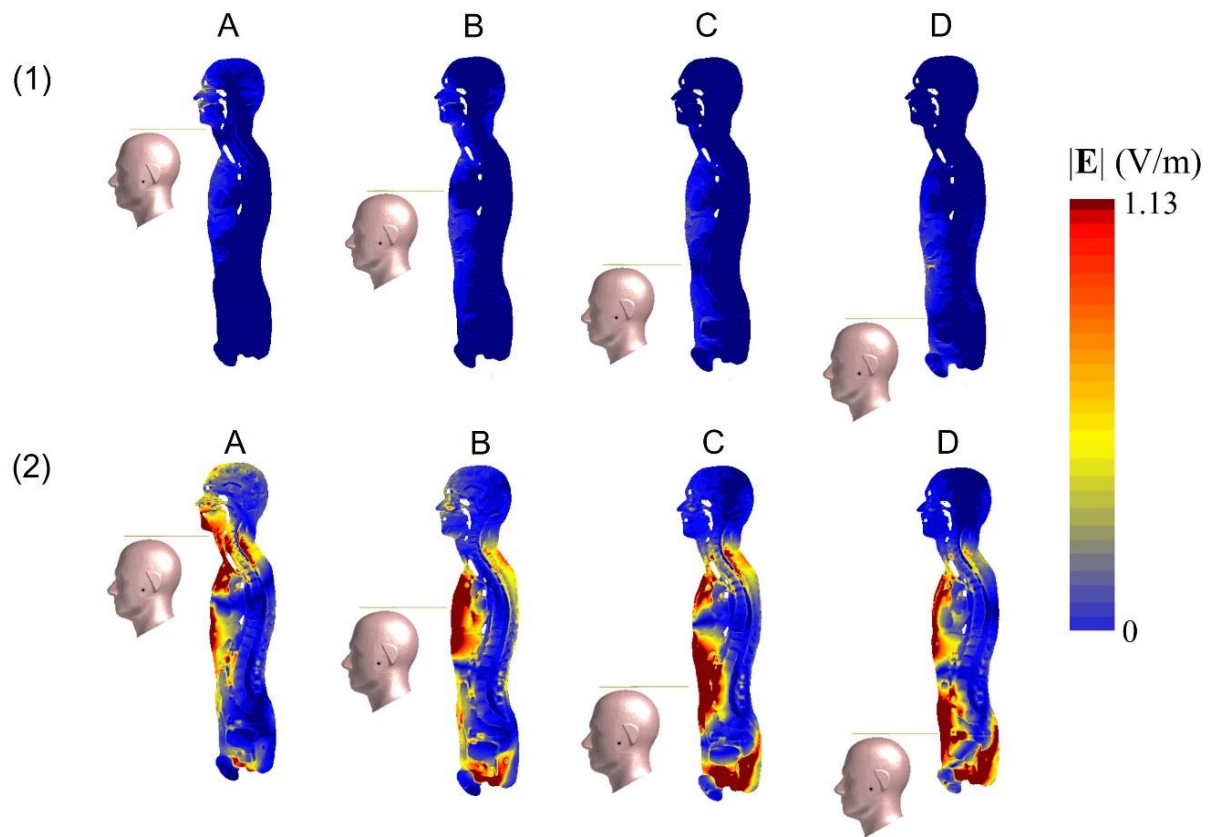


Figure IV. 4. E-field map at 50% of the maximum output for orientation I: (1) Exposure to the Double coil 9925-00 in the four cases, A-B-C-D; (2) Exposure to the Circular coil 9784-00 in the four cases, A-B-C-D.

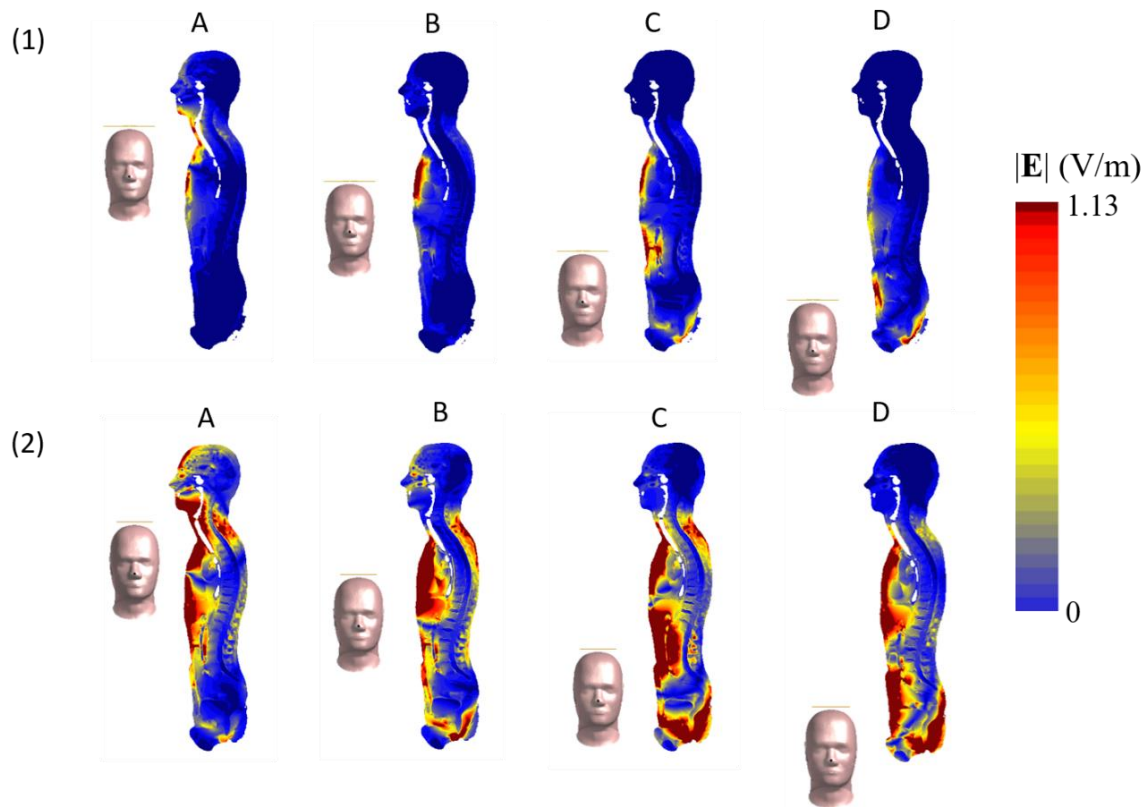


Figure IV. 5. E-field map at 50% of the maximum output for orientation II: (1) Exposure to the Double coil 9925-00 in the four cases, A-B-C-D; (2) Exposure to the Circular coil 9784-00 in the four cases, A-B-C-D.

In all conditions shown in Figures IV.4 and IV.5, the circular coil caused higher values of induced E-field in the human body, compared to the figure-of-eight. The mapping of the induced E-field shows that in most conditions, a large area of the body is affected by non-negligible E-fields. For instance, during the exposure of the abdomen to the figure-of-eight at orientation II (Figure IV.5, panel 1-C), the volume of the tissue in which the induced E-field exceeded the limit of 1.13 V/m is 0.12% of the total body, whereas it is 15% during the exposure to the circular coil. For all the scenarios, the exposure to intensities above the ICNIRP limit mainly involved the front of the operator, and some for which this condition reached the back of the model (e.g., Figure IV.4, panel 2 cases A-B-C-D and Figure IV.5, panel 1 cases C-D and panel 2 cases A-B-C-D). Considering the exposure to the figure-of-eight placed in position C and oriented according to orientation II (Figure IV.5, panel 1-C), the E-field induced on the back, at the hip joint reaches a maximum value of 1 V/m, even if in a small area. A more widespread exposure of the back to E-field intensities above 1.13 V/m occurs with the circular coil. Nevertheless, when placed as in case B and orientation II,

the E-field induced behind the neck is up to 0.9 V/m. Table IV-2 and Table IV-3 summarize the levels of exposure for orientations I and II respectively. For each of these, we reported the induced E-field in the case of a MSO of 30% and in the worst case of MSO of 100%. The comparison is also between the two models of coils: circular MAG-9784-00 and Std. Double MAG-9925-00.

**Table IV - 2. Orientation I - percentiles of detected induced E-field (V/m) as a function of %MSO**

	%MSO	Chin/neck (A)		Chest (B)		Abdomen (C)		Lower abdomen (D)	
		30%	100%	30%	100%	30%	100%	30%	100%
<i>Std. Double coil (MAG-9925-00)</i>	<b>99<sup>th</sup></b>	0.08	0.27	0.07	0.25	0.08	0.26	0.09	0.31
	99.9 <sup>th</sup>	0.15	0.50	0.12	0.38	0.13	0.43	0.16	0.53
<i>Circular coil MAG-9784-00</i>	<b>99<sup>th</sup></b>	1.13	3.77	1.21	4.01	1.30	4.34	1.51	<b>5.02</b>
	99.9 <sup>th</sup>	2.13	7.09	2.18	7.28	2.34	7.81	2.78	9.27

**Table IV - 3. Orientation II - percentiles of detected induced E-field (V/m) as a function of %MSO**

	%MSO	Chin/neck (A)		Chest (B)		Abdomen (C)		Lower abdomen (D)	
		30%	100%	30%	100%	30%	100%	30%	100%
<i>Std. Double coil MAG-9925-00</i>	<b>99<sup>th</sup></b>	0.33	1.11	0.31	1.04	0.40	1.34	0.38	1.26
	99.9 <sup>th</sup>	0.62	2.07	0.55	1.85	0.72	2.41	0.76	2.54
<i>Circular coil MAG-9784-00</i>	<b>99<sup>th</sup></b>	1.80	6.00	1.80	6.01	2.19	<b>7.32</b>	2.01	6.71
	99.9 <sup>th</sup>	3.44	11.48	3.01	12.87	4.00	13.33	3.91	11.73

The results indicated that the exposure to circular coil caused a 99<sup>th</sup> percentile of induced E-field that exceeded the ICNIRP limits of 1.13 V/m in all the conditions, whereas only two cases show values exceeding the guidelines for the figure-of-eight coil, i.e., C (abdomen) and D (lower abdomen), for orientation II.

Therefore, by addressing the critical conditions that could expose the operator to an induced E-field above the ICNIRP limits, the safety distances between the operator and the coil that would guarantee exposure below the limit at our working frequency were evaluated. Figures IV.6 and IV.7 show the data for the circular coil placed in the two worst-case scenarios: case- D in the orientation I and case- C in orientation II. For these cases, we evaluated the 99<sup>th</sup> percentile as a function of the distance for each considered percentage of the stimulator output<sup>50</sup>. The results are presented in Figures IV.6 and IV.7 for orientations I and II, respectively.

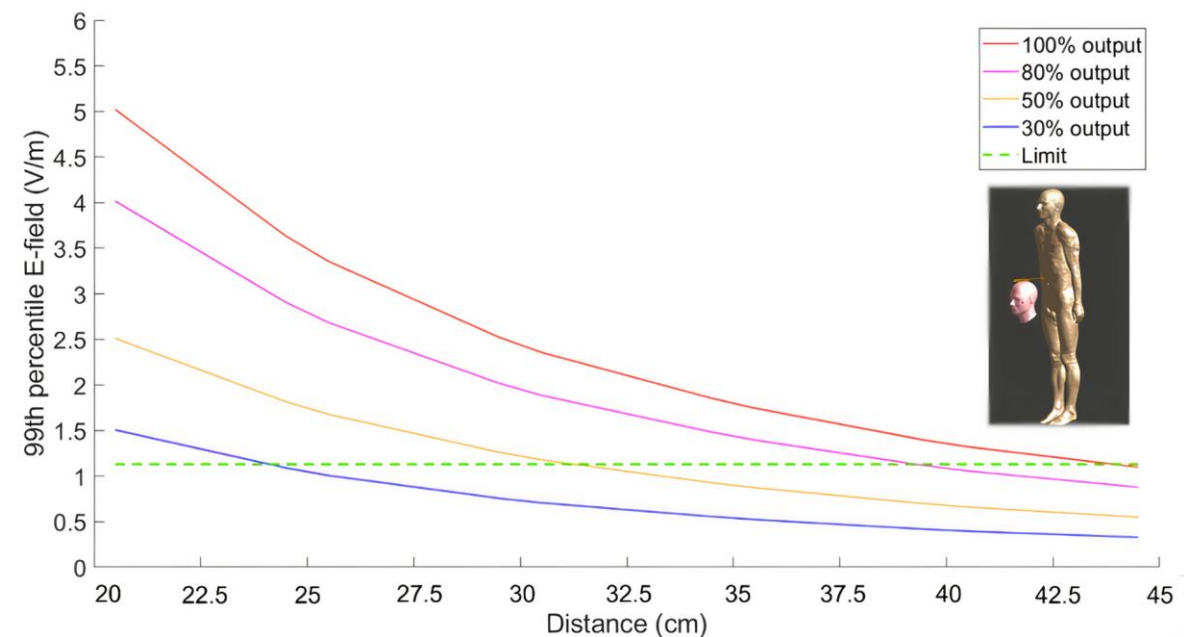


Figure IV. 6. 99<sup>th</sup> percentile of induced E-field for case D - lower abdomen (worst case scenario in orientation I owing to exposure to circular coil Magstim 9784-00) as a function of the distance from the center of the coil.



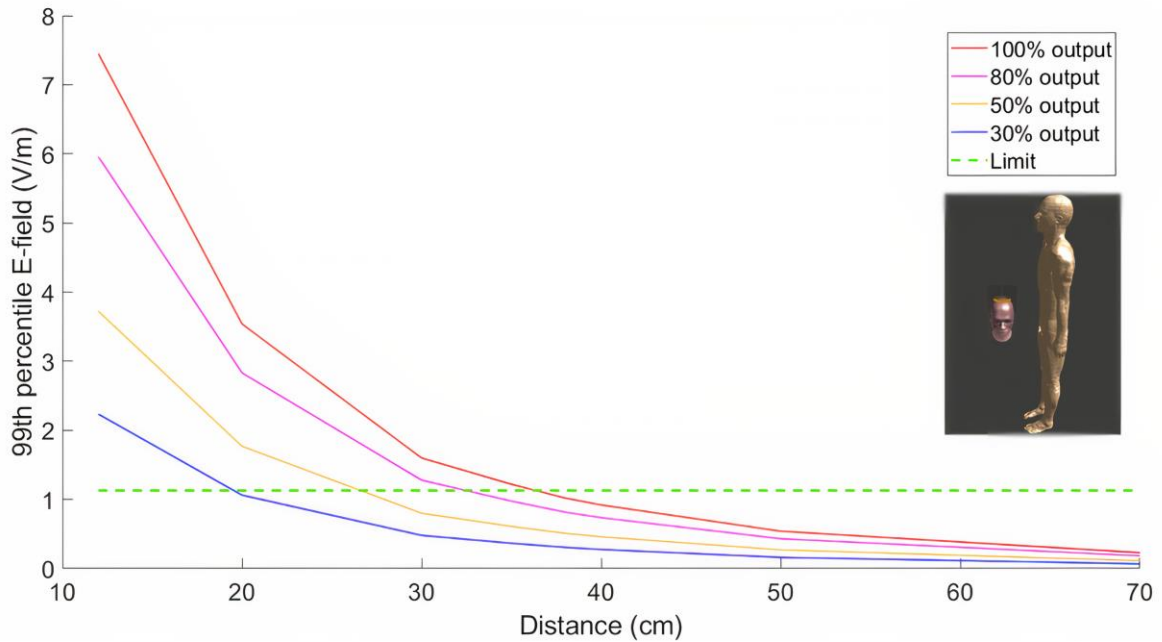


Figure IV.7. 99<sup>th</sup> percentile of induced E-field for case C - abdomen (worst case scenario in orientation II owing to exposure to circular coil Magstim 9784-00) as a function of the distance from the coil windings edge.

Generally, the induced E-field decreased as the distance increased and the stimulator's percentage of output decreased. Therefore, the possibility of exceeding the E-field limit could be considerably reduced when the operator stays at specific distances from the coil, which gradually increases as a function of the stimulator output. Considering exposure to the figure-of-eight coil, the induced E-field exceeds 1.13 V/m only in cases C and D of orientation II at a MSO of 100% (Table IV-3). In the worst-case scenario (i.e., case C), we established that the induced E-field decreases to 0.91 V/m at a distance of 15 cm, indicating that the exposure limits are respected if the coil is moved 3 cm away from the reference position (i.e., 12 cm from the edge of the coil). Conversely, a compliant scenario for the circular coil fed for MSO of 100% is obtained at 38 cm from the edge of the coil in orientation II (Figure IV.7, red line), or at approximately 44 cm from the center of the coil in the orientation I (Figure IV.6, red line). These distances can be reduced by feeding the coil with a lower %MSO, reaching values down to 19.8 cm and 24 cm for MSO of 30% for orientation II (Figure IV.7, blue curve) and orientation I (Figure IV.6, blue curve), respectively. From these data, it is confirmed that the circular coil herein considered remains the most "critical" device, and the distance that the clinician must keep avoiding the overcoming of the limits

during a TMS treatment is more than twice the distance that should be maintained with the figure-of-eight coil. It is also possible to consider a comparison between these two worst cases detected. In Figure IV.8, are reported the safe distances as a function of the %MSO. In red is reported the case shown in Figure IV.6 (exposure of lower abdomen, worst case for orientation I), while in blue is reported the case of Figure IV.7 (exposure of abdomen, worst case for orientation II)

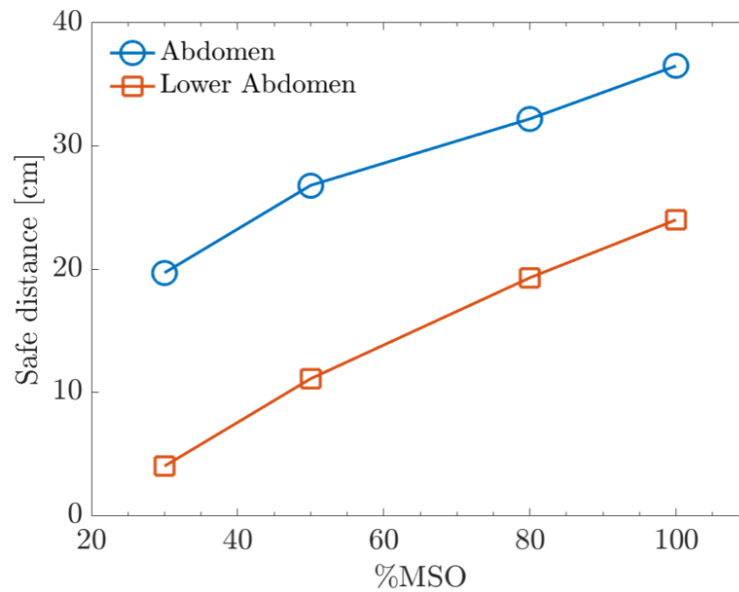


Figure IV. 8. Safe distances as a function of the MSO%. Red line the lower abdomen exposure in the I orientation; blue line the abdomen exposure in II orientation.

Since the worst case, it is fully noted in orientation II, for this exposure condition, it is chosen to compare the induced E-field caused by the exposure to the Magstim circular coils, with the exposure caused by the MC125 circular coil. This latter was not considered, since geometrically and also as power system (current and frequency) it is almost analogous to the Magstim circular coil. However, in order to take into account the other characterized coil, results are reported in the orientation II at 50% MSO caused by MC125 coil powered by MagPro30 (Figure IV.9):

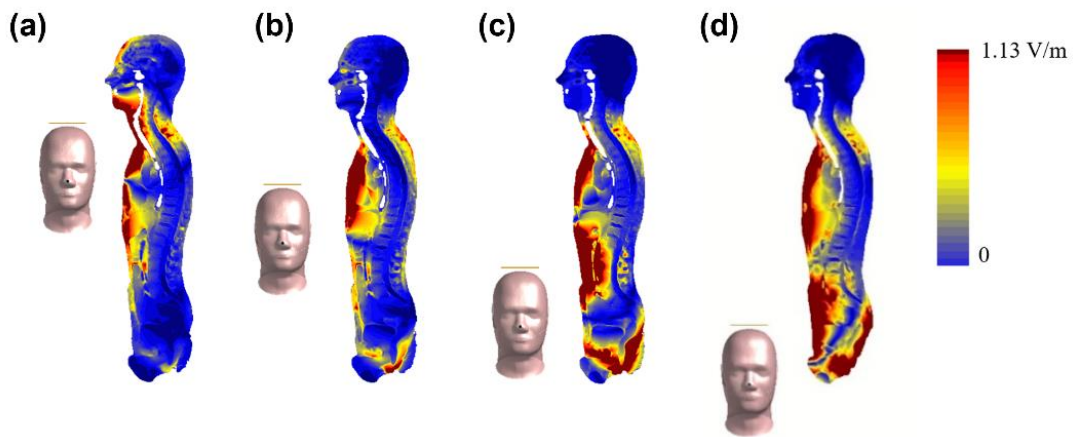


Figure IV. 9. Induced E-field map at 50% of the maximum output for orientation II. Coil placed in correspondence to: (a) chin/neck- case A, (b) chest- case B, (c) abdomen- case C, (d) lower abdomen -case D.

The MC-125 coil behaves similarly to the circular Magstim. The slight differences are, for example, due to the differences in geometry. The induced electric field generated inside the clinician’s body by the three coil models, in these four positions for orientation II, is shown in Figure IV.9 and is compared in terms of the 99<sup>th</sup> percentile, for different percentages of stimulator output, as reported in Table IV-4.

**Table IV - 4.** The 99<sup>th</sup> percentiles of induced E-field (V/m)

	Chin/neck		Chest		Abdomen		Lower abdomen	
%MSO	30%	100%	30%	100%	30%	100%	30%	100%
<i>Magstim figure-of-eight</i>	0.33	1.11	0.312	1.04	0.402	<b>1.34</b>	0.38	1.26
<i>Magstim circular</i>	1.80	6	1.8	6.01	2.19	<b>7.32</b>	2.01	6.71
<i>MagVenture circular coil MC-125</i>	1.19	3.98	1.13	3.77	1.58	<b>5.26</b>	1.31	4.38

As it can be seen, the magnetic field generated by the MagVenture MC125 induces an E-field estimated as the 99<sup>th</sup> percentile, which is comparable to those induced by the Magstim coils, in particular by the circular model. It should be noted that the MagVenture MC-125 coil works at a frequency of 3.45 kHz, at which the limit (BRs) suggested by ICNIRP 2010<sup>13</sup> for the occupational exposure, is 0.93 V/m (rms), i.e. 1.31 V/m (peak). Thus, in this case, as well, the induced E-field is far above the limit suggested by the ICNIRP 2010 guidelines, confirming that circular models expose the clinician to a more critical condition than exposure with a figure-of-eight. This is due to the different distribution of the magnetic field produced by this model of the TMS source, strongly dependent on the model.

For a complete analysis of the exposure scenario, a focus on the limb positioned close to the source, is carried out, in order to deepen the investigation on the E-field induced in the hand by simulating the condition of the operator that holds the TMS coil. In this case the exposure to the Std. Double MAG-9925-00 has been considered since it is the most frequently used device for long-lasting treatments (i.e., repetitive (r) TMS protocol). As described in paragraph 4.1, two configurations have been considered: i) the case of Duke holding the coil with a slightly open hand at two distances between the thumb and the outermost winding (2.5 cm and 5 cm, Figure IV.10 (a)), ii) the case of a closed hand at a distance of 5 cm. The distribution of the induced E-field on the surface of this area of the body is shown in Figure IV.10 (b) and (c) for the closed hand at 5 cm and open hand at 2.5 cm, respectively.

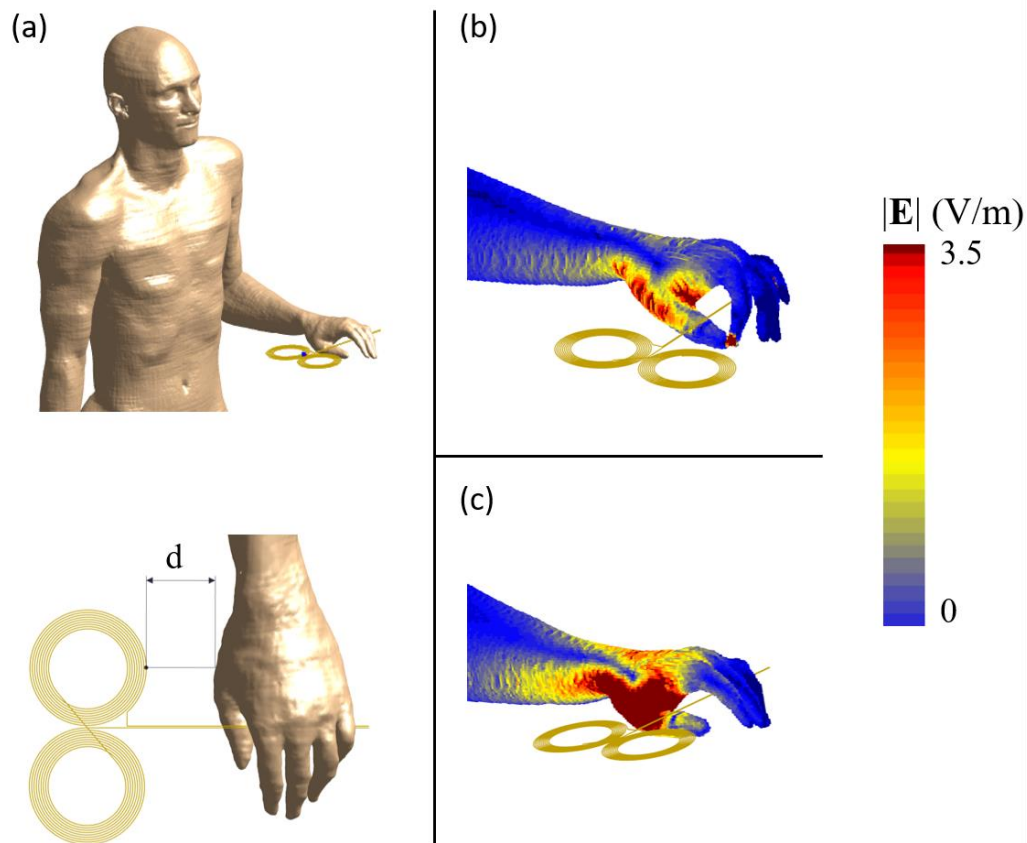


Figure IV. 10. Exposure condition: (a) On the top the human model of the Duke posable model, on the bottom the illustration of hand's distance  $d$ ; (b) E-field induced on the surface of the closed hand 5 cm from coil edge; (c) E-field induced on the surface of the open hand 2.5 cm from coil edge.

It is evident that the proximity to the source caused a non-negligible induced E-field in the thumb muscles, which is very evident for example in (c), where the open hand is much closer to the source than in all other cases. Furthermore, as shown in Figure IV.10 (b), for the closed hand, a peak of the E-field is induced at the contact between the thumb and index finger, suggesting that the type of grip affected the extent of the area exposed to non-compliant intensities. Table IV-5 summarizes the percentiles of the electric field distribution on the hand area to estimate the maximum values induced in the three conditions investigated in this study.

**Table IV - 5. Percentiles of the Induced E-field (V/m) in the operator's hand as a function of percentage of stimulator output**

		30%	50%	80%	100%
<b>Closed hand</b> <i>*d = 5 cm</i>	99 <sup>th</sup>	0.85	1.43	2.28	2.85
	99.9 <sup>th</sup>	1.03	1.71	2.74	3.42
	99.99 <sup>th</sup>	1.2	2	3.20	4.01
<b>Open hand</b> <i>*d = 5 cm</i>	99 <sup>th</sup>	0.9	1.5	2.4	3
	99.9 <sup>th</sup>	1.11	1.85	2.96	3.7
	99.99 <sup>th</sup>	1.23	2.06	3.3	4.12
<b>Open hand</b> <i>*d = 2.5 cm</i>	99 <sup>th</sup>	2.22	3.69	5.91	7.02
	99.9 <sup>th</sup>	3.01	5.03	8.04	10.06
	99.99 <sup>th</sup>	3.44	5.74	9.19	11.49

*\*d: distance between the coil edge and the hand, as shown in Figure IV.10 (a).*

To estimate the maximum value, we computed the percentile up to 99.99<sup>th</sup> because the area of interest was reduced to the hand only and lower values of percentiles (as the 99<sup>th</sup> percentile) may not be completely representative of the exposure because of the presence of local spikes. In fact, one of these local spikes occurs at the point of contact between the two fingers and is well detected by the 99.99<sup>th</sup> percentile to be 4 V/m in the case of maximum stimulator output. This is in accordance with how stated in Chapter II, considering the results of some research studies<sup>104,105</sup>, in which, in order to reduce numerical errors affecting the 100<sup>th</sup> percentile and to improve the underestimation relative to the 99<sup>th</sup> percentile, it was chosen to evaluate also the 99.9<sup>th</sup> percentile, since it is reasonable that this is the value that should be used for the assessment of exposure, especially in the condition here analyzed. An analysis of how the induced E-field depends on the percentile is, therefore, shown in comparison metric of dose reported in Figure IV.11, in the case of 50% MSO.

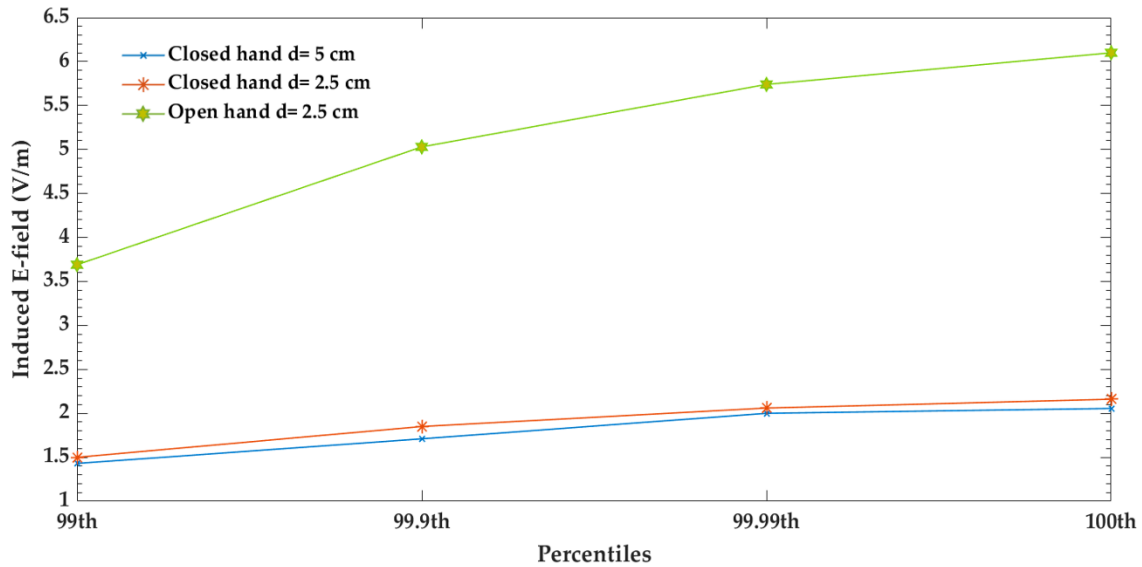


Figure IV. 11 Dose metric of the exposure in hand district.

Figure IV.11 shows how the extent of exposure could depend closely on the percentiles considered. In the case of this condition of local exposure, in which percentiles are evaluated only in the district of the hand, to exclude an underestimation of exposure, it is important to also consider the other percentiles, and not just the 99<sup>th</sup> percentile. The percentiles above 99<sup>th</sup> represent in these cases local peaks of the induced E-field, which should thus not be ignored.

In general, considering maximum output, for the closed hand, a 99<sup>th</sup> percentile of induced E-field in the hollow between the thumb and the forefinger of approximately 3.89 V/m (or 1.6 V/m with 30% of stimulator output) is achieved, whereas 3.5 V/m (or 1.05 V/m, at 30%) is achieved on the surface of the thumb. In the second case (open hand at 5 cm), in the hollow between the thumb and the forefinger, we evaluate the E-field that achieved 4.5 V/m (or 2.25 V/m, at 30%) and 4 V/m (or 1.2 V/m, at 30%). However, the surface of the thumb is characterized by a large area where 3.5 V/m (or 1.05 V/m, at 30%) is obtained. The last case (open hand at 2.5 cm) is characterized by an induced E-field peak equal to 12 V/m (or 3.6 V/m, at 30%) on the surface of the thumb, whereas we detected 10.5 V/m (or 3.15 V/m, at 30%) in the mentioned hollow between the fingers. These data indicate non-compliance with the corresponding limits suggested by the guidelines. These results may suggest the need for targeted interventions that can reduce the risk of exposure. Such as, for example, the use

of a stick on which to fix the coil (so that the operator remains at a distance) and, in conditions where the operator is forced to hold the coil, the introduction of a specific insulating material for each coil model that could limit exposure.

Finally, another induced quantity of equal importance has been considered: the induced current density. As a matter of fact, the exposure of the human body to the time-varying magnetic fields also results in the induction of a current density inside the human body. Our results indicated that such exposure may cause a non-negligible induced current density, as shown in Figure IV.12, which illustrates two exposure conditions: case A (exposure of the chin/neck) for orientation I and case C (exposure of the abdomen) for orientation II.

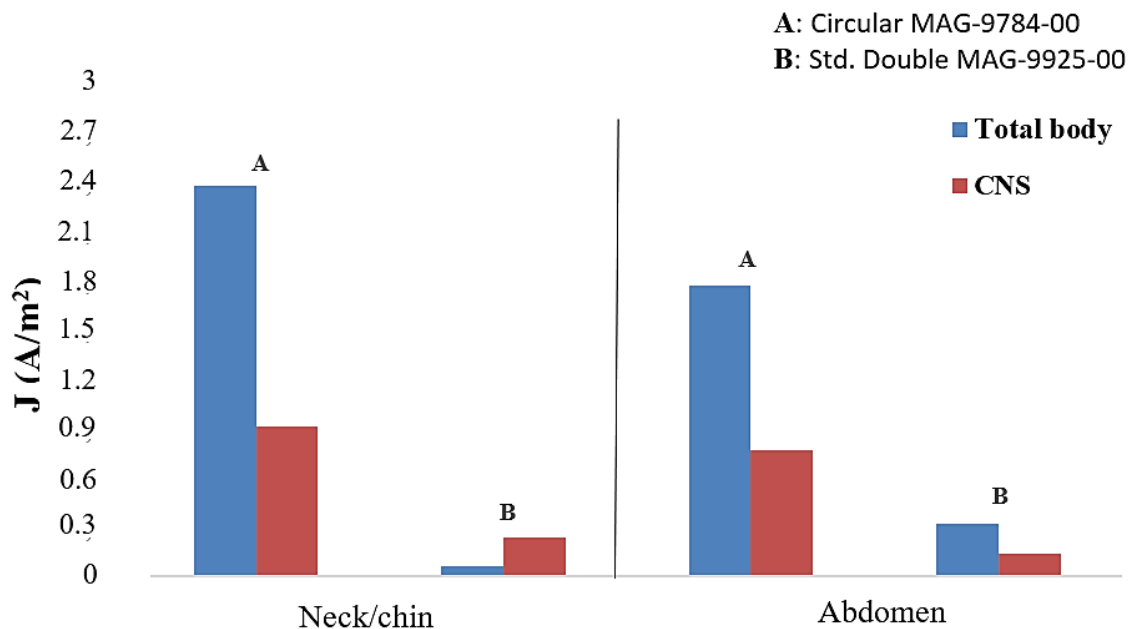


Figure IV. 12. Bar graph representing the 99th percentile of the current density induced in the whole body (blue) and in the Central Nervous System CNS only (red) by the circular coil (A) and the figure-of-eight coil (B) for two cases of exposure: neck/chin (case-A orientation I) and the abdomen (case-C orientation II).

The graph shows that the exposure to the magnetic field produced by Std. Double MAG-9925-00 causes a lower induced current density in the CNS than that caused by the circular MAG-9784-00. Furthermore, in all the evaluated exposure scenarios, J induced inside the CNS was lower than that induced in the whole body, except for the exposure of the chin/neck to the figure-of-eight coil, where a greater J is induced in the CNS with respect to the whole body.



### 4.3 Discussion of the results

In this chapter, a systematic numerical assessment of the operators' exposure to the EMF produced by a TMS was performed to rigorously investigate the risks for occupational health associated with TMS applications. The need for comprehensive studies on the operators' exposure to TMS arises from the lack of a standardized methodology for the conformity assessment of occupational exposure. Over the past decades, few computational studies have investigated this aspect and provided suggestions regarding the safety distance that the operator should maintain from the TMS coil. In 2010, Lu et al.<sup>152</sup> performed a dosimetric evaluation of the clinician exposure to a circular and a figure-of-eight coil, which resulted in a safety distance of 110 cm for both coils, oriented with their surface parallel to the surface of the chest, as would be done during a cerebellar TMS<sup>153</sup>. Furthermore, the exposure to different angular positions of the two coils was investigated. However, a cross analysis between angle and distance was not conducted, and the safety distance was estimated only in the aforementioned position, which is not commonly considered in clinical practice. A similar analysis was conducted in a more recent study by Bottauscio et al. 2016<sup>43</sup>, where they investigated the exposure of the clinician to a circular coil. The coil was placed at three heights from the ground (i.e., at the level of the chest, neck, and eyes), and it was evaluated in the same angular positions for each height, as in Lu et al., 2010<sup>152</sup>. Lu et al., 2010<sup>152</sup> computed the safety distance for all rotations of the coil. Furthermore, they proposed the use of a passive shield to reduce the safety distance between the operator and the coil from 64 to 38 cm. In both the aforementioned studies, the evaluation of the safety distance was limited to the coil placed at the level of the chest<sup>43,152</sup>, and some exposure scenarios evaluated were far from real ones, such as case #C (coil at the level of the eyes) in Bottauscio et al., 2016<sup>43</sup>. Generally, the different anatomical regions that might be exposed during TMS treatment depend on whether the patient is sitting or lying down and on the relative height between the patient and the clinician. Hence, in the previous chapter, it is conducted a review to common exposure scenarios to identify the positions generally assumed by the clinician while performing TMS treatment. In addition to the exposure of the chest, considered both in Lu et al. (2010<sup>21</sup>) and Bottauscio et al. (2016<sup>22</sup>),

and of the chin/neck considered only in Bottauscio et al., 2016<sup>22</sup>, we evaluated exposure of the abdomen and lower abdomen, thus conducting an in-depth analysis.

In all four exposure scenarios, we aimed to compare the behavior of two widely used types of coils (i.e., circular and figure-of-eight) placed along two different angular orientations with respect to the clinician's body. Further, because the exposure to a variable magnetic field, produced by TMS devices shows a strong reliance on the percentage of the stimulator output (%MSO), it was necessary to evaluate ways in which the operator exposure changed with different %MSO. Thus, in addition to the maximum stimulator output (%MSO=100%), we considered 30%, 50%, and 80%, while the literature studies considered exposure solely to the maximum stimulator output (100%)<sup>43,152</sup>. This can lead to conservative conclusions, given that TMS treatments are typically conducted at 50% of the stimulator output, and lower (30%) or higher (80%) stimulation intensities can be considered for research purposes<sup>150,151</sup>. Our results at 100% were consistent with the previous literature, particularly with those from Bottauscio et al., 2016<sup>43</sup>, where the 99<sup>th</sup> percentile of the induced E-field at the closest distance between the center of the coil and the operator body axis (i.e., 30 cm) was up to 4 V/m when the axis of the operator body and the axis of the coil are parallel. In similar conditions (i.e., circular coil at the level of the chest – case B, orientation I), an induced E-field of 4.01 V/m was found inside the operator's body at a distance of 21 cm between the center of the coil and the surface of the operator's body. From the investigation of the exposure of other body parts with respect to Bottauscio et al., 2016<sup>43</sup>, we estimated that the 99<sup>th</sup> percentile of the E-field above the limit suggested by the ICNIRP 2010 guidelines (1.13 V/m) occurred in all exposure conditions with the circular coil, and the highest value was induced with the coil placed at the level of the abdomen in orientation II (i.e. 7.32 V/m). For the latter our condition (case-C, orientation II), the safety distance was estimated as 38 cm (distance between the edge of the coil and body surface), which is closer than the distance estimated in Bottauscio et al., 2016<sup>43</sup>. This difference can be attributed to the different geometrical characteristics of the simulated coils, as can be observed by comparing Table III-7 with their Table I<sup>43</sup>. For the exposure to the figure-of-eight, the 99<sup>th</sup> percentile of the E-field never exceeds the ICNIRP limits in orientation I, whereas it

exceeded in cases C and D of orientation II, which are cases that were not investigated in the previous works<sup>43,152</sup>.

The dependence of the exposure from the MSO% has also been considered. As previously stated, all the discussed literature studies evaluated TMS exposure with the operator working at 100% of the stimulator output. Nevertheless, as shown in TMS clinical and research studies<sup>150,151</sup>, this treatment is usually adopted at lower stimulator outputs. Our results indicated that not only the choice of the TMS coil but also the selected stimulator output significantly affected the extent of the exposure. Notably, the percentage of machine output is chosen based on the TMS treatment; hence, the distance between the clinician's body and the coil is the principal quantity that should be varied to guarantee compliance with the guideline limits. Based on this, we evaluated the 99<sup>th</sup> percentile of the induced E-field with increasing distances between the source (i.e., TMS coil) and the body of the human model under %MSO other than 100% (i.e., 30%, 50%, and 80%). This analysis was conducted for the worst-case scenario of each coil orientation, that is, circular coil in case D (i.e., the lower abdomen) for orientation I (Figure IV.6) and case C (i.e., the abdomen) for orientation II (Figure IV.7). For the latter case, the induced E-field can be made compliant to the limits by moving the operator approximately 38 cm away from the edge of the source, if working at the maximum output or approximately 19.8 cm when working at 30% of the stimulator output. Conversely, under our investigated conditions, a stimulator output of 80% ensures that the electric field induced by the figure-of-eight coil is compliant with the guidelines in all the cases studied. It should be emphasized that these distances are obtained from dosimetric quantities, and not from environmental measurements because this study aimed to estimate the EM quantities induced inside the clinician's body, rather than providing indications regarding the zoning of the work environment (as explained in Chapter II). This analysis of operator exposure aims to make the worker aware of any possible risk while performing the treatment, as the quantities found are not negligible. It is revealed a considerably different behavior between the two coils, and we established that the circular coil induced an electric field greater than the figure-of-eight under the same exposure conditions, which is consistent with previous studies at the 100% stimulator output<sup>43,152</sup>.

Finally, to compare the two coils further, the fraction of body volume exposed to E-field over the guidelines limit was calculated. It was observed that in typical TMS working conditions of %MSO = 50%, the E-field above 1.13 V/m was induced in a small fraction of the body (0.12% of total body volume) by the figure-of-eight coil and in a larger fraction (15% of total body volume) by the circular coil. As a reference, it should be noted that the heart volume is equal to almost 0.85% of the total body for this male model of a standard man, Duke. Therefore, according to these results, the type of coil entails different general safe indications, depending on its angular orientation and the part of the body exposed. It is estimated that in orientation I, the figure-of-eight coil induces an E-field below the ICNIRP limits for all the stimulator output, even at the closest distance from the coil (Figure IV.4, Table IV-2). Conversely, in some cases studied for orientation II, the induced E-field exceeded the limits suggested by ICNIRP 2010, when considering both the circular and the figure-of-eight coil (see Figure IV.5 and Table IV-3). This implies that each treatment deserves specific attention.

Another important issue concerning operator exposure is the proximity of the upper limb to the source. Because the clinician often holds the handle of the TMS device without using any mechanical tools to maintain position, hence it is important to evaluate the exposure of this area of the body. Furthermore, after analyzing real working scenarios, it emerged that the operator may often hold the applicator during a TMS treatment. Thus, for a more realistic numerical analysis, we focused on reproducing a realistic configuration of the hand. Here, we excluded works that do not consider anthropomorphic virtual body models<sup>147,154</sup>, only one study that considered the operator with bent arm holding the coil was found in literature<sup>154</sup>. However, the influence of the hand aperture on exposure assessment was not investigated. Our results indicated that grip affected the exposure intensity. When the coil is held with the hand closed (i.e., touching the thumb and the index finger), the induced E-field is higher compared to when the coil is held with a slightly open hand, and it focuses on the tips of the two fingers (as a hot spot). We considered two distances to take into account the possibility of grabbing the coil with two hands, which would cause the hand to be closer to the coil, as well as the case in which the operator grabs the handle with only one

hand but closer to the source. Considering the 99<sup>th</sup> percentile of the internal E-field, we demonstrated that for a distance of 5 cm (for both configurations of the hand: open and closed), the compliance is achieved at 30% of the maximum output, indicating that the exposure of the hand can also be in compliance with the guidelines without the use of mechanical tools. For the case of the hand closer to the coil (2.5 cm from windings), the safety limits were exceeded at all the evaluated percentages of the stimulator outputs. As shown for the exposure of the total body, the distance increases when the output power increases. When considering the exposure focused on the hand, the maximum distance allowed is limited by the length of the coil handle, which may be too short and prevent respecting the ICNIRP limits (as well as the limits established by Directive 2013/35/EU<sup>1</sup>). Therefore, the aspect concerning auxiliary handpieces or insulating protection sleeves should be investigated in future analysis. As regards the methods to improve safety in the workplace, being pending the publication of relevant technical standards indicating, if any, which methods in the TMS use can guarantee the safety of the operator even if the limits for health effects are exceeded, similarly to the case of MRI equipment, the reduction of exposure levels can be achieved using, if medical practice allows, a plastic rod provided by the manufacturer to keep the applicator in place. This mode could effectively distance the operator from the applicator and result in compliance with the limits of the induced E-field. Finally, to elucidate the different exposure scenarios evaluated, the induced current density was studied (Figure IV.12), as it was done in the study by Lu and Ueno, 2010<sup>152</sup>, which addressed the issue of the internal currents in the body of the clinician, because they referred to the 1998 ICNIRP guidelines<sup>91</sup>. Their results indicated that the commercial figure-of-eight has less leakage magnetic field and a lower current density induced in the operator's body compared with the circular coil, as confirmed in our study. Furthermore, they established that at a distance of 70 cm, the current density induced by exposure to the figure-of-eight coil and the circular coil averaged in 1 cm<sup>2</sup> of CNS tissue were 13.9 mA/m<sup>2</sup> (or 19.2 mA/m<sup>2</sup> without simulating the cable, i.e. coil only) and 33.9 mA/m<sup>2</sup> (or 25.6 mA/m<sup>2</sup> without cable)<sup>152</sup>. Compliance with the ICNIRP 1998 BRs occurred at a distance of 110 cm for both coils. Although the induced current density is no longer a quantity considered for the exposure

compliance, it still provides a quantitative indication of what occurs inside the body of the clinician performing the treatments. Moreover,  $J$  ( $A/m^2$ ) is not negligible in our study as well, where the peak of the induced current density at the minimum distance of 12 cm between the body and the circular coil was  $2.37 A/m^2$  and  $0.9 A/m^2$ , considering the total body and the CNS exposure only, respectively (Figure IV.12). To better understand these values, they can be compared with the limits suggested by ICNIRP 1998<sup>91</sup>, set at 3 kHz a maximum acceptable induced current equal to  $0.04 A/m^2$  (peak) for occupational exposure.

## 4.4 Conclusions

A simulation-based safety assessment of operator exposure to three models of commercial coils was conducted to investigate the induced E-field and compare it with the limits suggested by the ICNIRP 2010 guidelines. The analysis demonstrated that during a TMS treatment, several factors can influence the exposure of the clinician, such as the type of coil, its vertical position, and orientation with respect to the clinician the stimulator output intensity, as well as the position and the degree of the aperture of the hand of the operator performing the TMS. In particular, the results of this study indicated that the circular coil induces a higher induced E-field with respect to the figure-of-eight coil owing to its geometric configuration that caused a greater dispersion of the magnetic field and resulted in exceeding the guideline limits in a higher number of configurations. For each exposure scenario, we conducted a whole-body analysis and evaluated the minimum distance allowed to maintain the induced E-field levels below the ICNIRP 2010 limits. Furthermore, we focused on the local exposure of the hand, and the results indicated that to reduce the induced E-field on the area of the hand, one should avoid holding the coil too close to the turns as well as holding it with a tightly closed hand. In this exposure assessment, a thorough analysis of different exposure scenarios of clinicians to TMS sources is reported, and a systematic numerical assessment of compliance with the ICNIRP 2010 guidelines was conducted, considering both the whole body and local exposure. However, the results of the dosimetry assessment presented in this analysis are specific to the exposure scenario

examined and therefore cannot be extended to all the practices performed with the TMS. Even they cannot extend to female exposure, if for example, we consider the female operator, since we consider that the anatomical characteristics could influence the extent of the exposure. Although a comprehensive risk analysis is beyond the scope of this analysis, the results obtained provide useful insights for future risk assessment studies.

# V. CHAPTER

---

## 5.1 Exposure gender-dependent: possible differences in risk assessment between male and female operator

The results obtained in the previous chapter open another important question regarding the possibility that the gender specificity can be decisive in EM exposure. In particular, the anatomical characteristics that differentiate a female subject from a male may have a significant role in the level of exposure. Among these, it is necessary to consider the shape of the body, the height (typically smaller in females than in human males), the presence of adipose tissues in body positions other than those in human males, and also the presence of the breast (which means a presence of gland and subcutaneous fat in the chest), that could be eventually directly exposed to the source, for example, if it is considered the exposure of the operator with the coil at the height of the chest (case-B, see chapter III and also Figure IV.1). The possibility that the final EM exposure and thus the assessment of the risk may be different starts from some results found in the literature. A study conducted by S. Gallucci et al. 2022<sup>55</sup> shows that a difference in terms of exposure response exists owing to gender although in a different frequency band; in this study, a numerical assessment of the risk of human exposure to RF-EMFs (2.45 GHz) emitted by a wearable antenna is executed. Results show how the value of SAR depends on gender, which means that the anatomy of the models could impact on the exposure. In particular, they obtained that when the antenna is posed on the arm, leg and shoulder, the exposure is much higher for the male model (Duke) than for the female one (Ella). They reported + 28% for the case of the shoulder, + 110.9% for the leg, and + 75.9% for the arm's case. These results lead the authors to state that a possible reason for the increase in the Duke's values is the greater amount of muscle compared to the female model, indeed, in the muscle tissue, higher values of SAR<sub>10g</sub> have been detected, unlike in the female model. An opposite situation occurs when the antenna is posed on the chest, in this case, the exposure resulted higher in Ella than in Duke (+8.1%), owing doubtless to the anatomical differences of the female model. Another study conducted by



A. Hirata et al. 2009<sup>155</sup>, examined the induced E-field and the current density (J) inside the Japanese human male and female models: Taro and Hanako respectively<sup>156</sup>. The paper aims to discuss the effect of gender and race on the induced quantities produced by an extremely low-frequency (ELF) uniform magnetic field exposure. The male model was 1.72 m tall and weighed 65 kg, while the female model is 1.6 m tall and 53 kg. In order to obtain the induced quantities, a computational analysis is made by using the QS FDT methods<sup>157</sup>. The exposure conditions consist of three orientations of the magnetic fields at 50 Hz. What is found is that the induced E-field in the male model was greater by 25% than those in the female model, and the authors assume that the reason is that the circumference of the male model is larger than that of the female. The same conclusions are achieved by A. Hirata et al. 2009 comparing their results with those of Dimbylow et al. 2000<sup>18</sup>, in which a study on European models is conducted. The female European model compared to the Japanese female model, show higher values of the induced E-field, and the reason, for A. Hirata et al., is again in the larger circumference of the European models compared to the Japanese. Although the differences strongly depend on the source (frequency of work, position, typology of field that spreads in the environment, etc.), from these results found in the literature, it is clear that the body characteristics (as for example the circumference), as well as the gender, could influence the assessment of the exposure. Therefore, to analyze the possible differences that could occur also with our source of interest (TMS), between the male (Duke) and female (Ella) models, a computational comparison dosimetry is carried out.

## 5.2 Assessment of gender exposure to TMS: comparison of the results

To obtain a comparative study, the same exposure conditions, analyzed in Chapter IV for the Duke model, are here considered for the female one (see Figure IV.1). As a guide, also, in this case, the human female model, represents the operator that performs the TMS treatment in standing position close to the patient. Therefore, the same exposure orientations and the same sources are here considered. Ella is a young adult female model

(26 years old, 1.63 m, 57.3 kg), that belongs to the member of the virtual population (ViP)<sup>23</sup>. Ella is a surface-based model obtained from the MRI scans of a healthy volunteer and she counts 312 different body structures<sup>158</sup>. To consider the same exposure conditions of the operator, previously identified (see Figure III.16 and Figure IV.1), and to obtain a comparison of the results between the male and female models, the exposure is set as following:

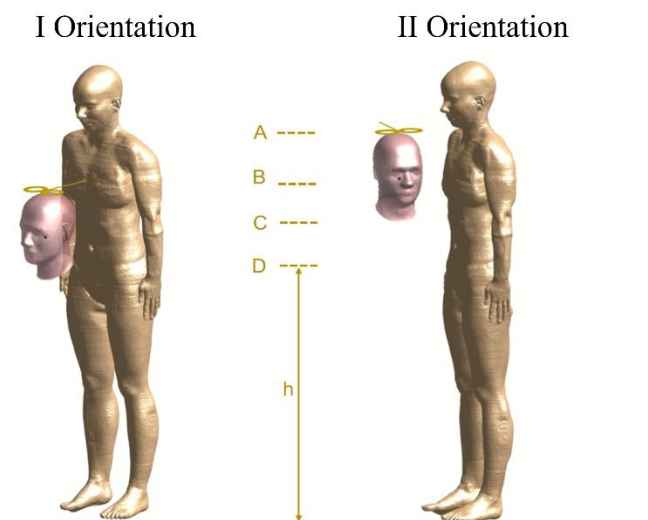


Figure V. 1. The exposure conditions. Two coil orientations (I and II) and four vertical positions: case A-exposure of the chin/neck ( $h_1 = 141.3$  cm), case B-exposure of the chest ( $h_2 = 125$  cm), case C-exposure of the abdomen ( $h_3 = 103$  cm), case D- exposure of the lower abdomen ( $h_4 = 87.7$  cm). For orientation I, the distance between the center of the coil and the surface of the clinician's body model is 21 cm, whereas, for orientation II, the distance between the edge of the coil and the surface of the clinician's body is 12 cm (as previously defined).

As can be seen from Figure V.1, the main differences occur in the coil's heights in reference to the ground, this is because the height of Ella is different from Duke and thus, the heights at which the coil needs to be positioned have been properly scaled. Conversely, the orientations and the distances of the operator with respect to the source, are the same reported in Table IV-1, defined for Duke.

As previously done, also in the case of Ella exposure, the sources used for the assessment of the risk are the Std. Double coil 9925-00 (figure-of-eight) and the circular coil Magstim 9784-00 (circular). Features are summarized in previous Table III – 7.

Since from the results obtained by the assessment of the exposure with the Duke model the exposure to the circular coil in orientation II results in the worst case, here, first of all, we evaluated the streamline of the B-field produced by the circular coil in orientation II, in the case in which the coil position involves the chest districts of the body models (case B). This choice considers the main difference that occurs between the male and female subjects. The B-field distribution in the free space and through the clinician's body is shown for the circular coil placed at the level of the chest (case B) and oriented according to the orientation II, in Figure V.2. As previously done, also, in this case, both simulation domains had the same dimensions and the same spatial resolution for a better comparison of the extent of the exposure.

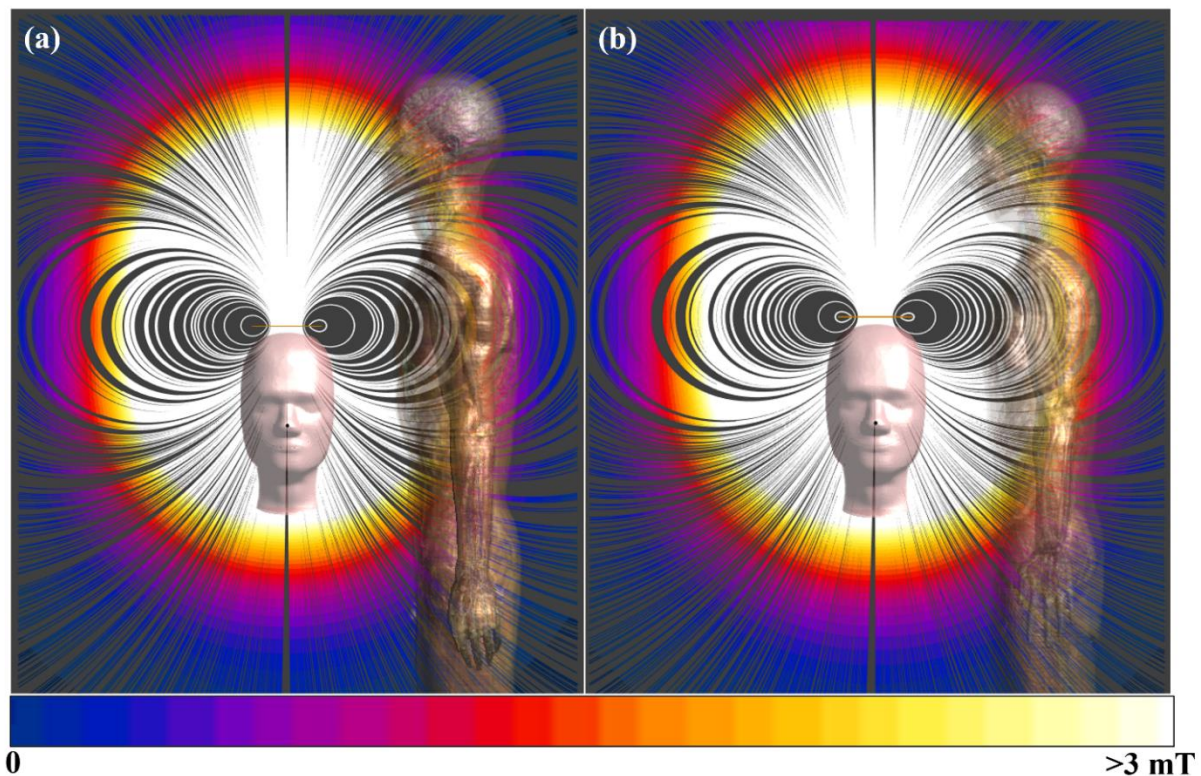


Figure V. 2. Streamline distribution with 100% MSO. Exposure case B (chest) produced by circular coil 9784-00, Magstim. (a) Duke male model, (b) Ella female model.

As it can be seen, the generated B-field is characterized by a great dispersion, since this is the typical behavior of the circular coil model. It is interesting to observe the differences in the way the B-field influences the two subjects. Although the B-field that spreads in the

environment is the same, the anatomical characteristics of the models mean that how the field invades the body is different. For example, the Ella's more curved back seems to cause a greater exposure in the head area, and in general, her more little shape means that the field involves the body differently than in Duke. Certain anatomical zones in Ella are reached by higher B-field values than in Duke, e.g., looking at the back, in Ella we have shades of red, while in Duke we have shades of blue. The percentiles of the induced E-field (inside the female operator), owing to the exposure to figure-of-eight and the circular coil, for the orientations I and II respectively, are evaluated. These results, (as done in chapter IV in Table IV-2 and -3 for Duke), are reported in the following Tables V-1 and -2:

**Table V - 1. Orientation I - percentiles of detected induced E-field (V/m) in Ella as a function of %MSO**

	%MSO	Chin/neck (A)		Chest (B)		Abdomen (C)		Lower abdomen (D)	
		30%	100%	30%	100%	30%	100%	30%	100%
		<i>Double coil</i> (MAG-9925-00)	99 <sup>th</sup>	0.12	0.40	0.07	0.25	0.08	0.27
	99.9 <sup>th</sup>	0.24	0.80	0.11	0.38	0.12	0.41	0.13	0.44
<i>Circular coil</i> MAG-9784-00	99 <sup>th</sup>	1.54	5.13	1.28	4.28	1.37	4.59	1.33	4.46
	99.9 <sup>th</sup>	2.47	8.26	2.04	6.80	2.29	7.63	2.14	7.15

**Table V - 2. Orientation II - percentiles of detected induced E-field (V/m) in Ella as a function of %MSO**

	%MSO	Chin/neck (A)		Chest (B)		Abdomen (C)		Lower abdomen (D)	
		30%	100%	30%	100%	30%	100%	30%	100%
		<i>Double coil</i> (MAG-9925-00)	99 <sup>th</sup>	0.49	1.63	0.32	1.09	0.41	1.35
	99.9 <sup>th</sup>	0.81	2.68	0.53	1.78	0.67	2.25	0.61	2.04
<i>Circular coil</i> MAG-9784-00	99 <sup>th</sup>	2.45	8.18	1.84	6.14	2.02	6.72	1.76	5.86
	99.9 <sup>th</sup>	3.93	13.13	2.95	9.83	3.33	11.11	2.86	9.54

As a first observation, only in three case the limit is exceed when the subject model is exposed to the figure-of-eight, and only in the orientation II at 100% MSO, similar at what occurs in Duke exposure. Moreover, comparing the results of these Tables, referring to Ella, with those of Chapter IV referring to Duke (Table IV-2 and -3), is obtained that in case of exposure to the circular coil, in both orientations I and II, the cases A and B present an induced E-field is slightly higher in Ella than Duke. In particular, in Ella, the percentiles in the case A are +26% (orientation I) and +26.6% (orientation II); while in the case B the values are +3.5% (orientation I) and +7.32% (orientation II). Similar behavior occurs in the case of the exposure to the figure-of-eight, wherein in all the cases the percentiles of the induced E-field are lower in Ella than Duke, except for case A for both orientations I and II, in which the induced E-field is +32.5%, in the orientation I, and +31.9 in orientation II, higher in Ella.

Except for these cases, in all the others the percentiles of induced E-field are lower in Ella than in Duke. What is obtained is in line with the literature, where overall, the induced quantities evaluated in female model were lower than in male one, with the exception of the chest exposure, where also in S. Gallucci et al. 2022 it is found a higher value in Ella (case A not considered in S. Gallucci et al.). However, this trend of lower values of the induced quantities in female model, we suppose cannot be valid in all exposure conditions, since, the results are strongly dependent on the type of source considered (geometry, frequency of work, orientation and so on), and also on the anatomical factors (not only the circumference of the body), as for example the electrical properties of the tissues and moreover the inter-variability of the subject, that mean intrinsic difference in the body structures. It is not a coincidence that in case A, in which Ella has a particular body characteristic (curvature), the resulting electric field is higher than in the male case.

For what concerns the circular coil, the induced E-field exceeds the suggested limits in all cases of exposure, even considering the 30% MSO. From the evaluated percentiles of the induced E-field, it can be detected the worst cases of exposure of Ella, that occurs in the orientation II caused by the circular coil, as happened for Duke's exposure. Therefore, a

comparison of the distribution of the induced E-field due to the circular coil in Orientation II at 50% MSO between Ella and Duke, is reported in Figure V.3:

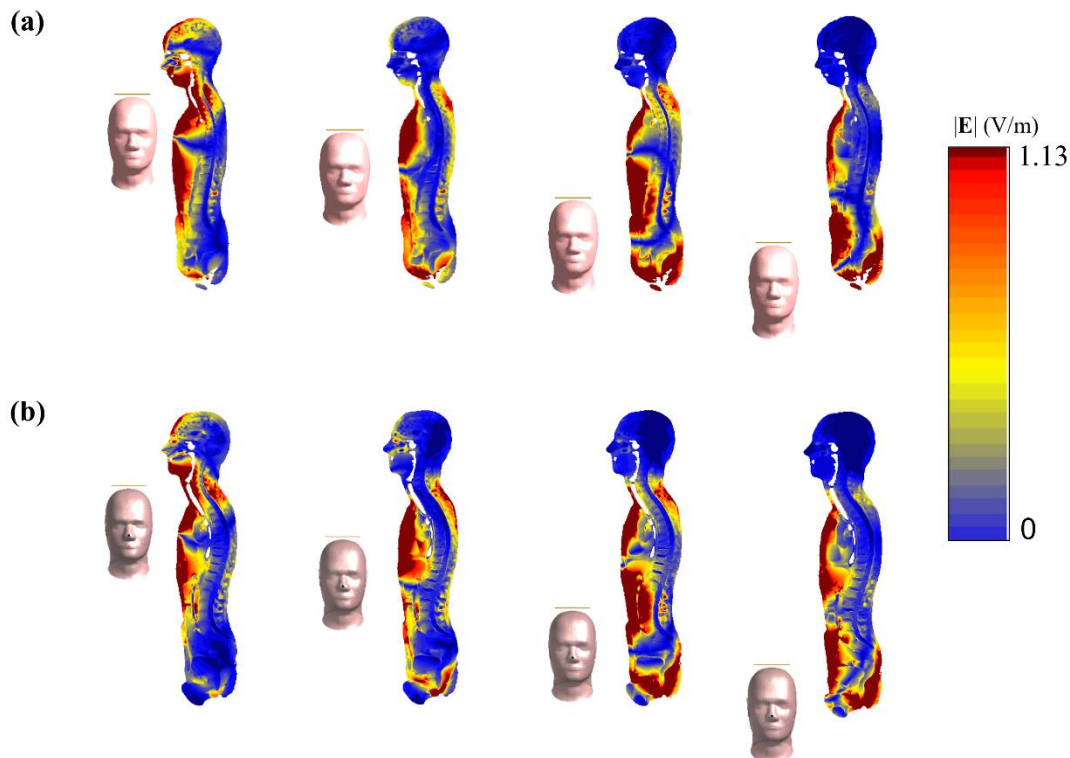


Figure V. 3. E-field map at 50% MSO for orientation II: (a) Exposure of Ella to circular coil 9784-00 in the four cases, A-B-C-D; (2) Exposure of Duke to the Circular coil 9784-00 in the four cases, A-B-C-D. The maximum color bar is set to the limit suggested by ICNIRP guidelines.

As we can observe, also in the case of Ella, the regions of the body interested by an induced E-field that exceeds the limit are not negligible. It is interesting to note the differences between the two models in cases A and B of exposure (as obtained from the calculated percentiles). In case A, the head of Ella is much more invaded by the induced E-field (i.e., intense red of the color bar). Whereas in case B, it is possible to note that a more defined region of intense red is present in the region of the breast of Ella, while in Duke the intense red involves a larger area of the chest, as if the characteristic of Ella's chest played a role not to be overlooked. Cases C and D seem to be sufficiently similar. For a direct understanding of the extent of the exposure, owing to the circular coil, Table V-3 summarizes the comparison of the percentiles of the induced E-field, for the cases A-B-C-D in orientation II (i.e., for the cases reported in

Figure V.3), for both human models. The evaluated percentiles refer to the 30% of stimulator output and to the maximum output (100%).

**Table V - 3. Orientation II – percentiles Induced E-Field (V/m) -exposure to a circular coil**

		<b>Chin/neck (A)</b>		<b>Chest (B)</b>		<b>Abdomen (C)</b>		<b>Lower abdomen (D)</b>	
<i>%MSO</i>		30%	100%	30%	100%	30%	100%	30%	100%
<i>Ella</i>	<b>99<sup>th</sup></b>	2.45	8.18	1.84	6.14	2.02	6.72	1.76	5.86
	99.9 <sup>th</sup>	3.93	13.13	2.95	9.83	3.33	11.11	2.86	9.54
<i>Duke</i>	<b>99<sup>th</sup></b>	1.80	6.00	1.80	6.01	2.19	7.32	2.01	6.71
	99.9 <sup>th</sup>	3.44	11.48	3.01	12.87	4.00	13.33	3.91	11.73

From these results, it can be noted that the worst cases exposure for Ella are different from those that occurs in Duke. Indeed, the induced E-field in Ella is lower than in Duke in the two cases of exposure of the abdomen and lower abdomen (that previously were the worst cases for Duke), while in cases A and B the induced quantity is higher in Ella than in Duke, as such was observed from the distribution of the induced E-field in Figure V.3.

In addition, for further deepening the analysis of the possible gender differences, it is considered the comparison of what occurs in specific districts of the bodies of the two operators exposed to the TMS source. Based on the obtained results, three conditions are more important to be compare than the others: case A, B and C in orientation II, exposed to the circular coil. This is because:

- Case A, represents the worst case in the Ella assessment of the exposure;
- Case B, refers to an important anatomical district of the female model, that therefore needs to be compared;
- Case C, represent the worst case in the Duke assessment of the exposure.

Following these steps, the comparison of the induced E-field in specific tissues, for the exposure in case A due to the circular coil in orientation II, is provided:

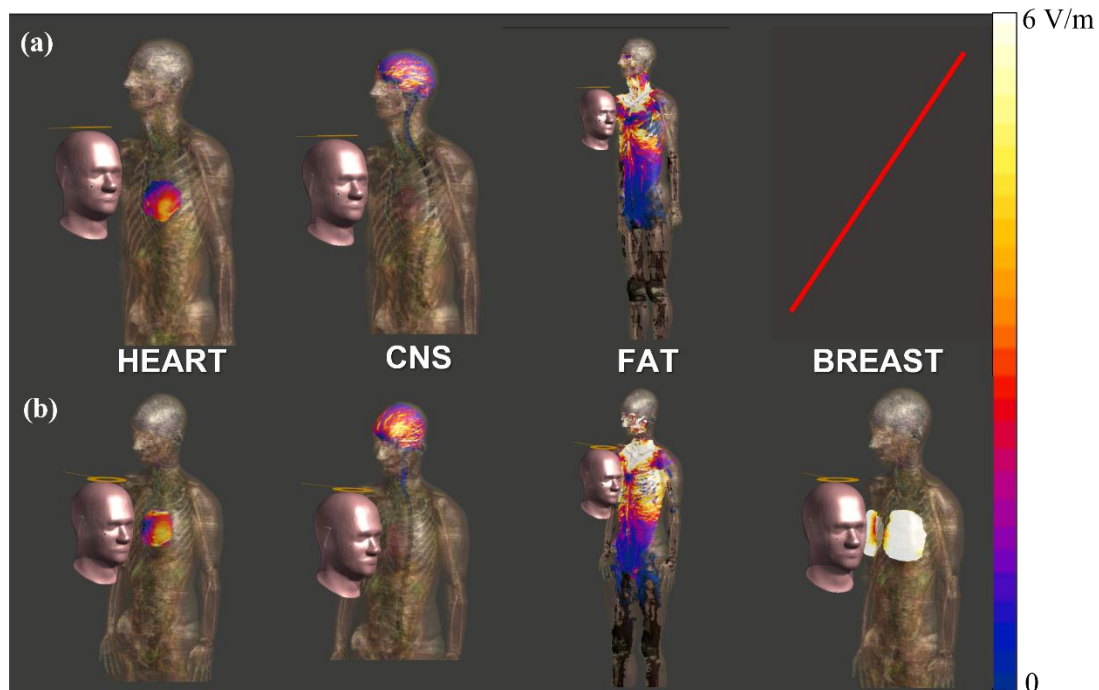


Figure V. 4. Exposure to the circular coil, orientation II, in the A (chin/neck). Electric field distribution in body tissues at 100%MSO (a) Duke, (b) Ella.

Figure V.4 helps us in understanding the extent to which the field distributes in tissues, which can be overlooked by focusing solely on percentiles. Starting from the heart, the distribution shows to be very different in the two subject models, since in Duke is present a larger area with blue color with respect to Ella, in which in turns is present a larger area with the yellow color of the bar. This behavior shows how the same tissue can behave differently, despite being exposed to the same source. This is because the heart intrinsically differs from subject to subject (bigger, more rotated, more inclined, and so on), and the same for example occurs in the fat, because of the different amount. Then, by directly observing the distribution of the induced E-field in the CNS tissue of the two models, it is confirmed that the exposure of the head of Ella is higher than in Duke. Indeed, what occurs in the tissues of the CNS is quite clear to justify what we found by the percentiles evaluated in the total body exposure. Of paramount importance is what occurs in the breast tissues; it can be seen that the entire tissue is uniformly affected by a high field value. Clearly, this does not appear in the Duke model where the tissue is absent. Table V.4 reports the percentiles evaluated in the considered tissues up to the 100<sup>th</sup>. In fact, in smaller regions the higher



percentiles could figure out the local hot spot (as it is observed in the case of local exposure of the limb of Duke reported in Table IV.5).

*Table V - 4. Percentiles of the Induced E-field (V/m) in the tissues*

	<b>Duke</b>				<b>Ella</b>			
	<i>Fat</i>	<i>Heart</i>	<i>CNS</i>	<i>Breast</i>	<i>Fat</i>	<i>Heart</i>	<i>CNS</i>	<i>Breast</i>
<b>99<sup>th</sup></b>	9.87	3.62	4.32	/	10.34	4.57	5.66	8.86
99.9 <sup>th</sup>	14.68	4.23	5.68	/	14.65	6.15	7.91	9.70
99.99 <sup>th</sup>	18.75	4.76	6.90	/	18.28	7.15	10.39	11.17
100 <sup>th</sup>	25.61	5.10	9.38	/	24.02	7.71	13.54	13.75

The local results of the above table, confirm that in this exposure condition (case A), Ella shows a higher induced E-field compared to Duke, that widely exceeds the suggested limits in all the tissues considered.

Finally, since the case B represents a region of crucial importance for female exposure, a deepening analysis of this region is carried out. In particular, to reveal possible difference in the distribution of E-field in the region of the chest, a local study in two slices of the body models is evaluated (Figure V.5), referring to the exposure to the circular coil in Orientation II.

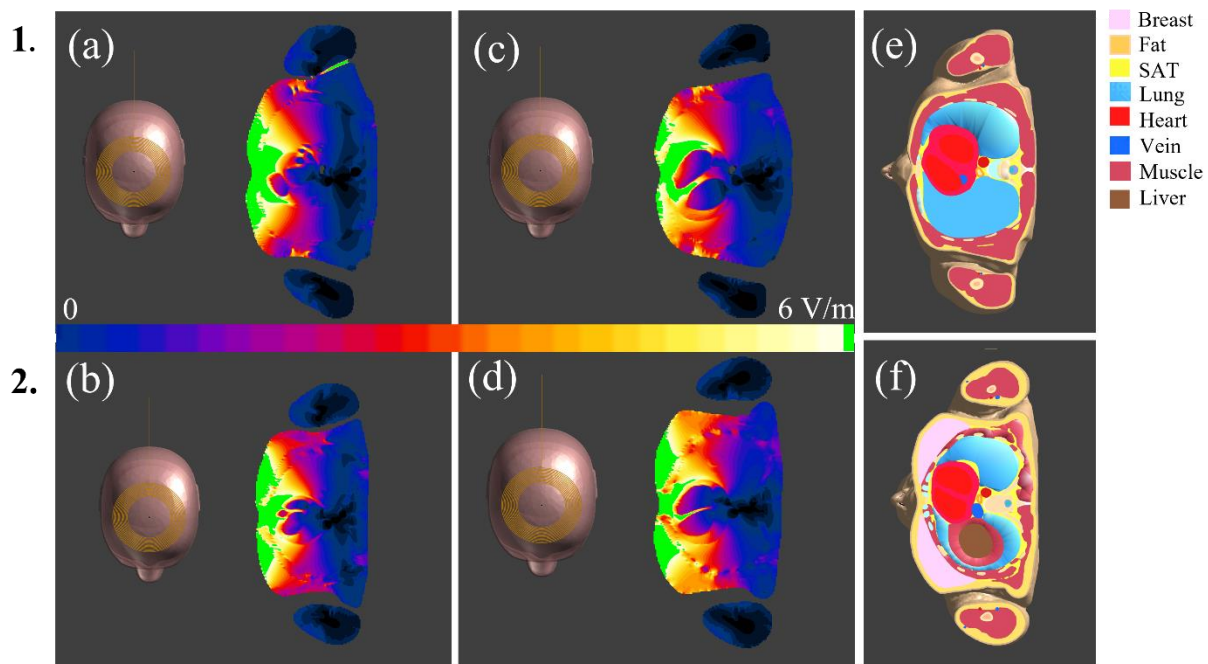


Figure V. 5. Exposure to circular coil in orientation II, case B. Panel 1 refers to Duke, panel 2 refers to Ella. Distribution of the induced E-field (a)-(b) on a transversal plane at the height of the coil of Duke and Ella respectively; (c)-(d) on a transversal plane in correspondence of the chest on the plane below 4.5 cm from the surface of the coil, in Duke and Ella respectively. (e)(f) slices of tissues in the correspondence of the Duke and Ella chest, respectively.

In Figure V.5 (a) and (b), is reported a comparison of the E-field distribution in the slice of the body at the height of the coil (passing through the surface of the coil) with highlighted in light green the maximum set in the color bar. In Figure V.5 (c) and (d), there is a comparison of the E-field distribution in the slice of the body on the transversal plane corresponding to the center of the chest (that is below 4.5 cm from the surface of the coil). Finally in Figure V.5 (e) and (f) are reported the same slices of (c) and (d), but with indication of the body tissues. What we can observe from these figures is that, in the transversal slices (a) and (b) the distribution of the E-field seems to be quite similar in the two models, with the particularity of Ella in which the profile of the maximum (light green) follows the breast tissue profile. What is interesting is what occurs in the plane below 4.5 cm from the source, in fact while within Duke there is a reduction in the region affected by the maximum E-field, in Ella the profile in light green remains almost the same of the previous slice, as if the presence of the breast tissue contributes to a slower decreasing in electric field value within it. It is important to note that the tissues that are directly exposed to the source between the two models are electrically different. In Duke we have the skin followed by a layer of

subcutaneous fat followed in turn by muscle; in Ella, there is a layer of subcutaneous fat under the skin, followed by the breast, and so on. To conclude, is clear that the tissue present in the female subject is of crucial importance in assessing exposure. Although the distribution of the induced electric field values is slightly different, the area where the high fields persist is not negligible in the female subject.

In the end, is evaluated the exposure of the abdomen (case C) in orientation II, produced by the circular coil. As well, are considered the slices of the bodies, in which could be present the main differences. The comparison between the two models of the distribution of the induced E-field is shown in Figure V.6:

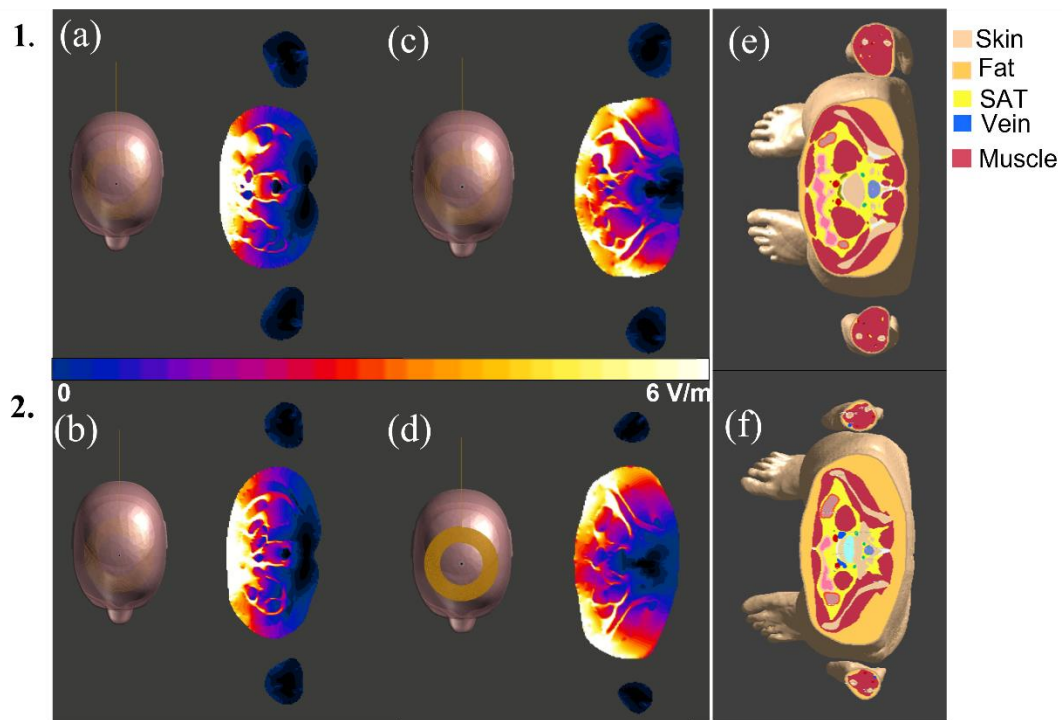


Figure V. 6. Exposure to circular coil in orientation II, case C. Panel 1 refers to Duke, panel 2 refers to Ella. Distribution of the induced E-field (a)-(b) on the transversal plane at the height of the coil of Duke and Ella respectively; (c)-(d) in a slice of the hip, below the coil; (e)(f) slices of the tissues corresponding to the hip slice.

As occurred for the worst case of Ella (case B), also in this case we can observe that, although in the slice at the height of the coil the profile of the distribution of the E-field is quite similar (but much more penetrating in Duke than in Ella), moving away from this slice, up to the hip region, the induce E-field remaining higher in Duke than in the Ella. In particular, in

this case we have to focalize on the shape of the map of the E-field. In the case (a) and (b), it is present a very compact area where the maximum of the bar color is reached. This area represents the anatomical district directly exposed to the coil: here we can say that the distribution profile is about the same, but as anticipated, in Duke it seems to be more penetrating and widens more towards the hips. Moving below to the height of hip, slices (c) and (d), in Ella we have areas with maximum electric field only in the zone of the flanks, while in Duke, we still find a high electric field in the frontal area (absent in Ella) and, as in the female subject, an extension of the maximum areas towards the lateral flanks. This behavior is only to attribute to the anatomical differences between the model (e)(f) since the exposure condition is exactly the same.

Therefore, in general, we find that our results follow the point of view found in the literature, but we believe that other factors can influence the results. However, based on what was found in the literature and what we obtained, we can conclude that, under the same conditions, some gender differences in the exposure could be observed.

### 5.3 Conclusions and suggestions for a better analysis of the risk

Based on the discussed results, emerges quite clearly that the anatomical characteristics of the human subjects have an important role in the evaluation of the assessment of the risk exposure, since several factors could influence the extent of the exposure. In the study of the exposure gender-dependent, here shown, it is evaluated that depending on the operator that performs the TMS treatment a slight difference in the extent of the exposure could be observed. First, the shape of the body of Ella model, resulting in a physiological curvature of the back, caused a wide exposure of the head, and consequently in the CNS, also due to smaller dimensions of the head compared to Duke. Then, it is found that where there are objective differences between the male and female (thus, not only in the models here considered), i.e., in the chest (for the presence of the breast) and in the abdomen (for a different anatomical composition of the muscle and fat in the male), wide differences in the

behavior of the distribution of the E-field are revealed. Therefore, by considering these differences, probably a more efficient assessment of the risk could be carried out.

As a whole this analysis would be a useful starting point for improved awareness of the importance of variability among human subjects in the assessment. These results, for example, could pave the way for the evaluation of an error percentage to be considered if the subject presents different body characteristics, such as those observed between male and female operators. However, the issue could also extend to other categories and thus to other differences (races, weight, etc.), opening a new method of the assessment of the exposure.



**SECTION III. AN INNOVATIVE  
APPROACH TO THE ANALYSIS OF THE  
RISK IN THE OCCUPATIONAL EXPOSURE**

---





# VI. CHAPTER

---

## 6.1 Drawback of the female models and enhancement of Ella model

Based on the results shown up to now, it is clear the important role of the numerical dosimetry in the exposure assessment, since it is necessary to have an accurate evaluation of the EM quantities induced inside the human body<sup>159</sup> and, at the same time, also the virtual models are a powerful tool for the numerical analysis, and for the evaluation of the risk due to some device, as in the case of this work. Several authors have developed various 3D human models representing a large sample of the population. To achieve good accuracy in the representation of tissue shape and distribution, these models are typically obtained from magnetic resonance (MR) or computed tomography (CT) images and successively processed with digital imaging techniques<sup>160</sup>. One of the first datasets of human body models is part of the Visible Human project, in which data were acquired from post-mortem scans, and includes the Visible Human Male (VHM) and Visible Human Female (VHF) models. Other models are those of the Virtual Population (ViP) project<sup>23</sup>, used in this work, which includes, among the others, the male (Duke, Jeduk, etc.) and female (Ella, Yoon-Sun, etc.) models, both obtained from MRI scans of healthy volunteers, as aforementioned. However, other works of literature have produced very detailed human models over the years<sup>161–163</sup>. Nevertheless, in all of them, the reconstruction based on medical images of subjects in supine positions implied a limit in accurately reproducing the realistic shape, in particular, that of the female body. In fact, in the female models elaborated by Mazzurana et al.<sup>164</sup>, Liu et al. 2005<sup>165</sup>, Dimbylow et al. 2005<sup>166</sup>, Nagaoka et al. 2004<sup>156</sup> as well as in Ella and Yoon-Sun models (belonging to ViP<sup>23</sup>) the representation of tissues in the thoracic area are unrealistic. The breasts and surrounding tissues are flattened out compared to how they would be in reality and therefore models obtained from the supine position are perhaps not

the most adequate to represent a standing female body. Therefore, an improved anatomical female is needed<sup>167</sup>.

From these assumptions, although some differences are already visible between the male and female models, to improve the assessment of the exposure, the second phase of the female exposure assessment was to obtain an enhanced model of Ella. Enhanced, means obtaining a form that better represents the realistic case of a female operator that performing a treatment in standing position. Based on the results previously found, it is reasonable to consider that a different shape in the body of the female subject could be impacted by the effects of the exposure. Therefore, a modification of the female human model is carried out.

## 6.2 Numerical dosimetry with Enhanced Ella: exposure dependent on anatomical structure

To conduct the dosimetric analysis on a more realistic female model, the reference model of the female human body Ella was considered. The Ella model, as mentioned, is obtained from MRI images in the supine position and therefore does not show a realistic distribution of the breast, fat, and skin tissues in the trunk area. To improve the model and thus obtain a realistic one to be used in numerical simulations, models of the breast tissue, subcutaneous adipose tissue (SAT), and skin tissue of the trunk area of interest needed to be modified. In order to convert the supine Ella anatomical model to a standing posture, the open-source software Blender (v.3.0, Stichting Blender Foundation, Amsterdam)<sup>168</sup> was used, and the following modeling steps were performed:

1. Reconstruction of the three *basic models* of the breast, SAT, and skin tissues, present in the thoracic area;
2. Sculpting deformation and surface manual adjustment to reposition and enlarge the three tissues of the model.

These steps are shown in Figure VI.1.

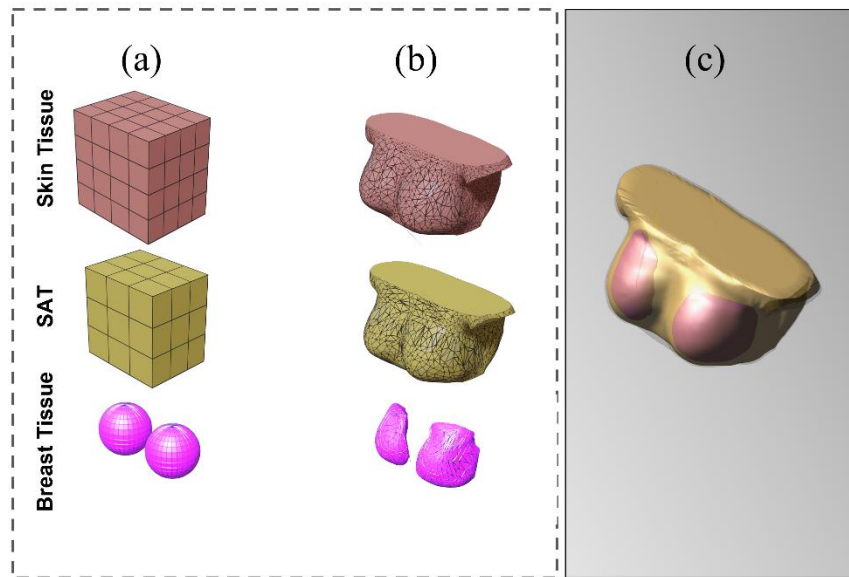


Figure VI. 1. Blender manipulation. (a) Basic tissues- the first step, (b) reconstruction of the real shape – second step, (c) improvement region of the thoracic area obtained- improved model.

The first step was to create three separate 3D numerical models representing a limited and localized area of the torso around the breast tissue. Taking the basic model of Ella (the one used so far) as an example, the breast tissue, subcutaneous fat, and skin were geometrically identified. These models are clearly modifiable but imitate the original tissue model in anatomical size. At this point, in the second stage, the surface modification of the three previously created objects is carried out using the deformation sculpting tools, powerful tools for intuitively modifying the shape of objects. This method makes it possible to modify only the surface of an object of interest in the shape of the tool's surface, maintaining the details and topology of the original models, controlling the mesh, and ensuring that the other structures of the whole-body model were not touched. Finally, the newly developed breast, SAT and skin models are incorporated into the complete Ella female human body model to obtain a new whole-body model called 'Enhanced Ella'. It is essential to underline that all tissues of the improved model are identical to those of the original one, except for the breast, the SAT, and the skin.

It is important to anatomically compare the two female operator models in order to have an overview of the crucial changes that have been made, and thus understand how these could

impact the assessment of TMS exposure and eventually the operator's posture itself. Therefore, in Figure VI.2 the two models of Ella are reported.

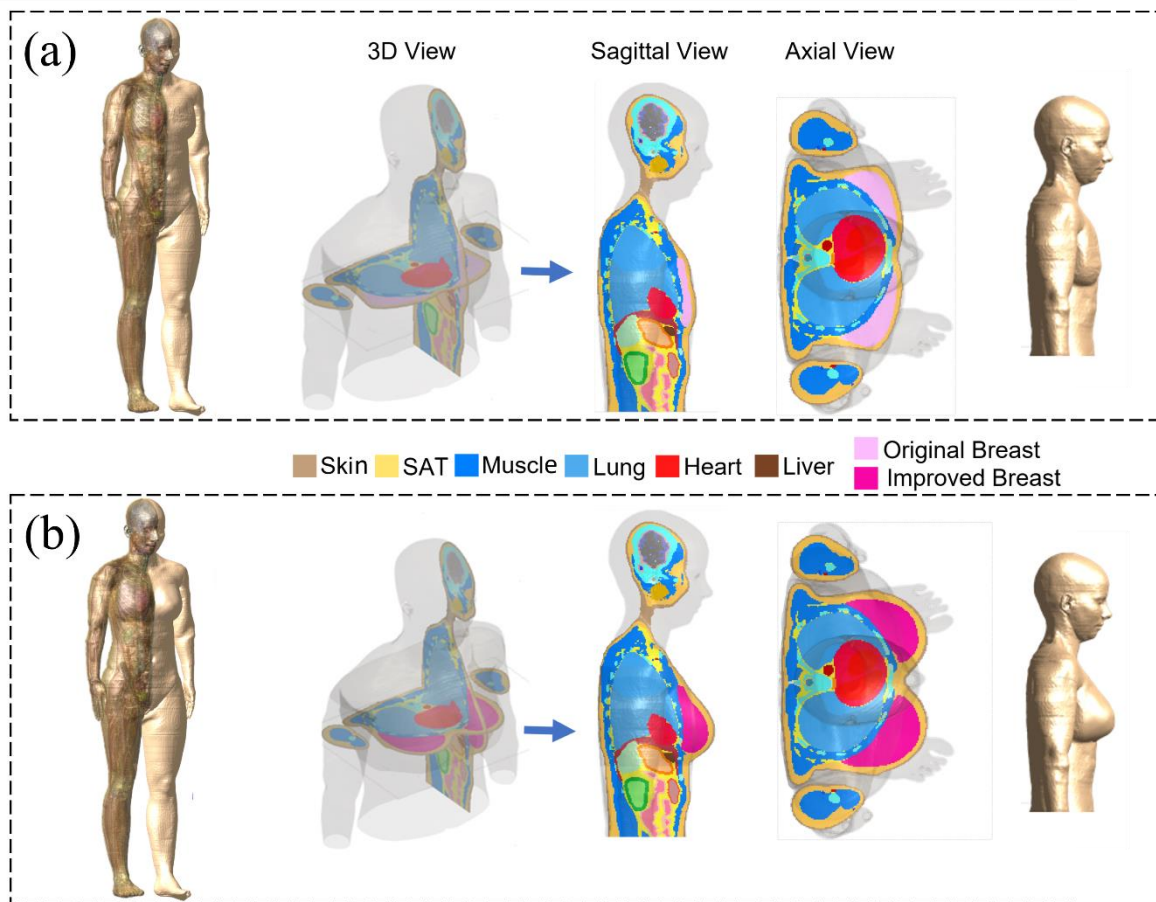


Figure VI. 2. Comparison between the anatomical female human models. (a) a panel of Ella original, with a section of tissues in 3D, sagittal and axial views, followed by the profile of the model; (b) panel of Enhanced Ella, with a section of tissues in 3D, sagittal and axial views, followed by the profile of the model, respectively.

In Figure VI.2, panel (a), is reported the model Ella in the original version, where it can be seen the slice of the body tissues in a different view, and in particular the volume occupied by the breast tissue. In panel (b), is shown the Enhanced Ella, in this case, it is possible to observe the modification of the breast tissue, which is characterized by a greater volume, and also it is possible to see that the other tissues (i.e., skin, SAT) only change their shape, following the new profile the female model. In particular, the SAT tissue shows a greater thickness than the original one since we want to mimic a real anatomical condition in which overall this region is characterized by a greater gland and SAT tissues. At this point, the

work aims to compare the behavior of these two female models, during the exposure to the TMS.

In this analysis, it is chosen to use as a source of exposure the circular coil powered by the Magstim Bistim (see features in Table III.7), that is the device characterized from the measurement campaign of INAIL<sup>123</sup> exposed in the Chapter III. For this comparison two exposure conditions were considered, that is case B (chest exposure) and case C (abdomen exposure) in orientation II. The case B is important in order to carry out a comparison between the different body shapes of the models; whereas case C, represents simultaneously a district quite distant from the new tissue to verify possible influence also in the region away from this one, and also this is a condition of exposure that, based on the results, figured to be one of the worst cases (i.e., for Duke model).

As explained in Chapter IV and in particular Table IV-1, in orientation II the distance between the coil windings and the operator's surface is set at 12 cm. For the exposure of Ella, the coil is positioned in orientation II at the height of the chest and at the height of the abdomen, maintaining a distance equal to 12 cm between the coil's windings and the body's surface. For the case of Enhanced Ella, it is necessary to add some considerations. Since the new shape of Ella, includes a modification of the surface of the operator, other distances need to be considered. Therefore, while for case C (abdomen), a distance of 12 cm from the coil windings is still considered, for case B intermediate distances are also considered. Therefore, the exposure of the abdomen is carried out in the same conditions for the two models, while, for the case B, for Enhanced Ella three distances are considered:

- d1, distance of 12 cm between the windings of the coil and the new tissue of the breast (green in c.1);
- d3, distance of 12 cm between the windings of the coil and the previously (original) external surface, this means that the new tissue is closer to the source (i.e., 8.6 cm between the windings and the surface of the new tissue, orange in c.1);
- d2, the intermediate distance between d1 and d3, i.e., 10.3 cm between the windings of the coil and the new tissue (purple in c.1);

The exposure conditions are summarized in Figure VI.3.

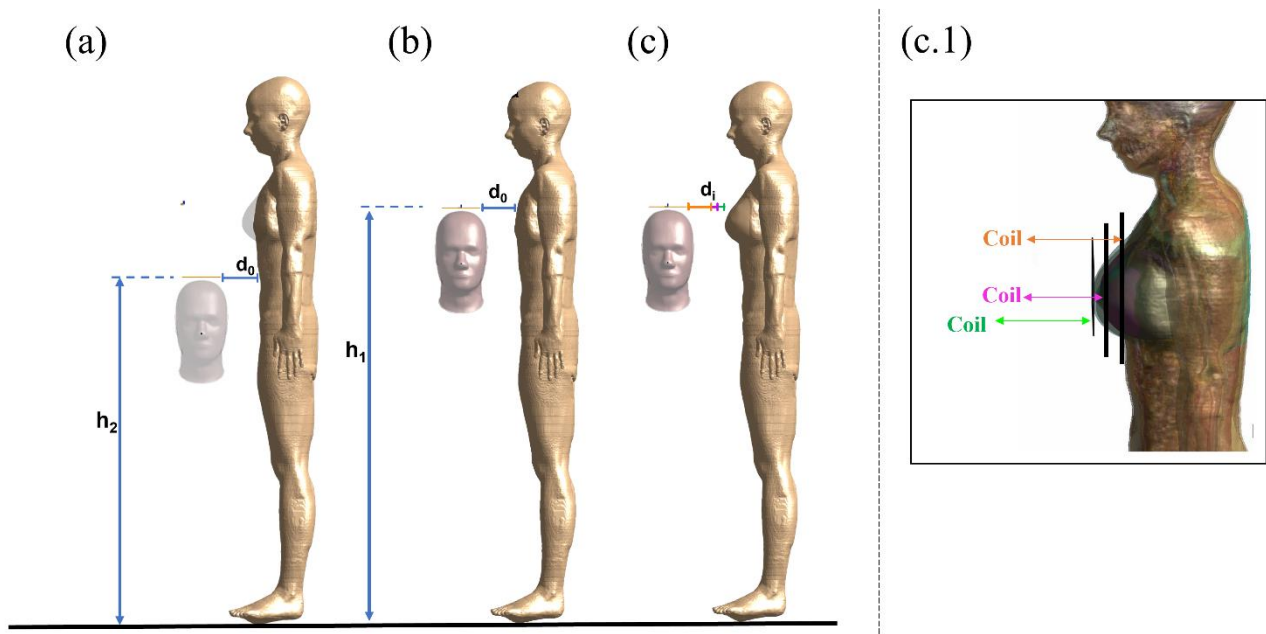


Figure VI. 3. Exposure to circular coil, orientation II: (a) exposure of the abdomen ( $h_2 = 112$  cm), the distance ( $d_0=12$ cm) was taken for both models, (b) exposure of the chest ( $h_1 = 136$  cm) with Original Ella ( $d_0 = 12$ cm), (c) exposure of chest of Enhanced Ella (in green  $d_1 = 12$ cm, in purple  $d_2 = 10.3$  cm, and in orange  $d_3 = 8.6$  cm); (c.1) explanation of the distances in Ella Enhanced

Starting from the case of the exposure of the abdomen, in the following is reported the distribution of E-field in some slices of the body, along the sagittal plane (Figure VI.4). The choice to consider several slices of the body refers to the possibility that some important differences could be present moving along the tissues, since the two models are different not only in the slice passing through the center of the body, but rather laterally.

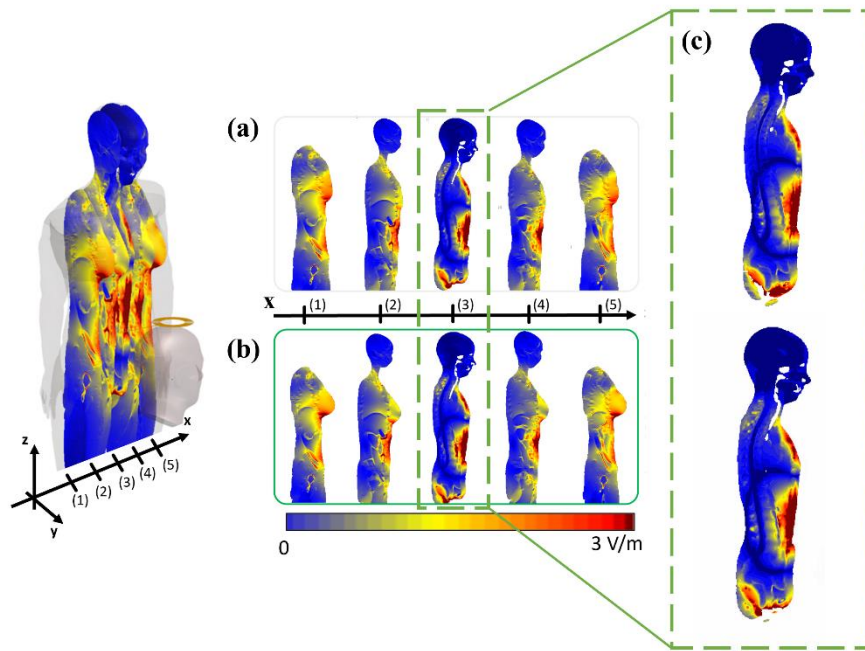


Figure VI. 4. Induced E-field distribution at 70% MSO on sagittal planes. Exposure of abdomen, orientation II: (a) Ella slices with steps of 5 cm, (b) Enhanced Ella slices.

The above figure reveals the differences in exposure between the two models, due to the anatomical differences. In panel (a) is the case of Ella, whereas in (b) is the case of Enhanced. Finally (c) shows a focus on the central slice which typically is chosen as reference for the analysis of the exposure. If we consider only this central slice, passing through the center of the coil (Figure VI.4 c), few differences in the distribution of E-field are evaluated, but by analyzing the other slices of the body, some changes appear. In particular, in slices (1) and (5) the profile of the maps of the induced E-Field takes a different form. The presence of a thicker layer of breast and SAT tissue in Enhanced Ella, helps to confine the electric field distribution. In fact, what we notice is a concentration of the maximum value (intense red) in the lower part of the breast (i.e., the one facing the surface of the coil), with a gradual decrease in the remaining tissue, which presents a greater field in the superficial section and a decrease as we penetrate inwards. On the other hand, in Ella (original), we notice that the field distributes with a certain homogeneity in the tissue. This could mean that the fatter tissue of the Enhanced creates hot spots, which we do not see in Ella, where overall the whole tissue participates in the exposure in the same way. However, it is evident that in

both models, the breast plays a key role in the exposure since the profile of the maximum E-field follows this tissue. Next, the percentiles of the induced electric field in the whole body are evaluated.

**Table VI - 1. Induced E-field (V/m) in the human female models**

Exposure of the abdomen to the circular coil, 70% MSO

	99 <sup>th</sup>	99.9 <sup>th</sup>	99.99 <sup>th</sup>	100 <sup>th</sup>
<i>Ella</i>	2.82	4.37	6.24	21.45
<i>Enhanced Ella</i>	2.86	4.34	6.11	19.78

From these results, it is clear that when we consider the whole body to evaluate the 99<sup>th</sup> percentile we lose the contribution of the tissue under test, indeed the results are almost the same. If we evaluate the induced electric field only in the tissue of the breast, we obtain the 99<sup>th</sup> percentile of 2.87 V/m for Ella and 3.27 V/m for Enhanced Ella, therefore a +12.23% in Enhanced with respect to the original shape of female model. This reflects the hot spot that we can appreciate in the maps of the induced E-field inside the Enhanced model. At this point, it is fundamental to assess the exposure of the chest (case B). Therefore, as previously done, first the distribution of the induced E-field is shown (Figure IV.5).



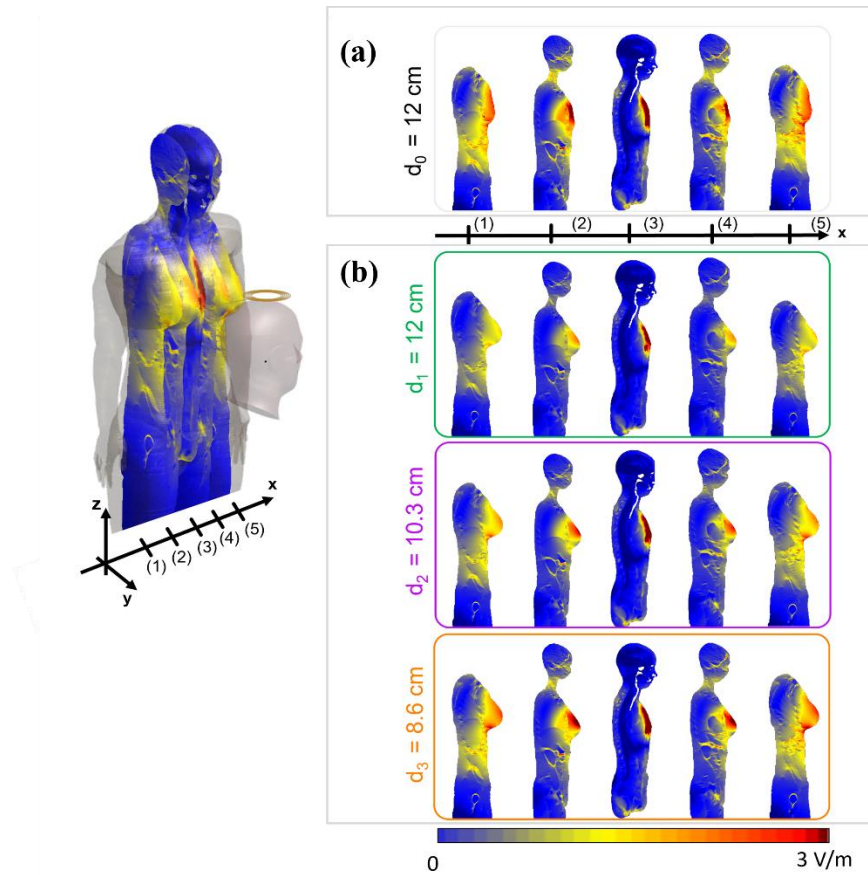


Figure VI. 5. Induced E-field distribution at 70% MSO on sagittal planes. Exposure of chest, orientation II: (a) Ella slices with steps of 5 cm, (b) Enhanced Ella slices at three different distances.

In this case three different distances for both models are considered. It is not possible to make an exact direct comparison, as the different shape leads us to the exposure conditions that are different from each other. What it is possible to observe is that in the Ella original model, the presence of the breast cause, as seen also before, an induced E-field that keeps higher values in the region in which is present the breast tissue. For example, it is evident how the higher values of E-field (intense red and orange), even when moving to the other slices, continue to delineate the profile of the breast tissue, persisting within this tissue. In the Enhanced model, we can attain different conclusions. In all three distances is clear how the breast helps to maintain a high value of the induced E-field also when considering a slice that is far from the source (as 1 and 5). Considering an overview analysis, also in this case of exposure, the maps of the distribution of E-field show hot spots in Enhanced Ella, while homogeneity is present in the original model. Therefore, the behavior is quite similar

to the case C, but in this case B, the area with intense red is larger than before. Further, is important to note how the slices (2) and (4) differs in the two models. Starting from Ella, the map of the induced E-field shows a maximum in the breast tissue, but also a great dispersion in the surrounding body districts, in particular in the abdominal area. This does not occur in the Enhanced Ella, in which the E-field is mainly confine in the trunk (and so in the breast), for all the distances considered.

For a complete overview of the differences in induced E-field the following Table is reported. Where skin and SAT refer to a crop of the only chest region.

**Table VI - 2.** *Induced E-field (V/m) in the human female models*

Exposure of the chest to the circular coil, 70% MSO

	<i>Ella</i> $d_0= 12\text{ cm}$	<i>Enhanced Ella</i> $d_1= 12\text{ cm}$	<i>Enhanced Ella</i> $d_2= 10.3\text{ cm}$	<i>Enhanced Ella</i> $d_3= 8.6\text{ cm}$
99 <sup>th</sup> whole body	2.43	1.63	1.99	2.82
99 <sup>th</sup> breast	3.32	2.04	2.56	3.09
99 <sup>th</sup> heart	1.85	1.05	1.29	1.54
99 <sup>th</sup> skin	5.13	3.36	4.21	5.03
99 <sup>th</sup> SAT	5.95	3.20	3.96	4.77

The results depend strongly on distance, since the closer the models are to the source, the higher the E-field and also the shape of the model could impact on the coupling with the external magnetic field, since we have completely different external shapes in the region of the chest. To have a better analysis of localized exposure distribution, in Figure VI.6 the histogram of the normalized probability distribution of E-field inside the tissues, referring to the chest exposure, are shown. The SAT tissue refers, as before done, to a crop of the chest section directly exposed to the coil.

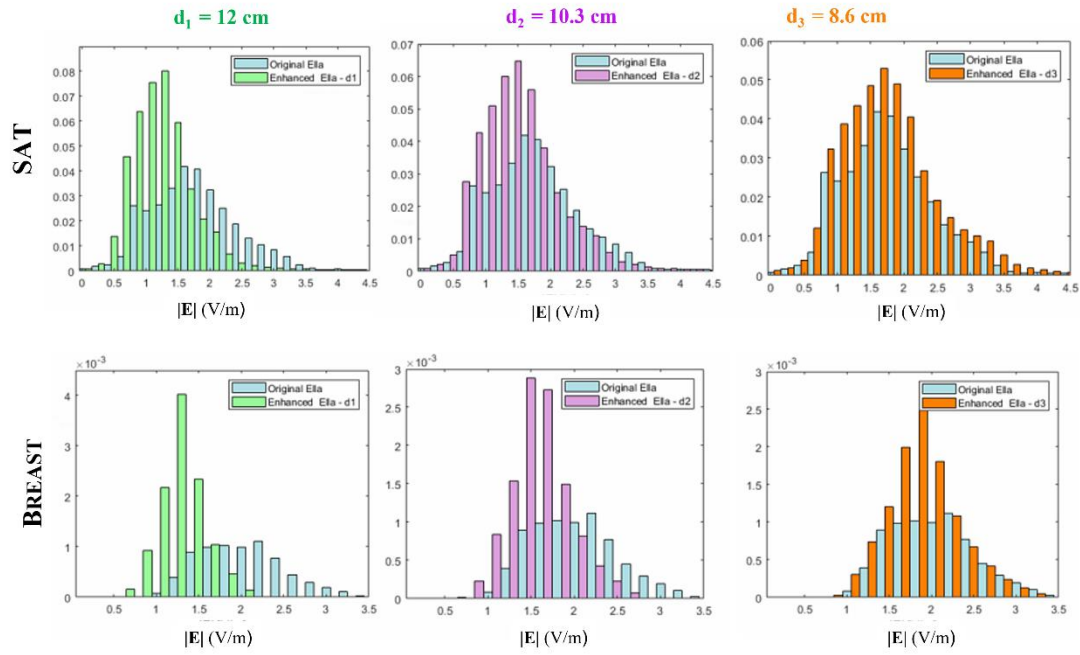


Figure VI. 6. Comparison between Ella and Enhanced Ella, of the normalized probability of the distribution of E-field intensity ( $|E|$ ) induced by TMS inside the tissues, in the case of exposure of the chest.

From this latter figure, the differences in the exposure, caused by the additional tissue added in the new model, are sufficient clear. Enhanced Ella shows, without a doubt, a higher value of the induced E-field, confirming the changes in the exposure owing to the anatomical differences.

### 6.3 Conclusions and suggestions

The analysis of the exposure to the TMS device in reference to the effect on the two different female models is carried out. The Ella original model belongs to the virtual population (ViP)<sup>23,45</sup> available in the software Sim4Life, whereas the enhanced Ella is obtained by means of a manipulation of the original model, by modifying the shape of some tissues present in the region of the chest: breast, skin and subcutaneous fat (SAT). The exposure conditions chosen for the assessment of the exposure are orientation II with the coil positioned at the abdomen and chest heights. These are chosen in order to take into account, on one hand the worst-case exposure condition, coming from the previous analysis on human body model, and on the other hand to consider the specific tissues characteristic of the female model, i.e.,

the chest. The evaluation of the exposure reveals that some differences occur, in particular in the distribution of the E-field in the trunk between the two models. It is observed that in the Enhanced Ella hot spots are created that are not observed in the Ella model. These could depend on the coupling with the external magnetic field (see the configuration of the streamline of the circular coil in Figure V.5), since the new tissue changes completely the external chest shape, but also could depend on the different thickness of the tissues, both for the breast and SAT. Overall no great changes are detected in the models in reference to the 99<sup>th</sup> percentiles of the induced E-field, since in this case the main factor is the distance from the source.

However, in the examined cases of Enhanced Ella, important conclusions can be carried out from the further analysis, in which evidence of the greater extension of the exposure for the Enhanced model is clear.

For example, the three distances chosen for analysis could represent three different ways of working of three different operators during TMS treatments. This is because the distances could indicate a different (and entirely personal) method of conducting the treatment in a way that is comfortable for the operator. We can suppose that the greater distance of 12 cm could represent a condition in which the operator feels the need to move the body away from the source and so from the patient, precisely because of its shape (i.e., the new additional tissues), while the shorter distance, on the contrary, could represent the operator's need to remain, despite the new tissues, close to the patient. These considerations, based on the results, may be important in order to give an awareness of the extent of the exposure, especially when dealing with an operator with a different shape than the standard one, such as this Enhanced.

Based on the results shown, we can conclude that the shape of the operator plays a key role in exposure assessment and, in particular, the intrinsic characteristics of the tissues seem to be equally significant (e.g., thickness, structure, position and so on). The suggestion is therefore to conduct an in-depth exposure analysis with the female subject. In the future, we would like to consider other positions and inclinations of the coil with respect to the

human body, also considering different coil models.. These results are preliminary to an important area that needs to be studied in order to improve the dosimetric occupational risk assessment.

# VII. CHAPTER

---

## 7.1 Human exposure variability and the importance of the anatomical characteristics in the risk assessment

From the results obtained in the gender dependent assessment of exposure described in Chapter V and VI emerged the possibility that the risk associated with the use of the TMS may depend on the clinician's body characteristics, such as size, height, or overall body structures. These factors may lead to differences in terms of the organs' size and location as well as in the distribution of tissues' conductivities, influencing the distribution of the induced electric field<sup>111,169-171</sup>. This issue is observed, for example, in the analysis reported in Figure V.4, in which the same organs show a different behavior, even though subjects are exposed to the source under the same conditions. In addition, different body shapes could cause different coupling with the external field, since the surface facing the source is different.

Thus the impact of human variability on risk assessment is largely unexplored to date, and typically regarded not the influence that the properties or the characteristics of the tissues could have in the distribution of the E-field inside the human body, rather the different sensitivity of the subjects and the inter-individual variations in populations' response to the exposure to the EM field<sup>172</sup>. Typically scientific research deepens the study of how sensitivity<sup>173</sup> and human variability influence the estimated thresholds<sup>174</sup> for the biological effects and thus the dose-response relationships, for the quantitative risk assessment. The detection of these thresholds is typically explored with the aim to establish in turn the limits of the exposure. In particular, the algorithm for deriving safety limits consists in the application of the reduction factors to the identified health effect thresholds. Thus, in order to detect these thresholds, the intersubject variability is studied, but no studies are conducted on the relation between the human body characteristics and the different behavior of induced quantities (such as distribution in the tissues, presence of the hot spots, or in general criticality of exposure due to anatomy). As part of the risk assessment, a recent

study by Hirata and co-workers<sup>175</sup> addressed the topic of the importance to use accurate human body models jointly to the own dielectric properties, highlighting the need to carry out an accurate measurement of dielectric human tissue properties for evaluating the induced field strength. The paper aimed at making a review up to date of the most important dosimetric studies (considering human body modeling and tissue dielectric properties) and analyzing the standardization process for compliance of certain products as wireless power transfer (WPT) or magnetic resonance systems. They did not conduct a comparative study on how the body anatomy could influence the induced E-field. Conversely, the cited study of S. Gallucci et al.2022<sup>176</sup> shows that a difference in terms of exposure response exists due to gender. From these results, it is clear that, wherefore, a thorough investigation should take into account the specificity of the sources (TMS in our case), but also the characteristics of the subject exposed, in order to obtain a complete analysis of the exposure. Just with regard to TMS, to date, studies on intersubjective variability mainly concern the therapeutic application (thus referred to the patient), while there are almost no indications in the context of risk assessment for workers. Therefore, this chapter aims to deepen the possible differences in the exposure among various human shape models, utilizing a model of a real work environment, and also using the same TMS source, derived from the measurement campaign<sup>177</sup> described in Chapter III. For this study, it is considered the exposure to the circular coil placed only in two positions among the four detected (i.e., cases B and C among the cases A-B-C-D) and in the detected worst orientation (i.e., II). As usual, the distribution of the induced E-field caused by the source inside the body tissues of the operators has been evaluated as well as the 99<sup>th</sup> percentile of the induced E-field in order to compare it with the limits reported in the ICNIRP guidelines and so to verify the compliance of the exposure. Additionally, the relationship between the distribution of the induced E-field and the specific tissues inside the body (taking also into account their electrical properties) has been considered, analyzing the influence of the body structure (shape, volume, and so on). Thus, the maps of the E-field and conductivity within tissues has been produced to assess how internal tissues may influence the distribution of the induced E-field. Finally, we evaluated the statistics of the induced E-field in specific

tissues included in a cubical box identified as the anatomical district of interest, showing the minimum, 25<sup>th</sup>, 50<sup>th</sup>, 75<sup>th</sup> percentile, and maximum in the boxplot.

## 7.2 Methods of analysis: four different human subjects to provide an intersubject variability

The exposure scenario considered for all the models examined for the Intersubject variability assessment is reported in Figure VII.1, in which only the profile of Duke model is reported, as representative of the orientation and the coil positions from the ground used.

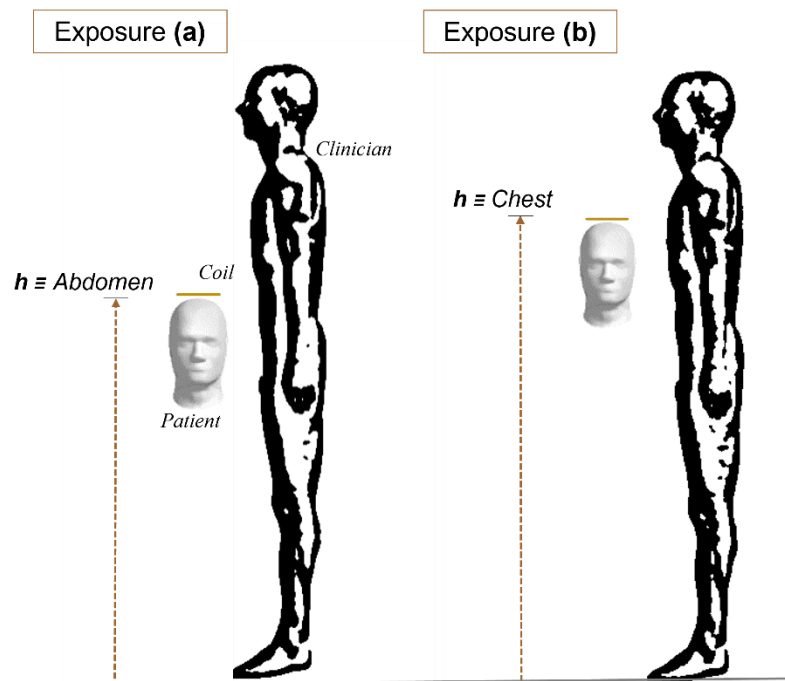


Figure VII. 1. The dosimetric exposure scenarios, representative of the intersubject analysis. The two coil positions are described: (a) at the height  $h$  of the abdomen; (b) at the height  $h$  of the chest. Both in the defined Orientation II

The coil used is the commercial Magstim MAG-9784-00 circular coil fed by the BiStim appliance<sup>124,125</sup>, characterized from the experimental data obtained by the measurement campaign and explain in Chapter III. The features of the TMS device are reported in Table III-7. In this chapter the system is considered working at 1 kHz with 9.7 kA when powered at 100% MSO.



As done in all the assessments of the exposure here considered, the work environment is reproduced using the numerical software Sim4Life (v.7, ZMT, Zurich MedTech AG) and consists of: the source, the clinician performing the treatment, and also the head of the patient (consisting again only of shell and liquid structures, with conductivities of 0.01 S/m and 0.33 S/m, respectively<sup>49</sup>). The coil was placed above Sam’s head at distance equal to approximately 1 cm.

To consider different shapes of the human body four members of the Virtual Population (ViP., v.3.0)<sup>23,45</sup> have been chosen, all available in the software Sim4Life as surface-based models obtained from the MRI scans of volunteers; they are: Duke, Ella, Fats, and Jeduk. The characteristics of each model are reported in the following Table VII-1.

**Table VII - 1. Characteristics of the human anatomical models**

	<b>Age (y)</b>	<b>Weight (kg)</b>	<b>Height (m)</b>	<b>Number of body structures</b>
<i>DUKE</i>	34	70.2 kg	1.77	319
<i>ELLA</i>	26	57.3	1.63	312
<i>JEDUK</i>	33	64.5	1.62	1186*
<i>FATS</i>	37	119	1.82	247

\* It includes a nerve that is separated for neuronal analysis.

Besides the differences shown in the table, which relate only to age, weight, and height, the subjects also appear with objective differences in the body structure. Duke and Ella, reflect standard European human models in which the woman is smaller than the man and characterized by less height. Jeduk is a Korean man model, which in comparison with the European one has a smaller height as well as a tiny cross-sectional size, more comparable in some aspects to the body characteristics of the European woman Ella. Finally, the Fats model was considered; as compared to the other subjects it presents a greater height, a larger size, and as the name suggests, a greater amount of fat (subcutaneous and visceral fat), which as

far as observed from the analysis on Ella and Enhanced Ella, could lead to important results in term of induced E-field distribution.

In this study is considered of crucial importance taking into account the organs (position, form, and so on) and similarly the electrical properties of the tissues, since from these characteristics it could be possible to derive some conclusions regarding the induced quantities behavior. The dielectric properties for the tissues of the four models have been assigned by LF IT'IS database v.4.0<sup>146,178</sup> available in Sim4Life, which includes measurements of electrical conductivity at low frequencies based on diffusion tensor imaging in recent publications; in particular, low-frequency parameters are based on a combination of the Gabriel<sup>179</sup> dispersion relations and a review of the available literature.

The two different coil positions chosen (coil at heights of abdomen and chest) take into account the district where the greatest differences among the models could be observed, such as the different quantity of adipose tissue and/or muscle in the male models (i.e., coil at the height of the abdomen) and the presence of the breast in the female one (i.e., chest exposure). The condition of abdomen exposure was detected as the worst case<sup>142</sup>. The distance between the windings' edge of the coil and the surface of the clinician is kept equal to 12 cm for all the conditions of the exposure and models, in order to have the possibility to carry on a direct comparison.

Furthermore, as previously done for the female model, also in this case because of the different heights of the models, the position of the coil was scaled appropriately, to correctly position the source at the selected district. Therefore, in Figure VII -2, the position of the coil is shown with a cross on the surface of the body for each model: Duke (light blue), Ella (pink), Jeduk (orange) and Fats (green).

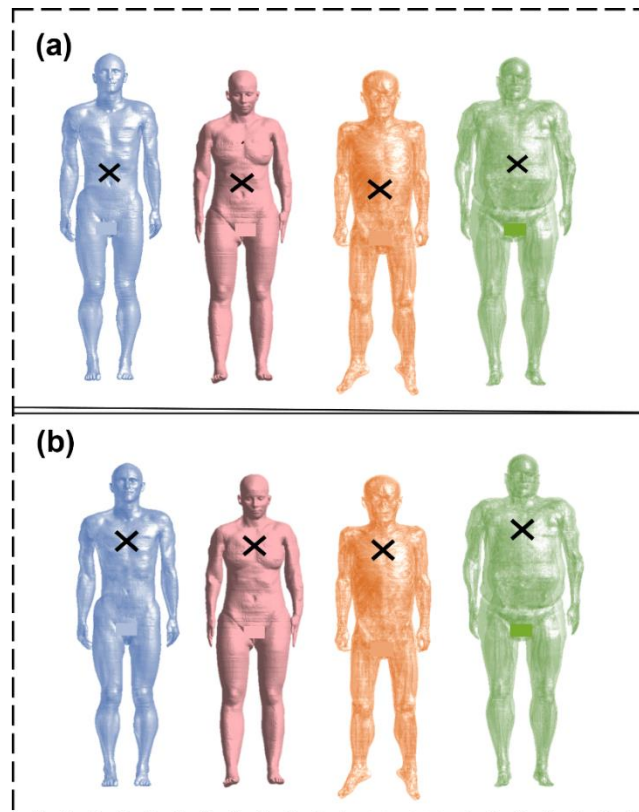


Figure VII. 2. Position of the coil as a function of the human height. The coil, marked with a cross, in (a) exposure of abdomen and (b) exposure of chest, in the four human models: Duke (light blue), Ella (pink), Jeduk (orange), Fats (green).

The simulations were implemented with the Magneto-Quasi Static solver as explained in Chapter III. All the human models were discretized in  $2 \times 2 \times 2$  mm cubic volumes within an environment space of the same dimensions, which results in a simulation domain that counts for a total number of cells ranging from approximately  $74 \div 99$  M-cells, depending on the human model.

To assess compliance with the limits, the 99<sup>th</sup> percentile of the induced E-field inside the human tissues is evaluated and subsequently compared with the limits, as suggested by the ICNIRP 2010 Guidelines<sup>13</sup> referring to BRs expressed in terms of induced E-field. These limits are frequency dependent and at our frequency of work, it corresponds to 1.13 V/m ( $E_{\text{peak}}$ ), since the guidelines stated that for the range 1 Hz – 3kHz, the BR for the internal electric field is equal to 0.8 V/m ( $E_{\text{rms}}$ ). Evaluation of the 99<sup>th</sup> percentile also allowed us to address a possible worst-case scenario and also to carry out an evaluation of the extent of exposure inside the body's tissues in the four models. In addition, we focused the attention also on the map of the distribution of the induced E-field, on the dielectric properties of the

tissues, and thus on their structure and geometry (taking into account the differences that distinguish the human models from each other). All of this is to identify possible correlations between gender and/or body shape and the extent of the exposure.

### 7.3 Comparison of the results among the human models

As previously mentioned, in all the cases examined the source worked at 70% of the MSO, to faithfully reproduce as we found during the aforementioned measurement campaign, in which the declared work conditions set by the clinician imply a 70% MSO. As previously done, both the 99<sup>th</sup> and the 99.9<sup>th</sup> percentiles are summarized in the following Table III-2.

*Table VII - 2. Percentiles of the induced E-field (V/m) in the human models*

70% MSO		DUKE	ELLA	JEDUK	FATS
<i>Exposure of Abdomen</i>	99 <sup>th</sup>	2.98	2.82	2.57	2.39
	99.9 <sup>th</sup>	5.12	4.37	4.06	3.88
<i>Exposure of Chest</i>	99 <sup>th</sup>	2.33	2.43	2.40	2.63
	99.9 <sup>th</sup>	4.15	3.86	5.68	4.39

Results indicate that the exposure to circular coil TMS causes a 99<sup>th</sup> percentile of the induced E-field that exceeds the suggested limit of 1.13 V/m in all the exposure conditions. In the case of the coil at the height of the abdomen, the worst case occurred in the Duke model, in which the 99<sup>th</sup> percentile reached 2.98 V/m (+163.7% with respect to the limit), whereas, in the case of exposure of the chest, the worst case occurred in the Fats model, in which the 99<sup>th</sup> percentile was 2.63 V/m (+132.74% with respect to the limit). Even in the case in which we found the lowest value of induced E-field ("safer case"), that is 2.39 V/m for the Fats model in the exposure of the abdomen, the limit is exceeded by +111.5%. Therefore, all the conditions represent a possible risk for the operators. Because these values are not completely representative of the individual response to the high magnetic field produced by the source, the distribution of the induced electric field along the bodies was evaluated.

To carry out this analysis, we divided the body into boxes 10 cm high, starting from the top of the head to the feet; this was made for each of the human models exposed to the source, in both configurations. In each of these boxes, we analyzed the 99<sup>th</sup> percentile of induced E-field at 70% MSO, and consequently, we obtain the distribution shown in Figures VII.3 and VII.4 for exposure of the abdomen and the chest, respectively.

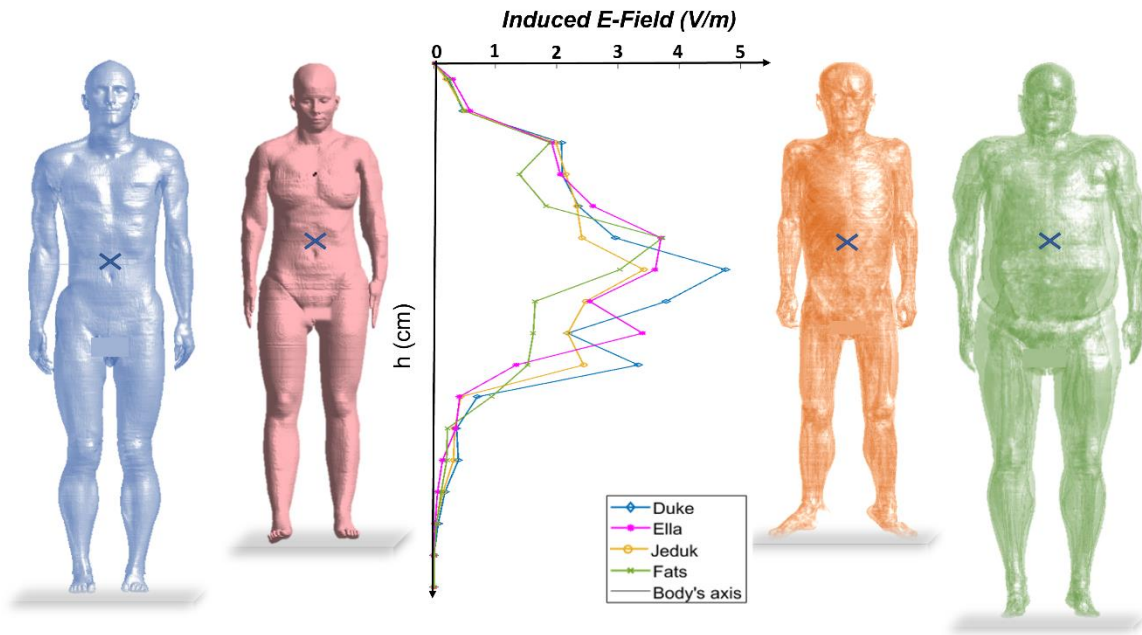


Figure VII. 3. Exposure of Abdomen at 70% MSO. Induced E-Field behavior along the body of human models. Marked with the cross the position of the coil.

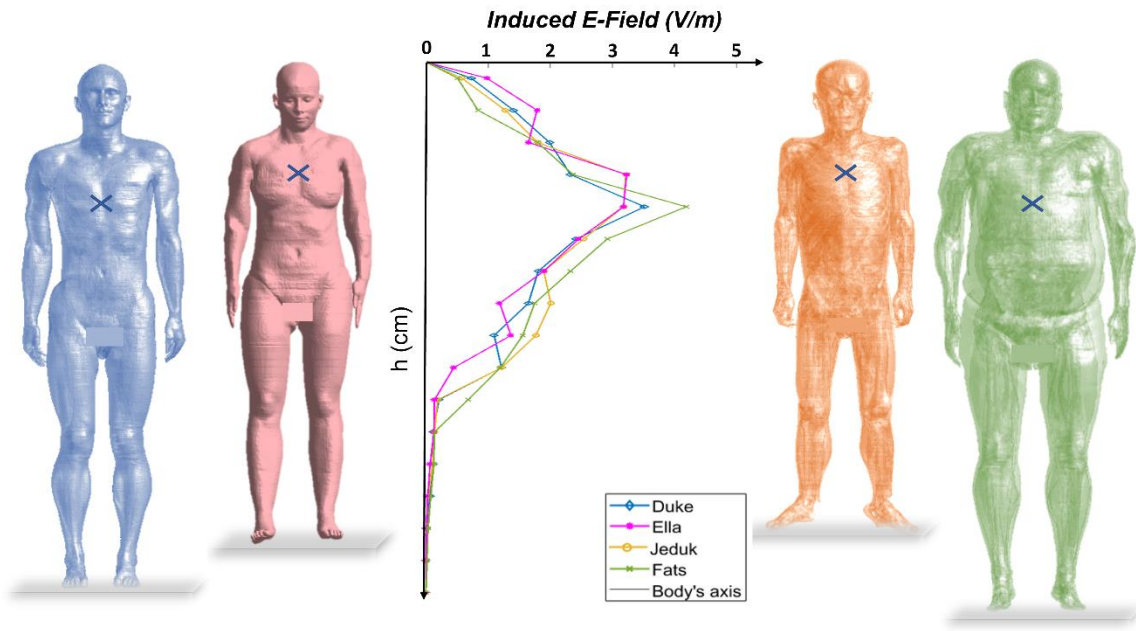


Figure VII. 4. Exposure of Chest at 70% MSO. Induced E-Field behavior along the body of human models. Marked with the cross the position of the coil.

The presence of the coil at the height of the abdomen showed a great variability of the E-field among the four anatomical clinician models. The maximum value of the induced E-field was obtained almost in correspondence to the position of the source in all examined cases, however, we can see another peak in correspondence to the reproductive system. The overall behavior of the 99<sup>th</sup> percentile along the staff bodies for the case of abdomen exposure (Figure VII.3) showed almost a linear increase from the top of the head to the thorax, where we obtained, in the area of the shoulder, a sort of plateau, followed by an increase until the abdomen, where another peak is reached (at the source), which in turn decreases in subsequent boxes, reaching another peak value in the area of the reproductive system. A general overview displays that, among the subject models, in the case of Fats we have a trend that differs from the others, showing greater variability in values of induced E-field. The same issue is shown by Duke in the abdominal area, in which compared to the other models, we see a tendency to maintain greater electric field (EF) values. Finally, Ella maintained a high value of induced EF for a larger area of the abdomen of about 20 cm, corresponding to the plateau around the position of the coil, where we found 3.70 V/m and 3.61 V/m for the two marked values. In addition, a maximum peak of the induced E-field at

the level of the reproductive system was found, and it was equal to 3.3 V/m in the Duke model, 3.4 V/m in Ella, and 2.44 V/m in Jeduk. In all three models, the peak fall in the SAT is present in the region of the bladder. Contrariwise, in the case of exposure of Fats, no peak of the E-field was found in the reproductive system, since the large layer of SAT could restrain the induced E-field in the abdominal region, where the only peak occurred.

Conversely, for what concerned the exposure of the chest (Figure VII. 4), we can see similar behavior in the distribution of the induced E-field along the height of the four human models. The 99<sup>th</sup> percentile of the E-field reached the maximum in correspondence of the box in which the source was present. Only in the case of Ella's exposure, the induced E-field remained at the peak values in a larger area of the chest (i.e., 3.23 V/m and 3.18 V/m in two consecutive boxes), compared to other models. This is probably due to the tissue that characterized the female chest; in fact, in the other models, we can observe a linear rise of the E-field, that achieved a maximum in the chest (in the area of is located the coil), followed by a decrease. It is important to highlight that also in this case of chest exposure, each model experienced a second peak of the induced E-field in correspondence to the pubic area. As expected, in this case, the intensity of this second peak was lower than that induced by the exposure of the abdomen, due to the closer distance from the source in this latter case.

At this point, since some studies<sup>104,105</sup> suggest evaluating the other percentiles in order to improve the evaluation of the exposure, also in this case, as done in Chapter IV, a comparison metric of dose is reported for each model. Figures VII.5 and VII.6 reported the total-body percentiles (99<sup>th</sup>, 99.9<sup>th</sup>, 99.99<sup>th</sup>, and 100<sup>th</sup>) of the induced E-field, comparing the values among the four human models. The 70% MSO is considered.

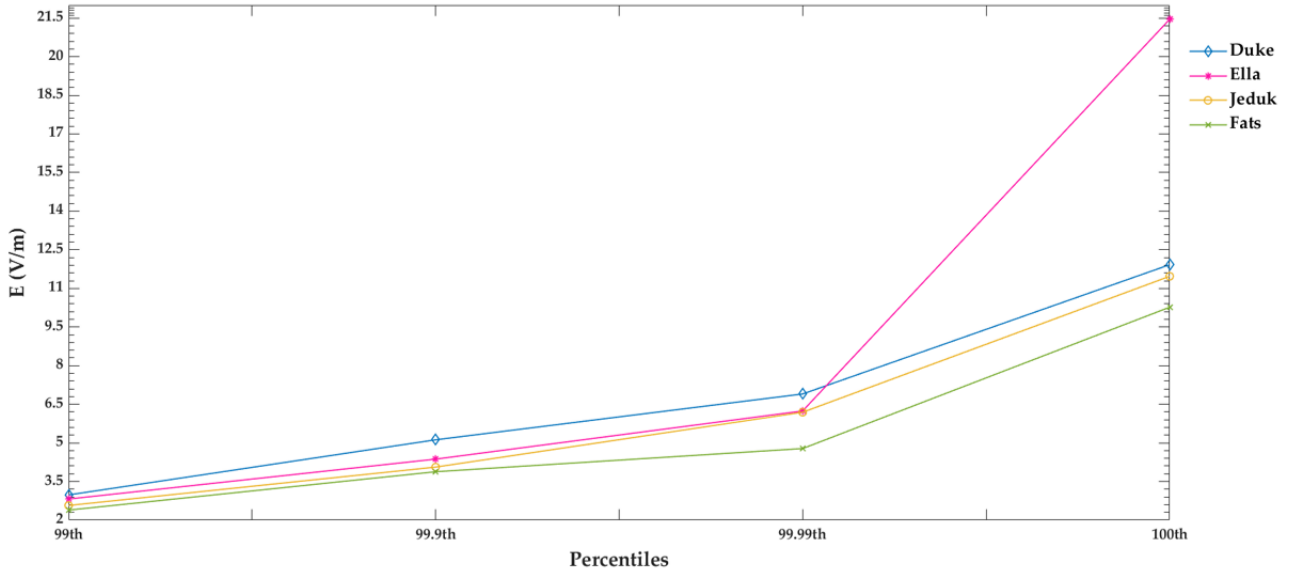


Figure VII. 5. Metric dose of the percentiles of the induced E-field in the exposure of the abdomen. Comparison among the four human models.

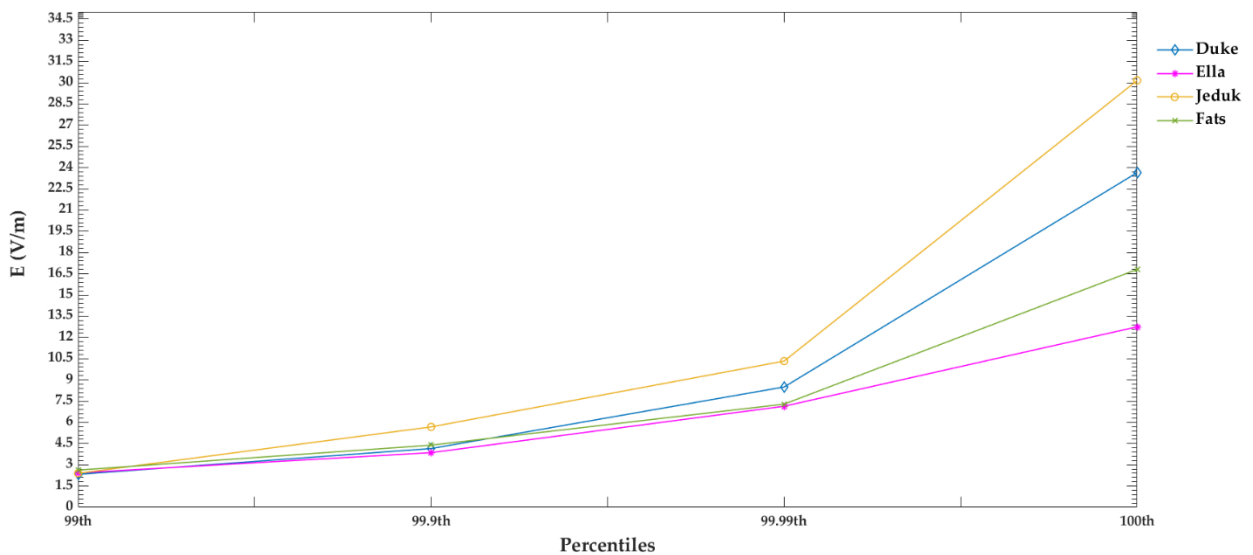


Figure VII. 6. Metric dose of the percentiles of the induced E-field in the exposure of the chest. Comparison among the four human models.

From the above figures, we can observe that, in the case of abdomen exposure, the other percentiles do not add relevant information, as the trends for the percentiles above the 99<sup>th</sup> reflect those of the 99<sup>th</sup> percentiles, thus adding no further information. In particular, Duke is represented by the line with the highest value, followed by Ella, then Jeduk, and then Fats, for all the percentiles considered. The only exception is present for the 100<sup>th</sup> percentile for Ella's model, as it far exceeds all the remaining values.



Looking instead at the percentiles for the chest case, we have that, while the 99<sup>th</sup> percentile suggests a maximum value in Fats, the 99.9<sup>th</sup> shows the highest value in Jeduk, which then maintains this trend, moving away from the others. The evaluation of the other percentiles could be very important, especially if we consider that the 99.9<sup>th</sup> percentile is sometimes considered more reliable in the literature for verifying compliance with the limits than the 99<sup>th</sup>, which in turn, as we have seen above, alone may not provide complete information on the extent of exposure. For example, in the case of chest exposure, the contribution of the female body characteristics (breast) is almost lost or however not totally appreciated. This is mainly because the 99<sup>th</sup> percentile is calculated in a total body evaluation, without showing how much the field is distributed in the tissues.

In Figure VII.7 and Figure VII.8, we describe the distribution of the induced E-field in the transversal plane, at the height of the source, where it is found the maximum induced E-field, accompanied by a cross-section of the conductivity maps of the tissues ( $\sigma$ ), followed by the body structures, separately reported in the third row of the figures.

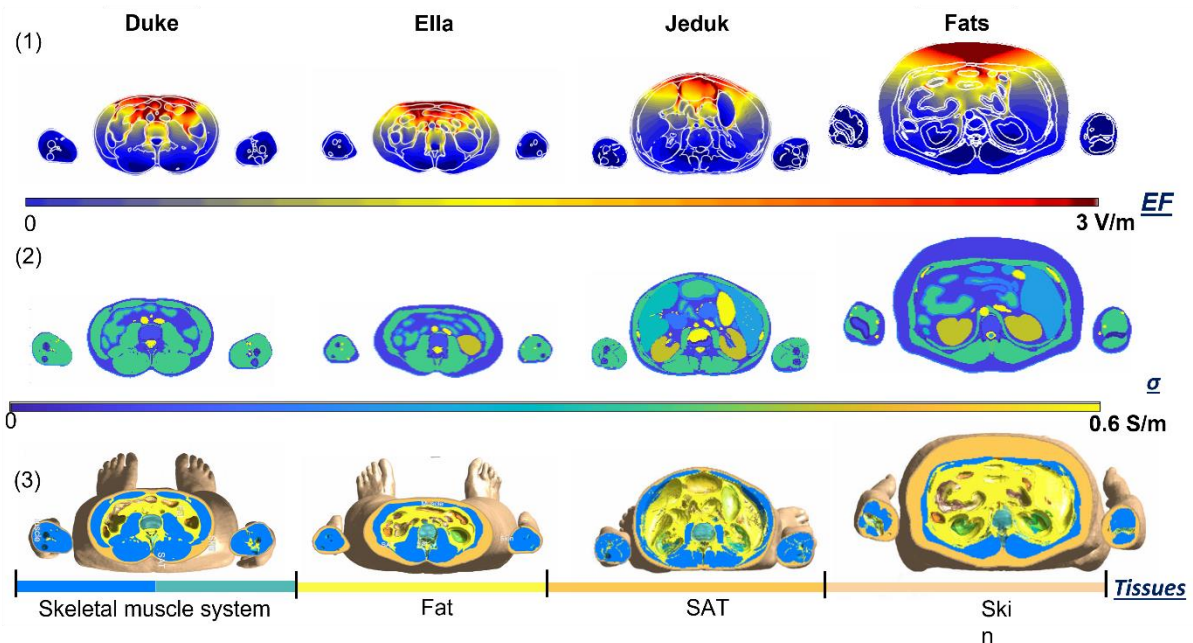


Figure VII. 7. Transverse slice, coil at height of the Abdomen at 70% MSO. Induced E-field (1), the conductivity of tissues (2), and real body tissues.

We first reported the case of exposure of the Abdomen (Figure VII.7). Here we can see that the maximum value of the induced E-field falls in the most superficial tissues of the bodies in front of the source, nevertheless, the shapes of the internal distribution are very different among the models. Although Duke and Ella showed a comparable distribution, Jeduk had a different behavior, with the electric field equal to the maximum (intense red, in the color bar) that covers a lower area of the tissues in the region of the abdomen exposed to the source. Furthermore, another different behavior was found in Fats, in which a very large and compact area interested by the maximum E-field was found and narrowed sharply inwards. To justify such observations, the conductivity maps of the tissues are needed. These latter are reported in Figure VII.7 (2) and are representative of the body structures reported in the third row (Figure VII.7 (3)). As is well known, visceral fat and subcutaneous adipose tissue (SAT) have a low conductivity (both 0.057 S/m), while the skin has a higher conductivity (0.17 S/m), followed by the muscular system which is even more conductive (0.35 S/m). These values are well representative of the maps of induced EF since the discontinuity of the conductivity seemed to spatially confine the electric field in the fat tissue, as we can see in Figure VII.7 (1). In this exposure condition, in the slice of Duke model, the maximum value of induced E-field of 4.4 V/m occurred in the fat tissue present in the region of the abdomen directly exposed to the source. The same situation occurred in Ella, where a maximum of 3.70 V/m is reached in the abdominal region in the subcutaneous adipose tissue (i.e., SAT). As regards the exposure of Jeduk, we found 3.64 V/m in the SAT. While, in the case of the Fats model, we computed a maximum of induced E-field equal to 3.58 V/m once again in the SAT located in the anterior abdominal area.

Successively, the second case of exposure where the coil is at the height of the chest is considered, with results reported in Figure VII.8.

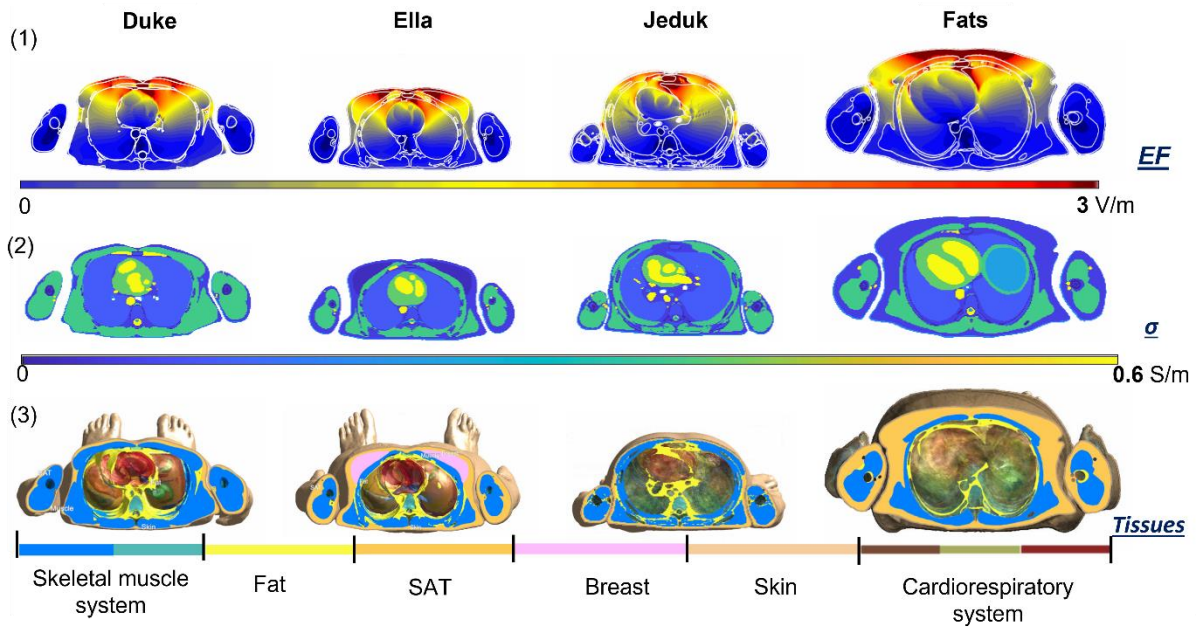


Figure VII. 8. Transverse slice, coil at height of the Chest at 70% MSO: Induced E-Field (1), the conductivity of tissues (2), and real body tissues.

A similar behavior can be observed. In row (1) of Figure VII.8, the intense red represents the maximum color bar for the E-field, and again occurred in the layers of the body directly exposed to the source, remaining confined in this area composed mainly of SAT. Analyzing each model, a maximum of induced field is achieved in fat or SAT tissues. Starting from Duke, we observed a maximum of 3.12 V/m in correspondence with the sternum at the discontinuity between SAT, bone, and fat. Ella showed a larger area of maximum equal to 3.16 V/m in the SAT and breast tissues (0.022 S/m). In Jeduk a maximum of 3.19 V/m was achieved in SAT and fat tissues. In the end, for the Fats model, a maximum value of EF of 3.51 V/m diffuses from the SAT toward the fat. All these values found in each model are observed in the region of the chest directly exposed to the source. Overall, it seemed to be confirmed that the layers of SAT and fat help to confine the induced E-field. Moreover, Figure VII.9 shows descriptive statistics (boxplot reporting minimum, 25<sup>th</sup>, 50<sup>th</sup>, 75<sup>th</sup>, 97<sup>th</sup> percentiles, and maximum) of the E field distribution evaluated in the tissues of the skin, SAT, fat, and breast, included in a cubical box of 24 cm identified in the anatomical district of interest concerning the coil positioned at the height of the chest.

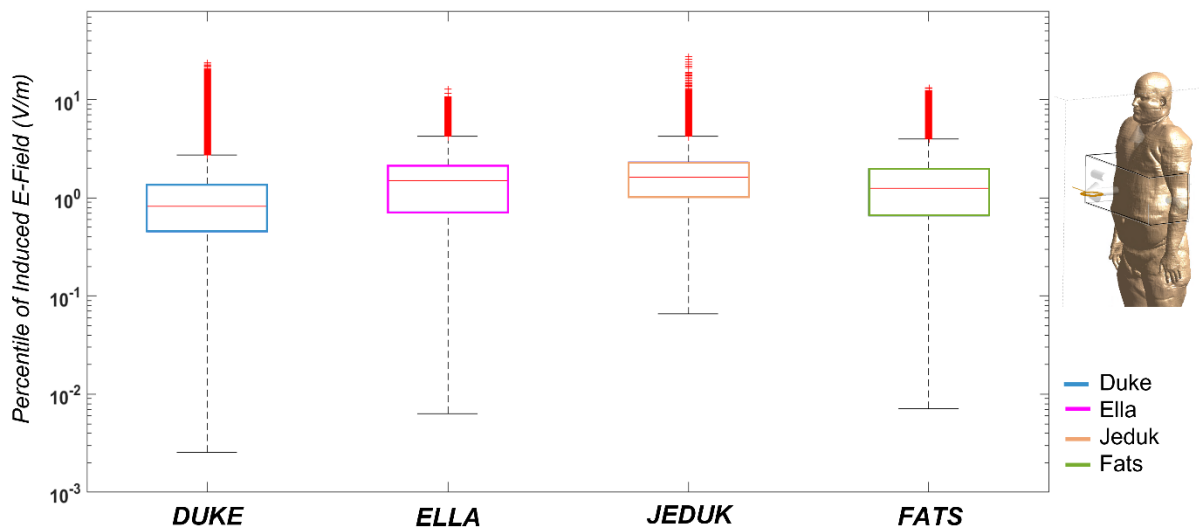


Figure VII. 9. Exposure of the Chest at 70% MSO. Boxplot of the E-field in SAT, fat, skin, and breast tissues, referred to a local area of the body in front of the coil

The boxplot shown in Figure VII.9 is in a logarithmic scale and describes how the induced electric field could depend on the anatomical characteristics of the human body. Analyzing the graph, we can see that the median is different among the four models and overall, each model, shows different behavior. In the case of Duke, the distribution is symmetrical, the first (25<sup>th</sup> percentile) and third quartiles (75<sup>th</sup> percentile) are at the same distance from the median, that is, the median line is exactly in the middle of the box, further the median value is the lower than the others. In the cases of Ella and Fats the observed distributions are characterized by a left asymmetry, that is, the median is closer to the third quartile than it is to the first quartile. Moreover, Fats' boxplot showed a larger dispersion than the other models, as can be seen from the box's higher height. Quite different is the behavior of Jeduk, in which we can observe that the median is higher than the other models, and the height of the box is the shortest (therefore we have less variability of data). Globally the upper whiskers plot are shorter than the inferior ones, and in the case of Jeduk, the inferior whisker is the shortest. To gain a deeper understanding, in Table VII- 3, the 99<sup>th</sup> percentiles computed in tissues chosen are reported, together with the values induced inside the only SAT, that is the tissue in which we observed the distribution of the higher values of the induced EF.

**Table VII - 3.** The 99<sup>th</sup> percentile of Induced Electric Field (V/m) for tissues of interest

70% MSO		DUKE	ELLA	JEDUK	FATS
<b>Abdomen</b>	SAT	5.89	4.38	5.61	4.01
	SAT + Skin + Fat	5.79	4.46	5.06	3.9
<b>Chest</b>	SAT	6.96	4.86	8.88	4.82
	SAT + Skin + Fat + Breast	3.55	4.13	7.89	4.80

The results refer to a local box of 24 cm of the region directly exposed to the source for the two exposure conditions (abdomen and chest). It is confirmed that concerning the induced E-field computed in the whole body, the percentiles found in the SAT tend to be higher than in the other tissues. The obtained 99<sup>th</sup> percentiles suggest that the value achieved in the tissue is inversely proportional to the dimension and/or thickness of subcutaneous fat, according to the fact that the lowest value was found for the Fats model. It is likely that a thinner thickness of SAT, which is a low conductive tissue, helps to confine the E-field in a small region with the consequence that the induced E-field reaches a higher value (as occurred in Jeduk).

## 7.4 Discussion

In this chapter an intersubject evaluation due to circular coil exposure, is proposed to investigate how single body characteristics can influence the electric field induced inside the operator during a TMS session. Four anatomical human body models from the Virtual Population<sup>145</sup> were considered, i.e. Duke, modeling the standard Caucasian male body, Ella, modeling the standard Caucasian female body, Fats, modeling an example Caucasian overweight man, and Jeduk, as a model of a non-Caucasian man. Such analysis has not been

taken into account in previous studies about exposure assessment of the medical staff to TMS, which conversely focused on the exposure variability due to different coil positions and orientations<sup>43,147,152,154</sup>. Nevertheless, it is well known that the body shape and its tissue distribution influence the electromagnetic quantities inside the body not only at the radio frequencies<sup>180</sup> but at low frequencies as well<sup>181,182</sup>. Hence here we evaluated how individual anatomies can influence the level of exposure induced in the operator. To the best of our knowledge, this is the first time that an intersubject variability study is performed in the frame of TMS occupational exposure. Following the method used in the other assessment of the exposure treated in this work, the TMS coil has been placed in two different positions, i.e., in front of the abdomen and the chest of the four human models, considering only the orientation II.

Two aspects are addressed: i) the assessment of risk shape-dependent and ii) the influence of intrinsic characteristics on the assessment of human exposure.

Regarding the first aspect, results of the 99<sup>th</sup> percentile show differences among the human body models up to 24.6% for the same exposure condition (as shown in Table VII- 2), which leads to conclude that there is an influence between the body characteristics and the exposure levels numerically estimated. The highest value occurs in Duke (2.98 V/m), for the exposure of the abdomen; and in Fats (2.63 V/m), for the exposure of the chest; However, also in the other models we obtained the 99<sup>th</sup> percentile of induced EF that exceeds limit, suffice it to say that the best case occurs in case of exposure of the chest in Duke model, with 2.33 V/m.

Particularly, in the exposure of the abdomen, we can observe a trend strongly dependent on the body. As expected, in all the models the peak of the induced EF is reached in correspondence with the coil, but the body characteristics seem to influence the values obtained in the remaining body sections, leading to different EF trends. For example, in the case of exposure of the abdomen, the obese model Fats, shows a behavior different from all other models, with an overall lower electric field intensity, almost uniform along the trunk. Such a result suggested a substantial role played by the fat and the SAT tissues in these

differences, owed to their greater thickness in the Fats model, compared to other subjects. Indeed, in the same case of the exposure, Duke shows a second peak of E-field, in correspondence with the reproductive system, where fat tissue is present as well, albeit thinner than Fats.

In the case of exposure of the chest, is the Ella model to show a particular behavior with respect to the other ones, since we found a plateau of the 99<sup>th</sup> percentile of EF, probably caused by the presence of breast tissue, that has a conductivity close to the one of the fat and SAT tissues. This seems to confirm the important role of the fat and SAT tissues, in the differences of exposure among the subjects. Even in this case of exposure, Duke, for example, has a second peak (in addition to the one at the source), right in the reproductive system, where we know there is a substantial layer of fat.

Results also show that the region with higher EF peak values is mainly located in the area in front of the coil and that, but the induced EF distributions along the body are strongly dependent on the anatomical characteristics of the clinicians. In addition, from the point of view of the risk assessment, Figures VII. 3 and .4, show that the limit is exceeded in the whole region of the bodies around the coil, and decreases below this only in the skull area and in the region between the knees and the feet.

Even considering the other percentiles of the E-field, since some studies suggest considering the 99.9<sup>th</sup> percentile for better verification of the compliance, these other percentiles, overall confirms the information provided by the 99<sup>th</sup> (see Figure VII. 5 and .6). Although this analysis allows us to obtain important information regarding the relationship between the acquired trend of induced EF and the shape of the clinician, that mean dependence of the intrinsic characteristics of the body structures; we chose to carry out a different evaluation, also considering the internal electrical property and anatomical geometry of the subjects.

Thus, to take into account the influence of intrinsic characteristics on the human exposure assessment, maps of the induced electromagnetic field were produced in the region where the highest induced electric field values were measured, i.e., the body slice in the transverse plane, at coil height. The maps help to understand the extent of the exposure in the body's

districts. In addition, we also considered important to associate them with the maps of the conductivity ( $\sigma$ ) of the body structures (Figures VII. 7 and 8). Based on these figures, we can conclude that the distributions of the induced field differ substantially among the models considered. It is crucial to observe how the maximum induced E-field profile seems to depend on the presence of the SAT and/or fat tissues. Another factor that influenced the distribution of the E-field was the geometry of these tissues, and, particularly, their thickness. The maps shown in Figures VII.7 and .8 showed that an important role in the E-field distributions was played by the discontinuity offered at the interface between tissues with different electric conductivity. Among the models such discontinuities could be placed differently, thus influencing the final distribution. For example, in the case of abdomen exposure, we can see that similar distributions are induced inside Duke and Ella, where resembling distributions of fat/SAT can be found. Both maps are characterized by “flames” that penetrate inward and become more penetrating in Duke, where, from what can be seen in the tissue cutaway, subcutaneous fat is directly in contact with visceral fat (light yellow color), giving continuity to the induced E field. Conversely, in the Ella model, we can observe that there is a layer of muscle interposed between SAT and visceral fat. Then the response of the induced field inside Jeduk shows a little area with the peak of the field (intense red in the maps), probably caused by the thin thickness of SAT under the surface of the model, where instead, in the conductivity maps, we can directly observe the presence of body structures with higher conductivity than the fat. It is interesting to observe that also in this case, only two lines of the peak of EF, penetrate internally, following exactly the profile of the SAT. Fats is characterized by a thicker SAT, that trapped the E-field in a “fan” shape, with an extension toward the visceral fat, again confirming the continuity of field induction between the SAT and fat.

In the case of exposure of the chest (Figure VII.8), the maps of induced E-field in Duke and Ella show a similar distribution, with a marked difference in the female model, likely owing to the presence of the breast, in which we can observe that the profile follows the shape of the breast, covering a larger area than in Duke. Furthermore, in both models, once again the penetration of E-field delineates the structure of the fat (subcutaneous and visceral).



Similarly, to what occurred with the abdomen exposure, we can observe that the very thin layer of SAT in Jeduk causes a smaller area in which E-field maximum is observed; such area is concentrated, in a circular shape, inside the fat. Fats model confirmed the behavior observed for the abdomen exposure, with the concentration of the maximum E-field in the thicker region of SAT, that in this model represents a large thickness under the skin. What we observed seems to suggest that the presence of the low conductive tissues of SAT and fat prevents the E-field from penetrating the other tissues. Thus, since the SAT is present immediately after the skin, this tissue, along with the fat tends to keep the field trapped inside. These preliminary results show the possibility that the presence of SAT, could be even protective in reference to internal organs, effectively trapping the E-field that seems to remain strongly confined in the fat layers. Jeduk remains the model that compared to the others, behaves more differently.

Finally results of Table VII-3 give us another crucial information, that is the importance of the geometry and thickness of the SAT in value that could achieve the induced EF inside the model. We can observe that the induced E-field appears to be in correlation with the thickness of the SAT. Indeed, the E-field seems to be inversely proportional to the width of this tissue. If we consider the case of the chest, the greatest amount of SAT appears in Fats, followed by Duke, then by Ella and finally by Jeduk. This precisely translates to a greater E field in Jeduk than in Fats.

In the case of exposure of the abdomen, the greater amount of SAT in Fats, confirms the lower 99<sup>th</sup> percentile of induced EF, followed by Ella (in which the interconnection between SAT and fat, that have same conductivity, resulting in a total greater layer); then by Jeduk whose layer of SAT is the thinnest, and finally by Duke, in which the presence of muscles (0.355 S/m), bones (up to 0.08 S/m) and also the tendon creates a discontinuity of conductivity, but especially interrupt the connection with the visceral fat, resulting in a lower thickness of SAT, and so in the higher value of induced EF.

These observations, although preliminary, must make us aware of the possibility that our intrinsic characteristics, could influence our response to a source of exposure and could help us for an improvement of the safety in the workplace.

## 7.5 Conclusions

In this chapter, a numerical dosimetry based safety assessment of the exposure of four anatomically different human body models, was conducted to investigate the distribution of the induced E-field and the role of an intersubject variability.

Our results show the existence of such variability, highlighting how anatomy could have a significant role in exposure assessment. We found that an important role is performed by the subcutaneous and visceral fat. This latter seems to be protective for the internal structures, since thanks to its low conductivity, tends to prevent the induced E field to circulate in the tissue layers and keep it concentrated in a limited area. If this area is large (as in the case of Fats) the electric field values tend to be lower than in a thin layer, where instead (as in the case of Jeduk) the field, although more concentrated, reaches higher values, (hence causing the presence of hotspots). Owing to the influence that the discontinuities of the tissues can have on the E-field distribution, it is not enough to consider whether an individual is obese or not, in order to come to safety conclusions, but one must also evaluate the intrinsic internal characteristics.

The results of this chapter, although strongly dependent on the source and the exposure conditions, prove the importance of an intersubject variability study using different human models, to obtain a more realistic workplace scenario of analysis. Moreover, they allow us to hypothesize that there may be scenarios in which not all the operators would be compliant with guidelines limits.

In future studies it could be important to evaluate also different working frequencies, other typologies of feeding systems, as well as other stimulating coils and other exposure

conditions, e.g., different coil orientations. This is a useful starting point for risk assessment, as it emphasises the importance of taking into account the different characteristics of the human body. In this way, it opens the way for a shape-specific risk assessment: shape-dependent. Possibly a correction factor that takes into account the worker's body characteristics could be considered in the risk assessment performed using the dosimetric method.

## VIII. CHAPTER

---

### 8.1 Possible health effects during TMS treatments: possible neuronal stimulation response

As widely supported in the ICNIRP guidelines<sup>13,14</sup>, exposure to low-frequency causes well-defined biological responses and the thresholds for the perception of some effects differ from the peripheral nervous system -PNS to the central nervous system- CNS. In particular, as is well note<sup>183</sup>, the basic restrictions have been derived by ICNIRP from biological thresholds of stimulation of excitable tissues introducing reduction factors to compensate for various sources of uncertainty, such as the extrapolation of animal data to effects on humans, differences in physiology and tolerance of different people, and statistical uncertainties in the results obtained from dosimetric analysis<sup>183,21</sup>. In the low-frequency range, experimental data indicate that the stimulation threshold of peripheral nerve fibers falls in the 4 – 6 V/m range of electric field strength and this assumption derives from the results obtained by So et al. 2004<sup>184</sup>, that carried out a study on heterogeneous high-resolution human models, by Reilly et al. 2002, through theoretical studies on the nerve fiber, Nyenhuis et al. 2001<sup>185</sup>, through homogeneous human models.

Conversely, the thresholds of both skeletal and myocardial muscle cells, although variable, are significantly higher than those of nerve fibers. When deriving the basic restriction for workers, a reduction factor of 5 has been applied to the minimum identified stimulation

threshold to account for the uncertainties described above. By studying some research conducted by Reilly (in a temporary gap of 1989 – 2002), it is found that the minor thresholds of the stimulation due to an external magnetic field, are equal to 6.15 V/m (or 7.3 V/m in the case of sinusoidal stimulation) for fiber with a diameter of 20  $\mu\text{m}$ , equal to 12.3 V/m for 10  $\mu\text{m}$  and 24.6 V/m for 5  $\mu\text{m}$ , with a uniform stimulus field (or current) oriented along the length of the fiber axis<sup>186</sup>. This threshold achieved 6.2 V/m<sup>186</sup> or 12 V/m<sup>187-189</sup> for the cardiac tissue, 5.9 V/m for the tissue of the forearm, and 6 -12 V/m for the tissues of the muscular-skeletal system<sup>188</sup>, in the end, 0.075 V/m for phosphenes.

In addition is also important to consider another study by Laakso et al. 2016<sup>190</sup> in which they showed that the thresholds found, precisely through the use of a TMS on a patient, deviated from the ICNIRP basic limits by a factor of 22, quite different from both the factor 5 and 10 that the body uses to protect both workers and the general public respectively.

It should also be pointed out that an ICNIRP Note on the use of guidelines (1999) states: "There is no solid basis for the precise determination of safety factors. The safety factors are based on a conservative value judgment by a group of experts. In the new ICNIRP guidelines, safety factors range from 2 to >10 depending on the degree of uncertainty about the knowledge of thresholds for direct and indirect health effects due to interaction with fields at different frequencies." Obviously, a mere exceeding of the BRs does not imply inevitably a nerve stimulation; however, when considering a specific individual exposure, it cannot be excluded that, for her/his particular sensitivity, a stimulation effect occurs at exposure levels between the BR and the identified threshold. Therefore, it is not possible to guarantee the health of workers exposed to levels exceeding the health effects of BR for low-frequency fields. For this purpose, it is necessary to consider that the lowest biological effect threshold corresponds to the mere perception of the electric currents induced. It has also to be considered that the thresholds of painful perceptions, and potentially dangerous effects, such as involuntary muscle contraction and cardiac stimulation up to the induction of ventricular fibrillation, are increasingly higher. The protection of workers could be assured if it is guaranteed that just minor effects like non-painful perception can occur<sup>101</sup>. From what is found in the literature, it is clear that it is possible that in the exposure conditions

considered in this work, some possible exceeding of the biological thresholds could occur, also owing to the hot spot that we have observed and also because, from the analysis of the distribution of the induced E-field in the body of the operator it is evaluated that sometimes the 99<sup>th</sup> percentile could underestimate the exposure since, in its the total body evaluation, some information could be lost. It is to be noted that at our frequency of work, the threshold indicated of ICNIRP is equal to 4 V/m (rms), that in more than only one circumstances is exceeded in the assessment of the exposure treated in the previous chapters. For this reason, in this chapter, an analysis of the possible stimulation of the human fiber is carried out.

## 8.2 Neuronal analysis: Jeduk and Yoon-Sun neurofunctional models

For the study of the possible neuronal stimulation, owing to the exposure to the high magnetic field produced by the TMS device is necessary to consider the neuro-functionalized human computational models. In particular, they allow us to study the mechanisms of neurostimulation and ensure the safety of the device. In the software, Sim4life two human neuro-functionalized models are available, that are: Jeduk and Yoon-Sun. Jeduk is the Korean male model, previously described, which through an improvement conducted jointly by the Visible Korean team<sup>191</sup> and IT'IS<sup>19</sup>, has been transformed into its neuro-functionalized version. This model was obtained from the original high-resolution cryosection images used to obtain the basic Korean model. The image quality and resolution made it possible to segment previously unaccomplished details in the peripheral nerves, arteries, veins, and other small structures. Therefore, in this neuronal version, the muscles, nerves, and blood vessels have been segmented, named, and meshed as separate objects, allowing for more accurate analysis. This male model is added to a female neuro-functionalized model, also obtained by the cooperation of the IT'IS and the Visible Korean team, which have collaborated project called *Neuroman*. Yoon-Sun model includes neuro-functionalized nerve trajectories modeled as splines. All major peripheral nerves, muscles, and blood vessels have been separately named and meshed. The neuronal analysis allows to evaluate the EM-induced neuronal activation, inhibition, and synchronization

using either complex, multi-compartmental representations of the neuronal trajectories. To do this Sim4Life uses the *Neuron solver* (see Chapter III for more information) developed at Yale University<sup>192</sup> which is ideal for studying neuronal interaction mechanisms. The presence of both the models, male and female, is an important extension that allows us to compare simulation results and predictions obtained with both male and female adult models, e.g., to investigate differences due to anatomical variability, as done in this work for all the exposure conditions.

The two models are young adults: Jeduk is 33 years old, 1.62 m, 54.5 kg; whereas Yoon-Sun is 26 years old, 1.52 m, 54.6 kg. Jeduk includes a set of 1186 tissues, and Yoon-Sun counts a total of 1144 tissues, both at high resolution. Nerves, muscles, veins, and arteries are separated. Anatomically correct nerve trajectories have been extracted from the segmentation and functionalized as splines for use with Neuron. Both models support the Poser function in Sim4Life, which is a tool that allows modification of the pose of the model, as done for Duke in chapter IV, to simulate the operator that grips the handle of the coil.

In this type of analysis, it has been chosen to consider the exposure to the figure-of-eight coil, which is one of the most used devices for TMS treatments, power by the Rapid2 of the Magstim Co.; this means to work at 3 kHz with current  $\approx 4$  kA (see Chapter III). The two human models (Jeduk and Yoon-Sun) grip the coils but with both their hands, keeping the standing position adjacent to the patient, again simulated with the head of Sam. In this case, the conditions of exposure would be to reproduce real working conditions, paying attention to the position of the hands, which have to reproduce as real as possible what during medical practice was possible to observe, for some types of treatments. The importance that is given to know to the position of the hands, comes precisely from what has been found for Duke, where high values of induced electric field have been detected. Assuming therefore that such fields are also present in Jeduk and Yoon-Sun, and since the hands are highly innervated, there is a great attention to possible nerve stimulation eventually induced by the TMS exposure.

Together with these considerations there are other parameters to be considered as the type of fiber to be used in the simulations (comprehensive of its diameter) and the selection of the nerve trajectories that may be of interest. Regarding the type of the fiber, the software Sim4life offers different types of fibers, such as Spatially extended nonlinear node (SENN), the rat sciatic nerve, the unmyelinated Sundt C-fiber (fiber with specific membrane resistivity) and also the Modified MRG models for both the myelinated sensory and motor axon fibers. For the present study the modified MRG models has been chosen. Moreover, since from the literature<sup>186-189</sup>, it is found that the fiber with greater diameter has a lower threshold of stimulation compared to the fiber with the others, a preliminary test was carried out to confirm if as the diameter increases the threshold of stimulation decreases, and indeed the results prove this. Further, as reported also in the above-mentioned studies, the sensory fiber has a lower threshold of stimulus compared to the motor fibers (with the same diameter and the same location). Therefore, in our analysis, we chose to consider only the sensory fibers with a maximum diameter considerable, which is 20  $\mu\text{m}$  (the range of the choice is from 5  $\mu\text{m}$  up to 20  $\mu\text{m}$ ). Therefore, we have created a condition in which the probability of obtaining stimulation is higher.

For the choice of the trajectories involved in the neuron analysis, a preliminary consideration had to be made. From the assessment of the exposure carried out in this work, what emerged is that the region of the body in which it is found considerable values of the induced E-field is the one directly exposed to the source. For example, a negligible induced E-field in the head is observed when the coil is at the height of the chest or of the abdomen, and conversely, when the coil is at the height of the chest, very low induced E-field is present in the legs. Finally, in all the conditions, a small E-field reaches the back. From these assumptions, the choice has been to consider only the nerve trajectories that are involved in the trunk and in the limb.

As a preliminary analysis, we evaluated what it is possible to obtain (in terms of induced E-field) when the figure-of-eight is in an inclined position, that occurs typically in the later motor treatment, Figure VIII.1:

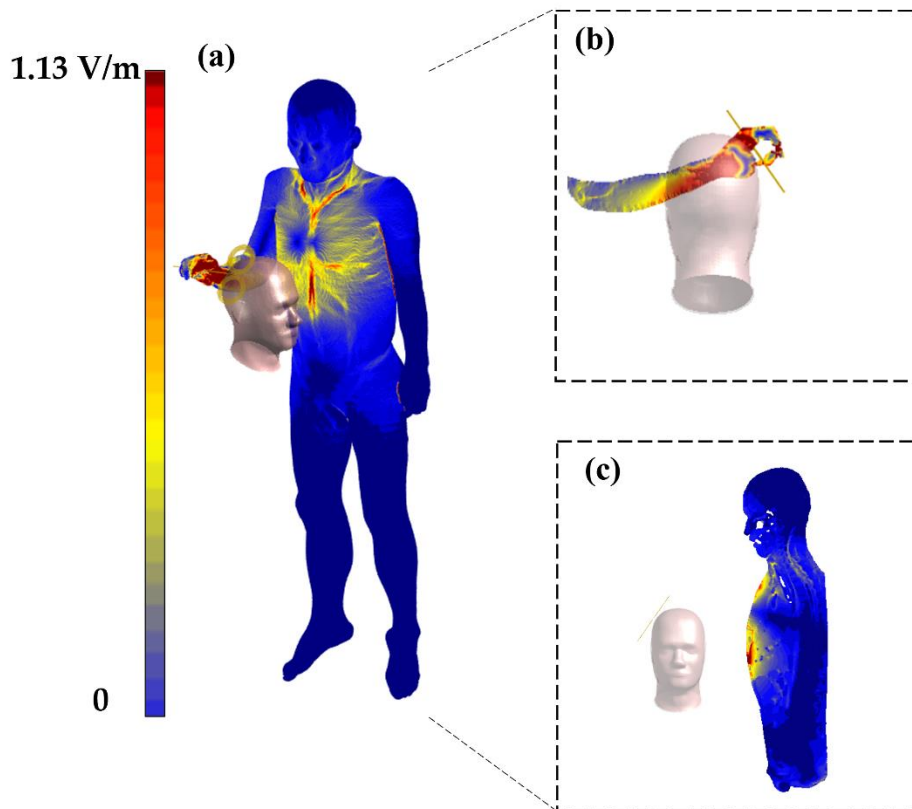


Figure VIII.1. Exposure operator-dependent. Distribution of the induced E-field with the figure-of-eight inclined of about  $55^\circ$  on the head of the patient. (a) whole body exposure on the surface, (b) focus on the limb, (c) focus on the central slice of the body.

This preliminary analysis is important to verify that also with the inclined coil, the district of the body involved in the exposure does not change from those observed so far. Indeed, considering this position in which the operator holds the inclined coil at about chest height, what has been detected is confirmed: the front part of the trunk and the forearm are interested by intense E-field. From these results, a direct consequence is the choice of trajectories. Focusing on the thorax area, the study is reduced to the trajectories present where an important field is present, Figure VIII.2, shows this consideration:



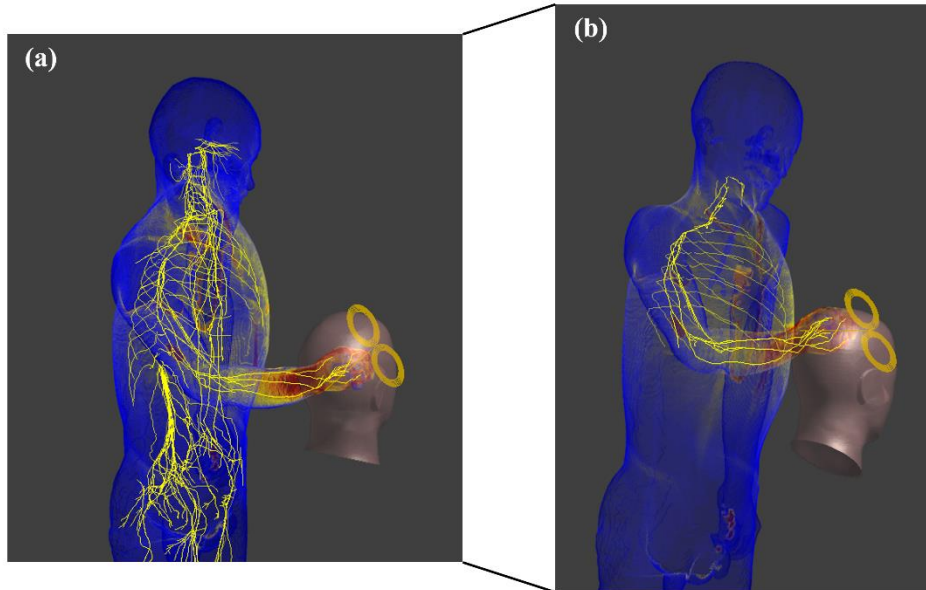


Figure VIII. 2 Choice of the trajectories to involve in the neuron study. (a) All the trajectories present in the upper part of the body, (b) selected trajectories forming part of the body region in which we have a relevant E-field.

Figure VIII.2 (a), shows all the trajectories present in the body, focusing on the upper part of the body. From what observed in Figure VIII.1, it makes sense to consider those nerve trajectories where the E-field distribution reaches values high enough to eventually produce a stimulus (i.e., above the limits). Thus, thoracic and brachial (ulnar, median and radial)trajectories will be analyzed. This will be applied to both models.

The final step is to define the environment of the exposure and set the position of the two models with respect to the coil. A possible real position, which an operator may assume, during a later-motor cortex treatment, i.e., with an inclined coil, was considered. In particular, two configurations have been chosen:  $\alpha$ ) in which the Patient's ear faces the clinical chest, and  $\beta$ ) in which the Patient's nape of the neck faces the clinical chest. For both conditions, the operator holds the coil with his/her two hands. The distance between the ear and the nape of the neck is equal to 12 cm, as previously considered.

The positions are reported in Figure VIII.3:

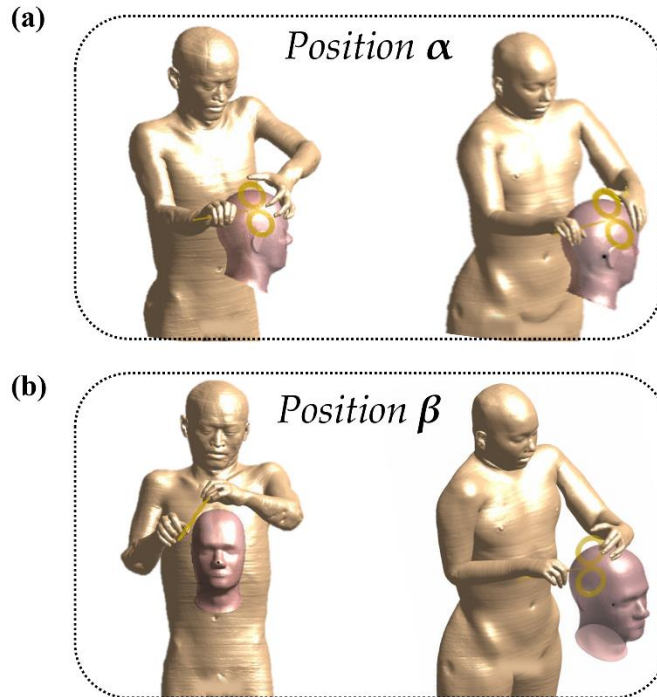


Figure VIII. 3 Exposure conditions. (a) Position  $\alpha$ , ear of the patient facing the chest of the operator, that keeps the coil in positions with both hands, (b) Position  $\beta$ , nape of the neck of the patient facing the chest of the operator, that keeps the coil in positions with both hands. Coil inclined of about  $55^\circ$ .

In both positions, the right hand of the operator is positioned on the handle of the coil while gripping this latter. The left hand is positioned close to the windings, and likewise keeps in position the coil, this is a typical configuration assumed by the operator, which most often helps with the second hand to hold the coil, placing the latter one so as to hold the coil sideways and therefore supporting it externally where there are windings. The positions of Yoon-Sun are similar but not exactly equal to Jeduk, since the aim is to carry out an analysis operator-dependent and not a comparative study between male and female, as before done. The following analysis starts the positions previously described.

### 8.3 Results

The assessment of the exposure carried out with the Neuron solver, implies as the first step the evaluation of the solutions of the Quasi-Static LF solver, i.e., the neuron exposed to an EM field detects an electric potential ( $\phi$ ) distribution that can be extracted directly as the

quantity of QS LF solvers, as explained in Chapter III. Therefore, the induced E-field is first evaluated, to verify compliance with the limits suggested by the guidelines and possibly find out how much the limit has been exceeded. Starting from Jeduk, is reported the surface distribution of the induced E-field in the body, but the aim is in particular to highlight what occurs in the hands since they are the part of the body closer than the other to the source.

Figure VIII.4 reported the exposure of Jeduk, with the power of the system set to 70% MSO.

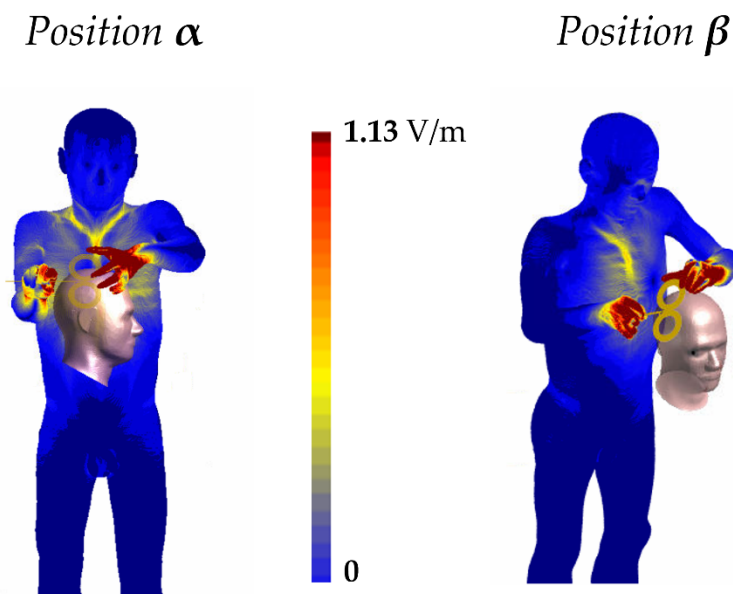


Figure VIII. 4. Distribution of the induced E-field in the surface of the body of the Jeduk model, in the two configurations:  $\alpha$  on the left and  $\beta$  on the right. Maximum color bar set to the limit.

As it can be seen, the hand is highly exposed, indeed a large area is affected by an induced E-field that probably exceeds the basic restrictions since the maximum of the color bar is already set to the limit suggested for the frequency of the working source. Clearly, the left hand that is near the windings is affected by a larger intense red area, compared to the right hand, that at the same time results likewise interest by a not negligible E-field, in particular in the position  $\beta$ , since the back of the hand is all facing the windings. At this point, a post-processing of the data was carried out and the 99<sup>th</sup> percentile of the induced E-field was calculated; thus Table VIII.1 summarizes what it is found:

**Table VIII - 1.** The 99<sup>th</sup> percentiles of the induced E-field (V/m) in the district of the hand and forearm

		%MSO	30%	50%	70%	100%
<i>Position <math>\alpha</math></i>	<i>Right hand</i>		0.99	1.65	2.32	3.31
	<i>Left hand</i>		2.77	4.61	6.46	9.23
<i>Position <math>\beta</math></i>	<i>Right hand</i>		0.84	1.41	1.97	2.81
	<i>Left hand</i>		3.15	5.24	7.34	10.49

From these results, is clear that both the hands are exposed to an induced E-field that exceeds the limit in all the conditions, except for the case of the right hand in both positions, in which the induced E-field decreases below the limit with the 30% MSO. In addition, in the left hand, the threshold indicated by ICNIRP is exceeded. The lowest exposure of the right hand is because by comparing with the left hand, the right one is farther from the source than the left one, which instead holds the surface of the coil near the windings. In addition, the right hand in the position  $\beta$  shows a larger area affected by an induced E-field that achieved the limits; the higher value of the E-field is recorded in the position  $\alpha$ , this is because in this latter configuration the right hand is inclined toward the coil and thus closer to the windings, even if in a smaller area. No other percentiles are evaluated, since the aim of the chapter is to consider the overexposure, thus we refer only to a comparison with ICNIRP limits.

Considering the exposure of the female human model, the distribution of the induced E-field is shown in Figure VIII.5.

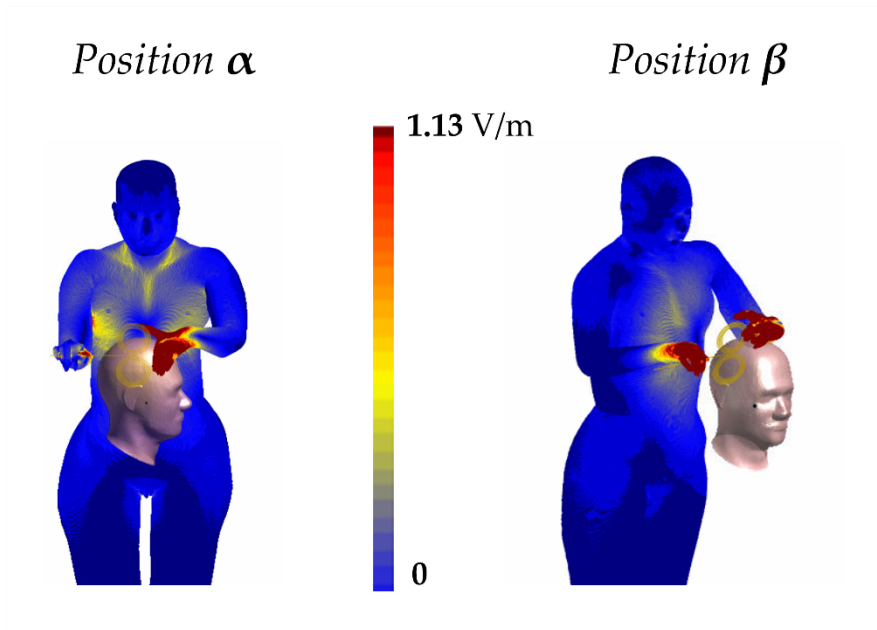


Figure VIII. 5. Distribution of the induced E-field in the surface of the body of the Yoon-Sun female model, in the two configurations:  $\alpha$  on the left and  $\beta$  on the right. Maximum color bar set to the limit.

In this case, it is possible to observe that in both conditions the left hand is invaded by an intense red (maximum color bar), while differences occur in the right hand. Notably, in the position  $\alpha$ , the right hand is farther than in the case  $\beta$ , and also is positioned horizontally, following the handle; while in the position  $\beta$ , the hand is closer to the source and inclined with the thumb and the index pointing towards the coil while the hand grips the coil. The hand itself in turn is slightly tilted forward. Subsequently, the evaluation of the 99<sup>th</sup> percentile of the E-field is carried out and reported in Table VIII-2:

**Table VIII - 2.** The 99<sup>th</sup> percentiles of the induced E-field (V/m) in the district of the hand and forearm

	%MSO	30%	50%	70%	100%
<i>Position <math>\alpha</math></i>	<i>Right hand</i>	0.41	0.68	0.95	1.37
	<i>Left hand</i>	4.04	6.74	9.44	13.48
<i>Position <math>\beta</math></i>	<i>Right hand</i>	1.78	2.97	4.16	5.94
	<i>Left hand</i>	6.35	10.58	14.81	21.16

The results show that in position  $\alpha$ , the limit is exceeded with all the percentages of MSO, while for the right hand it occurs only if the device is powered by 100% MSO. In this case, the left hand seems to be in a position less safe, as observed by the analysis of the distribution of the induced E-field. For position  $\beta$ , all the percentages of MSO, and for both the hands, cause the limits to be exceeded.

From these results is clear that the extent of the exposure strongly depends on the subjectivity with which treatment is done, or on the position of the hands. It is certain that keeping a close distance from the source often results in high exposure, but it also depends on how the hands are positioned (slanted, straight, with fingers spread out, etc.).

Analyzing these values of the induced E-field, we can conclude that the possibility of producing a stimulus is not remote, since from the literature the electric value is around 4-6 V/m (indeed the limit at our frequency is derived from the 4 V/m by applying the reduction factor of 5). Therefore, a Titration analysis (see Chapter III for more details) is carried out. From the Titration, it is possible to detect the value of the current needed to produce a stimulus in the nervous trajectories chosen for the study. In other words, if, for example, the Titration indicates that the current value required to produce a stimulus must be greater than 4 kA, the source under consideration will not be able to induce any neuronal stimulation, since at 100% MSO the maximum current will be 4 kA. To this end, remember that lower power percentages (30% ÷ 80% MSO) are always used in medical practice.

Starting from Jeduk, in the following Figure VIII.6 the trajectories chosen are shown, including the brachial and thoracic nerves, but only relative to the area in which it is possible to find an important field, that from the preliminary study regard only the surface of the trunk and the limbs. The nervous fiber are the sensory ones with diameters equal to 20  $\mu\text{m}$ , for the two human models.

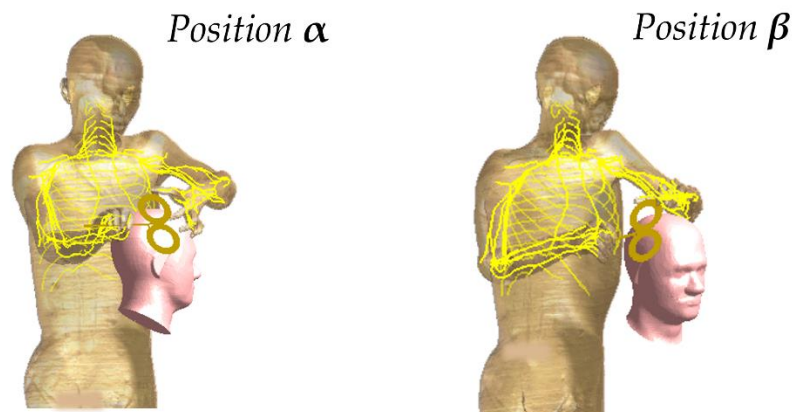


Figure VIII. 6. Trajectories under test for the Titration analysis. Sensory MRG neuron of 20  $\mu\text{m}$  diameter.

Thanks to the Titration analysis it is found that, that the possibility for the figure-of-eight to produce a stimulus is not very likely, since it occurs only in a few nodes along the axon. Exactly in the position  $\alpha$ , in several nodes about twenty, it is possible to produce a stimulus if the source work at  $\approx 85\text{-}94\%$  MSO, in all the other cases is needed a current much higher (up to  $\approx 286$  kA). In position  $\beta$ , the stimulus occurs in a lower number of nodes, belonging to the left brachial plexus median, but in this case, is needed a current equal to  $\approx 96\text{-}99\%$  MSO. The average current value necessary for an induced stimulus, in the remaining nerve fibers ranges from 100 kA up to  $10^6$  kA. What is obtained, demonstrates that the possibility of the stimulus is remote, since occurs in a few nodes of different axons and also with a high value of MSO, hardly used during medical treatments.

In the case of Yoon-Sun the trajectories are shown in Figure VIII.7:

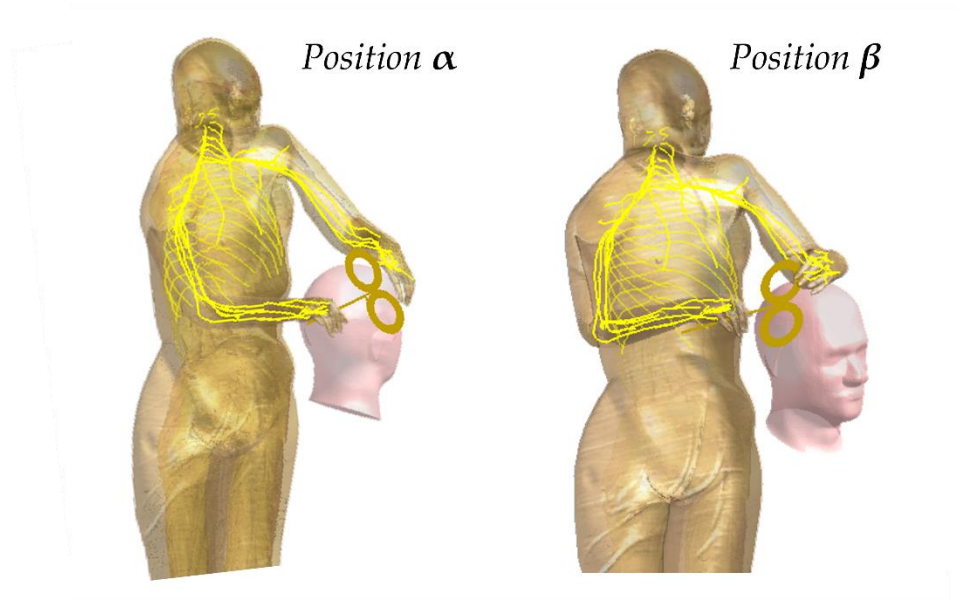


Figure VIII. 7. Trajectories under test for the Titration analysis. Sensory MRG neuron of 20  $\mu\text{m}$  diameter.

For this case it is obtained that, in the position  $\alpha$ , the stimulus is produced in correspondence of twenty nodes, belonging to different axon fitting to the only left brachial plexus (median and radial), but is necessary a current equal to the  $\approx 73\text{-}77\%$  MSO. The average current value necessary for there to be an induced stimulus, in the remaining nerve fibers ranges from 10 kA up to  $\approx 524$  kA. On the other hand, for the position  $\beta$ , it is found that in several nodes equal about to thirty, is produced a stimulus when the coil is powered by a percentage of MSO ranging from 65% up to 89% and this occurs again in the left brachial plexus (median, radial and ulnar). In the remaining axons, the activation of the nerve nodes requires an external current ranging from 200 kA up to values of the order of  $10^6$  kA.

The results, for both models, are summarized in Table VIII-3, in which are reported the range of the percentage of MSO necessary to produce a stimulation, the number of nodes in which it is possible to obtain this latter, and finally the maximum current needed for the coil to activate the neuronal response in the all nodes evaluated.



*Table VIII - 3. Results of the Titration analysis*

		<i>MSO%</i>	<i>Number of nodes interested in stimulus</i>	<i>Maximum Current needed</i>
<i>Jeduk</i>	Position $\alpha$	85-94%	20	up to $\approx 286$ kA
	Position $\beta$	96-99%	9	up to $10^6$ kA
<i>Yoon-Sun</i>	Position $\alpha$	73-77%	20	up to $\approx 524$ kA
	Position $\beta$	65% - 89%	34	up to $10^6$ kA

Based on these results it is possible to conclude that the effects of stimulation are improbable, even though Yoon-Sun shows a higher probability of their occurrence. Therefore, although the evaluated induced electric field exceeds the limits and, in many cases, even the biological thresholds, overall no relevant stimulus event at the neuronal level is detected, since high percentage of MSO would be required.

This is probably due to the fact that the ICNIRP adopts a conservative approach, whereby overexposure need not cause an effect.

## 8.4 Discussion and conclusions

In this chapter, a neuronal analysis is carried out. Since the results obtained from the assessment of the exposure with all the human models used in this work have shown that in many conditions the operators are exposed to an induced E-field that exceeds the suggested limits by the ICNIRP guidelines, it is chosen to analyze better the overexposure condition. Indeed, when E-field induction values are above the limits the possibility that the threshold for neuronal stimulation was also exceeded cannot be remote. To perform this type of analysis, the software Sim4life provides two neurofunctionalised human models, through which an accurate neuronal study can be carried out. In order to set up the case study in the best possible way, different steps were necessary: a) choosing sensory nerve fibers with a diameter of 20  $\mu\text{m}$ , b) positions of the models mimicking those assumed by an

operator during a treatment involving latero-motor stimulation of the patient's head, c) two orientations (positions  $\alpha$  and  $\beta$ ) of the patient's head. As done in the other chapters, the E field distribution was evaluated as well as the areas of the body where a field sufficiently wide to exceed the limits, and hence suitable for neuronal stimulation. This led to the identification of nerve trajectories, to be used for Titration, which therefore only affect the trunk and arm area. The 99<sup>th</sup> percentile values confirmed that the limits (and threshold values) were exceeded and therefore *Titration* was carried out. Results showed that although the limits are exceeded, the E field values do not reach a threshold in the nerve fibers that would induce stimuli of significant magnitude. Indeed, in the few nodes where the possibility of producing a stimulus was recorded, the MSO values to be used were higher than those expected in medical practice in most of the cases examined. We can therefore conclude that the figure-of-eight, although it causes an overcoming of limits, especially in the area of the hands, is not capable of causing a nerve stimulus. However, since the results are strongly influenced by the position of the hand and also by the position of the coil (as well as the model of the coil itself), the suggestion is in any case to keep hands as far as possible away from the coil in order to avoid any possible risk.

In the future, we might consider carrying out the same study for the circular coil, which has always proved to be the less safe according to our results. The objective remains to improve safety in the workplace and thus provide the means to improve it. No less important is the scientific contribution that such a study can make to the literature, as to date no such study has been carried out on TMS concerning the possibility that this device could produce a stimulus when used.



## **SECTION IV. TECHNICAL SUPPORT IN INAIL MISSION**

---



# IX. CHAPTER

---

## 9.1 Aims of the Institute and measurement campaigns

The research project shown in this work started from a collaboration between the National Institute for Insurance against Accidents at Work- INAIL and Sapienza University. In particular, the departments involved in the research are the Department of Medicine, Epidemiology, Occupational Hygiene and Environment (DiMEILA of INAIL, which provides funding support) and the Department of Information Engineering, Electronics, and Telecommunications (DIET). Since the work combines the aims of both departments, it was of paramount importance to consider the purposes that characterize both institutions, that is from one side the scientific mission of the DIET Department and from the other side the interest in the health and safety in workplaces jointly to the interest in the research area of INAIL. In particular, research, study, experimentation, and advanced training activities in the field of occupational health and safety are carried out by INAIL following the expansion of its institutional functions as a result of the incorporation of Ispesl - Istituto Superiore per la prevenzione e la Sicurezza del Lavoro (Higher Institute for Occupational Prevention and Safety). Through its research activities, the Institute pursues the objective of improving health and safety conditions and reducing the phenomenon of accidents and the occurrence of occupational diseases. Therefore, adapting to the changes introduced by new forms of work organization and production processes and by technological innovation, the Institute implements solutions capable of preventing and managing risks in the workplace. Some of the most important results achieved thanks to INAIL's research activities include the development of technological tools to reduce risks to the musculoskeletal system, devices for working in safety, the design of new ways of managing different types of risk, for example, electromagnetic risk, and analyses on the development and use of nanotechnologies in the workplace. The research activity is carried out by two scientific departments: the Department of Medicine, Epidemiology, Occupational and Environmental

Hygiene, with a health vocation, and the Department of Technological Innovation and Safety of Anthropic Installations and Settlements (DIT), with a technological vocation, in the field of occupational health and safety. DIMEILA carries out and promotes the study, scientific research, and experimentation activities, according to the principles of occupational medicine, occupational epidemiology, and occupational and environmental hygiene. It collaborates with the World Health Organization (WHO) and the Central Prevention Directorate for the coordination of the activities of the Focal Point for Italy of the European Agency for Safety and Health at Work. As part of its departmental activities, the Occupational and Environmental Epidemiology Laboratory plans and conducts epidemiological studies to deepen knowledge of the state of health of workers and living environments. The Laboratory also conducts research activities for the epidemiological surveillance of exposure to carcinogenic and biological agents, and in general on all physical risk agents (electromagnetic fields, optical radiation, noise, vibration, and so on), in the workplace and related diseases. Within this framework, numerous studies have been conducted on risk mitigation and prevention of health effects. Therefore, the present work has considered both the aspects of the research and novelty and also the improvement of safety in the workplace. During the years of the Ph.D. project, part of the activity carried out has also seen myself involved in activities that are purely typical of INAIL, i.e., measurement campaigns also conducted in collaboration with other Institutions. Due to the pandemic period, unfortunately, the number of measurement campaigns carried out was much less than usual, due to the impossibility of reaching workplaces. This is precisely because one of the peculiarities of these measurements is that they are conducted in the working environment, with the presence of the worker who sets the measurement site together with the team, such as the actual working conditions. This is very important to detect criticalities, also due to bad practice in the execution of the work activity. Although I also participated in other measurement campaigns, through a research grant that preceded the period of the Doctoral course, the campaigns conducted during these three years mainly concerned: i) the exposure owing to an aesthetic machine and ii) the immunity analysis of the pacemaker exposed to E-field produced in GTEM cell.

The first measurement campaign was carried out, to deepen a new device that was beginning to expand in Italian beauty centers following high usage in the United States, where the device has now become part of aesthetic practice. What led INAIL towards this campaign was the similarity of this device to TMS. In fact, this device is characterized by two applicators, each of which consisting of a circular coil, and can produce a magnetic field up to 7 T.

This is a non-invasive therapeutic device, that produces an electromagnetic field that interacts with the tissues of the human body. The device has two outputs that enable simultaneous treatment by the two applicators. The purpose of this machine is to improve fitness through the rising of muscle tone and firmness, strengthening the muscles of the arms, abdomen, and so on. To achieve this goal, it is necessary to cause a muscle stimulus, therefore an important induced electric field must be produced. The system consists of two applicators, an elastic band to keep in position the coils on the surface destined to the treatment, and a power system that produces a signal equivalent to a pure sinusoid with a period of 350  $\mu\text{s}$  (corresponding to an equivalent frequency of 2.8 kHz).

The applicator is shown in Figure IX.1.

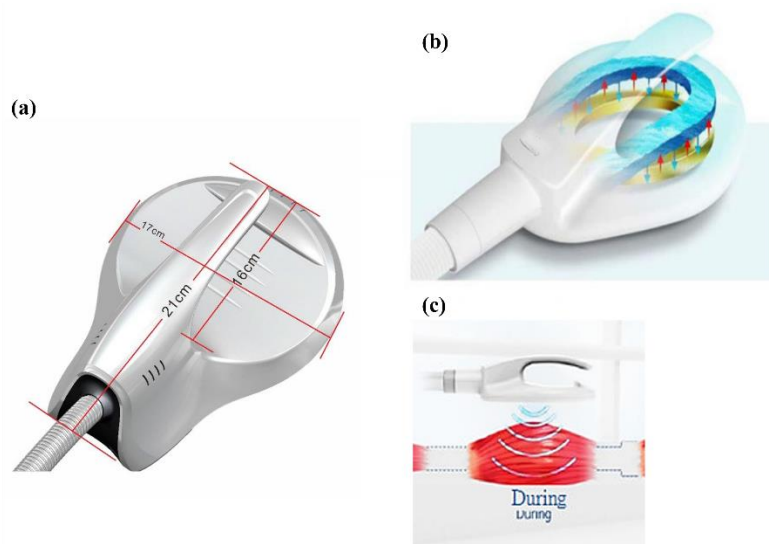


Figure IX. 1Applicator of the aesthetic device. (a) dimension of the coat of the coil, (b) an image of the interior with the scheme of the windings of the coil, (c) an example of the exposure. Image adapted by the user manual.



From the user manual (name and model of the device are private materials) this pulse magnetic stimulator is fed by a maximum power of 2800 W and the produced current density is 1.5 mA/cm<sup>2</sup>. Further, it is defined as a biphasic pulse stimulator with a pulse range of 1-150 Hz. As before mentioned, the maximum magnetic field produced by this device can achieve 7 T. This latter is equal to that produced by some models of TMS, but in this case, the subject is not a patient but a member of a general population since this is an aesthetic treatment and not a clinical one. Therefore, in the analysis of the exposure, it is necessary to evaluate the exposure of the worker but also the exposure of the population.

To obtain the evaluation of the kind of the exposure a NARDA ELT 400 E field probe was used, with the following measurement chain (Figure IX.2).



Figure IX. 2 Measurement chain of instrument NARDA ELT 400

The Narda ELT-400 instrument was used by inserting it into a measurement chain consisting of an Agilent U2531A acquisition board (DAQ) and a personal computer. This chain, managed by software specially developed in the LabView language (from LabView 2009, National Instruments Corporation, Austin, TX 78759, USA), makes it possible to take the voltage signals supplied by the magnetic induction sensors via the probe's analog outputs, digitize them and make them available for post-processing.

By means of the personal computer, it is also possible to directly display and record the signal waveform providing both the real-time measurement of the emitted fields and the exposure index value. For the occupational assessment of the exposure, it should be noted

that in the National regulatory framework, the reference is the Legislative Decree 81/08<sup>193</sup> (subsequent modifications and integrations)<sup>194</sup>. For E field measurements, it is necessary to refer to action levels (AL), these are properly operational values and are expressed in terms of the EM quantities (electric, magnetic, electromagnetic field) that can be measured in the exposure environment. They are established to simplify the process of demonstrating compliance with the relevant Exposure Limit Values (ELVs), equivalent to the BRs established by the ICNIRP guidelines and referring to induced quantities. The environmental limits expressed in terms of Action Levels (ALs) for environmental magnetic fields are given below, Table IX-1:

**Table IX - 1. AL for environmental magnetic fields at frequencies between 1Hz – 10 MHz**

*Non-thermal effects - Table B2 of Annex XXXVI – D. Lgs. 81/08*

Frequency range	AL <sub>Low</sub> B(μT) rms	AL <sub>High</sub> B(μT) rms	AL for local exposure B(μT) rms
1 ≤ f < 8 Hz	2,0 × 10 <sup>5</sup> /f <sup>2</sup>	3,0 × 10 <sup>5</sup> /f	9,0 × 10 <sup>5</sup> /f
8 ≤ f < 25 Hz	2,5 × 10 <sup>4</sup> /f	3,0 × 10 <sup>5</sup> /f	9,0 × 10 <sup>5</sup> /f
25 ≤ f < 300 Hz	1,0 × 10 <sup>3</sup>	3,0 × 10 <sup>5</sup> /f	9,0 × 10 <sup>5</sup> /f
300 Hz ≤ f < 3 kHz	3,0 × 10 <sup>5</sup> /f	3,0 × 10 <sup>5</sup> /f	9,0 × 10 <sup>5</sup> /f
3 kHz ≤ f ≤ 10 MHz	1,0 × 10 <sup>2</sup>	1,0 × 10 <sup>2</sup>	3,0 × 10 <sup>2</sup>

The low ALs for the magnetic field are set directly to ensure compliance with ELVs for sensory effects at frequencies between 1 Hz and 400 Hz. Above this frequency, they coincide with the high ALs, which are set to ensure compliance with the ELVs for health effects. Furthermore, Legislative Decree 81/2008 provides that the assessment of occupational exposure in the frequency range 1 Hz ÷ 10 MHz is carried out by applying the Weighted Peak (WP) method. Since ALs varies with frequency, this method allows an index, I<sub>WP</sub>, to be defined, which can provide a more well founded exposure assessment metric than parameters such as peak or RMS values, which are of little significance when dealing with complex signals characterized by numerous spectral components. According to the WP method, the frequency content of an impulsive signal is processed by weighing the amplitudes of the spectral components against the relevant limits (workers/population) at the corresponding frequencies, also considering the phases of the components. The

maximum absolute value of the waveform thus weighed constitutes the index required ( $I_{WP}$ ), the value of which must be less than 1 (or 100% depending on the chosen normalization criterion) to ensure compliance with the exposure condition. Another index, referred to as  $I_{pop}$ , again based on the weighted sum of spectral contributions, without taking phases into account, is used to estimate the exposure of workers exposed for not professional reasons and thus comparable to the general population (see Chapter II). This index is therefore more conservative. With regard to the restrictions established for the protection of the population (or for the workers exposed for not professional reasons), the Reference Levels derived from Recommendation 1999/519/EC<sup>92</sup> are reported (Table IX-2), as the two decrees of 8 July 2003<sup>195,196</sup> implementing the Framework Law 36/01<sup>197</sup> for the type of sources under consideration refer to it.

**Table IX - 2. Limits for the electric, magnetic, and electromagnetic fields (0 Hz – 300 GHz). From Recommendation 1999/519/EC**

Frequency range	B (mT)	J (mA/m <sup>2</sup> ) rms	SAR total body (W/kg)	Local SAR (head and trunk) (W/kg)	Local SAR (limbs) (W/kg)	Power Density S(W/m <sup>2</sup> )
0 Hz	40	—	—	—	—	—
>0-1 Hz	—	8	—	—	—	—
1-4 Hz	—	8/f	—	—	—	—
4-1 000 Hz	—	2	—	—	—	—
1 000 Hz-100 kHz	—	f/500	—	—	—	—
100 kHz-10 MHz	—	f/500	0,08	2	4	—
10 MHz-10 GHz	—	—	0,08	2	4	—
10-300 GHz	—	—	—	—	—	10

\*Frequency expressed in Hz.

In the following measurement campaign, in order to have a complete analysis three different types of measures are carried out: the first to evaluate the weighted peak ( $I_{WP}$ ) refers to the occupation exposure, the second to evaluate the exposure of the general population (referring to the limits reported in Table IX-2), and finally, the measurement of the magnetic field (B) for the comparison with the limits AL (referring to the limits reported in Table IX-1).

The preliminary measurement showed a non-negligible B-field in correspondence of the surface of the coil, with the machine powered at 50% MSO. Indeed, the instruments evaluated a magnetic field equal to 110 mT on the surface facing in opposite directions of the muscle (side of the operator) and 170 mT on the surface facing the subject under treatment.

Successively, for the evaluating the risk assessment, the device was set in the real condition of work, which implies 75% of MSO. A qualitative example of the measurement, detected to evaluate the  $I_{wp}$  in several points around the device setup, is shown in the figures below. Two conditions of measurements are carried out: to analyze emissions along the radial direction, the applicator is fixed on a support, keeping the axis pointing upwards (Figure IX.3); to study the emissions along the axial direction, the axis of the applicator was oriented horizontally (Figure IX.4).

In the first case (Figure IX.3), the applicator is positioned with the active surface facing the ground.

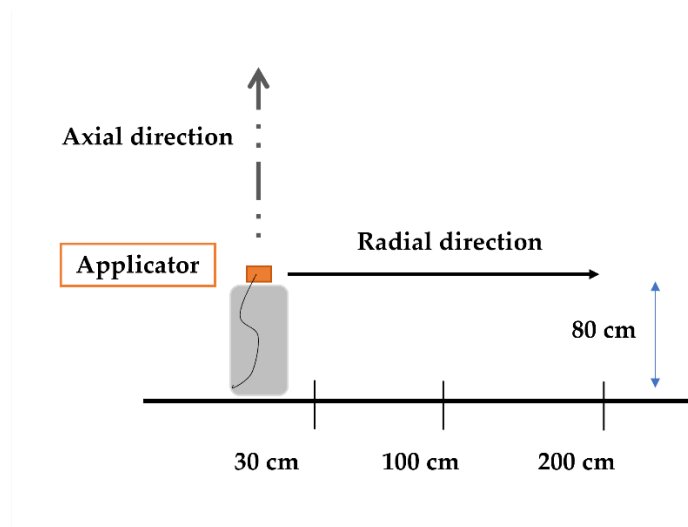


Figure IX. 3 Measurement set-up. Points of measure are chosen along the radial direction. The applicator is positioned with the active surface facing the ground on support at 80 cm from the ground.

The measures of the index as a function of the radial distance, are reported below.

*Table IX - 3. Measurements along radial direction for the I<sub>WP</sub> index*

<b>Radial distance (cm)</b>	<b>I<sub>WP</sub></b>
30	1700%
50	311%
70	122%
90	58%
100	41%
120	24.6%
140	15.8%
160	10.9%
180	8.8%
200	0.6%

From the measurements and their subsequent processing, it emerged that the respect distances for workers and the population, respectively, in the radial direction are as follows:

- With reference to the lower VA, Legislative Decree 81/08, the respect distance is approximately 50 cm;
- With reference to the exposure of the general population, Recommendation 1999/519/EC, the respect distances is about 140 cm.

In the second case (Figure IX.4), the applicator is turned laterally with the axis of the active surface parallel to the ground.

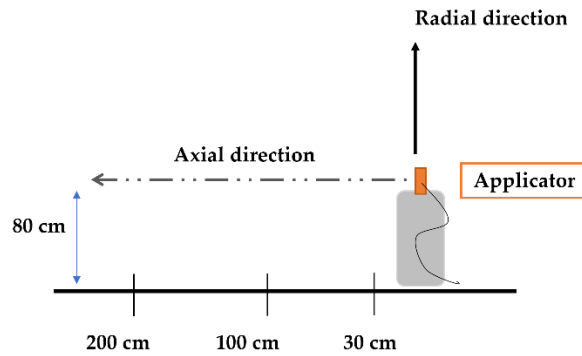


Figure IX. 4, Measurement set-up. Points of measure are chosen along the axial direction. The applicator is positioned with the axis of the active surface perpendicular to the ground. It is also on support at 80 cm from the ground.

The measures of the index as a function of the axial distance, are reported below.

**Table IX - 4. Measurements along axial direction for the IWP index**

Axial distance (cm)	IWP
40	986%
70	205%
90	93%
100	68%
120	39%
140	25.7%
160	16.9%
180	12.1%
200	9.4%
220	7.4

The measurements and their subsequent processing showed that the respect distances for workers and the general population, respectively, in the axial direction are as follows:

- With reference to the lower AL, Legislative Decree 81/08, the respect distance is approximately 60 cm;
- With reference to the general population, Recommendation 1999/519/EC, the respect distance is approximately 150 cm.

From these results, it is concluded that operators using this machinery must be classified as exposed to electromagnetic fields for professional reasons and assessed as suitable for exposure. Subjects with previously reported contraindications to exposure to magnetic fields (pregnant women, minors, wearers of pacemakers and implanted devices, metal prostheses, etc.) may not use the equipment unless specifically assessed by the competent doctor. Furthermore, since the population limit is respected at a distance of approximately 1.50 m, it follows that this means that the client undergoing treatment is exposed to a level of the electromagnetic field that is higher than that provided for by Law No 36 of 22 February 2001, "Framework law on the protection from exposure to electric, magnetic and electromagnetic fields"<sup>198</sup>, which only provides for such excess for professional or medical reasons. Finally, from the evaluations carried out, this apparatus represents a relevant source of the magnetic field that is very similar to the transcranial magnetic stimulation used in the medical field. To use it safely, appropriate prevention and protection procedures must be put in place, including the training of all operators involved. For these reasons, at present this type of apparatus is not among those that can be used in aesthetic centers.

The second measurement campaign started in a collaboration with the Italian National Institute of Health (ISS). This campaign regards the study of the immunity of the active implantable medical device (pacemaker) and E-field in the far field condition, using the GTEM cell jointly with a phantom filled with saline solution. This latter is important to reproduce the trunk of the subject in which the active device is implanted.

The GTEM cell is a TEM waveguide with an upper-frequency limit extended to GHz. This is used for both the radiated emission and the immunity measurement. Indeed, it is included in the recently standard IEC 31000-4-20<sup>199</sup> regards the "Emission and Immunity in Transverse Electromagnetic Waveguide" as a measurement facility for EMC emission and immunity testing<sup>200</sup>. Moreover, GTEM cells (Giga-hertz Transversal Electro-Magnetic cells) are waveguide structures intended for electromagnetic compatibility measurements, as well as biomedical applications. The electromagnetic field distribution inside the cell is in TEM

mode. Therefore, the field components are strictly perpendicular. In this campaign, the aim is to consider the exposure of the pacemaker in the far field, since in the international standards for Active Implantable Medical Devices (AIMD), at frequencies above 385 MHz, immunity levels are assessed in near-field conditions and expressed in terms of net power at the antenna input (Watt). In addition, the limits for occupational exposure are expressed in terms of E-field, thus it is not immediately possible to compare these two quantities. Therefore, during this campaign, an exposure setup able to investigate AIMD immunity in terms of far-field E-field has been setup, producing in the GTEM cell a field that achieved (and possibly exceeding) the workers' limits. The exposure setup consists of GTEM cell (model GTEM 5311 by Emco) signal generator R&S 9kHz - 3.2GHz; Amplifiers (KALMUS, 200 MHz – 1 GHz of 50 W; 10S1G4A Research 800 MHz – 4.2 GHz of 10 W and directional coupler Amplifier Research DC7144), and RF Power meter Boonton operating in the range 10 kHz - 100 GHz. The pacemaker (PM) under test is placed inside the cylindrical PVC phantom (diameter 17 cm, width 7 cm). The entire setup is shown in Figure IX.5 The phantom is filled with saline solution ( $\sigma=0.3$  S/m), and the PM is fixed 1 cm below the solution surface and attached to a spiral-shaped lead, in a unipolar configuration. The PVC phantom and PM are owned by the ISS. This setup is in accordance with standard ISO 14117<sup>201</sup>. PM activity signal is acquired using LabVIEW, after passing through a conditioning and A/D conversion board. The board also generated a heart-simulated signal able to inhibit the PM.



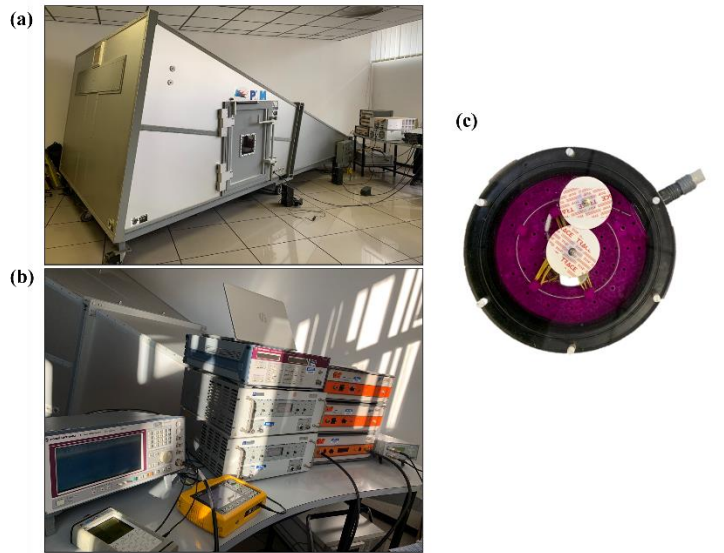


Figure IX. 5 Measurement setup: (a) GTEM cell; (b) Generator, amplifiers, and measurement instrument; (c) cylindrical PVC phantom with PM.

During the analysis both continuous and pulse RF signals are generated. For each frequency under test, the unperturbed E-field was measured at 1.4 m from the apex of the GTEM, where the uniform field is produced, as reported in the user manual. In this location, in the second step, the phantom is placed and the PM activity is monitored in order to detect possible malfunctions (i.e., oversensing, under-sensing, and asynchronous pacing) which may occur in both continuous and pulsed RF signals. The measurements of the E-field inside the GTEM are following reported:

**Table IX - 5. Measured values of the unperturbed E-field and produced Power**

Frequency (MHz)	Power (W)	E-field (V/m)
450	35.3	98.0
600	41.8	96.4
700	45.3	89.7
800	47.6	94.9
825	48.1	110.0
850	48.5	98.1
875	49.0	96.8
900	49.5	100.0
930	50.0	96.4
1610	21.0	44.7
1850	18.6	44.5
1910	18.2	48.9
2450	19.7	49.0
3000	18.0	47.8

The AIMD minimum immunity levels are derived from the European Recommendation 1999/519/EC<sup>92</sup>, which set the E-field reference levels (for the environment measurements) for the general public at  $1.375\sqrt{f}$  (V/m) in the range 400 – 2000 MHz and 61 V/m above 2 GHz. Workers can be exposed to higher values (Directive 2017/35<sup>1</sup>,  $3.0\sqrt{f}$  (V/m) and 137 (V/m) above 2 GHz). For frequency below 1 GHz, we were able to test PM immunity at field values notably greater than reference values and up to workers exposure levels. Further campaigns are planned in the future to study other PM configurations to identify the worst condition. In addition, different signals will be tested to ensure the immunity of devices to next-generation EM sources, such as 5G. The results of this campaign are disseminated at the 2022 44th Annual International Conference of the IEEE Engineering in Medicine & Biology Society (EMBC), with the contribution “Exposure set up for the far-field EMI assessment of pacemakers”.

Another important campaign was carried out jointly with ARPA Lazio, in which also the ISS and a manufacturer of signal processing equipment are involved. This campaign

concerns the preliminary study for a correct methodology of acquisition of the signal produced by some antennas of 5G technology. To date, the measurements have concerned the antennas present in the territory of Rome, but other analyses have already been planned to deepen this issue, very important also from a protectionist point of view.

## 9.2 An overview of the contributions to the research activity in INAIL

During the years of my Ph.D. course, I have been also involved in some studies carried out mainly in the DiMEILA department. This resulted in different contributions that are presented at National and International Conference, as well as an article in a Journal and supplement in a national Journal. Therefore, in this section, a review of these contributions is reported, since also these studies have contributed to integrating and improving my health and safety knowledge.

*“Uncertainty in determining respect distance for electromagnetic fields by spatial interpolation of exposure indices”*. Submitted to URSI GASS 2020 and published as proceedings of the conference. Authors: N. Zoppetti, D. Andreuccetti, S. Ceccherini, M. Comelli, S. D’Agostino and R. Falsaperla. In this work is proposed a method to determine the respect distance. This latter refers to another important quantity which is the exposure index ( $I_{wp}$ ), which is significant in the assessment of human exposure to electromagnetic fields. Some measurement instruments allow the measurement of this index, by expressing it as a percentage or unit value. However, in many situations, a parameter that allows the characterization of the exposure and gives synthetic and effective indications on risk assessment and risk reduction is the respect distance.

This work describes how the respect distance could be determined starting from exposure index measurements, thanks to a flexible interpolation method to be used in combination with different source models that allow to propagate of the uncertainty of each measurement on the result of the interpolation and therefore determine the uncertainty

related to the respect distance. The method has been implemented as an online application, equipped with a clear operating interface, which allows the user to manage the selection of the data to be processed and the personalization of the processing results flexibly and completely. This application is distributed through the free access WebNir platform<sup>202</sup> developed jointly by INAIL and IFAC-CNR.

*“Protection of workers from electromagnetic fields (EMF) and health surveillance: preliminary data of a research within the INAIL Call for Research Collaboration (BRiC) 2016 ”* published as a journal supplement in the Italian Journal Of Occupational Medicine And Ergonomics<sup>203</sup> and submitted to the 82<sup>nd</sup> National Congress of Italian Society of Occupational Medicine, 2019. Authors: A. Modenese, D. Carlotti, GM Contessa, S. D’Agostino, R. Falsaperla, C. Grandi, V. Lopresto, R. Pinto, A. Polichetti, R. Pozzi, F.M. Gobba.

In this article, we present the preliminary results of the assessment of aspects of medical interest related to the possible occurrence of indirect adverse health effects in workers exposed to EMF. Recent reviews of the publications by ICNIRP, WHO e SCENIHR<sup>204</sup> are carried out; while for the years 2015 to 2018, not covered by the documents cited, an ad hoc review of the literature was conducted. This study has led to important conclusions. That is, the analysis of the literature on the indirect effects of EMF confirms the need for a careful investigation by the competent physician into the presence of particularly risk-sensitive workers, and in particular DMIA carriers, among those also exposed to levels of EMF that comply with the exposure limits for workers. Other indirect effects attributable to contact currents, which may range from the mere perception of the current to more serious accident-type events, are generally associated with significantly higher levels of EMF exposure. Furthermore, with regard to the identification of workers with particular risk sensitivity, no indications have been found in the scientific literature of possible human pathological or para-physiological conditions in which increased risk for the induction of effects attributable to contact currents can be identified.

*“Muscle stimulators for aesthetic use as relevant sources of magnetic field protection aspects”*. This contribution regards the measurement campaign conducted on the aesthetic device and before described. The work was submitted to the Italian Association of Radiation Protection (Airp) National Conference, 2021. Authors: A. Bogi I. Pinto, N. Stacchini, R. Pozzi, R. Falsaperla, S. D’Agostino, A. Polichetti, C. Giliberti, M. Comelli and N. Zoppetti. This work analyzed the protective aspects that referring to the muscle stimulators that produce high magnetic fields. This type of apparatus, whose operating principle has long been used in rehabilitation and aesthetic medicine, is now also becoming widespread in Italy in the purely aesthetic field. From the evaluations carried out, it represents a relevant source of the magnetic field that is very similar to the transcranial magnetic stimulation used in the medical field. In order to use it safely, appropriate prevention and protection procedures must be put in place, including the training of all operators involved. By law, the use in beauty salons is limited to equipment that corresponds to that provided in the technical data sheets of Ministerial Decree 206/2015<sup>205</sup>. The muscle stimulators with a magnetic field, that are the subject of this work, are based on a completely different operating principle from that allowed for the aesthetic equipment, and cannot be traced back to any of the apparatuses envisaged by the decree before mentioned, in particular, they cannot be assimilated into the stimulators envisaged in datasheet n.19 (that referring to the pulse electrostimulation by means the electrodes), which thus entail a completely different level of exposure and consequent different limitations on use. Similar reasons exclude the belonging of the apparatus to those envisaged in technical sheet n.6 of Ministerial Decree 206/2015 (equipment for massage by means of the mechanical tool). Furthermore, as highlighted by the measurements reported in this work and also set out in the previous paragraph, the subject that receives the treatment, which is to be considered as the general population, is exposed to a level of magnetic field higher than the reference level for the general population and this can only occur for therapeutic or diagnostic purposes. For the results obtained, at present, this type of apparatus would not be among those that can be used in aesthetic centers.

*“Intercomparison of measuring instruments used for the evaluation of complex electromagnetic field signals using the weighted peak method”*, submitted to the 38<sup>th</sup> National Congress of Industrial and Environmental Hygiene (Aidii), 2022. Authors: Giancarlo Burriesci, Andrea Bogi, Moreno Comelli, Simona D’Agostino, Riccardo Di Liberto, Rosaria Falsaperla, Marco Valentini, Nicola Zoppetti. In this paper, the results of an experimental study comparing three electromagnetic field measuring instruments implementing the weighted peak method were reported. The evaluation of the weighted peak index ( $I_{wp}$ ) was carried out both based on the limits adopted by Legislative Decree 81/08 relevant to the protection of occupationally exposed workers and concerning the reference values indicated by Recommendation 1999/519/EC, relevant to the protection of sensitive subjects, first and foremost the wearers of active implantable medical devices. The instruments examined and the signal generation systems are supplied to the DiMEILA Laboratory of EMF. In particular, the instruments used for the comparison were:

- Narda ELT 400 (1 Hz - 400 kHz) with a 100 cm<sup>2</sup> isotropic probe;
- Microrad NHT3DL (1 Hz - 1 MHz) with 33S isotropic probe;
- Narda EHP-50F (1 Hz - 400kHz), with internal isotropic probe.

A comparison of the results shows a comparable response between the instruments, thus showing good reliability in assessing the  $I_{wp}$  for the purposes of verifying compliance with protectionist and legal limits. In particular, a fairly similar response is noted between the two Narda instruments and a slight underestimation of the Microrad instrument. The latter is attributed in particular to a different location of the sensitive elements of the probes.

*“Protection of Workers Exposed to EMFs above Occupational Exposure Limits”*. Submitted to the VI edition of the National Conference "Interactions between Electromagnetic Fields and Biosystems", ICEmB 2022. Authors: A. Polichetti, G. M. Contessa, S. D’Agostino, R. Falsaperla, C. Grandi. In this contribution, we have discussed how to deal with the conditions of overexposure to electromagnetic fields permitted by the European Directive 2013/35/EU, suggesting some possible approaches in the case of time-varying electric,

magnetic and electromagnetic fields, while we have highlighted the critical issues related to static magnetic fields. The approach to managing health and safety requirements in overexposure conditions may be different for static magnetic fields, low-frequency electric and magnetic fields, and radiofrequency electromagnetic fields. Concerning the exposure to the static magnetic field, we are not aware of further studies investigating the possibility of health effects in volunteers exposed over 8 T and ICNIRP has not updated its recommendations about static magnetic field exposures then, owing to the persistent lack of knowledge, in our opinion it is not possible to guarantee the health of workers exposed to these levels. As regards the exposure to the electric and magnetic fields at low frequencies, we conclude that the protection of workers could be assured if it is guaranteed that just minor effects like non-painful perception can occur. In the end, the exposure to RF-EMF leads us to distinguish between whole-body and localized exposures. In the first case, in the light of the recent pertinent ICNIRP guidelines<sup>14</sup>, derogation from compliance to the ELV of 0.4 W/kg on the whole-body SAR, could be considered acceptable up to 2 W/kg, a value implying only slight thermal stress, unless the worker works in severe thermal environments and/or wears heat-insulating clothing, which requires a more detailed risk assessment. For localized exposures, derogations from compliance with the local SAR ELVs, seem not to be justified.

This issue is set out more exhaustively in a contribution published in a scientific journal, below reported:

*“Issues in the implementation of Directive 2013 35 /EU regarding the protection of workers against electromagnetic fields”*, published in the International Journal of Environmental Research and Public Health, 2022<sup>101</sup>. Authors: G.M. Contessa, S. D’Agostino, R. Falsaperla, C. Grandi and A. Polichetti. In this paper are analyzed the main concerns in interpreting and managing some provisions of Directive<sup>1</sup> with particular reference to the issue of how the employer can manage the situations of overexposure. These issues started from the innovative approach of the Directive that, in some circumstances, allows the conditions of overexposure (exceeding the exposure limits), which undoubtedly presents some difficulties in application. Strictly connected to the possibility of overexposures is the distinction between

the health effects ELVs (above which workers might be subject to adverse health effects), and the sensory effects (transient disturbed sensory perceptions). What regards to these latter, in the case of transient effects, is introduced the concept of “*flexibility*” and is based on the approach first introduced by ICNIRP<sup>95,13</sup> in its guidelines on static magnetic fields and on time-varying electric and magnetic fields. In the flexibility approach, the eventuality that a worker can experience transient minor effects is accepted if the consequences for safety are controlled. On the contrary, the possibility of exceeding the exposure limits for health effects, formally recognized in the article of the Directive dealing with derogations, is not included in the ICNIRP guidelines. In this work are discussed all these issues, with the aim to analyze the main concerns in the interpretation and handling of the Directive's provisions.

The last contribution was submitted to the 10<sup>th</sup> Jubilee International Conference on Radiation in Various Fields of Research, 2022. With the title:

*“WebNir: Web-based tools for assessing occupational exposure to Non-Ionizing Radiation”.*

Authors: M. Comelli, D. Andreuccetti, N. Zoppetti, E. Mattei, G. Burriesci, R. Falsaperla, S. D'Agostino, C. Grandi, M. Valentini, A. Bogi, N. Stacchini, R. Di Liberto. This article is thought to present the WebNir platform. Therefore, are presented the currently available tools, following summarized:

- Display standardized intervention procedures for certain classes of occupational EMF sources;
- Analysing EMF regulations, visualizing the development of their limit values as a function of frequency and time, and calculating exact values at specific frequencies and/or time intervals;
- Plot and compare the frequency-dependent trends of two or more regulatory limits;
- Determine the respect distance to an EMF source by interpolating measured data along a straight line at progressively increasing distances;
- Evaluate and compare exposure to the electric field and magnetic flux density near power lines;



- Evaluate the magnetic flux density generated by any conductor configuration, choosing from a wide variety of geometries;
- Process a sequence of measurements of the perceived magnetic field in the case of movement of a subject in a magnetostatic field and determine relevant radiation protection indices;
- Analysing in the time domain an appropriately sampled waveform in the low to intermediate frequency range and calculating weighted peak indices relevant to applicable standards;
- Load, recognize and process time or frequency domain measurement data files from any type of instrument chain;
- Calculate the shielding effectiveness of an ideal screen;
- Estimate the induced voltage at the input of a pacemaker exposed to EMF;
- Generate interactive graphs to dynamically visualize compliance with EMF-related operating procedures.

This platform is mainly realized by the CNR-IFAC (“Nello Carrara” Institute for Applied Physics of the Italian National Research Council), and jointly involved the DiMEILA department, as well as other public institutions, which are:

- IRCCS "Scientific Hospitalization and Care Institute" Polyclinic San Matteo;
- ISS (Italian National Institute of Health);
- Environmental Protection Agency of Lazio;
- USL (Local Health Authority) of Tuscany.

### 9.3 Working Group of physical agents portal- PAF: presentation of the database for the prevention and protection from the physical agents

During the Ph.D. course my activity at DiMEILA I have been included in the working group of the Physical Agents Portal (PAF), which comprises several researchers also belonging to

other institutes and different INAIL sites: A. Bogi, F. Picciolo, I. Pinto, N. Stacchini, G. Burriesci, S. D'Agostino, M. Diano, I. Di Gesu, C. Grandi, M. Valentini. In this paragraph, an overview of this portal is carried out. The PAF is available at the web address <https://www.portaleagentifisici.it/> and originates in 2008 from a project of INAIL, Tuscany region and Local Health Services of Siena and Modena, also supported and funded by the Italian Health Ministry. This portal aims at making available a technical tool to support employers in the risk assessment, regarding the physical agents such as defined in Legislative Decree 81/08. Actually, the Italian framework on occupational exposure has undergone significant innovation thanks to the transposition in particular of four different European Directives, concerning the vibrations (Directive 2002/44/EU)<sup>206</sup>, noise (Directive 2003/10/EU)<sup>207</sup>, electromagnetic fields (Directive 2013/35/EU)<sup>1</sup> and artificial optical radiation (Directive 2006/25/EU)<sup>208</sup>. All these Directives are incorporated into Decree 81/08 and subsequent amendments and are the object of a specific title.

In particular, Title VIII contains general provisions about the physical agents. Despite the physical agent being a traditional risk factor, in Italy, there is still a lack of competent services and technicians able to correctly carry out a proper assessment of the risk in the workplace, and thus in this framework, the usefulness of PAF becomes evident. The PAF is continuously upgraded and consultable also in the English version to be consulted even outside the national territory. Until now it is counted that more than 300000 users per month have consulted this database starting from November 2011, which is the official opening date.

Going more specific, today the portal contains the sections following reported: noise, vibration, electromagnetic field, hyperbaric atmosphere, natural and artificial ionizing radiation, natural and artificial optical radiation, and microclimate. After the access on the home page, the user is addressed to the main menu of each physical agents. All the sections provide a description of the risk associated with the specific agent, and also it is possible to check the database (divided for the type of equipment that causes the risk), and also the

information supports, simplified procedures for the risk evaluation, technical documentation, and several guidelines.

At this point, the attention can be focused on the electromagnetic section, in which I am directly involved. It is important to highlight that following the publication of Legislative Decree 159/2016 (that modify 81/08), the electromagnetic database can be used for the risk assessment purpose in accordance with art. 28, 181, and 209 of the Legislative Decree 81/08. The EMF section counts different topics that are: risk descriptions, a guide for the use of the database, Database, assessment method, Legislation, exposure calculator, information regarding prevention and protection, documentation, and FAQ. The main feature, which avails of the scientific support of the Institute IFAC-CNR of Florence, is a database of EMF sources that contain measured data from about 150 sources and currently remains under development for the following purposes:

- Ensuring easy finding exposure values related to the levels of the electromagnetic fields produced by widely industrial, medical, and research machines/sources, in order to improve safety by preventing and reducing risk, without making measurements that are often expensive, complex, and in some cases useless, as for the case of equipment that is already compliant to a harmonized technical standard, like the wi-fi apparatus.
- Allow the employers to identify the source that could minimize the exposure of the workers, when purchasing new machines or replacing obsolete ones.

Further, for each source reported in the database of this section, the following data are provided:

- Registered equipment, to properly identify the sources of the exposure itself;
- Specific protection measurement to be implemented for the workers with particular risks, such as those wearing the AIMD;
- Zoning of the area around the source of exposure, concerning the limits for workers but also for the population (that also identified the worker not exposed for professional reasons and also for the workers with particular risk);

- Specific data related to the source to which measures reported in the portal refer. In this respect, it must be noted that the same equipment can have different applicators mounted inside in the operating condition of use. If this occurs, the data related to the applicator of interest must be looked for.

Another important item of this section is without a doubt the FAQ. This latter tries to respond to the most common questions related to risk assessment and management. They cover different topics, as well: health effects, health surveillance, measurement method and instrumentation, assessment of the risk procedure, risk control, and management of the risk. Also, the FAQ is continuously updated based on the questions posed by the users.

It is clear that to obtain a portal that can be really useful, this must be continuously updated, thus the research conducted in the laboratory of EMF of DiMEILA aims also to improve the database with constantly updated results. Therefore, some of the results of the Ph.D. project will in the future be included in the section concerning the TMS, where it is already possible to consult some reports of measurements carried out on this device.

Finally, a tool is being worked on to help the employer manage the risk in the presence of workers with AIMD. In essence, this will be a risk assessment wizard for wearers of active implantable medical devices, following the procedure laid down in standard 50527-1<sup>209</sup>. The aim is to make this tool available in the next few months.

# CONCLUSIONS

---

In this work, occupational exposure to transcranial magnetic stimulation (TMS), a treatment widely used in the clinical practice, has been fully evaluated. The research project involved the National Institute for Insurance against Accidents at Work - INAIL and Sapienza University of Rome. The project involving two different Institutions had to find a fair compromise between the missions of both centers: occupational medicine, occupational epidemiology, and occupational and environmental hygiene for DIMEILA-INAIL, bioelectromagnetic scientific research activity for DIET-Sapienza University. Taking these aspects into account, we identified a project that would be able to combine the two Institutions and from which results obtained could be affordable for both research Centers: the evaluation of the occupational exposure to electromagnetic fields evaluating the risk assessment of operators performing TMS treatments.

The starting point has been a careful evaluation of the scientific literature to identify working conditions that could be of both scientific and protectionist interest. The research led to the identification of a precise working environment in the clinical field, which involves the use of a transcranial magnetic stimulation device: TMS. This instrument, from the "INAIL point of view", needs to be investigated since to date there are large gaps in the risk assessment associated with it. As extensively discussed in Chapters I and II, there is a lack of a technical standard for the TMS that can regulate its use, and at the same time, through the study of the user manuals, it has emerged that this equipment is not designed in accordance with certain directives typically used for medical devices. Given all this, means that there is a high degree of variability both in the way the device is used and in the risk assessment, with obvious possible health and safety problems at the workplace as a result. On the other hand, from the "University point of view", the literature concerning the assessment of workers' exposure to TMS has proved to be very lacking, in fact, the studies found in the literature are so few that one cannot think of them as exhaustively dealing with this issue.

The issue relates precisely to the exposure to which the operator performing the treatment is subjected, who is exposed to a high magnetic field for several hours a day, during work shifts. To assess this exposure, a characterization of various devices used in the medical field, using both experimental data and comparisons of data with the literature has been provided. In other words, the Verification and Validation process (V&V), previously described, was carried out to ensure that the sources worked exactly as they do. This led to the characterization of four different sources. Once obtained this, the analysis began by reproducing the authentic working conditions (machine settings, coil position, operator position, etc.) in a numerical dosimetry environment, to assess, by post-processing the EM quantities induced in human tissues, with the aim of obtaining a risk assessment by comparison with regulatory limits.

The first analyses involved the use of the Duke male human model, thanks to which all the critical issues related to the use of the machine were identified: high limb exposure, worst-case condition of exposure (coil at the height of the abdomen), and, above all, the safety distances. Results were evaluated according to the type of treatment, i.e., according to the percentage of chosen MSO and it is important to highlight that the exposure MSO-dependent had never before been addressed in the literature.

Successively a different human body model has been considered: the female model Ella. This was considered important since several studies in the literature had shown differences in terms of induced quantities, between men and women models when exposed in the same conditions. The results of this analyses have revealed differences in the exposure of the two models, depending on geometric characteristics, such as height, cross-section, the shape of the body (for example, having Ella the curved back exposes the skull more), and also intrinsic body characteristics (difference in muscle mass and amount of fat, as well as different sizes between organs). Moreover, maps of the E-field inside the tissues have shown to be strongly dependent on body characteristics, which has proved evident in the study of the chest of Ella, where the presence of breast tissue did emerge significant differences with the male subject.

This important difference led us to analyze it in more depth Ella, highlighting a drawback of the model, which is the fact that it was obtained from images of magnetic resonance, and therefore with the subject lying supine. This caused the flattening of the most important tissue for the gender comparison, i.e., the breast. Therefore, a modified model, called Enhanced Ella, more similar to a real subject in a standing position, was produced which allowed us to make further exposure assessments focusing on the tissue that has proven to be crucial in risk assessment. Effectively the real shape of the female subject leads us to obtain the correct evaluation of the exposure, of paramount importance to educate the female workers doing the treatment about the potential risks they incur.

Further improving the analysis towards an intersubject variability, four different human models were used: Duke, Ella, Jeduk and Fats, with the aim of quantifying a risk assessment that can result from exposure to the same source by completely different subjects. Without any doubt, this type of analysis was never done for TMS, and from our studies, it was never even conducted for risk assessment in the occupational environment. Typically, the concept of variability is mainly associated with sensitivity as a perception of an effect. Usually, intersubject studies effectively concern the study of thresholds of perception of an effect and not the study of different responses in terms of induced quantities. Indeed, the results obtained showed that the different body shapes, together with intrinsic body characteristics (quantity and thickness of fat, tissues distribution, dielectric discontinuity, and so on), lead to important variations, observable in terms of percentiles of induced E-field, induced E-field distribution, peak of E-field that could be achieved in the body and the quantitative analysis carried out with the boxplot. Therefore, these results have made us think about the need to take into account, during a risk assessment, the specificity of the subject. For example, one might consider including a correction factor that considers the differences between one operator and another. This would certainly make the risk assessment more realistic. On the other hand, it would already be important to inform operators about how their physicality may affect exposure, to adopt specific risk reduction procedures.

From a general point of view of the exposure risk assessment of the TMS, it emerged that under our exposure conditions, this device in many situations can cause operator exposure

that exceeds the regulatory limits. Moreover, among the geometries of coils analyzed in this work (circular and figure-of-eight), the circular had proven to be the least safe, exposing the operator to an induced electric field considerably higher than the limits, even when the process involves the use of the machine at 30% of MSO. This happens also when the exposure is the one of the limbs due to the figure-of-eight. Therefore, it appears the necessity to train and inform the operator about the not negligible exposure that involves the limbs, if he/she decides to hold the coil with one hand, or with two as in most cases occurred.

One suggestion to reduce the exposure is to provide distances at which the limbs are no longer exposed to field values that exceed the limits and possibly provide them depending on the coil model and the type of treatment (i.e., the percentage of MSO, as done in this work). As well, if the treatment or coil model cannot ensure exposure below the limits, the suggestion is to use the rod, sometimes supplied with the coil, which serves to keep the coil in place at a distance. Finally, you can think of external insulation for the coil that can decrease the exposure on the "operator side", obviously this presupposes a careful study as such insulation is strongly dependent on the coil model (frequency, power, and so on).

Finally, to complete the assessment of exposure to TMS, it was decided to investigate the aspect of possible nerve stimulation. Since it was estimated that in several situations the induced E-field exceeded the limits, it was thought to investigate the condition of overexposure. Since the threshold detected by ICNIRP has been exceeded in several situations, it was decided to use neurofunctionalized models for the study of possible conditions of stimulation caused by the use of TMS. The analysis was conducted on both male and female subjects (Jeduk and Yoon-Sun) for the figure-of-eight. Results showed that neither male nor female subjects experience stimulation events. However, as the results are highly dependent on the coil model, this assessment should be considered on a case-by-case basis. Therefore, the possibility of stimulation events occurring cannot be definitively ruled out. The suggestions given to reduce the exposure of the limbs are therefore confirmed.

In conclusion, it can be said that the objectives set have been achieved, partially filling the gaps identified in the literature, and at the same time bringing about new security

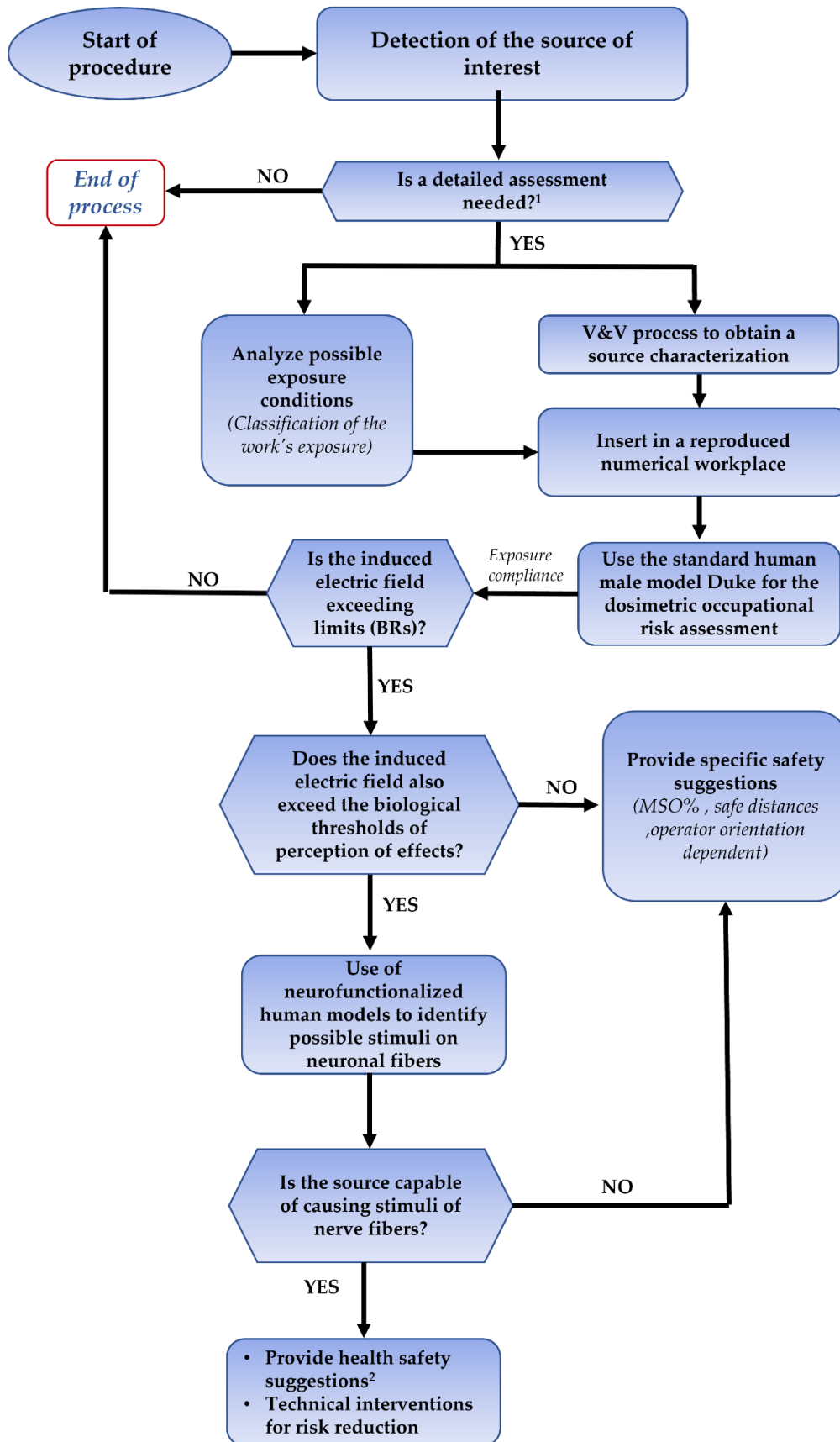


awareness. What is reported in this study can be considered a starting point, and not an end, for further analysis that can additionally deepen the topic, also considering other sources and other exposure conditions, since it has emerged that the results are highly dependent on the circumstances chosen.

From these conclusions, we can consider suggesting a sort of protocol, that based on our results could be necessary for an extensive assessment of the risk, owing to the exposure to the TMS and/or for any other source for which there is no specific procedure. This could be more useful in the conditions in which the dosimetric analysis is needed.

The proposal for an analysis procedure for the assessment of occupational exposure by means of numerical dosimetry can be divided into two phases, where: the first phase is characterized by the basic analysis to be carried out for risk assessment; whereas the second phase takes into account an innovative approach aimed at making the outcome of the dosimetric assessment more realistic. This is shown in the following flowcharts:

**Step 1: Basic protocol of analysis**



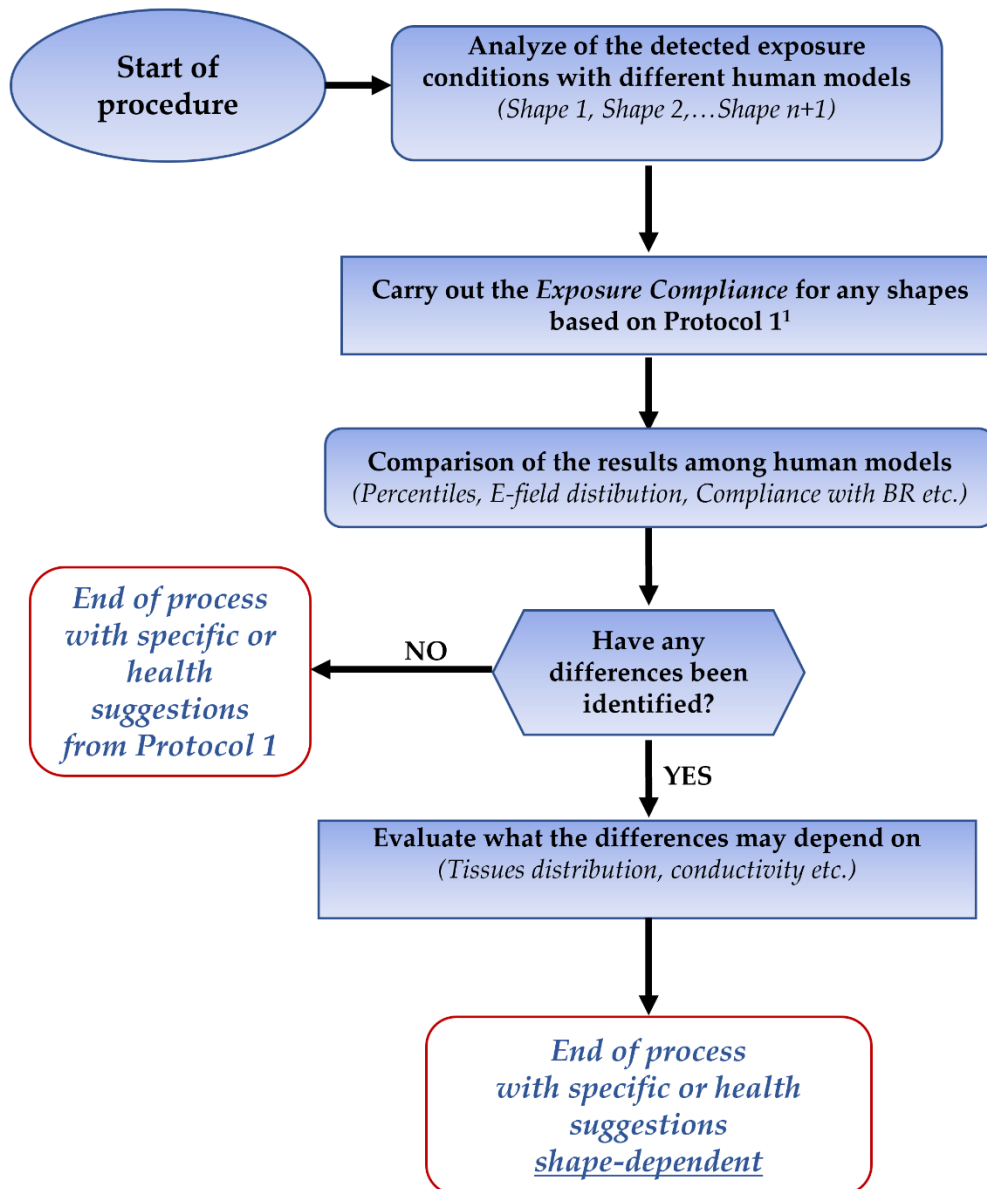
### **Note**

1. *The census of the equipment, following the Table 3.2 of Non-binding Guide, reveals the necessity to carry out a specific evaluation of the exposure., and also, in order to continue with the procedure, one of the following cases, must exist:*

- *The ALs (or RLs for ICNIRP), exceed the limits;*
- *The condition of the exposure consists of a very localized source with a distance of a few centimeters from the body of the worker, thus the exposure assessment necessarily requires determining dosimetrically the induced electric field.*

2. *From the titration analysis we are capable to know in which condition the source can causes the stimuli, thus some suggestions could be proposed.*

## Step 2: Innovative protocol of analysis



### Note

1. Replace the male human model Duke with the subject you consider appropriate (Ella, Jeduk, Fats, etc.) and continue with the basic protocol.



# BIBLIOGRAPHY

---

1. European Union. Directive No. 2013/35/EU, of 26 June 2013, on the minimum health and safety requirements regarding the exposure of workers to the risks arising from physical agents (electromagnetic fields). *Off. J. Eur. Union* **L179**, 1–21 (2013).
2. Modenese, A. & Gobba, F. Occupational exposure to electromagnetic fields and health surveillance according to the european directive 2013/35/eu. *Int. J. Environ. Res. Public Health* **18**, 1–12 (2021).
3. EN IEC 62822-1:2018. EN IEC 62822-1:2018. Electric welding equipment - Assessment of restrictions related to human exposure to electromagnetic fields (0 Hz to 300 GHz) - Part 1: Product family standard. (2018).
4. EN 62822-2:2016. IEC 62822-2:2016 applies to equipment for arc welding and allied processes designed for occupational use by professionals and for use by laymen. (2016).
5. CEI EN 50444. Basic standard for the evaluation of human exposure to electromagnetic fields from equipment for arc welding and allied processes. (2008).
6. CEI EN 50445. Product family standard to demonstrate compliance of equipment for resistance welding, arc welding and allied processes with the basic restrictions related to human exposure to electromagnetic fields (0 Hz - 300 GHz). (2008).
7. Karpowicz, J. & Gryz, K. The pattern of exposure to static magnetic field of nurses involved in activities related to contrast administration into patients diagnosed in 1.5 T MRI scanners. *Electromagn. Biol. Med.* **32**, 182–191 (2013).
8. Di Nallo, A. M. *et al.* Monitoring of people and workers exposure to the electric, magnetic and electromagnetic fields in an Italian national cancer Institute. *J. Exp. Clin. Cancer Res.* **27**, 16 (2008).
9. European Commission. European Commission, Directorate-General for

Employment, Social Affairs and Inclusion, Non-binding guide to good practice for implementing Directive 2013/35/EU Electromagnetic Fields. Volume 2, Case studies, Publications Office, 2016,. (2016).

10. De Sousa, I. P. & Costa Monteiro, E. Transcranial magnetic stimulation conformity assessment. *XXI IMEKO World Congr. "Measurement Res. Ind.* 2–5 (2015).
11. IEC 60601-1:2005+A1:2012+A2:2020. IEC 60601-1 Medical electrical equipment – Part 1: General requirements for basic safety and essential performance. 1740 (2020).
12. IEC 60601-1-2 Standard (edition 4.0). CEI - EN 60601-1-2/A1 Medical electrical equipment Part 1: General requirements for basic safety and essential performance - Collateral Standard: Electromagnetic disturbances - Requirements and tests. (2021).
13. International Commission on Non-Ionizing Radiation Protection (ICNIRP). Guidelines for limiting exposure to time-varying electric and magnetic fields (1 Hz TO 100 kHz). *Health Phys.* **99**, 818–836 (2010).
14. International Commission on Non-Ionizing Radiation Protection (ICNIRP). Guidelines for limiting exposure to electromagnetic fields (100 kHz to 300 GHz). *Health Physics* vol. 118 483–524 (2020).
15. Laakso, I. & Hirata, A. Reducing the staircasing error in computational dosimetry of low-frequency electromagnetic fields. *Phys. Med. Biol.* **57**, 5057–5057 (2012).
16. Gomez-Tames, J. *et al.* Computational Artifacts of the In Situ Electric Field in Anatomical Models Exposed to Low-Frequency Magnetic Field. *IEEE Trans. Electromagn. Compat.* **60**, 589–597 (2018).
17. Laakso, I. Computational Dosimetry at Low Frequencies: Recent Progress and Open Issues. *Proc. 2020 Int. Symp. Electromagn. Compat. - EMC Eur. EMC Eur. 2020 2020–2023* (2020) doi:10.1109/EMCEUROPE48519.2020.9245772.
18. Dimbylow, P. J. Current densities in a 2 mm resolution anatomically realistic model of the body induced by low frequency electric fields. *Phys. Med. Biol.* **45**, 1013–1022

(2000).

19. IT'IS Foundation. <https://itis.swiss/news-events/news/latest-news/>.
20. Aga, K. *et al.* Intercomparison of In Situ Electric Fields in Human Models Exposed to Spatially Uniform Magnetic Fields. *IEEE Access* **6**, 70964–70973 (2018).
21. Bakker, J. F. *et al.* Children and adults exposed to low-frequency magnetic fields at the ICNIRP reference levels: theoretical assessment of the induced electric fields. *Phys. Med. Biol.* **57**, 1815–1829 (2012).
22. Soldati, M. *et al.* A multi-scale computational approach based on TMS experiments for the assessment of electro-stimulation thresholds of the brain at intermediate frequencies. *Phys. Med. Biol.* **63**, 225006 (2018).
23. Gosselin, M.-C. *et al.* Development of a new generation of high-resolution anatomical models for medical device evaluation: the Virtual Population 3.0. *Phys. Med. Biol.* **59**, 5287–5303 (2014).
24. website. Physical Agents Portal.
25. Kamil . J. Ali. Measurement of Magnetic Fields Emitted From Welding Machines. *Diyala J. Eng. Sci.* **5**, 114–128 (2012).
26. Kos, B., Valič, B., Kotnik, T. & Gajšek, P. Induced electric fields in workers near low-frequency induction heating machines. *Bioelectromagnetics* **35**, 222–226 (2014).
27. STAM, R. & YAMAGUCHI-SEKINO, S. Occupational exposure to electromagnetic fields from medical sources. *Ind. Health* **56**, 96–105 (2018).
28. Wilén, J. Exposure assessment of electromagnetic fields near electrosurgical units. *Bioelectromagnetics* **31**, 513–518 (2010).
29. Munteanu, C., Topa, V., Racasan, A., Visan, G. & Pop, I. T. Computation methods and experimental measurements of the electric and magnetic field distribution inside high voltage substations. in *2009 International Conference on Electromagnetics in*



- Advanced Applications* 253–256 (IEEE, 2009). doi:10.1109/ICEAA.2009.5297453.
30. Thielens, A., Vermeeren, G., Kurup, D., Joseph, W. & Martens, L. Compliance boundaries for multiple-frequency base station antennas in three directions. *Bioelectromagnetics* **34**, 465–478 (2013).
  31. Hocking, B. & Gobbo, F. Medical aspects of overexposures to electromagnetic fields. *J. Heal. Saf. Environ.* **27**, 185–195 (2011).
  32. Shellock, F. G. & Crues, J. V. Temperature, heart rate, and blood pressure changes associated with clinical MR imaging at 1.5 T. *Radiology* (1987) doi:10.1148/radiology.163.1.3823445.
  33. Dimbylow, P. J. The calculation of SAR from limb current in the female voxel phantom, NAOMI. *Radiat. Prot. Dosimetry* **121**, 236–239 (2006).
  34. European Standard. European Standard 50499- Procedure for the assessment of the exposure of workers to electromagnetic fields. (2020).
  35. Petrov, P. I., Mandija, S., Sommer, I. E. C., Van Den Berg, C. A. T. & Neggers, S. F. W. How much detail is needed in modeling a transcranial magnetic stimulation figure-8 coil: Measurements and brain simulations. *PLoS One* **12**, e0178952 (2017).
  36. Karlström, E. F., Lundström, R., Stensson, O. & Mild, K. H. Therapeutic staff exposure to magnetic field pulses during TMS/rTMS treatments. *Bioelectromagnetics* **27**, 156–158 (2006).
  37. Møllerlækken, O. J., Stavang, H. & Hansson Mild, K. Staff exposure to pulsed magnetic fields during depression treatment with transcranial magnetic stimulation. *Int. J. Occup. Saf. Ergon.* **23**, 139–142 (2017).
  38. Guidance on determining compliance of exposure to pulsed and complex non-sinusoidal waveforms below 100 kHz with ICNIRP guidelines. *Health Phys.* **84**, 383–387 (2003).
  39. Rossi, S. *et al.* Safety, ethical considerations, and application guidelines for the use of

- transcranial magnetic stimulation in clinical practice and research. *Clin. Neurophysiol.* **120**, 2008–2039 (2009).
40. Guidelines for limiting exposure to electromagnetic fields (100 kHz to 300 GHz). *Health Physics* vol. 118 483–524 (2020).
  41. Guidelines for limiting exposure to time-varying electric and magnetic fields (1 Hz TO 100 kHz). *Health Phys.* **99**, 818–836 (2010).
  42. Lu, M. & Ueno, S. Dosimetry of typical transcranial magnetic stimulation devices. *J. Appl. Phys.* **107**, 09B316 (2010).
  43. Bottauscio, O., Zucca, M., Chiampi, M. & Zilberti, L. Evaluation of the Electric Field Induced in Transcranial Magnetic Stimulation Operators. *IEEE Trans. Magn.* **52**, 2–5 (2016).
  44. Air Force Research Laboratory. website. <https://www.afrl.af.mil/711HPW/RH/>.
  45. Christ, A. *et al.* The Virtual Family—development of surface-based anatomical models of two adults and two children for dosimetric simulations. *Phys. Med. Biol.* **55**, N23–N38 (2010).
  46. Temesi, J., Gruet, M., Rupp, T., Verges, S. & Millet, G. Y. Resting and active motor thresholds versus stimulus–response curves to determine transcranial magnetic stimulation intensity in quadriceps femoris. *J. Neuroeng. Rehabil.* **11**, 40 (2014).
  47. Schecklmann, M. *et al.* Resting motor threshold and magnetic field output of the figure-of-8 and the double-cone coil. *Sci. Rep.* **10**, 1644 (2020).
  48. Zucca, M., Bottauscio, O., Chiampi, M. & Zilberti, L. Operator Safety and Field Focality in Aluminum Shielded Transcranial Magnetic Stimulation. *IEEE Trans. Magn.* **53**, 1–4 (2017).
  49. Rutherford, G., Lithgow, B. & Moussavi, Z. Transcranial magnetic stimulation safety from operator exposure perspective. *Med. Biol. Eng. Comput.* **58**, 249–256 (2020).

50. De Leo, A., Primiani, V. M., Russo, P., Moglie, F. & Cerri, G. Safety Investigation of a Magnetic Pulse Applicator for Heart Stimulation. *IEEE Trans. Magn.* **50**, 5–12 (2014).
51. Bailey, W. H. & Erdreich, L. S. ACCOUNTING FOR HUMAN VARIABILITY AND SENSITIVITY IN SETTING STANDARDS FOR ELECTROMAGNETIC FIELDS. *Health Phys.* **92**, 649–657 (2007).
52. McCann, J. Cancer risk assessment of extremely low frequency electric and magnetic fields: a critical review of methodology. *Environ. Health Perspect.* **106**, 701–717 (1998).
53. Leitgeb, N., Schröttner, J. & Cech, R. PERCEPTION OF ELF ELECTROMAGNETIC FIELDS: EXCITATION THRESHOLDS AND INTER-INDIVIDUAL VARIABILITY. *Health Phys.* **92**, 591–595 (2007).
54. Hirata, A. *et al.* Assessment of Human Exposure to Electromagnetic Fields: Review and Future Directions. *IEEE Trans. Electromagn. Compat.* **63**, 1619–1630 (2021).
55. Gallucci, S. *et al.* Human Exposure Assessment to Wearable Antennas: Effect of Position and Interindividual Anatomical Variability. *Int. J. Environ. Res. Public Health* **19**, 5877 (2022).
56. Barker, A. T., Jalinous, R. & Freeston, I. L. NON-INVASIVE MAGNETIC STIMULATION OF HUMAN MOTOR CORTEX. *Lancet* **325**, 1106–1107 (1985).
57. Valero-Cabré, A., Amengual, J. L., Stengel, C., Pascual-Leone, A. & Coubard, O. A. Transcranial magnetic stimulation in basic and clinical neuroscience: A comprehensive review of fundamental principles and novel insights. *Neurosci. Biobehav. Rev.* **83**, 381–404 (2017).
58. Lefaucheur, J.-P. *et al.* Evidence-based guidelines on the therapeutic use of repetitive transcranial magnetic stimulation (rTMS): An update (2014–2018). *Clin. Neurophysiol.* **131**, 474–528 (2020).
59. Sakreida, K. *et al.* High-resolution language mapping of Broca's region with transcranial magnetic stimulation. *Brain Struct. Funct.* (2017) doi:10.1007/s00429-017-

1550-8.

60. Gunduz, M. E. *et al.* Motor Cortex Reorganization in Limb Amputation: A Systematic Review of TMS Motor Mapping Studies. *Front. Neurosci.* **14**, (2020).
61. Padovani, A. *et al.* Diagnosis of Mild Cognitive Impairment Due to Alzheimer's Disease with Transcranial Magnetic Stimulation. *J. Alzheimer's Dis.* **65**, 221–230 (2018).
62. Brunoni, A. R. *et al.* Repetitive Transcranial Magnetic Stimulation for the Acute Treatment of Major Depressive Episodes. *JAMA Psychiatry* **74**, 143 (2017).
63. Carmi, L. *et al.* Efficacy and Safety of Deep Transcranial Magnetic Stimulation for Obsessive-Compulsive Disorder: A Prospective Multicenter Randomized Double-Blind Placebo-Controlled Trial. *Am. J. Psychiatry* **176**, 931–938 (2019).
64. He, Y., Li, K., Chen, Q., Yin, J. & Bai, D. Repetitive Transcranial Magnetic Stimulation on Motor Recovery for Patients With Stroke. *Am. J. Phys. Med. Rehabil.* **99**, 99–108 (2020).
65. Yang, C. *et al.* Repetitive transcranial magnetic stimulation therapy for motor recovery in Parkinson's disease: A Meta-analysis. *Brain Behav.* **8**, e01132 (2018).
66. Schoisswohl, S. *et al.* RTMS parameters in tinnitus trials: a systematic review. *Sci. Rep.* **9**, 12190 (2019).
67. VanHaerents, S., Chang, B. S., Rotenberg, A., Pascual-Leone, A. & Shafi, M. M. Noninvasive Brain Stimulation in Epilepsy. *J. Clin. Neurophysiol.* **37**, 118–130 (2020).
68. Yang, S. & Chang, M. C. Effect of Repetitive Transcranial Magnetic Stimulation on Pain Management: A Systematic Narrative Review. *Front. Neurol.* **11**, (2020).
69. Awad, B. I., Carmody, M. A., Zhang, X., Lin, V. W. & Steinmetz, M. P. Transcranial Magnetic Stimulation After Spinal Cord Injury. *World Neurosurg.* **83**, 232–235 (2015).
70. Di Lazzaro, V., Rothwell, J. & Capogna, M. Noninvasive Stimulation of the Human

Brain: Activation of Multiple Cortical Circuits. *Neurosci.* **24**, 246–260 (2018).

71. Wagner, T., Valero-Cabre, A. & Pascual-Leone, A. Noninvasive Human Brain Stimulation. *Annu. Rev. Biomed. Eng.* **9**, 527–565 (2007).
72. Lefaucheur, J.-P. *et al.* Evidence-based guidelines on the therapeutic use of repetitive transcranial magnetic stimulation (rTMS). *Clin. Neurophysiol.* **125**, 2150–2206 (2014).
73. Arai, N. *et al.* Comparison between short train, monophasic and biphasic repetitive transcranial magnetic stimulation (rTMS) of the human motor cortex. *Clin. Neurophysiol.* **116**, 605–613 (2005).
74. Klomjai, W., Katz, R. & Lackmy-Vallée, A. Basic principles of transcranial magnetic stimulation (TMS) and repetitive TMS (rTMS). *Ann. Phys. Rehabil. Med.* **58**, 208–213 (2015).
75. Sommer, M. *et al.* Half sine, monophasic and biphasic transcranial magnetic stimulation of the human motor cortex. *Clin. Neurophysiol.* **117**, 838–844 (2006).
76. Kammer, T., Beck, S., Thielscher, A., Laubis-Herrmann, U. & Topka, H. Motor thresholds in humans: a transcranial magnetic stimulation study comparing different pulse waveforms, current directions and stimulator types. *Clin. Neurophysiol.* **112**, 250–258 (2001).
77. Maeda, F., Keenan, J. P., Tormos, J. M., Topka, H. & Pascual-Leone, A. Interindividual variability of the modulatory effects of repetitive transcranial magnetic stimulation on cortical excitability. *Exp. Brain Res.* **133**, 425–430 (2000).
78. Guadagnin, V., Parazzini, M., Fiocchi, S., Liorni, I. & Ravazzani, P. Deep Transcranial Magnetic Stimulation: Modeling of Different Coil Configurations. *IEEE Trans. Biomed. Eng.* **63**, 1543–1550 (2016).
79. Roth, Y., Amir, A., Levkovitz, Y. & Zangen, A. Three-Dimensional Distribution of the Electric Field Induced in the Brain by Transcranial Magnetic Stimulation Using Figure-8 and Deep H-Coils. *J. Clin. Neurophysiol.* **24**, 31–38 (2007).

80. Zewdie, E. & Kirton, A. TMS Basics. in *Pediatric Brain Stimulation* 3–22 (Elsevier, 2016). doi:10.1016/B978-0-12-802001-2.00001-1.
81. Deng, Z.-D., Lisanby, S. H. & Peterchev, A. V. Electric field depth–focality tradeoff in transcranial magnetic stimulation: Simulation comparison of 50 coil designs. *Brain Stimul.* **6**, 1–13 (2013).
82. Peterchev, A. V., D’Ostilio, K., Rothwell, J. C. & Murphy, D. L. Controllable pulse parameter transcranial magnetic stimulator with enhanced circuit topology and pulse shaping. *J. Neural Eng.* **11**, 056023 (2014).
83. Guerra, A. *et al.* Detecting cortical circuits resonant to high-frequency oscillations in the human primary motor cortex: a TMS-tACS study. *Sci. Rep.* **10**, 7695 (2020).
84. Cantone, M. *et al.* Age, Height, and Sex on Motor Evoked Potentials: Translational Data From a Large Italian Cohort in a Clinical Environment. *Front. Hum. Neurosci.* **13**, (2019).
85. Ueno, S., Tashiro, T. & Harada, K. Localized stimulation of neural tissues in the brain by means of a paired configuration of time-varying magnetic fields. *J. Appl. Phys.* **64**, 5862–5864 (1988).
86. Ilmoniemi, R. J., Ruohonen, J. & Karhu, J. Transcranial magnetic stimulation--a new tool for functional imaging of the brain. *Crit. Rev. Biomed. Eng.* **27**, 241–84 (1999).
87. Paffi, A., Liberti, M., Apollonio, F. & Tampieri, P. Experimental Characterization of a Figure of Eight Coil for Transcranial Magnetic Stimulation. *MeMeA 2018 - 2018 IEEE Int. Symp. Med. Meas. Appl. Proc.* 1–5 (2018) doi:10.1109/MeMeA.2018.8438691.
88. Lontis, E. R., Voigt, M. & Struijk, J. J. Focality Assessment in Transcranial Magnetic Stimulation With Double and Cone Coils. *J. Clin. Neurophysiol.* **23**, 463–472 (2006).
89. Zangen, A., Roth, Y., Voller, B. & Hallett, M. Transcranial magnetic stimulation of deep brain regions: evidence for efficacy of the H-Coil. *Clin. Neurophysiol.* **116**, 775–779 (2005).

90. Deng, Z.-D., Lisanby, S. H. & Peterchev, A. V. Coil design considerations for deep transcranial magnetic stimulation. *Clin. Neurophysiol.* **125**, 1202–1212 (2014).
91. International Commission on Non-Ionizing Radiation Protection (ICNIRP). *ICNIRP Guidelines for limiting exposure to time-varying electric, magnetic and electromagnetic fields (up to 300 GHz)*. vol. 74 (4) (Health Physics, 1998).
92. European Council. 1999/519/EC: Council Recommendation of 12 July 1999 on the limitation of exposure of the general public to electromagnetic fields (0 Hz to 300 GHz). *Off. J. L 199 L 199*, 59–70 (1999).
93. European Commission. European Commission, Directorate-General for Employment, Social Affairs and Inclusion, Non-binding guide to good practice for implementing Directive 2013/35/EU Electromagnetic Fields. Volume 1, Practical guide, Publications Office, 2016,. **1**, (2016).
94. European Parliament and of the Council. Directive 2004/40/EC of the European Parliament and of the Council of 29 April 2004 on the minimum health and safety requirements regarding the exposure of workers to the risks arising from physical agents (electromagnetic fields) (18th individual Directi. **L 159**, (2004).
95. International Commission on Non-Ionizing Radiation Protection (ICNIRP). Guidelines on limits of exposure to static magnetic fields. International Commission on Non-Ionizing Radiation Protection. *Health Phys.* **66**, 100–106 (2009).
96. IEC 60601-1-3:2008+A1:2013+A2:2021. (2021).
97. International Standard. IEC 60601-2-1:2020 Medical electrical equipment - Part 2-1: Particular requirements for the basic safety and essential performance of electron accelerators in the range 1 MeV to 50 MeV. (2020).
98. EN 60601-2-33:2010 - Medical electrical equipment - Part 2-33: Particular requirements for the basic safety and essential performance of magnetic resonance equipment for medical diagnosis (IEC 60601-2-33:2010). (2010).

99. IEC 60601-2-2:2017 Medical electrical equipment - Part 2-2: Particular requirements for the basic safety and essential performance of high frequency surgical equipment and high frequency surgical accessories. (2017).
100. Regulation (EU) 2017/745 of the European Parliament and of the Council of 5 April 2017 on medical devices, amending Directive 2001/83/EC, Regulation (EC) No 178/2002 and Regulation (EC) No 1223/2009 and repealing Council Directives 90/385/EEC and 93/42/EE. **L 117/1**, (2017).
101. Contessa, G. M., D'Agostino, S., Falsaperla, R., Grandi, C. & Polichetti, A. Issues in the Implementation of Directive 2013/35/EU Regarding the Protection of Workers against Electromagnetic Fields. *Int. J. Environ. Res. Public Health* **18**, 10673 (2021).
102. Dawson, T. W., Caputa, K. & Stuchly, M. A. Influence of human model resolution on computed currents induced in organs by 60-Hz magnetic fields. *Bioelectromagnetics* **18**, 478–90 (1997).
103. Hirata, A., Takano, Y., Fujiwara, O., Dovan, T. & Kavet, R. An electric field induced in the retina and brain at threshold magnetic flux density causing magnetophosphenes. *Phys. Med. Biol.* **56**, 4091–4101 (2011).
104. Laakso, I. & Hirata, A. Evaluation of the induced electric field and compliance procedure for a wireless power transfer system in an electrical vehicle. *Phys. Med. Biol.* **58**, 7583–7593 (2013).
105. Ahn, J. *et al.* Improved Calculation Method of Coupling Factors for Low-Frequency Wireless Power Transfer Systems. *Int. J. Environ. Res. Public Health* **19**, 44 (2021).
106. IEC. IEC 62233:2005 Measurement methods for electromagnetic fields of household appliances and similar apparatus with regard to human exposure. (2005).
107. IEC. IEC 62311:2019 Assessment of electronic and electrical equipment related to human exposure restrictions for electromagnetic fields (0 Hz to 300 GHz). (2019).
108. Kaune, W. T., Guttman, J. L. & Kavet, R. Comparison of coupling of humans to



electric and magnetic fields with frequencies between 100 Hz and 100 kHz.

*Bioelectromagnetics* **18**, 67–76 (1997).

109. Andreuccetti, D. & Zoppetti, N. Quasi-Static Electromagnetic Dosimetry: From Basic Principles to Examples of Applications. *Int. J. Occup. Saf. Ergon.* **12**, 201–215 (2006).
110. Sim4Life website. <https://zmt.swiss/>. <https://zmt.swiss/>.
111. Colella, M., Paffi, A., De Santis, V., Apollonio, F. & Liberti, M. Effect of skin conductivity on the electric field induced by transcranial stimulation techniques in different head models. *Phys. Med. Biol.* **66**, 035010 (2021).
112. Fiocchi, S., Chiaramello, E., Ravazzani, P. & Parazzini, M. Modelling of the Current Density Distributions during Cortical Electric Stimulation for Neuropathic Pain Treatment. *Comput. Math. Methods Med.* **2018**, 1–12 (2018).
113. Samoudi, A. M., Tanghe, E., Martens, L. & Joseph, W. Deep Transcranial Magnetic Stimulation: Improved Coil Design and Assessment of the Induced Fields Using MIDA Model. *Biomed Res. Int.* **2018**, 7061420 (2018).
114. Yale University. <http://www.neuron.yale.edu>.
115. Kim, J. H., Lee, J.-K., Kim, H.-G., Kim, K.-B. & Kim, H. R. Possible Effects of Radiofrequency Electromagnetic Field Exposure on Central Nerve System. *Biomol. Ther. (Seoul)*. **27**, 265–275 (2019).
116. Pall, M. L. Electromagnetic fields act via activation of voltage-gated calcium channels to produce beneficial or adverse effects. *J. Cell. Mol. Med.* **17**, 958–965 (2013).
117. D’Agostino, S. *et al.* Extremely High Frequency Electromagnetic Fields Facilitate Electrical Signal Propagation by Increasing Transmembrane Potassium Efflux in an Artificial Axon Model. *Sci. Rep.* **8**, 9299 (2018).
118. Buckner, C. A., Buckner, A. L., Koren, S. A., Persinger, M. A. & Lafrenie, R. M. Inhibition of Cancer Cell Growth by Exposure to a Specific Time-Varying

- Electromagnetic Field Involves T-Type Calcium Channels. *PLoS One* **10**, e0124136 (2015).
119. Tekieh, T., Sasanpour, P. & Rafii-Tabar, H. Electrophysiological effects of low frequency electrical radiation on the neural compartment: a theoretical investigation. *Biomed. Phys. Eng. Express* **4**, 025040 (2018).
120. Gaines, J. L., Finn, K. E., Slopsema, J. P., Heyboer, L. A. & Polasek, K. H. A model of motor and sensory axon activation in the median nerve using surface electrical stimulation. *J. Comput. Neurosci.* **45**, 29–43 (2018).
121. McIntyre, C. C., Richardson, A. G. & Grill, W. M. Modeling the Excitability of Mammalian Nerve Fibers: Influence of Afterpotentials on the Recovery Cycle. *J. Neurophysiol.* **87**, 995–1006 (2002).
122. Thacker, B. H. *et al.* Concepts of Model Verification and Validation. (2004).
123. Physical Agents Portal.  
[https://www.portaleagentifisici.it/fo\\_campi\\_elettromagnetici\\_viewer\\_for\\_macchiana\\_rio.php?lg=IT&objId=21453](https://www.portaleagentifisici.it/fo_campi_elettromagnetici_viewer_for_macchiana_rio.php?lg=IT&objId=21453).
124. Müller-dahlhaus, F. *et al.* Brain Stimulation Short-interval and long-interval intracortical inhibition of TMS-evoked EEG potentials. *Brain Stimul.* **11**, 818–827 (2018).
125. Nelson, A. J., Hoque, T., Gunraj, C., Ni, Z. & Chen, R. Bi-directional interhemispheric inhibition during unimanual sustained contractions. **13**, 1–13 (2009).
126. Premoli, I. *et al.* Short-interval and long-interval intracortical inhibition of TMS-evoked EEG potentials. *Brain Stimul.* **11**, 818–827 (2018).
127. Bottauscio, O., Zucca, M., Chiampì, M. & Zilberti, L. Evaluation of the Electric Field Induced in Transcranial Magnetic Stimulation Operators. *IEEE Trans. Magn.* **52**, 1–4 (2016).

128. Paffi, A. *et al.* A Computational Model for Real-Time Calculation of Electric Field due to Transcranial Magnetic Stimulation in Clinics. *Int. J. Antennas Propag.* **2015**, 1–11 (2015).
129. Petrov, P. I., Mandija, S., Sommer, I. E. C., van den Berg, C. A. T. & Neggers, S. F. W. How much detail is needed in modeling a transcranial magnetic stimulation figure-8 coil: Measurements and brain simulations. *PLoS One* **12**, e0178952 (2017).
130. Gomez-Tames, J., Laakso, I. & Hirata, A. Review on biophysical modelling and simulation studies for transcranial magnetic stimulation. *Phys. Med. Biol.* **65**, 24TR03 (2020).
131. Gomez, L. J., Dannhauer, M., Koponen, L. M. & Peterchev, A. V. Conditions for numerically accurate TMS electric field simulation. *Brain Stimul.* **13**, 157–166 (2020).
132. Christ, A. *et al.* The Virtual Family - Development of surface-based anatomical models of two adults and two children for dosimetric simulations. *Phys. Med. Biol.* **55**, (2010).
133. Magstim Corporation. <https://www.magstim.com/row-en/product-category/coils/>.  
<https://www.magstim.com/row-en/product-category/coils/>.
134. Magstim Co Ltd. <https://www.magstim.com/row-en/product/90mm/>.
135. Pascual-Leone, A. MAGSTIM Rapid 2 - Operating manual. *System* (2009).
136. Joulinous, R. Guide to Magnetic Stimulation. (1998).
137. Paffi, A. *et al.* A computational model for real-time calculation of electric field due to transcranial magnetic stimulation in clinics. *Int. J. Antennas Propag.* **2015**, 23–27 (2015).
138. Roth, F. Guide to Magnetic Exploration. 1–8 (2005).
139. MagVenture medical device. Explore the brain - Advance your neuroscience research with TMS. 1–16.

140. Carlo Miniussi. La stimolazione magnetica transcranica: nuove prospettive d'intervento tra clinica e ricerca. in (ed. 2° congresso Nazionale di Neuroscience of Addiction) (2010).
141. Val, A. *et al.* RAPPORTO DI MISURA Rilevazione campi elettromagnetici emessi da un apparecchio per la stimolazione transcranica modello Magstim 200. 1–5 (2009).
142. D'Agostino, S., Colella, M., Liberti, M., Falsaperla, R. & Apollonio, F. Systematic numerical assessment of occupational exposure to electromagnetic fields of transcranial magnetic stimulation. *Med. Phys.* **49**, 3416–3431 (2022).
143. Gomez-Tames, J., Laakso, I. & Hirata, A. Review on biophysical modelling and simulation studies for transcranial magnetic stimulation. *Phys. Med. Biol.* **65**, (2020).
144. Gomez, L. J., Dannhauer, M., Koponen, L. M. & Peterchev, A. V. Conditions for numerically accurate TMS electric field simulation. *Brain Stimul.* **13**, 157–166 (2020).
145. Gosselin, M.-C. *et al.* Development of a new generation of high-resolution anatomical models for medical device evaluation: the Virtual Population 3.0. *Phys. Med. Biol.* **59**, 5287–5303 (2014).
146. Hasgall, P. *et al.* IT'IS Database for thermal and electromagnetic parameters of biological tissues, Version 4.0. *IT'IS* (2018) doi:10.13099/VIP21000-04-0.
147. Rutherford, G., Lithgow, B. & Moussavi, Z. Transcranial magnetic stimulation safety from operator exposure perspective. *Med. Biol. Eng. Comput.* **58**, 249–256 (2020).
148. Stuchly, M. A. & Dawson, T. W. HUMAN BODY EXPOSURE TO POWER LINES: RELATION OF INDUCED QUANTITIES TO EXTERNAL MAGNETIC FIELDS. *Health Phys.* **83**, 333–340 (2002).
149. Jokela, K. ASSESSMENT OF COMPLEX EMF EXPOSURE SITUATIONS INCLUDING INHOMOGENEOUS FIELD DISTRIBUTION. *Health Phys.* **92**, 531–540 (2007).
150. Schecklmann, M. *et al.* Resting motor threshold and magnetic field output of the

- figure-of-8 and the double-cone coil. *Sci. Rep.* **10**, 1–6 (2020).
151. Temesi, J., Gruet, M., Rupp, T., Verges, S. & Millet, G. Y. Resting and active motor thresholds versus stimulus-response curves to determine transcranial magnetic stimulation intensity in quadriceps femoris. *J. Neuroeng. Rehabil.* **11**, (2014).
  152. Lu, M. & Ueno, S. Dosimetry of typical transcranial magnetic stimulation devices. *J. Appl. Phys.* **107**, 1106 (2010).
  153. Çan, M. K., Laakso, I., Nieminen, J. O., Murakami, T. & Ugawa, Y. Coil model comparison for cerebellar transcranial magnetic stimulation. *Biomed. Phys. Eng. Express* **5**, (2019).
  154. Zucca, M., Bottauscio, O., Chiampi, M. & Zilberti, L. Operator Safety and Field Focality in Aluminum Shielded Transcranial Magnetic Stimulation. *IEEE Trans. Magn.* (2017) doi:10.1109/TMAG.2017.2709402.
  155. Hirata, A., Wake, K., Watanabe, S. & Taki, M. In-situ electric field and current density in Japanese male and female models for uniform magnetic field exposures. *Radiat. Prot. Dosimetry* **135**, 272–275 (2009).
  156. Nagaoka, T. *et al.* Development of realistic high-resolution whole-body voxel models of Japanese adult males and females of average height and weight, and application of models to radio-frequency electromagnetic-field dosimetry. *Phys. Med. Biol.* **49**, 1–15 (2004).
  157. Taflove, A. & C.Hagness, S. In Computational Electrodynamics: The Finite-Difference Time-Domain Method. *Artech House* 51–105 (2003).
  158. ViP, S. Ella tissues list. [https://itis.swiss/assets/Downloads/VirtualPopulation/Tissue-list-cV3-1/Ella\\_26y\\_f\\_v3-1b01\\_TissueList.txt](https://itis.swiss/assets/Downloads/VirtualPopulation/Tissue-list-cV3-1/Ella_26y_f_v3-1b01_TissueList.txt).
  159. Hand, J. W. Modelling the interaction of electromagnetic fields (10 MHz–10 GHz) with the human body: methods and applications. *Phys. Med. Biol.* **53**, R243–R286 (2008).

160. *Handbook of Anatomical Models for Radiation Dosimetry*. (CRC Press, 2009).  
doi:10.1201/EBK1420059793.
161. Kim, C. H., Choi, S. H., Jeong, J. H., Lee, C. & Chung, M. S. HDRK-Man: a whole-body voxel model based on high-resolution color slice images of a Korean adult male cadaver. *Phys. Med. Biol.* **53**, 4093–4106 (2008).
162. Bibin, L. *et al.* Whole-body pregnant woman modeling by digital geometry processing with detailed uterofetal unit based on medical images. *IEEE Trans. Biomed. Eng.* **57**, 2346–2358 (2010).
163. Wu, T. *et al.* Slice-based supine to standing postured deformation for Chinese anatomical models and the dosimetric results by wide band frequency electromagnetic field exposure: morphing. *Radiat. Prot. Dosimetry* **154**, 26–30 (2013).
164. Mazzurana, M. Development of numerical phantoms by MRI for RF electromagnetic dosimetry: a female model. *Radiat. Prot. Dosimetry* **111**, 445–451 (2004).
165. Liu, W., Collins, C. M. & Smith, M. B. Calculations of B<sub>1</sub> distribution, specific energy absorption rate, and intrinsic signal-to-noise ratio for a body-size birdcage coil loaded with different human subjects at 64 and 128 MHz. *Appl. Magn. Reson.* **29**, 5–18 (2005).
166. Dimbylow, P. Development of the female voxel phantom, NAOMI, and its application to calculations of induced current densities and electric fields from applied low frequency magnetic and electric fields. *Phys. Med. Biol.* **50**, 1047–1070 (2005).
167. Dolciotti, N., Colella, M., D’Agostino, S., Apollonio, F. & Liberti, M. Improved Anatomical Female Breast Model: 3D Realization and Its Application to Numerical Plane Wave Exposure. in *2022 IEEE 21st Mediterranean Electrotechnical Conference (MELECON)* 1274–1278 (IEEE, 2022). doi:10.1109/MELECON53508.2022.9843025.
168. Community, B. O. (2018). Blender - a 3D modelling and rendering package. Stichting

Blender Foundation, Amsterdam. Retrieved from <http://www.blender.org>.

169. Cvetković, M., Poljak, D., Rogić Vidaković, M. & Đogaš, Z. Transcranial magnetic stimulation induced fields in different brain models. *J. Electromagn. Waves Appl.* **30**, 1820–1835 (2016).
170. Parazzini, M., Fiocchi, S., Liorni, I. & Ravazzani, P. Effect of the Interindividual Variability on Computational Modeling of Transcranial Direct Current Stimulation. *Comput. Intell. Neurosci.* **2015**, 1–9 (2015).
171. Lucano, E. *et al.* A numerical investigation on the effect of RF coil feed variability on global and local electromagnetic field exposure in human body models at 64 MHz. *Magn. Reson. Med.* **79**, 1135–1144 (2018).
172. Bailey, W. H. & Erdreich, L. S. ACCOUNTING FOR HUMAN VARIABILITY AND SENSITIVITY IN SETTING STANDARDS FOR ELECTROMAGNETIC FIELDS. *Health Phys.* **92**, (2007).
173. McCann, J., Kheifets, L. & Rafferty, C. Cancer risk assessment of extremely low frequency electric and magnetic fields: A critical review of methodology. *Environ. Health Perspect.* **106**, 701–717 (1998).
174. Leitgeb, N., Schröttner, J. & Cech, R. Perception of ELF electromagnetic fields: Excitation thresholds and inter-individual variability. *Health Phys.* **92**, 591–595 (2007).
175. Hirata, A., Diao, Y., Onishi, T., Sasaki, K., Ahn, S., Colombi, D., De Santis, V., Laakso, I., Giaccone, L., Wout, J. & Rashed, E. A., Kainz, W., & Chen, J. Assessment of Human Exposure to Electromagnetic Fields. *IEEE Trans. Electromagn. Compat.* **63**, 1619–1630 (2021).
176. Gallucci, S. *et al.* Human Exposure Assessment to Wearable Antennas : Effect of Position and Interindividual Anatomical Variability. *Int. J. Environ. Res. Public Health* **19**, 5877 (2022).

177. Andrea Bogi, Nicola Zoppetti, I. P. RAPPORTO DI MISURA Rilevazione campi elettromagnetici emessi da un apparecchio per la stimolazione transcranica modello Magstim 200.  
*[https://www.portaleagentifisici.it/BO/getPdfForCaseById.php?case=public\\_download\\_pdf\\_report\\_misura\\_nir&id=13](https://www.portaleagentifisici.it/BO/getPdfForCaseById.php?case=public_download_pdf_report_misura_nir&id=13)* 1–5 (2009).
178. IT'IS Foundation. Tissue Properties Database V4.0. *IT'IS Foundation* (2018).
179. Gabriel, C. Compilation of the Dielectric Properties of Body Tissues at RF and Microwave Frequencies. **Occupation**, (1996).
180. Lucano, E. *et al.* A numerical investigation on the effect of RF coil feed variability on global and local electromagnetic field exposure in human body models at 64 MHz. *Magn. Reson. Med.* **79**, 1135–1144 (2018).
181. Colella, M., Paffi, A., de Santis, V., Apollonio, F. & Liberti, M. Effect of skin conductivity on the electric field induced by transcranial stimulation techniques in different head models. *Phys. Med. Biol.* **66**, (2021).
182. Tzirini, M. *et al.* Electric Field Distribution Induced by TMS: Differences Due to Anatomical Variation. *Appl. Sci.* **12**, (2022).
183. Contessa, G. M., D'agostino, S., Falsaperla, R., Grandi, C. & Polichetti, A. Issues in the implementation of directive 2013/35/eu regarding the protection of workers against electromagnetic fields. *Int. J. Environ. Res. Public Health* **18**, (2021).
184. So, P. P. M., Stuchly, M. A. & Nyenhuis, J. A. Peripheral nerve stimulation by gradient switching fields in magnetic resonance imaging. *IEEE Trans. Biomed. Eng.* **51**, 1907–1914 (2004).
185. Nyenhuis JA, Bourland JD, Kildishev AV, S. D. *Health effects and safety of intense gradient fields*. In: *Shellock FG, ed. 630 Magnetic resonance procedures: Health effects and safety*. (2001).
186. Reilly, J. P. Magnetic field excitation of peripheral nerves and the heart: a



- comparison of thresholds. *Med. Biol. Eng. Comput.* **29**, 571–579 (1991).
187. REILLY, J. P. Principles of Nerve and Heart Excitation by Time-varying Magnetic Fields. *Ann. N. Y. Acad. Sci.* **649**, 96–117 (1992).
188. Reilly, J. P. *Applied Bioelectricity*. *Applied Bioelectricity* (1998). doi:10.1007/978-1-4612-1664-3.
189. Reilly, J. P. & Diamant, A. M. Neuroelectric mechanisms applied to low frequency electric and magnetic field exposure guidelines - Part II: Non sinusoidal waveforms. *Health Phys.* **83**, 356–365 (2002).
190. Laakso, I. & Murakami, T. Thresholds of central nervous system stimulation at intermediate frequencies. *2016 URSI Asia-Pacific Radio Sci. Conf. URSI AP-RASC 2016* 733–736 (2016) doi:10.1109/URSIAP-RASC.2016.7601395.
191. Visible Korean Project. [Http://vkh3.kisti.re.kr/?q=node/24](http://vkh3.kisti.re.kr/?q=node/24).  
<http://vkh3.kisti.re.kr/?q=node/24>.
192. Yale University. <https://neuron.yale.edu/neuron/>.
193. Normativa. D.Lgs. 9 aprile 2008, 81. (2008).
194. DECRETO LEGISLATIVO 1° agosto 2016 , n. 159. Attuazione della direttiva 2013/35/UE sulle disposizioni minime di sicurezza e di salute relative all'esposizione dei lavoratori ai rischi derivanti dagli agenti fisici (campi elettromagnetici) e che abroga. 1–4 (2011).
195. *Decreto del Presidente del Consiglio dei Ministri 8 luglio 2003 "Fissazione dei limiti di esposizione, dei valori di attenzione e degli obiettivi di qualità" per la protezione della popolazione dalle esposizioni a campi elettrici, magnetici ed elettromagnetici*". *Gazzetta Ufficiale* n. 199 (2003).
196. *DECRETO DEL PRESIDENTE DEL CONSIGLIO DEI MINISTRI 8 luglio 2003 Fissazione dei limiti di esposizione, dei valori di attenzione e degli obiettivi di qualità' per la protezione della popolazione dalle esposizioni ai campi elettrici e magnetici alla frequenz.* GU

- n. 200 (2003).
197. *Legge quadro 22 febbraio 2001, n. 36 Sulla protezione dalle esposizioni a campi elettrici, magnetici ed elettromagnetici. Gazzetta ufficiale n. 55 (2001).*
  198. *Legge 22 febbraio 2001, n. 36 Legge quadro sulla protezione dalle esposizioni a campi elettrici, magnetici ed elettromagnetici. G.U. n. 55 del 7 marzo 2001 (2001).*
  199. International Electrotechnical Commission. Geneva Switzerland. IEC 610004-20 Electromagnetic Compatibility (EMC) -'F'a1t4: Testing and measurement techniques Section 20: Emission and Immunity Testing in Transvcnc Elechomagnctic (EM) Waveguides. (2003).
  200. Bozec, D., McCormack, L. M., Marvin, A. C., Nothofer, A. & Alexander, M. J. A good practice guide for the use of GTEM cells in EMC measurements according to IEC 61000-4-20. in *2004 International Symposium on Electromagnetic Compatibility (IEEE Cat. No.04CH37559)* vol. 2 660–665 (IEEE).
  201. ISO 14117:2019 Active implantable medical devices — Electromagnetic compatibility — EMC test protocols for implantable cardiac pacemakers, implantable cardioverter defibrillators and cardiac resynchronization devices. (2019).
  202. <https://webnir.ifac.cnr.it/>.
  203. Moretto, A. La Caratterizzazione Degli Effetti Degli Agenti Chimici: Problemi Nella Definizione Della Relazione Dose-Risposta Alle Basse Dosi. *G. Ital. Med. Lav. Ergon.* **XLI**, (2019).
  204. Scientific Committee on Emerging and Newly Identified Health Risks (SCENIHR). Health Effects of Exposure to EMF. European Commission; 2015.
  205. Ministero dello Sviluppo economico. Regolamento recante modifi che al decreto 12 maggio 2011, n. 110, concernente il regolamento di attuazione dell'articolo 10, comma 1, della legge 4 gennaio 1990, n. 1, relativo agli apparecchi elettromeccanici utilizzati per l'attività di estetista. 1–4 (2011).

206. Directive 2022/44/EU: laying down rules for the application of Regulation (EU) 2021/1139 as regards the criteria for establishing the level of financial corrections and for applying flat-rates linked to serious non-compliance with Common Fisheries Policy . (2022).
207. Directive Directive 2003/10/EU: on the minimum health and safety requirements regarding the exposure of workers to the risks arising from physical agents (noise) (Seventeenth individual Directive within the meaning of Article 16(1) of Directive 89/391/EEC.
208. Directive 2006/25/EC on the minimum health and safety requirements regarding the exposure of the workers to risks arising from physical agents (artificial optical radiation, 19th individual Directive within the meaning of Article 16(1) of Directive 89/391.
209. EN 50527-1:2017 Procedure for the assessment of the exposure to electromagnetic fields of workers bearing active implantable medical devices - Part 1: General. (2017).

# CURRICULUM VITAE

---

# SIMONA D'AGOSTINO

## PERSONAL INFORMATION

Date of birth: June 12, 1989  
Place of birth: Soriano Calabro (VV), ITALY  
Citizenship: ITALIAN  
Address: Via Arcinazzo Romano, 18, 00171, Rome (RM)

## PERSONAL CONTACTS:

Phone: +39 3407969178  
Personal e-mail: [dagostino.simona@yahoo.it](mailto:dagostino.simona@yahoo.it)  
Work e-mail: [simona.dagostino@uniroma1.it](mailto:simona.dagostino@uniroma1.it); [s.dagostino-sg@inail.it](mailto:s.dagostino-sg@inail.it)

## EDUCATIONAL BACKGROUND

- (2019- 2022) **Ph.D. Course**  
Sapienza University of Rome, Department of Information Engineering, Electronics and Telecommunications (DIET), Division of Engineering Electronics, Rome, Italy.
- (2012 - 2014) **Master's degree in Biomedical Engineering**  
Sapienza University of Rome
- Main subjects of the study: Bioelectromagnetic Interaction, Radioprotection and Complements of Physics, Biomechanics, Technological Applications in Surgery and Hospital Environment Diseases, Biomedical Instrumentation, Data Processing, and Biomedical Signals, and Hospital Systems.
  - Thesis title: "Numerical characterization of systems for drug delivery applications based on the magnetic field "
  - Vote: 110/110
- (2008 - 2012) **Bachelor's degree in Clinical Engineering**  
Sapienza University of Rome
- Main subjects of the study: Machines and Mechanics Applied to Machines, Fluid Mechanics, Models of Biological Systems, Electronics, Electrotechnical Systems, and Electrical Machines, Construction Science, Measures for Clinical Diagnostics, and Fundamentals of Human Anatomy and Physiology.
  - Thesis title: "Circuit analysis of the Trimprob probe: power supply signal generation"
  - Vote: 103/110

## TRAINING COURSE

- (27-28 January 2022) Theoretical/practical course on radioprotectionist and metrological aspects of 4G and 5G telephony, aimed at the correct assessment of population exposure".  
61<sup>st</sup> Course of the Scuola Superiore di Radioprotezione "Carlo Polvani"
- (14 December 2021) Electromagnetic fields - Basic course  
Webinar event. INAIL, USL Tuscany
- (4 July 2019) Electromagnetic fields and artificial optical radiation - measurement and evaluation in the workplace  
Phoenix ESD s.r. l
- (December 2017 – November 2018) Mandatory internship for the qualification to the profession of Expert in Radiation Protection  
Study of sources whose surveillance belongs to a qualified expert of I and II degree
- (3 March 2018) Legislative Decree 81/08, art 37 - Occupational safety - Mandatory training for Inail Institute employees  
INAIL National Institute for Insurance against Accidents at Work.
- (May 2012 – July 2012) Training internship for undergraduates.  
ENEA, National Agency for New Technologies, Energy and Sustainable Economic Development. Casaccia Research Center (RM).

## QUALIFICATIONS

- (20 May 2019) Qualification to the profession of Expert in Radiation Protection, I degree  
Ministry of Labor and Social Policies enrolled in the National Directory with identification number 1133

## WORK EXPERIENCE

(1 December 2017 – 31 October 2019)

### Grant in research projects

INAIL, Research Center DiMEILA (Department of Medicine, Epidemiology, Occupational and Environmental Hygiene) - Laboratory for physical agents risk. Monte Porzio Catone (RM).

- Collaboration for the realization of the research program: "Innovative safety management systems for risks connected to the evolution of production processes."
- The aim of the project is also the formulation of operational indications for assessing the risk associated with equipment that generates ionizing and non-ionizing radiation and the supervision of workers exposed to electromagnetic fields. The grant provides for the performance of activities in collaboration with the National Institute of Health- ISS of Rome, measurement campaigns at various institutions throughout the country, dosimetric analyzes with dedicated software, and knowledge of the regulatory aspects regarding electromagnetic exposure.

[Activity or sector](#) Scientific research.

(March 2016 – March 2017)

### External collaborator in experimental studies

CNR, National Research Council; Institute of Translational Pharmacology (IFT). ARTOV. Tor Vergata (RM).

- Collaboration in experimental studies as an external biomedical engineer expert.
- This work is carried out as part of the Research Project entitled "Non-invasive therapies for the treatment of various neurological diseases", the purpose of which is to carry out experimental laboratory work, use of microwave-generating antennas, and partly realized display systems during the study itself.

[Activity or sector](#) Scientific research.

(December 2015 – March 2016)

### Clinical Assistant

Motustech srl, Castel Fusano (RM).

- Training activities
- Evaluative analysis of the musculoskeletal system. This work is carried out working with a team of experts, making use of innovative, validated, and highly accurate tools for the functional assessment of the movement. The fields of application concern the sports, clinical, and rehabilitation fields.

[Activity or sector](#) Biomechanical

## GENERAL WORKING TASKS

- March 2022 [Lecturer](#) to the Advanced Training Course (as part of the Sapienza-INAIL Master)  
 " Integrated risk management from physical agents in the workplace and new ergonomic technologies for prevention".
- 28 August – 4 September 2021 [Staff](#). Coordinator of the volunteer staff present on-site and online; I also support the LOC on the occasion of the "XXXIV General Assembly and Scientific Symposium (GASS) of the International Union of Radio Science." Rome
- 20 – 24 June 2016 [Staff and Lecturer](#), of the International Summer School: on the advanced topics on cell model systems.  
 Lecture in " *Laboratory: vesicles preparation* "  
 Organized in collaboration with COST Action BM1309. At the Institute of Translational Pharmacology (IFT-CNR), Tor Vergata (RM).

## CERTIFICATIONS

- November 2021 [Certificate of "Qualified Teacher Trainer for Health and Safety at Work \(D.I: 6 March 2013\)"](#) according to criterion 1 and for Teaching C (Hygienic Health Risks of Legislative Decree 81/08 (Titles VI VIII IX X).  
 Certificate Nr AA2021003290.
- July 2015 [English language certificate](#)  
 Recognized by MIUR – level B2. The new British Centre (RM).

## AWARDS

- August 2021 [Young Scientist Award](#).  
 Award received on the occasion of the "34<sup>th</sup> General Assembly and Scientific Symposium", awarded by "The International Union of Radio Science", Rome.
- September 2021 [Student travel award](#)  
 BioEM2021 Annual Joint Meeting, Ghent, Belgium;

## TECHNICAL SKILLS AND COMPETENCES



- **Programming:** Matlab for data postprocessing, LabView for computer/instrument interface; basic C++,
- **Electromagnetic and electronic simulation software:** Sim4Life, Comsol Multiphysics, basic CST Computer Simulation Technology, basic LT Spice;
- **Software platform for medical image processing and 3D modeling:** MeshMixer;
- **Devices for electromagnetic measurements:** Oscilloscope, digital multimeter, NARDA ELT-400, NARDA EHP-50, Enertech EMDEX-LITE, Wandel & Goltermann EFA-3, Metrolab THM1176;
- **Application Software:** KaleidaGraph, OptoGait, Gyko RePower

## PARTICIPATION IN NATIONAL AND INTERNATIONAL CONFERENCES

- 29 May - 3 June 2022 Conference: “3rd URSI AT-AP-RASC 2022”, Gran Canaria, Spain.  
Presentation: Oral  
 Title: “Occupational exposure to TMS treatment: variability among human anatomical models”.  
 Authors: S. D’Agostino, M. Colella, M. Liberti, R. Falsaperla and F. Apollonio,
- 29 August – 4 September 2021 Conference: “XXXIV General Assembly and Scientific Symposium of the International Union of Radio Science (URSI GASS)”, Rome.  
Presentation: Oral  
 Title: “Dosimetric assessment of clinical staff exposed to the magnetic field produced by a transcranial magnetic stimulation circular coil”.  
 Authors: S. D’Agostino, M. Colella, M. Liberti, R. Falsaperla and F. Apollonio.
- 26 September - 1 October 2022 Conference: “BioEM 2021 - International Conference in the area of bioelectromagnetics”. Ghent, Belgium  
 Presentation: Poster  
 Title: “Numerical assessment of the exposure to Transcranial Magnetic Stimulation coil male and female anatomical model comparison”.  
 Authors: S. D’Agostino; M. Colella; M. Liberti; R. Falsaperla; F. Apollonio.
- October 2019 Conference: “National Conference dBA 2019, Physical agents and health in the workplace”, Bologna (BO).  
Presentation: Oral  
 Title: “Radiation protection between Consolidated Law and Legislative Decree.”.  
 Authors: S. D’Agostino, G.M. Contessa, E. Ragno.
- October 2018 Conference: “National Conference dBA 2018, physical risks in the workplace”. Bologna (BO).  
Presentation: Oral  
 Title: “Development and use of a web tool for the processing of low-frequency magnetic field exposure measurements and the determination of the weighted peak index”.
- 04 October 2017 – 06 October Conference: “8th International THz-Bio workshop”, ENEA, Frascati (RM).

2017 Presentation: Poster  
Title: Characterization of the electrical signal of artificial axon model for exposure to millimeter waves.  
Authors: C. Della Monica, E. Palizzi, S. D'Agostino, F. Di Pietrantonio, M. Benetti, D. Cannatà, M. Cavagnaro, D. Sardari, P. Stano and A. Ramundo-Orlando.

25 September 2016 – 30 September 2016 Conference: "*41st International Conference on Infrared, Millimeter and Terahertz waves*", organized by The International Society of Infrared, Millimeter, and Terahertz Waves; Copenhagen, Denmark.  
Presentation: Poster  
Title: Small-size wire phantom to study effect of MMW on nerve fiber  
Authors: S. D'Agostino, F. Di Pietrantonio, M. Benetti, D. Cannatà, M. Cavagnaro, D. Sardari, P. Stano and A. Ramundo-Orlando;

## SOCIETY MEMBERSHIP

**From August 2021:** Student member of the European Bioelectromagnetics Association (EBEA), now Society BIOEM;

## ACADEMIC SERVICES

Trainer for four bachelor students in Clinical Engineering during their intern period, under the The direction of Prof. Francesca Apollonio. With thesis on:

- Numerical characterization of a circular coil for transcranial magnetic stimulation: exposure assessment of clinician;
- Analysis of wireless power transfer in dispersive tissues;
- Occupational exposure assessment during TMS treatment: comparison of two anatomical models;
- Evaluation of the exposure of a healthcare professional to the field produced by a "figure-of-eight" coil for transcranial magnetic stimulation by numerical dosimetry applied to poser anatomical models;

## PARTICIPATION AT NATIONAL CONFERENCES AND SEMINARS FOR AN INCREASE IN KNOWLEDGE

26 April 2022 Webinar: *Characterizing Signal Integrity on Interconnections and Digital Interfaces*  
Organized by Rohde & Schwarz Italia.

22 March 2022 Seminar (webinar), *"Electromagnetic fields and 5G"*  
Organized by ARPA Lazio

- 21 January 2021 Seminar on "Risk from exposure to physical agents in outdoor activities."  
Organized by SST and USL Tuscany Centre
- 30 September 2020 AIRP National Radiation Protection Conference  
The Italian Association of Radiation Protection promotes scientific and cultural actions in the field of protection against ionizing and non-ionizing radiation.
- 3-4 December 2020 5G International Ph.D. School 2019, aggregated to the conference "5G Italy"  
Faculty of Industrial and Civil Engineering, Sapienza University of Rome, (RM).
- 15 November 2019 Conference on "Project BRIC INAIL ID 26 presentation of final results"  
Faculty of Industrial and Civil Engineering, Sapienza University of Rome, (RM).
- 9 October 2019 Seminar on: "Occupational health and safety regulations and insurance protection to the test of the IV industrial revolution".  
Inail, via IV Novembre (RM).
- 11 April 2019 Seminar on: " Technological innovation for the assessment of biomechanical risk and rehabilitation to work "  
INAIL Research Center Monte Porzio Catone (RM).
- 21 March 2019 Seminar on: "Muscles and vibrations"  
INAIL Research Center Monte Porzio Catone (RM).
- 28 February 2019 Seminar on: " Mapping of health risks and outcomes in the area "  
INAIL Research Center Monte Porzio Catone (RM).
- 27 February 2019 Seminar on: "MATLAB for the development of IoT device monitoring platforms"  
MathWorks Event (RM).
- 8 November 2018 Seminar on: " Indoor radon exposure in living and working environments: average levels, current regulation, and future prospects "  
INAIL Research Center Monte Porzio Catone (RM).
- 26 October 2018 Conference on: "Radon geological risk from the earth an invisible danger to health: how many know it?"  
CNR, Piazzale Aldo Moro 7, (RM). Organized by the National Geologist Council.
- 9 October 2018 Seminar on: "Radiation Protection in Healthcare".  
INAIL Research Center Monte Porzio Catone (RM).
- 20 September 2018 Seminar on: " Active control of noise and vibrations: state of the art and prospects "

INAIL Research Center Monte Porzio Catone (RM).

- 4 July 2018 Conference on: " Prevention through design and business 4.0. The contribution of Inail research. "  
Auditorium Inail, P.le Pastore 6, Rome .
- 25 January 2018 Seminar on: "Natural radioactivity in building materials".  
National Research Council, P. le Aldo Moro, 7 (RM).  
In collaboration with the National Professional Association of Qualified Radioprotection Experts (ANPEQ) and the Order of Engineers of the Province of Rome.
- 11 December 2017 Seminar on: " Optimization of radiation protection in interventional radiology procedures ".  
INAIL Research Center Monte Porzio Catone (RM).
- 14 February 2017 – 16 February 2017 COST Meeting BM1309, "5th WGMs with Workshops: COST EMF-MED, the European network for innovative uses of EMFs in biomedical applications."  
CIOP- Central Institute for work Protection – National Research Institute, Warsaw, Poland.
- 2 May 2016 Conference on: "New frontier in the field of RF and Microwave measurements: News 5G Technology".  
Rohde & Schwarz Italia SpA, Rome.

## PUBLICATIONS ON JOURNAL PAPERS AND BOOKS

February 2022

Authors: **S D'Agostino** , M Colella ,M Liberti, R Falsaperla and F Apollonio.

Title: "Systematic numerical assessment of occupational exposure to electromagnetic fields of Transcranial Magnetic Stimulation".

Journal: The International Journal of Medical Physics Research and Practice. DOI: 10.1002/mp.15567

October 2021

Authors: G M Contessa, **S. D'Agostino** , R Falsaperla, C Grandi, A Polichetti.

Title: "Issues in the implementation of Directive 2013 35 /EU regarding the protection of workers against electromagnetic fields"

Journal: International Journal of Environmental Research and Public Health. 2021, **18**, 10673.

<https://doi.org/10.3390/ijerph182010673>

June 2018

Authors: **Simona D'Agostino**, C. Della Monica, E. Palizzi, F. Di Pietrantonio, M. Benetti, D. Cannatà, M.

Cavagnaro, D. Sardari, P. Stano and A. Ramundo-Orlando.

Title: "Extremely high-frequency electromagnetic fields facilitate electrical signal propagation by increasing transmembrane potassium efflux in an artificial axon model."

Journal: **Scientific Reports** volume 8, Article number: 9299 (2018). DOI: 10.1038/s41598-018-27630-8  
[www.nature.com/articles/s41598-018-27630-8](http://www.nature.com/articles/s41598-018-27630-8)

June 2022.

Authors: N. Dolciotti, M. Colella, **S. D'Agostino**, M. Liberti and F. Apollonio

Title: "Improved anatomical female breast model: 3D realization and its application to numerical plane wave exposure", Conference IEEE MELECON, Palermo, 14 - 16 June 2022;

Publisher: IEEE Xplore, DOI:10.1109/MELECON53508.2022.9843025

Published in: 2022 IEEE 21st Mediterranean Electrotechnical Conference (MELECON)

October 2021

Authors: **S. D'Agostino**; M. Colella; M. Liberti; R. Falsaperla; F. Apollonio.

Title: "Dosimetric assessment of clinical staff exposed to magnetic field produced by a transcranial magnetic stimulation circular coil".

Collection: XXXIV General Assembly and Scientific Symposium of the International Union of Radio Science (URSI GASS).

Publisher: IEEE Xplore

DOI: 10.23919/URSIGASS51995.2021.9560280

October 2019

Authors: A. Modenese, D. Carlotti, G.M. Contessa, **S. D'Agostino**, R. Falsaperla, C. Grandi, V. Lopresto, R. Pinto, A. Polichetti, R. Pozzi, F.M. Gobba

Title: "Protection of workers from electromagnetic fields (EMF) and health surveillance: preliminary data of a research within the INAIL Collaborative research (BRiC) 2016 call"

Journal: GIMLE- Italian Journal of Occupational Medicine and Ergonomics, Volume XLI n.4.

December 2016

Authors: **Simona D'Agostino**, F. Di Pietrantonio, M. Benetti, D. Cannatà, M. Cavagnaro, D. Sardari, P. Stano, A. Ramundo-Orlando.

Title: "Small-size wire phantom to study the effect of MMW on nerve fiber."

Collection: IEEE 2016 41st International Conference on Infrared, Millimeter, and Terahertz waves (IRMMW-THz). Copenhagen, Denmark.

Publisher: IEEE Xplore; ISBN 9781467384858, ISSN 2162-2035, DOI: [10.1109/IRMMW-THz.2016.7758455](https://doi.org/10.1109/IRMMW-THz.2016.7758455)

## PROCEEDINGS OF NATIONAL AND INTERNATIONAL CONFERENCES

September 2022

Authors: N. Dolciotti, M. Colella, **S. D'Agostino**, M. Liberti and F. Apollonio

Title: "Improvement of Breast Shape in a Female Whole-Body Model: A Numerical Evaluation of the Exposure to 2.45 GHz Plane Wave"

European Microwave Week - EuMW2022, Milano, 25-30 September 2022.

#### July 2022

Authors: M. Comelli, D. Andreuccetti, N. Zoppetti, E. Mattei, G. Burriesci, R. Falsaperla, **S. D'Agostino**, C. Grandi, M. Valentini, A. Bogi, N. Stacchini, R. Di Liberto.

Title: "WebNir: Web-based tools for assessing occupational exposure to Non-Ionizing Radiation"  
10<sup>th</sup> Jubilee International Conference on Radiation in Various Fields of Research (Jubilee RAD 2022 Conference Summer Edition). Herceg Novi, Montenegro, from 25<sup>th</sup> to 29<sup>th</sup> of July, 2022

#### July 2022

Authors: C. Vivarelli, E. Mattei, F. Censi, G. Burriesci, **S. D'Agostino**, R. Falsaperla, G. Calcagnini.

Title: "Exposure set up for the far-field EMI assessment of pacemakers";

44<sup>th</sup> Annual international conference of the IEEE Engineering in Medicine and Biology Society. EMBC2022, Glasgow, Scotland.

#### July 2022

Authors: Alessandro Polichetti , Gian Marco Contessa, **Simona D'Agostino**, Rosaria Falsaperla, Carlo Grandi.

Title: "Protection of Workers Exposed to EMFs above Occupational Exposure Limits".

ICEmB2022. VI edition of the National Conference "Interactions between Electromagnetic Fields and Biosystems", Cagliari

#### June 2022

Authors: Giancarlo Burriesci, Andrea Bogi, Moreno Comelli, **Simona D'Agostino**, Riccardo Di Liberto, Rosaria Falsaperla, Marco Valentini, Nicola Zoppetti

Title: Intercomparison of measuring instruments used for the evaluation of complex electromagnetic field signals using the weighted peak method.

38<sup>th</sup> National Congress of Industrial and Environmental Hygiene - Aidi 2022. Cagliari

#### June 2022

Authors: **S. D'Agostino**, M. Colella ,M. Liberti, R. Falsaperla and F. Apollonio.

Title: Occupational exposure to transcranial magnetic stimulation coil: a systematic numerical risk assessment.

BioEM 2022 - International Conference in the area of bioelectromagnetic. Nagoya, Japan, 19 -24 June 2022.

#### June 2022

Authors: **S. D'Agostino** , M. Colella ,M. Liberti, R. Falsaperla and F. Apollonio,

Title: " Occupational exposure to TMS treatment: variability among human anatomical models",  
3rd URSI AT-AP-RASC, Gran Canaria, 29 May - 3 June 2022;

#### October 2021

Authors: **S. D'Agostino**; M. Colella; M. Liberti; R. Falsaperla; F. Apollonio.

Title: "Numerical assessment of the exposure to Transcranial Magnetic Stimulation coil male and female anatomical model comparison".

BioEM 2021 - International Conference in the area of bioelectromagnetics. Ghent, Belgium, 26 September 01 October 2021

#### October 2021

Authors: A Bogi I Pinto, N Stacchini, R Pozzi, R Falsaperla, **S. D'Agostino**, A Polichetti C Giliberti, M Comelli, N Zoppetti.

Title: "Muscle stimulators for aesthetic use as relevant sources of magnetic field protectionist aspects".

Airp National Conference Rome, 29 September - 1 October 2021

#### September 2020

Authors: N. Zoppetti, D. Andreuccetti, S. Ceccherini, M. Comelli, **S. D'Agostino** and R. Falsaperla

Title: Uncertainty in determining respect distance for electromagnetic fields by spatial interpolation of exposure indices.

URSI GASS 2020, Virtual Meeting.

#### October 2019

Authors: **S. D'Agostino**, G.M. Contessa, E. Ragno, P. Rossi.

Title: "The radiation protection between the Consolidated Law and Legislative Decree."

National Conference dBA 2019, Physical agents and health in the workplace", ISBN 978-88-944190-3-0

#### September 2019

Authors: A. Modenese, D. Carlotti, G.M. Contessa, **S. D'Agostino**, R. Falsaperla, C. Grandi, V. Lopresto, R. Pinto, A. Polichetti, R. Pozzi, F.M. Gobba

Title: "Protection of workers from electromagnetic fields (EMF) and health surveillance: preliminary data of a research within the INAIL Collaborative research (BRiC) 2016 Call" 82<sup>nd</sup> National Congress of Occupational Medicine (SIML), 25-27 September, Trieste.

#### June 2019

Authors: R. Pinto, A. Coniglio, G.M. Contessa, **Simona D'Agostino**, R. Falsaperla, V. Lopresto and A. Polichetti.

Title: "Occupational environments where electromagnetic fields exposure can exceed Directive 2013/35/EU limits: identification of scenarios and preliminary measurement survey".

BioEM2019 23-28 June, Montpellier (France).

#### June 2019

Authors: N. Zoppetti, D. Andreuccetti, M. Comelli, **Simona D'Agostino**, R. Falsaperla.

Title: "Uncertainty in the determination of the distance of respect by spatial interpolation of indices of exposure to electromagnetic fields".

Collection: VII National Conference of Physical Agents - Environmental monitoring: from production to data analysis 5-7 June 2019 ISBN 9788888648477, Stresa (VCO).

#### November 2018

Authors: R. Pinto, G.M. Contessa, **S. D'Agostino**, R. Falsaperla, V. Lopresto and A. Polichetti.

Title: "Scientific Review for the Identification of Occupational Scenarios where Electromagnetic Fields Exposure can exceed Exposure Limits."

V National Conference on Interactions between Electromagnetic Fields and Biosystems (ICEmB), Fisciano (SA).

October 2018

Authors: D. Andreuccetti, M. Comelli, **S. D'Agostino**, R. Falsaperla, N. Zoppetti.

Title: "Development and use of a Web tool for the processing of low-frequency magnetic field exposure measurements and the determination of the weighted peak index."

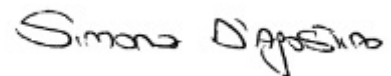
Collection: Proceedings of the Conference "dBA2018 - Physical risks in the workplace", ISBN 978-88-940868-6-7

*In compliance with the Italian legislative Decree no. 196 dated 30/06/2003, I hereby authorize you to use and process my personal details contained in this document.*

*Date*

31/10/2022

*Signature*

A handwritten signature in black ink that reads "Simona D'Agostino". The signature is written in a cursive style with a large initial 'S'.